The influence of hypoxia-inducible factor-2 (HIF-2) on synaptic transmission under normoxia and hypoxia

Dissertation

for

the doctoral degree of

Dr. rer. nat.

from the Faculty of Biology

University of Duisburg-Essen

Germany

submitted by

Theresa Quinting

born in Unna

September 2023

The experiments underlying the present work were conducted under supervision of Prof. Dr. med. Joachim Fandrey at the Institute of Physiology, University of Duisburg-Essen, University Hospital Essen, from October 2019 to July 2023.

1. Examiner: Prof. Dr. med. Joachim Fandrey
2. Examiner: Prof. Dr. med. Ursula Felderhoff-Müser

Chair of the board of examiners: Prof. Dr. rer. nat. Nicole Dünker

Date of the oral examination: 12.12.2023

DOI: 10.17185/duepublico/81349
URN: urn:nbn:de:hbz:465-20240109-114554-7

TABLE OF CONTENTS

ABSTRACT VII

ZUSAMMENFASSUNG IX

1. INTRODUCTION 1

1.1. Hypoxia and hypoxia-inducible factors (HIFs) 1

1.1.1. Molecular mechanisms and regulation of HIFs 2

1.1.2. Role of HIFs in cellular response to hypoxia 4

1.2. Synapses and brain function 6

1.2.1. Synapses and their role in neural communication 6

1.2.2. The tripartite synapse 9

1.3. Hypoxia in the brain 10

1.3.1. Expression and function of HIFs in the brain 11

1.3.2. HIF-2α – implications for synapses 15

1.4. Aim of the study 18

2. MATERIAL AND METHODS 19

2.1. Material 19

2.1.1. Experimental animals and cell culture 19

2.1.2. Machines and devices 20

2.1.3. Consumables and plastic ware 21

2.1.4. Chemicals, reagents and solutions 23

2.1.5. Buffers and media 25

2.1.6. Antibodies 27

2.1.7. Oligonucleotides / primers 28

2.1.8. Software 31

2.2. Methods 31

2.2.1. Cell culture 31

2.2.1.1. Isolation and culture of cortical astrocytes 32

2.2.1.2. Freezing of cortical astrocytes 33

2.2.1.3. Preparation of paraffin dots, PDL coating and seeding of cortical astrocytes for co-culture 33

2.2.1.4. PORN/laminin coating, isolation of hippocampal neurons and co-culture with astrocytes 34

2.2.2. Gene expression analysis 37

2.2.2.1. RNA isolation from hippocampal neurons (kit-extraction) 37

2.2.2.2. RNA isolation from cortical astrocytes and tissue (phenol-chloroform-extraction) 37
2.2.2.3. Complementary DNA (cDNA) synthesis....38
2.2.2.4. Polymerase chain reaction (PCR)....39
2.2.2.5. Genomic DNA (gDNA) isolation and genotyping PCR 40
2.2.2.6. Quantitative PCR (qPCR) 41
2.2.2.7. RT² Profiler™ PCR Array....42
2.2.3. Immunocytochemistry 42
2.2.4. Protein analysis....43
2.2.4.1. Cell lysis and protein extraction 43
2.2.4.2. Protein concentration analysis 43
2.2.4.3. SDS-PAGE and Western Blotting 44
2.2.5. Transmission electron microscopy analysis 45
2.2.5.1. Perfusion, fixation, cutting and embedding of brain tissue 45
2.2.5.2. Image acquisition....47
2.2.5.3. Image analysis....47
2.2.6. Environmental enrichment study 48
2.2.7. Brain tissue analysis 50
2.2.7.1. Dissection of brain hemispheres, cortices and hippocampi....50
2.2.7.2. Shredding of brain tissue for RNA and protein analysis 50
2.2.7.3. Tissue fixation, dehydration and embedding....51
2.2.7.4. Tissue cutting and serial sectioning 51
2.2.7.5. Nissl staining 52
2.2.7.6. Analysis of hippocampal tissue....52
2.2.8. Statistics 53
3. RESULTS **54**
3.1. Functions of cerebral HIF-2α in vivo 54
3.1.1. Brain development and synapse formation in WT and HIF-2α KO mice....54
3.1.1.1. Morphological analysis of the hippocampus of P3, P20 and adult WT and HIF-2α KO mice 54
3.1.1.2. Quantitative analysis of synapse-associated genes in the brain of P3, P20 and adult WT and HIF-2α KO mice 60
3.1.1.3. Quantitative analysis of (potentially) HIF-2α-associated genes in the brain of P3, P20 and adult WT and HIF-2α KO mice 62
3.1.2. Ultrastructure of hippocampal synapses of WT and HIF-2α KO mice....69

3.1.3. Effects of environmental enrichment on WT and HIF-2α KO mice.....72
3.1.3.1. Quantitative analysis of synapse-associated genes in the cortex and hippocampus of enriched and standard housed WT and HIF-2α KO mice.....72
3.1.3.2. Quantitative analysis of HIF-2α-associated genes in the cortex and hippocampus of enriched and standard housed WT and HIF-2α KO mice.....78
3.1.3.3. BDNF content in the cortex and hippocampus of enriched and standard housed WT and HIF-2α KO mice.....81
3.2. Functions of cerebral HIF-2α in vitro.....83
3.2.1. Establishment of a neuron-astrocyte co-culture system under normoxic and hypoxic conditions.....83
3.2.2. Establishment of an experimental set-up and induction of hypoxic target genes in neurons and astrocytes.....90
3.2.3. HIF-2α KO efficiency in neurons and astrocytes under NOX and HOX conditions93
3.2.4. Stability of neuronal and astrocytic marker expression over the experimental time course.....95
3.2.5. Quantitative analysis of synapse-associated and hypoxia-inducible genes in WT and HIF-2α KO astrocytes under HOX conditions.....97
3.2.6. HIF-1α and HIF-2α protein and gene levels in WT and HIF-2α KO astrocytes under HOX conditions.....100
3.2.7. Quantitative analysis of hypoxia-inducible genes in WT and HIF-2α KO neurons under HOX conditions.....102
3.2.8. Quantitative analysis of neuron- and synapse-associated genes in WT and HIF-2α KO neurons under HOX conditions.....104
4. DISCUSSION 113
4.1. Aspects of brain development in neonatal (P3), juvenile (P20) and adult WT and HIF-2α KO mice.....113
4.1.1. WT and HIF-2α KO mice exhibit a similar hippocampal development.....113
4.1.2. The width of the synaptic cleft is reduced in the Stratum radiatum of adult HIF-2α KO mice.....114
4.1.3. Differences in expression of cerebral genes are mainly found in neonatal mice and resolve during adulthood.....115
4.2. Effects of environmental enrichment on a cerebral HIF-2α KO.....118
4.2.1. Environmental enrichment does not enhance differences in gene expression levels in the cortex and hippocampus between HIF-2α KO and WT mice.....118

4.2.2. Environmental enrichment does not induce overall neuro- and synaptogenesis on gene level 119
4.3. Effects of a HIF-2α KO on neurons and astrocytes in vitro under hypoxic conditions 122
4.3.1. Hypoxic response of WT and HIF-2α KO astrocytes 122
4.3.1.1. The hypoxic response in astrocytes is not influenced by neuronal HIF-2α ...122
4.3.1.2. *Epo* and *Vegf* are target genes of HIF-2α in astrocytes 123
4.3.1.3. *Phd2* expression is increased in HIF-2α KO astrocytes compared to WT astrocytes....124
4.3.1.4. Adora2a, but not Adora1, is a hypoxia target gene in astrocytes, though independent of HIF-2α....125
4.3.1.5. The hypoxic up-regulation of target genes is more prominent in astrocytes than in neurons 127
4.3.2. Hypoxic response of WT and HIF-2α KO neurons....127
4.3.2.1. The expression of hypoxia target genes *Vegf*, *Phd2* and *Phd3* is not HIF-2α-dependent in neurons....127
4.3.2.2. The up-regulation of neuronal *Vegf* and *Phd2* depends on the HIF-2α status of astrocytes....128
4.3.2.3. Neuronal HIF-2α is not important for expression of genes associated with synaptic formation and function 131
4.3.2.4. The HIF-2α status of astrocytes affects the neuronal expression of genes associated with synaptic function and hypoxic adaptation 132
4.4. Conclusion 136
4.5. Outlook....138
5. REFERENCES **140**
6. APPENDIX **154**
6.1. Supplementary figures....154
6.2. List of figures....162
6.3. List of tables 165
6.4. List of abbreviations....165
6.5. List of publications and congress contributions....168
ACKNOWLEDGEMENTS **170**
CURRICULUM VITAE **171**
DECLARATIONS **172**

ABSTRACT

Hypoxia is a condition characterized by inadequate oxygen levels in tissues or organs, which can have widespread and detrimental effects on various physiological processes. Sufficient oxygen supply is fundamental for maintaining normal brain functions and synaptic transmission. Prolonged hypoxia as in an ischemic stroke can lead to irreversible brain injury with symptoms like epilepsy, speech and language deficits or even paralysis. In acute hypoxia, the cells adapt in different ways to the decreased oxygen supply for protection of neurons, including decreased synaptic signaling or changes in excitation and inhibition of neuronal and glial cells.

Key factors of the cellular response to low oxygen are a group of heterodimeric transcription factors, the *hypoxia-inducible factors* (HIF-1, HIF-2 and HIF-3). HIFs alter the expression of oxygen-related genes and play an important role during brain development and neural regeneration after hypoxic events. The function of HIFs thereby varies based on the specific brain region or cell type, such as neurons or astrocytes. In addition, the isoforms HIF-1 and HIF-2 exhibit different, sometimes opposing effects on cellular adaptation to hypoxia.

Synapses are highly susceptible to changes in oxygen availability based on their high energetic demand. Although many of the response mechanisms to hypoxia take part at the synapse, the exact role of HIF-2 in synaptic transmission and plasticity is not yet known.

Previous studies found implications of HIF-2 on brain development, learning and memory in vivo under normoxic conditions and under hypoxia in vitro. Therefore, this study investigates the functions of HIF-2 in synaptogenesis and synaptic transmission in a mouse model of a brain-specific HIF-2α knockout (KO) on a molecular level. Under normoxic conditions, HIF-2α had no major impact on hippocampal development and synaptic ultrastructure in vivo. Additionally, a global HIF-2α KO did not lead to any significant differences in the expression of synapse-associated genes in cortex and hippocampus of adult animals, even under environmentally enriched conditions. However, in an in vitro model of brain hypoxia, using a neuron-astrocyte co-culture system, HIF-2α abundance in astrocytes played a significant role. In the absence of astrocytic HIF-2α, the neuronal adaptation to hypoxic stress is dampened, independent of the neuronal genotype. Neurons exhibited reduced activation of hypoxia-responsive genes like *Vegf* and *Phd2*, along with increased expression of genes linked to the excitatory glutamatergic system and decreased expression of genes related to the inhibitory GABAergic system.

Astrocytes recently emerged as new regulators in synaptic activation by interacting with neurons through paracrine effects. In this study, astrocyte-derived neurotrophic factors like *Vegf* and *Epo* were less expressed when HIF-2α was knocked out in astrocytes, potentially

resulting in the disturbed fine-tuning of neuronal response to hypoxia and altered balance between excitatory and inhibitory synapses.

Collectively, astrocytic HIF-2α emerged as a key player for the interplay between astrocytes and neurons during neuronal adaptation mechanisms to hypoxia whereas neuronal HIF-2α seems to be of only limited importance at the synapse. Since synapses are crucial for communication between neurons and play a vital role in cognitive functions, understanding how they respond to hypoxia can shed light on the mechanisms underlying cognitive impairment, memory deficits and various neurological disorders that are associated with oxygen deprivation in the brain.

ZUSAMMENFASSUNG

Hypoxie ist ein Zustand, der durch unzureichende Sauerstoffversorgung in Geweben oder Organen gekennzeichnet ist und weitreichende, schädigende Auswirkungen auf verschiedene physiologische Prozesse haben kann. Eine ausreichende Sauerstoffversorgung ist entscheidend für die Aufrechterhaltung normaler Gehirnfunktionen und synaptischer Übertragung. Langanhaltende Hypoxie, wie bei einem ischämischen Schlaganfall, kann zu irreversiblen Hirnverletzungen führen, die sich in Symptomen wie Epilepsie, Sprachstörungen oder sogar Lähmungen äußern können. In akuter Hypoxie passen sich die Zellen auf unterschiedliche Weise an die verminderte Sauerstoffversorgung an, um die Neurone zu schützen. Dazu gehört zum Beispiel eine Abnahme der synaptischen Signalübertragung oder Veränderungen in der Erregung und Hemmung von neuronalen und glialen Zellen.

Schlüsselfaktoren der zellulären Antwort auf niedrigen Sauerstoff sind eine Gruppe von heterodimeren Transkriptionsfaktoren, die Hypoxie-induzierbaren Faktoren (HIF-1, HIF-2 und HIF-3). HIFs verändern die Expression von Sauerstoff-bezogenen Genen und spielen eine wichtige Rolle während der Gehirnentwicklung und der neuralen Regeneration nach hypoxischen Ereignissen. Die Funktionen von HIFs variieren dabei je nach spezifischer Hirnregion oder Zelltyp, wie Neuronen oder Astrozyten. Darüber hinaus zeigen die Isoformen HIF-1 und HIF-2 unterschiedliche, manchmal gegensätzliche Effekte auf die zelluläre Anpassung an Hypoxie.

Synapsen reagieren aufgrund ihres hohen Energiebedarfs besonders empfindlich auf Veränderungen der Sauerstoffverfügbarkeit. Obwohl viele der Anpassungsmechanismen unter Hypoxie an der Synapse stattfinden, ist die genaue Rolle von HIF-2 in synaptischer Übertragung und Plastizität bisher nicht bekannt.

Vorherige Studien fanden Hinweise auf Auswirkungen von HIF-2 auf die Gehirnentwicklung sowie auf Lernen und Gedächtnis unter normoxischen Bedingungen in vivo und unter Hypoxie in vitro. Daher untersucht diese Studie die Funktionen von HIF-2 in Synaptogenese und synaptischer Übertragung in einem Mausmodell eines Gehirn-spezifischen HIF-2α-Knockouts (KO) auf molekularer Ebene. Unter normoxischen Bedingungen hatte HIF-2α keine wesentlichen Auswirkungen auf die hippocampale Entwicklung und synaptische Ultrastruktur in vivo. Darüber hinaus führte ein globaler HIF-2α-KO nicht zu signifikanten Unterschieden in der Expression von Synapsen-assoziierten Genen in Kortex und Hippocampus adulter Tiere, selbst unter *environmental enrichment* Bedingungen. In einem in-vitro-Modell der Gehirnhypoxie, unter Verwendung eines Neuron-Astrozyten-Co-Kultursystems, spielte HIF-2α in Astrozyten eine wichtige Rolle. In Abwesenheit von astrozytärem HIF-2α wurde die neuronale Anpassung an hypoxischen Stress vermindert, unabhängig vom neuronalen Genotyp. Neuronen zeigten eine reduzierte Aktivierung von Hypoxie-reaktiven Genen wie *Vegf*

und *Phd2* sowie eine erhöhte Expression von Genen, die mit dem exzitatorischen glutamatergen System in Verbindung stehen und eine verringerte Expression von Genen, die mit dem inhibitorischen GABAergen System in Verbindung stehen.

Erst kürzlich sind Astrozyten als neue Regulatoren in der synaptischen Aktivierung hervorgetreten, indem sie auf parakrine Weise mit Neuronen interagieren. In dieser Studie wurden die von Astrozyten sekretierten neurotrophen Faktoren *Vegf* und *Epo* weniger exprimiert, wenn HIF-2α in Astrozyten ausgeschaltet wurde. Dies führte möglicherweise zu einer gestörten Feinabstimmung der neuronalen Reaktion auf Hypoxie und einem veränderten Gleichgewicht zwischen exzitatorischen und inhibitorischen Synapsen.

Insgesamt erwies sich astrozytäres HIF-2α als Hauptakteur für das Zusammenspiel zwischen Astrozyten und Neuronen während der neuronalen Anpassungsmechanismen an Hypoxie, wogegen neuronales HIF-2α in der Synapse nur von begrenzter Bedeutung zu sein scheint. Da Synapsen für die Kommunikation zwischen Neuronen entscheidend sind und eine wichtige Rolle für kognitive Funktionen spielen, kann das Verständnis ihrer Anpassung auf Hypoxie dazu beitragen, Aufschluss über die Mechanismen von kognitiver Beeinträchtigung, Gedächtnisstörungen und verschiedenen neurologischen Störungen geben, die mit Sauerstoffmangel im Gehirn in Verbindung stehen.

1. INTRODUCTION

1.1. Hypoxia and hypoxia-inducible factors (HIFs)

Hypoxia, a condition characterized by a deficiency of oxygen supply to tissues and organs, is a significant physiological challenge that cells must overcome to restore oxygen homeostasis and maintain their survival and function. One crucial player in the cellular response to hypoxia is the hypoxia-inducible factor (HIF) family. HIFs are transcription factors that coordinate adaptive responses to low oxygen levels by regulating the expression of numerous target genes mainly involved in angiogenesis, erythropoiesis, metabolism and cell survival (for review, see for example Fandrey *et al.*, 2019; Wenger, 2002).

Hypoxia can occur in both physiological and pathophysiological contexts. Physiological hypoxia refers to a temporary and controlled decrease in tissue oxygenation, typically observed during high-altitude exposure or intense exercise. Physiological hypoxia furthermore occurs in the developing vertebrate embryo, where HIFs promote anaerobic metabolism, drive vasculature formation and support the development of heart, bones, placenta, nervous system and other organs. In addition, low oxygen levels can regulate the differentiation of embryonic stem and progenitor cells (Dunwoodie, 2009; Simon and Keith, 2008).
In contrast, pathophysiological hypoxia arises from various medical conditions, including respiratory disorders like chronic obstructive pulmonary disease, cardiovascular diseases or anemia. Hypoxia is furthermore a characteristic feature of solid tumors due to an inadequate and disorganized tumor vasculature, limited oxygen diffusion and high oxygen consumption by rapidly proliferating cancer cells. Hypoxic conditions in tumors activate HIFs, which regulate the expression of genes involved in angiogenesis, metabolism and resistance to therapy, thereby contributing to tumor progression and metastasis (Semenza, 2012).
HIFs also play a critical role in neuroprotection under hypoxic conditions like in ischemic stroke. In addition, dysregulations of HIF signaling and chronic or repetitive hypoxic insults have been implicated in the pathogenesis of neurodegenerative disorders such as Alzheimer's disease (Mitroshina *et al.*, 2021).

Understanding the structure, regulation and functions of HIFs is vital for unraveling the complex mechanisms underlying cellular responses to hypoxia and holds promising prospects for therapeutic interventions in hypoxia-related diseases like cancer, ischemia or anemia. It was therefore well reasoned that the Nobel Prize in Physiology or Medicine in 2019 was awarded jointly to William G. Kaelin Jr., Sir Peter J. Ratcliffe and Gregg L. Semenza for their pioneering work in “discoveries of how cells sense and adapt to oxygen availability” (NobelPrize.org, 2019).

1.1.1. Molecular mechanisms and regulation of HIFs

The structure of HIFs intricately links with their function and regulation, enabling them to respond to changes in oxygen levels and modulate gene expression accordingly. HIFs are heterodimeric proteins composed of an oxygen-sensitive α-subunit and a constitutively expressed β-subunit (also named ARNT = aryl hydrocarbon receptor nuclear translocator) (Wang *et al.*, 1995; Wang and Semenza, 1995). The stability of HIF-α is regulated by oxygen availability and it is responsible for sensing and responding to changes in oxygen levels while the β-subunit provides stability and helps to facilitate DNA binding. To date, three different isoforms of the α-subunit, namely HIF-1α, HIF-2α and HIF-3α, have been identified (Gu *et al.*, 1998; Tian *et al.*, 1997; Wang *et al.*, 1995). The structural organization of HIF-α isoforms is highly conserved and encompasses several functional domains such as the basic helix-loop-helix (bHLH) and Per-Arnt-Sim (PAS) domains located at the N-terminus (Semenza *et al.*, 1997). Figure 1.1 depicts the functional domains of the different subunits and their isoforms.

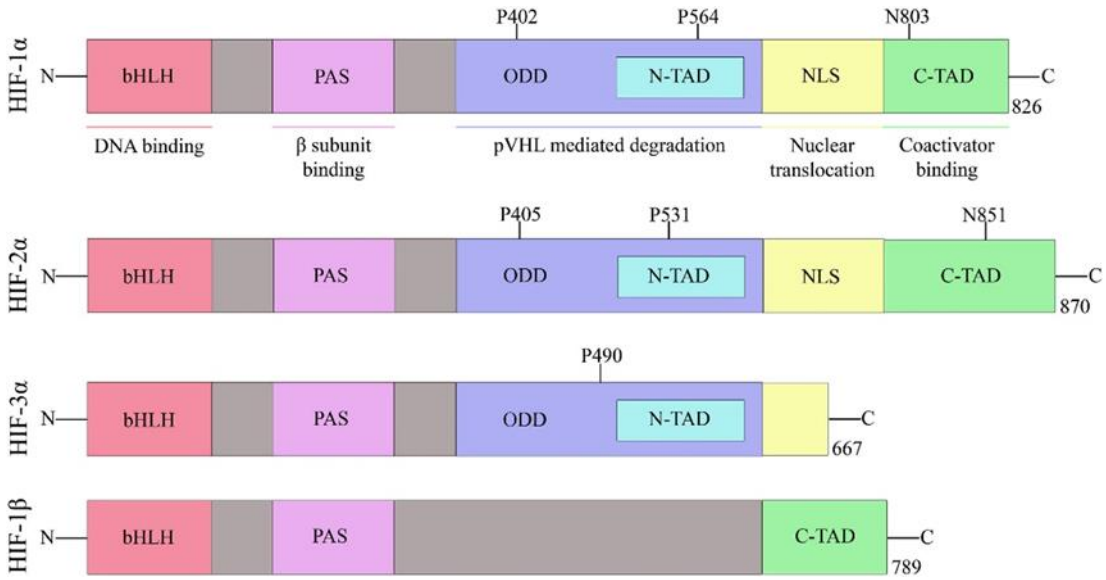

Figure 1.1: Domain structure of human HIF subunits and isoforms (Davis *et al.*, 2018).

The bHLH domain facilitates DNA binding to specific DNA sequences known as hypoxia-responsive elements (HREs) within target gene promoters, while the PAS domain enables heterodimerization with the β-subunit. Moreover, a nuclear localization signal (NLS) directs the α-subunit to the nucleus (where binding to HRE sequence takes place). Additionally, the C-terminal region of HIF-α contains two oxygen-dependent transactivation domains: the amino-terminal transactivation domain (N-TAD) and the carboxy-terminal transactivation domain (C-TAD). These domains interact with histone acetyltransferases and the co-activator p300/CBP (CREB binding protein) to regulate gene expression (Jiang *et al.*, 1997; Kallio *et al.*, 1998; Semenza *et al.*, 1997). Within the NAD domain, the oxygen-sensitive degradation domain (ODD) is located, which contains two proline residues that can be hydroxylated for HIF regulation (Huang *et al.*, 1998).

HIF-α stability is mainly regulated post-translationally through hydroxylation events. The hydroxylation of HIF-α is carried out by a family of enzymes known as prolyl hydroxylases (PHDs), which require oxygen, iron and 2-oxoglutarate as cofactors. Under normoxic conditions, when enough oxygen is available, the PHDs hydroxylate specific proline residues within the ODD of HIF-α (Srinivas *et al.*, 1999)(Figure 1.2, left). This hydroxylation event serves as a signal for the recruitment of the von Hippel-Lindau tumor suppressor protein (VHL), leading to ubiquitination and subsequent degradation of HIF-α by the proteasome (Cockman *et al.*, 2000; Maxwell *et al.*, 1999; Salceda and Caro, 1997). However, under hypoxic conditions, reduced oxygen availability limits PHD activity, resulting in the stabilization and accumulation of HIF-α subunits (Figure 1.2, right). The α-subunit translocates into the nucleus, where it dimerizes with the β-subunit and recruit co-activators, including p300/CBP, to initiate the transcriptional activation of target genes (Arany *et al.*, 1996).

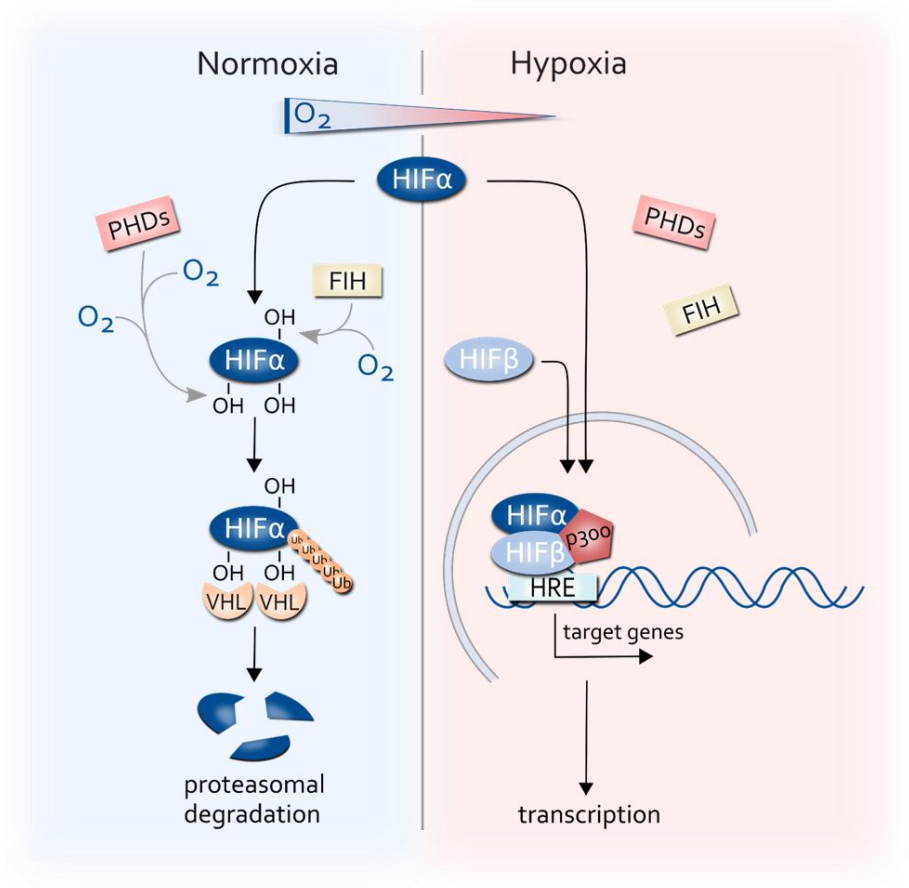

Figure 1.2: O_2-dependent regulation of hypoxia-inducible factors.

HIF activity is mainly regulated at a post-translational level. In the presence of O_2, HIF-α is hydroxylated by prolyl hydroxylases (PHDs) and factor inhibiting HIF (FIH) enzymes. This leads to subsequent ubiquitination mediated by the von Hippel-Lindau protein (VHL) which targets the α-subunit for proteasomal degradation. Under hypoxic conditions, reduced oxygen availability limits PHD activity, resulting in the stabilization and accumulation of the HIF-α subunit. HIF-α and HIF-β dimerize in the nucleus at genomic hypoxia-responsive elements (HREs) and, together with co-factors such as P300, initiate the transcription of target genes.

Three oxygen-dependent prolyl hydroxylases have been identified: PHD1, PHD2, and PHD3 (Epstein *et al.*, 2001). These enzymes are generally inactive or exhibit reduced activity under hypoxic conditions. PHD2 is likely to predominantly regulate HIF-1α and is ubiquitously expressed (Berra *et al.*, 2003). In contrast, the expression of PHD1 and PHD3 is rather tissue-specific, as proven in cell culture experiments derived from various tissues. In addition, PHD3 is predominantly associated with the regulation of HIF-2α under hypoxic conditions (Appelhoff *et al.*, 2004; Metzen *et al.*, 2005).

In addition to prolyl hydroxylation, HIF-α undergoes asparaginyl hydroxylation within the C-TAD domain. This hydroxylation event is mediated by the factor inhibiting HIF (FIH), which blocks the interaction of HIF-α with coactivators such as p300/CBP (Hewitson *et al.*, 2002; Lando *et al.*, 2002). The hydroxylation of proline and asparaginyl residues within HIF-α is crucial for its regulation. Moreover, several signaling pathways, such as those activated by growth factors and cytokines, can modulate HIF activity through mechanisms that affect HIF stability, subcellular localization and interactions with other transcriptional regulators in an oxygen-independent way (Iommarini *et al.*, 2017; Ziello *et al.*, 2007).

1.1.2. Role of HIFs in cellular response to hypoxia

The cellular response to hypoxia orchestrated by HIFs is essential for the adaptation, survival and proper function of cells under low oxygen conditions. HIFs mediate the transcriptional activation of genes involved in various adaptive processes directly or indirectly linked to maintaining oxygen balance (Figure 1.3).

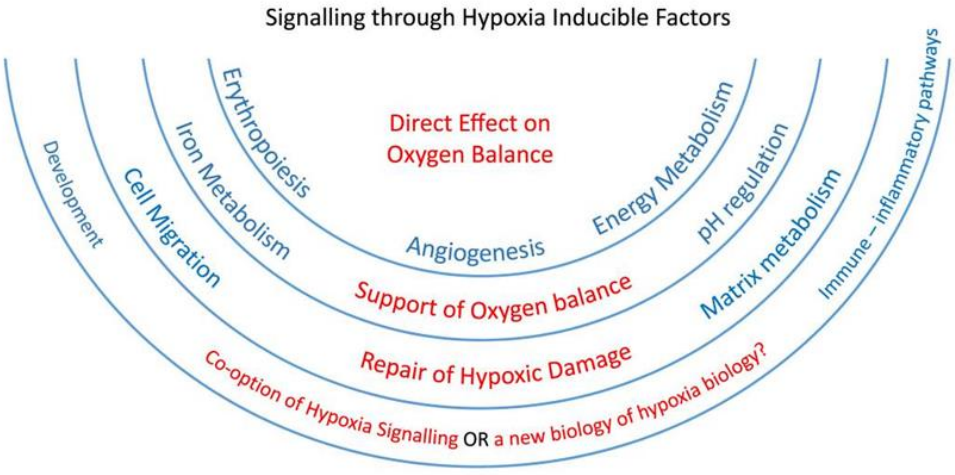

Figure 1.3: Different ways of HIFs for regulating processes that are directly or indirectly associated with maintaining oxygen balance.

Initially, the genes identified as targets of HIF were primarily associated with direct effects on maintaining oxygen balance. However, as more HIF targets have been discovered, it has become evident that many of them are indirectly linked to oxygen homeostasis, particularly in relation to processes such as development and immune-inflammatory pathways (Pugh and Ratcliffe, 2017).

This involves the regulation of genes involved in erythropoiesis, angiogenesis and energy metabolism like glycolysis and mitochondrial functioning, as well as genes affecting iron transport or pH regulation, cell migration or regarding inflammatory or immune-modulating pathways (Pugh and Ratcliffe, 2017).

While the structural features of HIF-α isoforms are highly conserved, they exhibit distinct functional characteristics. HIF-1α and HIF-2α function as transcription factors when dimerized with HIF-β, whereas the precise role of HIF-3α remains less understood and is believed to modulate HIF signaling through complex interactions and negative regulations with other HIF isoforms, especially with HIF-1 (Duan, 2016; Maynard *et al.*, 2005).
HIF-1α and HIF-2α have similar DNA-binding motifs and overlapping targets, but the pathways targeted by each of the subunits differ considerably (Loboda *et al.*, 2012). While the C-TAD domain is highly similar in structure and function across both isoforms and facilitates the expression of their shared target genes, the N-TAD domain plays a significant role in determining target gene specificity of HIF-1α and HIF-2α (Hu *et al.*, 2007).
HIF-1α is widely expressed and has been extensively studied. It is involved in the regulation of angiogenesis, cell survival and displays a preference for inducting the glycolytic pathway. HIF-1 plays a crucial role in the adaptation to acute hypoxia, promoting anaerobic metabolism, enhancing oxygen delivery and maintaining energy homeostasis. It is associated with the response to inflammation, immune cell function and tumor growth (McGettrick and O'Neill, 2020; Semenza, 2012).
HIF-2α, also known as endothelial PAS domain protein 1 (EPAS1), exhibits a more restricted expression pattern. It is primarily expressed in endothelial cells, liver, lungs, kidneys, heart, brain and intestine and plays a critical role in embryonic development, erythropoiesis and vascular homeostasis and angiogenesis (Loboda *et al.*, 2012; Tian *et al.*, 1997; Wiesener *et al.*, 2003). HIF-2 is implicated in cellular responses to chronic or prolonged hypoxia. It contributes to tissue remodeling, angiogenesis and organ development and is particularly critical for erythropoiesis and iron homeostasis. In addition, HIF-2 is involved in regulating genes crucial for tumor growth, cell cycle progression and maintenance of stem cell pluripotency. Examples of such genes include the proto-oncogene c-Myc (Gordan *et al.*, 2007) and the stem cell factor OCT-3/4 (Covello *et al.*, 2006).

The distinct functions and target gene specificities of HIF-1 and HIF-2 contribute to their differential involvement in disease pathogenesis, highlighting the need for isoform-specific research.

1.2. Synapses and brain function

Neurons are the primary functional units of the brain and are responsible for transmitting and facilitating communication within the nervous system through electrical and chemical signaling. There are several types of neurons, including sensory neurons, which convey information from the external environment, motor neurons, which initiate muscle contractions and interneurons, which facilitate communication between different regions of the brain. At the cellular level, neurons consist of three main parts: the cell body (soma), dendrites and axons. The cell body contains the nucleus and other organelles necessary for metabolic functions of the neuron, like the synthesis of proteins and neurotransmitters, which are vital for the function and maintenance of the cell. The axon is a long projection that plays a crucial role in transmitting signals from one neuron to other neurons or effector organs. Dendrites are the primary structures responsible for receiving incoming signals from other neurons or sensory receptors. They possess numerous branches and specialized protrusions called dendritic spines, which increase the surface area available for synaptic connections. Through these connections, neurons can receive input from multiple sources and integrate signals from different neurons, which allows the processing of complex information and the generation of an appropriate response. Neurons communicate with each other at specialized junctions called synapses. When an action potential reaches the end of an axon, it triggers the release of chemical transmitters into the synaptic cleft. These neurotransmitters bind to receptors on the dendrites or cell bodies of neighboring neurons, initiating electrical signals in the recipient neuron and continuing the transmission of information (Bear *et al.*, 2018).

In addition to neurons, glial cells, often referred to as the non-neuronal cells of the brain, play a critical role in supporting neuronal function. Glial cells include several subtypes, for example astrocytes, oligodendrocytes and microglia. Each glial cell subtype possesses distinct properties and functions, collectively contributing to brain development, metabolism, immune response and neuronal survival. Astrocytes, the most abundant glial cells in the brain, provide structural and metabolic support to neurons. They provide nutrients like lactate, maintain the extracellular ion balance and contribute to the blood-brain-barrier, which protects the brain from potential harmful substances. Once considered as only supportive cells, astrocytes have also emerged as active modulators of synaptic function and plasticity through various mechanisms that are further referred to in 1.2.2.

1.2.1. Synapses and their role in neural communication

Synapses are essential for the transmission of information and communication between neurons through electrical or chemical signaling. Research on synaptic structures dates back

to as early as the late 19th century, when the Spanish histologist Cajal employed the Golgi staining technique to visualize individual neurons and their connections with each other, thereby proposing that neurons are discrete individual cells that communicate through specialized contact points, now known as synapses (Jones, 1994).

At the cellular level, a synapse consist of a pre-synaptic terminal, the synaptic cleft and a post-synaptic terminal. The standard structure of a chemical synapse and the process of synaptic transmission is depicted in Figure 1.4.

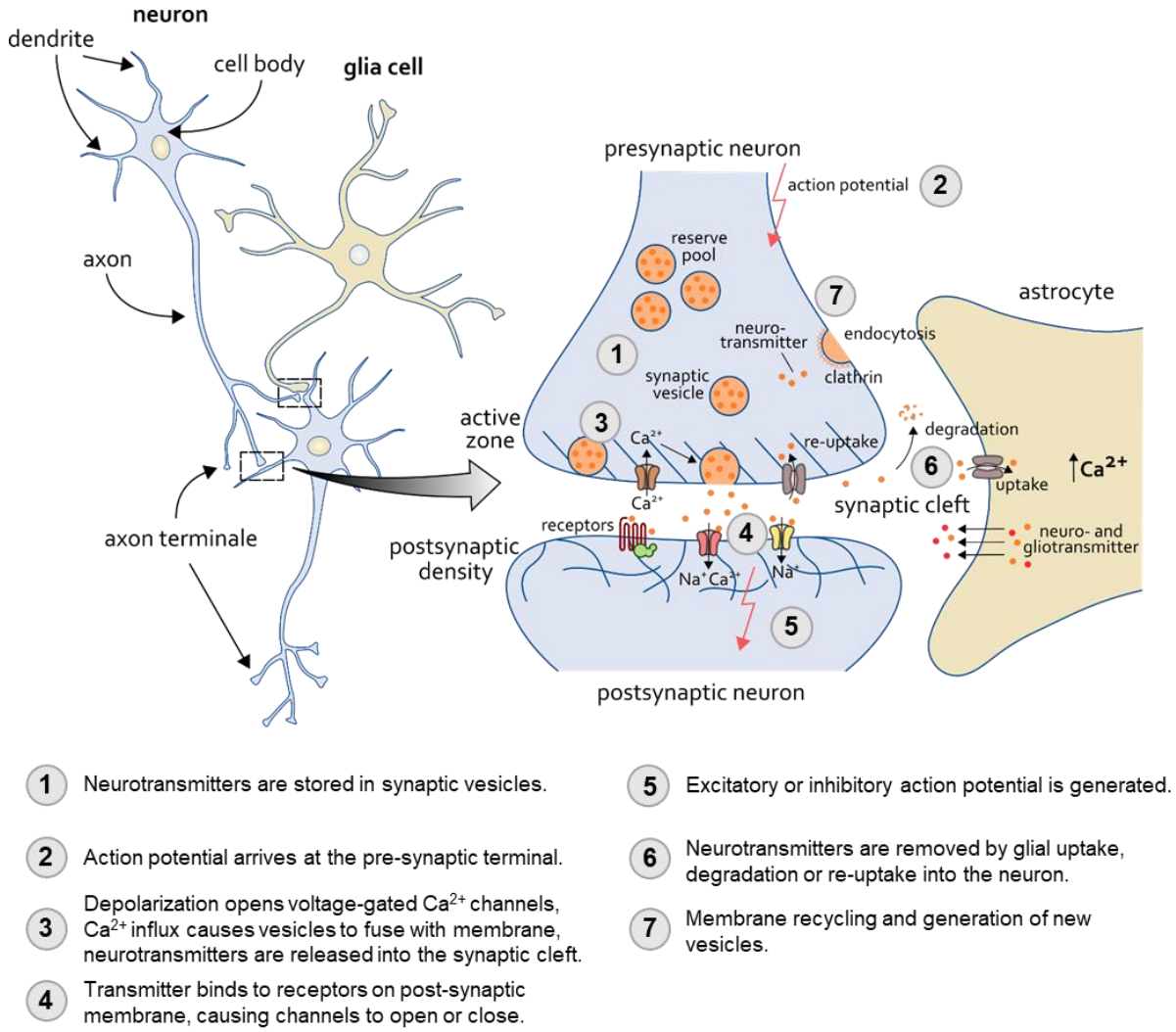

Figure 1.4: Schematic overview of chemical synapses and synaptic transmission.

Chemical synapses transmit signals from axon terminals of one neuron to the dendrites of another neuron through release of neurotransmitters as messengers between the two cells. The general structure of a chemical synapse is composed of the pre-synaptic compartment containing the vesicles with neurotransmitters and the post-synaptic compartment with a high concentration of receptors at the post-synaptic density. Astrocytes may contribute to the synaptic transmission as part of a tripartite synapse through release of neuro- and gliotransmitters and degradation of neurotransmitters.

The process of synaptic transmission begins with the arrival of an action potential at the pre-synaptic terminal. The depolarization of the pre-synaptic membrane triggers the opening of voltage-gated calcium channels, allowing calcium ions (Ca^{2+}) to enter the cytoplasm. The

increase in intracellular Ca^{2+} concentration triggers the fusion of the neurotransmitter-containing vesicles with the pre-synaptic membrane, leading to exocytosis and the release of neurotransmitters, like glutamate as the main excitatory or GABA as the main inhibitory neurotransmitter, into the synaptic cleft (Bear *et al.*, 2018). The exocytosis is thereby restricted to a small section of the pre-synaptic membrane that contains electron-dense material and is therefore referred to as the active zone (Sudhof, 2012). The neurotransmitters diffuse across the synaptic cleft and bind to specific receptors located on the post-synaptic membrane at a specialized zone, the post-synaptic density (PSD, Figure 1.4). The PSD is an electron-dense region that functions in concentrating and organizing neurotransmitter receptors so they are in close proximity to the opposite neurotransmitter release sites of the pre-synapse. These receptors can be classified into two main categories: ionotropic receptors and metabotropic receptors. Ionotropic receptors such as NMDA (N-methyl-D-aspartate) receptors and AMPA (α-amino-3-hydroxy-5-methyl-4-isoxazolepropionic acid) receptors, with glutamate and glycine as ligands, directly regulate the flow of ions across the post-synaptic membrane. Upon neurotransmitter binding, ionotropic receptors undergo conformational changes, leading to the opening or closing of the ion channels. This results in the generation of post-synaptic potentials, either excitatory (EPSP) or inhibitory (IPSP), depending on the nature of the neurotransmitter and the associated receptor (Figure 1.4). In contrast, metabotropic receptors initiate signaling cascades through G-protein activation, which mediate the transmission of the signal to downstream effectors (Bear *et al.*, 2018).

The PSD is composed of many more proteins besides the neurotransmitter receptors, as proteomics analyses revealed. PSDs also contain cell adhesion molecules, scaffold proteins, signaling enzymes, proteins of the cytoskeleton and membrane trafficking proteins, all of them crucial for synaptic transmission and plasticity (Kaizuka and Takumi, 2018).
To ensure the precise and timely termination of synaptic transmission, excess neurotransmitters must be eliminated from the synaptic cleft (Figure 1.4). There are two primary mechanisms for neurotransmitter clearance: enzymatic degradation or reuptake by transporters. Enzymes, such as acetylcholinesterase, catalyze the breakdown of neurotransmitters, thereby terminating their function in the synaptic cleft. Additionally, specialized transporters located on the pre-synapse or neighboring glial cells actively transport neurotransmitters back into the pre-synaptic terminal or surrounding cells, where they can be recycled for subsequent use (Bear *et al.*, 2018).

The ability of synapses to change their transmission efficiency is called synaptic plasticity. It is a fundamental property of the nervous system and important for learning and memory processes. Long-term potentiation (LTP), an increase in efficiency, and long-term depression

(LTD), a decrease in efficiency, are two well-studied forms of synaptic plasticity that are thought to be involved in information storage and synaptic remodeling (Citri and Malenka, 2008).
Altogether, the precise and complex regulation of synapse formation and synaptic signaling depends on a variety of proteins and protein complexes performing different functions, with more than 2000 different proteins found through proteomics analyses over the last 20 years (Dieterich and Kreutz, 2016). Besides the different receptors and ion channels, there are proteins essential for synaptic vesicle formation, membrane fusion and therefore transmitter release and recycling processes, like Synaptophysin, Synaptotagmin and Synaptobrevin or other members of SNARE proteins (Sudhof, 2013). Scaffolding proteins are involved in organizing and anchoring the components of the synapse. They provide a structural framework for the assembly of signaling molecules, receptors and ion channels (Sheng and Kim, 2011).
Synaptic adhesion molecules are involved in establishing and maintaining cell-cell contacts at the synapse. They promote synapse formation, regulate synaptic stability and influence synaptic plasticity (Sudhof, 2008).

1.2.2. The tripartite synapse

Astrocytes have emerged as active and dynamic players in synaptic function and plasticity and take part in so-called “tripartite” synapses, where astrocytic processes can be found in close proximity to the pre- and post-synaptic compartment (Figure 1.4).
One significant role of astrocytes at the synapse is the regulation of extracellular neurotransmitter levels. Astrocytes express neurotransmitter transporters on their membranes, allowing them to take up released neurotransmitters from the synaptic cleft. For instance, glutamate, the primary excitatory neurotransmitter in the brain, is efficiently taken up by astrocytic transporters, which prevents the excessive accumulation of glutamate in the synaptic cleft. Astrocytes then convert glutamate into glutamine through the enzyme glutamine synthetase, which is released back to neurons for the re-synthesis of glutamate (Mahmoud *et al.*, 2019). Astrocytes are further equipped with calcium-permeable channels and receptors that, upon activation, trigger intracellular calcium signaling. Elevated intracellular calcium in astrocytes can then induce the release of gliotransmitters, including glutamate, ATP, D-serine and BDNF. These gliotransmitters can act on neuronal receptors and modulate synaptic transmission and connectivity (Parpura and Zorec, 2010). For example, D-serine can act as a co-agonist at the NDMA receptor, a crucial player in LTP induction (Henneberger *et al.*, 2010).
Astrocytes are further involved in synaptic pruning and structural remodeling during brain development and synaptic plasticity. They actively participate in the elimination of excess synapses, induction of new synapse formations and refinement of neural circuits through secretion of different factors. The first family of proteins that was identified to be a major

synaptogenic factor secreted by astrocytes was the thrombospondin group of extracellular matrix proteins (Christopherson *et al.*, 2005; Chung *et al.*, 2015). Astrocytes also contribute to the formation and maintenance of the extracellular matrix, which is crucial for neuronal migration and axonal guidance during development (Faissner *et al.*, 2010).

1.3. Hypoxia in the brain

The brain is particularly susceptible to hypoxic injury because of its high metabolic demands and limited capacity for energy storage (Vangeison *et al.*, 2008). Hypoxia in the brain as result of for example stroke, cardiac arrest or high-altitude exposure triggers a cascade of adaptive responses and cellular changes to maintain oxygen homeostasis. While the brain has mechanisms to cope with short-term hypoxia, prolonged or severe hypoxia can lead to neuronal damage such as cognitive impairments, motor deficits and cell death (Sharp and Bernaudin, 2004).

Figure 1.5 summarizes how prolonged or severe hypoxia disrupts the cellular homeostasis of the brain by impairing important processes including the ubiquitin-proteasome-system, endoplasmic reticulum, mitochondrial dynamics, autophagy and Ca^{2+} and iron homeostasis (Jha *et al.*, 2018).

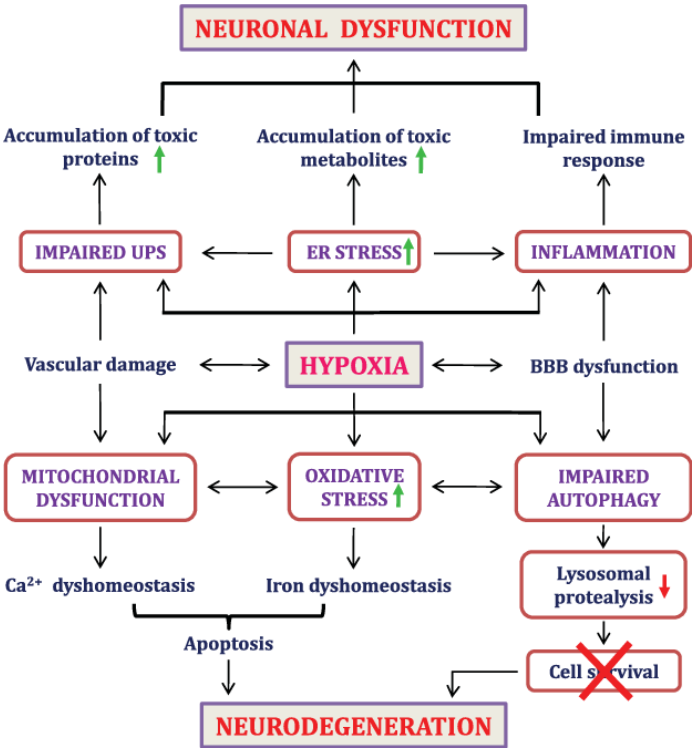

Figure 1.5: Pathological roles of hypoxia in neuronal dysfunction and neurodegeneration.
Upon hypoxia, the disruption of brain homeostasis is triggered by a broad range of biological processes such as mitochondrial dysfunctions, oxidative stress, impaired autophagy, inflammation, ER stress and an impaired UPS, leading to neuronal dysfunctions or even cell death. UPS = ubiquitin-proteasome-system, ER = endoplasmic reticulum, BBB = blood-brain-barrier (Jha *et al.*, 2018).

As master regulators of cellular adaptation to low oxygen levels, HIFs are also important players of the adaptive processes in the hypoxic brain. Studying HIFs in the context of cerebral hypoxia thereby allows for a deeper understanding of how the brain adapts to oxygen deprivation. Further research is needed to unravel the intricate mechanisms involved in hypoxic brain injury and develop targeted interventions to protect and promote brain health under hypoxic conditions.

1.3.1. Expression and function of HIFs in the brain

To date, there are several studies dealing with the function of HIFs in the developing or pathophysiological brain or in different adapted cell culture models using brain-derived cell types. MCAO (middle cerebral artery occlusion) systems in rat- or mouse-related models can be used as mimics for stroke pathology whereas primary neurospheres or neuron-astrocyte co-culture systems can be directly challenged with different intensities of hypoxia or oxygen-glucose-deprivation. The generation of overall or cell-type specific *Hif-1* or *Hif-2* knockouts in animals, tissue or cell culture thereby helped to identify mechanisms of HIF activity and function. It became evident, that the role of HIFs is dependent on the specific brain area or cell type like neurons or astrocytes and that HIF-1 and HIF-2 can differentially modulate cellular adaptation mechanisms.

Jha and colleagues (2018) comprehensively reviewed and summed up some of the most prominent functions of HIF-1 and HIF-2 (Figure 1.6).

One of the major cellular adaptation mechanisms to hypoxia is the change in energy homeostasis, which is mediated by HIFs. Under normal oxygen conditions, glucose is primarily metabolized through aerobic glycolysis, in which glucose is converted into pyruvate, which then enters the mitochondria for further energy production through the tricarboxylic acid cycle and oxidative phosphorylation. However, during brain hypoxia, the reduced oxygen levels impair mitochondrial function and the efficient utilization of pyruvate via oxidative phosphorylation. As a compensatory response, the brain undergoes a metabolic shift towards anaerobic glycolysis. In this pathway, glucose is converted to lactate through glycolysis, even in the presence of oxygen. This metabolic shift allows for the generation of ATP, though at a lower efficiency compared to oxidative phosphorylation. The lactate produced during anaerobic glycolysis can furthermore be utilized as an energy source by neurons and astrocytes (Dienel, 2012). HIF-1α, in particular, has been shown to increase the expression of glucose transporter 1 (GLUT1) and glucose transporter 3 (GLUT3) in brain cells, facilitating enhanced glucose uptake by brain cells (Sharp and Bernaudin, 2004). Once glucose is taken up by brain cells, HIFs further impact glucose metabolism by modulating glycolysis. HIF-1α activation has been shown to upregulate the expression of various glycolytic enzymes, including hexokinase

2 (HK2), phosphofructokinase 1 (PFK1) and lactate dehydrogenase A (LDHA), promoting glycolytic flux (Sharp and Bernaudin, 2004). Besides, HIF-1 was shown to be an important player of neurogenesis, angiogenesis, mitochondrial trafficking and autophagy in the brain (Jha *et al.*, 2018)(Figure 1.6).

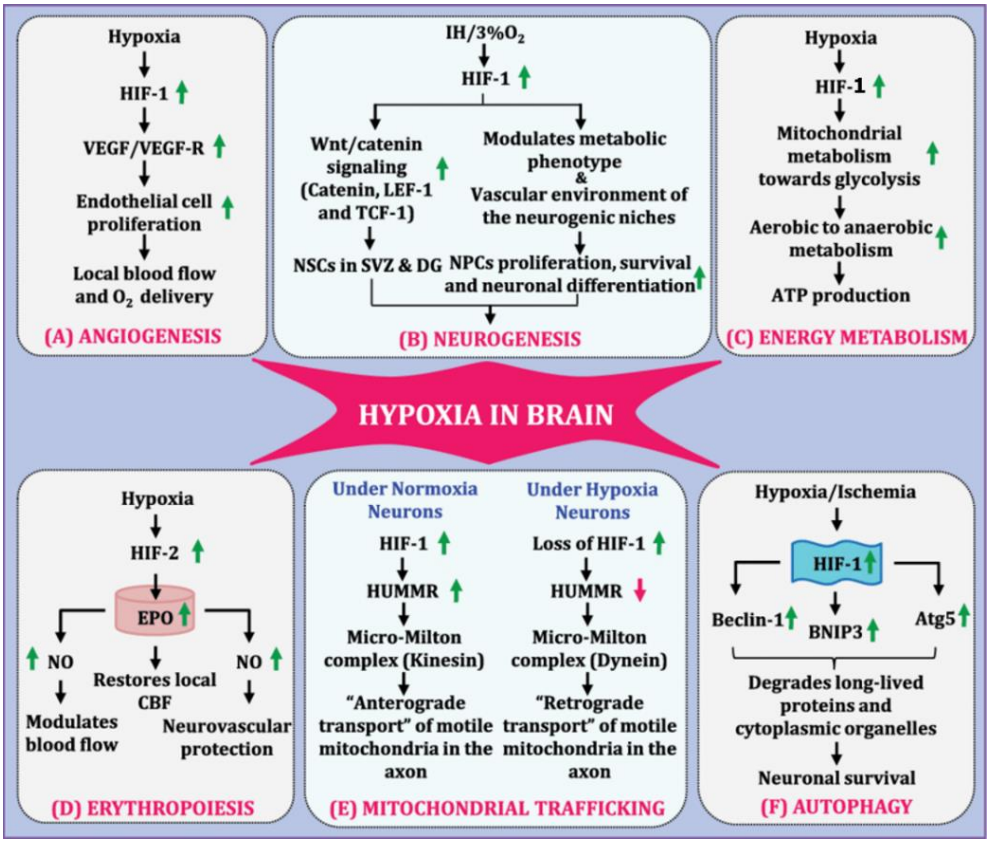

Figure 1.6: HIF-1 and HIF-2 dependent mechanisms of cellular adaptation to brain hypoxia.
VEGF = vascular endothelial growth factor, VEGF-R = vascular endothelial growth factor-receptor, IH = intermittent hypoxia, LEF-1 = lymphoid enhancer-binding factor-1, TCF-1 = T-cell factor-1, NSCs = neural stem cells, SVZ, = subgranular zone, DG = dentate gyrus, NPCs = neural progenitor cells, EPO = erythropoietin, NO = nitric oxide, CBF = cerebral blood flow, BNIP3 = BCL2 Interacting Protein 3, Atg5 = autophagy protein 5, HUMMR = hypoxia upregulated mitochondrial movement regulator. Adapted from Jha *et al.* (2018).

HIF-1 also shows cell-type specific effects as investigated in an elegant study from Vangeison *et al.* (2008), where they induced a loss of HIF-1α function in either neurons, astrocytes or both cell types combined. Whereas a HIF-1 loss in neurons reduced neuronal viability under hypoxic conditions, the selective loss in astrocytes protected the neuronal cells from hypoxia-induced death in co-cultures. On the other hand, the expression of HIF-1α in astrocytes under hypoxia has a protective effect on astrocytes itself in maintaining cell morphology and viability in response to glutamate excitotoxicity, potentially mediated by EPO, VEGF and adenosine (Badawi *et al.*, 2012). In a more recent study, Guo *et al.* (2019) tested the functions of HIF-1 and HIF-2 in astrocytes under different combinations of hypoxic severity and glucose concentrations, demonstrating that both severity of hypoxia during pretreatment and glucose

availability alter the balance of HIF-1 and HIF-2 signaling during chronic hypoxia and subsequently influence the interaction of astrocytes and neurons.

Hypoxic adaptation mechanisms also take place in terms of erythropoiesis (Figure 1.6). *Epo*, one of the main target genes of HIFs, is primarily produced by the kidney and, to a lesser extent, the liver. This hormone is traditionally associated with regulating erythrocyte production. However, it also exhibits non-erythropoietic effects, particularly in the brain, which have been extensively studied in recent years. It acts through its receptors, EPO receptors (EpoRs), which are abundant on neural progenitor cells, to stimulate their proliferation and subsequent differentiation into mature neurons (Chen *et al.*, 2006). Neurons, astrocytes, microglia and endothelial cells also express *EpoRs*, allowing them to respond to EPO signals (Nagai *et al.*, 2001).

One of the primary functions of EPO is the modulation of apoptosis or programmed cell death. EPO has been shown to inhibit apoptosis in neuronal cells, thereby preventing cell death and preserving the integrity of the brain tissue. EPO also modulates oxygen delivery through regulation of endothelial NO production. Endothelial cells respond to EPO through production of factors that regulate blood flow, endothelial cell survival, endothelial progenitor cell mobilization and secretion of factors that affect neurogenesis and neuroblast migration (Noguchi *et al.*, 2007). Additionally, EPO can enhance angiogenesis, the formation of new blood vessels, in the brain, facilitating improved blood supply and oxygen delivery to hypoxic regions (Ghezzi and Brines, 2004; Noguchi *et al.*, 2007).

In addition, EPO exhibits neuroprotective effects that have been elucidated in diverse studies. EPO abundance is significantly induced during hypoxic events and functions as a protectant for surrounding cell types. In this, astrocytes seem to be the main source of EPO production which than promote neuronal survival in a paracrine manner with an up-regulation of up to 100 fold (Marti *et al.*, 1996). Although HIF-1 was thought to be the main inductor of EPO for a long time, it was later shown that the EPO production in astrocytes is mainly induced in a HIF-2 dependent manner (Chavez *et al.*, 2006; Toriuchi *et al.*, 2020).

Much is known about the role of HIF-1 in brain hypoxia, however there are less studies dealing with the functions of HIF-2, although the role of HIF-2 in EPO expression in cortical astrocytes was already examined in 2006 (see above) and further hypothesized in other studies (Barteczek *et al.*, 2017). Barteczek *et al.* investigated the impact of HIF-1 and HIF-2 on neuronal survival upon stroke in a MCAO model with *Hif-1α*-, *Hif-2α*- or *Hif-1α/Hif-2α*-deficient mice. They found that both *Hif-1α*- and *Hif-2α*-deficient mice showed no altered infarct and edema size, suggesting that the two HIF-α subunits might compensate for each other. In the double knockout animals, the infarct size was reduced, but only in the early acute phase during

the first 24 h of reperfusion, not in the acute phase after 72 h. This was potentially caused by the reduced expression of anti-survival genes in the early acute phase due to the double HIF-1/HIF-2 loss that, on the other hand, resulted in an increased apoptosis and reduced angiogenesis in the following phase.

In a study of embryogenesis in zebrafish, Ko *et al.* (2011) showed a protective role of HIF-2 on neural progenitor cells and neural differentiation through up-regulation of apoptosis inhibitors birc5a and birc5b (orthologues of Survivin).

Although not tested in brain-residing astrocytes, HIF-2 in retinal astrocytes seems to have important functions in regulating astrocyte development by maintaining the supply of astrocyte progenitors through slowing down their differentiation into non-proliferative mature cells (Duan *et al.*, 2014). In addition, HIF-2 is required for growth and survival of oxygen sensitive glomus cells of the carotid body, the central organ of O_2 sensing (Macias *et al.*, 2018). Global HIF-2α, but not HIF-1α, inactivation in adult mice was furthermore shown to impair carotid body growth and associated ventilatory acclimatization to chronic hypoxia (Hodson *et al.*, 2016).

Studies of our group further evaluated the role of HIF-2α in a knockout mouse model investigating its functions in brain development (Kleszka *et al.*, 2020) and neuronal responses to ischemia with special regards to neurogenesis (Leu *et al.*, 2021). Mice lacking a functional version of HIF-2α exhibited a decrease in the number of pyramidal neurons in the retrosplenial cortex (RSC), a region in the brain that plays a crucial role in various cognitive abilities such as memory and navigation. Moreover, native HIF-2α seemed to be stabilized even under normoxic conditions in the WT mice and the HIF-2α deficit let to disturbances in learning, memory and fear induction, providing new evidence for a significant role of HIF-2α in normal brain functioning and its involvement in developmental processes. HIF-2α KO neurospheres, as an in vitro model for brain development, showed deficits in migration capabilities especially in neurons under normoxic condition, accompanied by reduced expression of genes associated with neural migration and patterning (Kleszka *et al.*, 2020).

In a neurosphere model using oxygen-glucose deprivation (OGD) with or without reperfusion time serving as model of ischemia, HIF-2α was found to be important for promoting neurogenesis after ischemia. Furthermore, there seems to be a HIF-2 dependent expression of *Vegf* in neurospheres (Leu *et al.*, 2021), indicating again that the functions of HIF-1 and HIF-2 are depending on the exact cell type studied, the cellular differentiation stage and the timing and severity of hypoxia, ischemia or OGD.

1.3.2. HIF-2α – implications for synapses

The brain is the organ with the highest energy consumption, making up more than 20% of the overall oxygen metabolism. It is believed that neurons utilize approximately 75% - 80% of the energy generated within the brain and that the major energy consumption takes part at the synapse in restoring the membrane potentials, vesicle recycling, neurotransmitter synthesis or axonal trafficking processes (Watts *et al.*, 2018). Hypoxia can negatively impact synaptic energy metabolism due to the reduced oxygen supply necessary for cellular respiration and the generation of ATP that is essential for various energy-dependent processes at the synapse. As a result, synaptic transmission and plasticity may be compromised, affecting the overall function and communication between neurons and processes of learning and memory. Indeed, there are studies showing an effect of HIF depletion on behavioral performance, as observed for an overall HIF-2α KO in the brain of mice in the study of Kleszka *et a*l. (2020) even under normoxic conditions. In a different study, double knockout mice (HIF-1 and HIF-2 depleted) that were kept under 8% oxygen for three weeks also changed the behavioral performance in these animals, although the sample size of the experiments was rather small and they did not test single knockouts (Ma *et al.*, 2021).

One study dealing with differences between HIF-1 and HIF-2 in terms of synaptic transmission and plasticity was published in 2018 by Leiton *et al*. They tested the hypothesis that astrocyte HIF supports synaptic plasticity and learning upon hypoxia. For this purpose, animals with HIF-1 or HIF-2 depletion in astrocytes were tested for behavioral, learning and electrophysiological LTP responses to mild hypoxic challenge. They found an impaired learning, accompanied by an attenuated response to induction in LTP, showing that loss of HIF-2, but not HIF-1, in astrocytes has consequences on cognitive performance and synaptic plasticity and function.

There is also evidence for a modularly role of PHD2, belonging to the hypoxia-HIF-axis, in synaptic plasticity in the hippocampus. In acute hippocampal tissue slices of rats, field excitatory post-synaptic potentials and excitatory post-synaptic currents were measured after treating the tissue with PHD inhibitors. The study found the induction of LTPs to be strongly impaired. A neuron specific PHD2 knockout in murine tissue also prevented hippocampal LTP (Corcoran *et al.*, 2013). A different research study demonstrated that the suppression of PHD2 leads to the reduction of dendritic spine formation in hippocampal neurons. As a result, this diminishes the density of synapses and overall neuronal activity throughout the network (Segura *et al.*, 2016).

When looking for interaction points between HIFs (particularly HIF-2α) and synapses, there might be different potential mechanisms of HIF-involvement in synaptic functioning. Tyrosine hydroxylase (TH), the rate-limiting enzyme in the synthesis of catecholamines such as

dopamine, comprises HRE sequences in its promotor region and is up-regulated under hypoxia. It was shown that both HIF isoforms are able to activate this promoter in a reporter construct assay (Schnell *et al.*, 2003) although several studies implicate a preference for HIF-2 (Richter *et al.*, 2013).

The brain derived neutrophic factor (BDNF) is a growth factor with multiple important functions in the brain, for example in neuronal development, differentiation and survival; in synaptogenesis and synaptic plasticity of both excitatory and inhibitory synapses; or in long-term memory (for reviews see Colucci-D'Amato *et al.*, 2020; Huang and Reichardt, 2001; Kowianski *et al.*, 2018). BDNF is synthesized as an immature precursor form that is stored in either dendrites or axons and is released and activated in an activity-dependent manner as either pro or mature BDNF that can have opposing effects. Reduced levels of BDNF have furthermore been observed during the natural process of aging but also in neurodegenerative disorders, such as Huntington's disease, Alzheimer's disease and Parkinson's disease (Miranda *et al.*, 2019). In addition, interactions between BDNF and hypoxia are known, for example a higher induction and secretion of BDNF after hypoxia in pulmonary human cells in a HIF-1α-dependent manner (Helan *et al.*, 2014) or a promotion of neurite regrowth after oxygen-glucose deprivation in rat neurons (Xue *et al.*, 2021). *Bdnf* overexpression in neurons enhanced the preconditioning effect of brief episodes of hypoxia in a rat neuroglial hippocampal cell culture and promoted a tolerance of GABAergic neurons to hypoxia/ischemia (Turovskaya *et al.*, 2020). Tyrosine kinase receptors that serve as receptors of the mature BDNF form are also hypoxia-inducible and contain three HREs upstream of the transcription site, although the induction of gene expression rather seems to be HIF-1 and not HIF-2 specific (Martens *et al.*, 2007).

Another factor in neuronal activity and synaptic transmission is adenosine. Adenosine can be generated by ectonucleotidases, in particular astrocytic ecto-5′-nucleotidase (CD73), through extracellular catabolism of ATP released by astrocytes. In addition, adenosine can also be released directly through equilibrative nucleoside transporters (ENT). The adenosine system in the CNS mostly operates through inhibitory adenosine A1 receptors (Adora1) and facilitating adenosine A2A receptors (Adora2a) that are predominantly expressed on glutamatergic excitatory pre- and post-synapses. Adora1 suppresses voltage-gated calcium channels and decreases the probability of neurotransmitter release at the pre-synapse and post-synaptic activation of Adora1 inhibits activation of NMDA-R. This contrasts with the role of Adora2a that enhances glutamate release as well as NMDA-R activation, regulating the induction and expression of LTPs and LTDs (for reviews, see Chen *et al.*, 2014; Lopes *et al.*, 2021). Astrocytes also express Adora1 and Adora2a, which seem to play a significant role in regulating the morphological and functional responses of astrocytes especially in pathological situations. For example, Adora2a is linked to Alzheimer’s disease (Lopes *et al.*, 2021).

Although HIF-1 also has implications for the adenosine pathway, for example through induction of CD73 leading to higher adenosine levels or through activation of Adora2b gene expression under hypoxic condition (Poth *et al.*, 2013), Adora2a was shown to be transcriptionally induced in human pulmonary endothelial cells in a HIF-2 dependent manner (Ahmad *et al.*, 2009).

One surprising finding in the study of Kleszka *et al.* (2020) was that a HIF-2α deficiency affects synaptogenesis and the expression of the synapse-associated genes *Neurogranin* and *Synapsin* in the cortex of adult animals, although electron microscopy did not reveal structural differences of cortical synapses in HIF-2α KO compared to WT mice. In neurospheres that were challenged with normoxia and hypoxia, the neurospheres furthermore showed reduced expression levels of *Synapsin* and *SAP90/PSD-95-associated protein 4 (Dlgap4)* under both conditions.
Additionally, a study investigating target genes of HIF-1α and HIF-2α in human embryonic kidney cells (HEK293T) found that CACNA1a, a subunit of voltage gated calcium channels at the pre-synapse, is strongly induced by HIF-2α (Wang *et al.*, 2005).
Last but not least, EPO, which is primarily secreted from astrocytes in a HIF-2 dependent manner, was shown to improve affected learning, memory and synaptic plasticity in fimbria-fornix lesion rat models (Almaguer-Melian *et al.*, 2023; Almaguer-Melian *et al.*, 2018; Almaguer-Melian *et al.*, 2016). Furthermore, it was shown that EPO administration enhanced LTP and memory in young mice under normoxic conditions (Adamcio *et al.*, 2008) and EPO administration in young rats reduced spatial learning effects when exposed to chronic intermittent hypoxia (Al-Qahtani *et al.*, 2014).

Taken together HIF-2 might be involved in several mechanisms and processes at the synapse but only a limited number of studies have dealt with this topic so far. Besides the work of our group (Kleszka *et al.*, 2020), most prominent is the beforehand mentioned study of Leiton *et al.* (2018). However, they only researched on functions of astrocytic HIF-2 and not neuronal HIF-2. As synaptic transmission and plasticity is highly affected by changes of oxygen levels as an adaptive mechanism, it is of greater interest to intensify research dealing with functions of HIF-2 in synaptic transmission and plasticity in different cell types.

1.4. Aim of the study

Hypoxia is a challenging condition that affects the brain's normal functioning. As neurons are the major consumer of energy in the brain with high-energetic processes taking part at the synapse, a fine-tuning of synaptic function is of high importance for the brain's resilience and adaptation to oxygen-deprived conditions. Therefore, understanding the exact mechanisms of how the brain preserves neuronal communication and synaptic plasticity under hypoxia can be of great interest in aiding the development of therapeutic strategies against severe pathologies such as neonatal hypoxia-ischemia, ischemic stroke or neurodegenerative diseases.

The activation of hypoxia-inducible factors (HIFs) in response to low oxygen levels is a crucial adaptive mechanism of the brain and other organs. HIFs are heterodimeric transcription factors that regulate various cellular processes, including oxygen homeostasis, energy metabolism, neuronal survival, neurogenesis and synaptic plasticity.

Although much is known about the role of HIF-1 in cerebral adaptation to hypoxia, the isoform HIF-2 is less well studied. Previous studies of our working group found an impact of HIF-2α on brain development and learning and memory in vivo even under normoxic conditions, as well as in vitro functions regarding neurogenesis and synapse-associated gene expressions under both normoxia and hypoxia. As many of the adaptation mechanisms of the brain directly affect synaptic processes and HIF-2α may take part in synaptic transmission and plasticity, this study aims to investigate functions of HIF-2α in synaptogenesis and synaptic transmission in more detail on a molecular level.

For this, one part of the study is focusing on the in vivo effects in HIF-2α KO mice regarding morphological alterations in synapse-dense regions and changes in the expression of synapse-associated genes using histological techniques, electron microscopy and qPCR analysis. To enhance effects of HIF-2α on synaptic plasticity, an environmental enrichment study will be conducted and qPCR and Western Blot analyses performed for HIF-2α KO and WT mice.

The second part of the study will investigate the role of HIF-2α under hypoxic conditions using a neuron-astrocyte co-culture as a model system for synaptic networks, where different combinations of WT and HIF-2α neurons and astrocytes can be directly challenged with hypoxia. As it is known that astrocytes actively take part in neuronal signaling through paracrine effects, the separate analysis of both cell types by Western Blot and qPCR will reveal cell-type specific functions of HIF-2α and allow for the identification of possible paracrine effects of astrocytes on neuronal gene expressions.

2. MATERIAL AND METHODS

2.1. Material

2.1.1. Experimental animals and cell culture

All research was conducted using male and female inbred C57BL/6J mice carrying a conditional brain-specific knockout (KO) of exon 2 of the *Hif-2α* gene, resulting in a non-functional version of HIF-2α, as exon 2 is coding for the DNA-binding domain of the protein.
Mice were generated with help of the Cre/loxP system, where the exon 2 of both *Hif-2α* alleles is flanked by loxP sites and a Cre recombinase is expressed under control of the *Nestin* promotor. *Nestin* expression is only present in cells of the developing central nervous system, guaranteeing a conditional KO in the brain of these mice.
Mice homozygous for the loxP sites (Hif-2α+fl/+fl, purchased from the Jackson Laboratory, Bar Harbor, ME, USA) were mated with mice heterozygous for the Cre recombinase under control of a rat *Nestin* promotor (B6.Cg-Tg(Nes-cre)1Kln/J, purchased from the Jackson Laboratory, Bar Harbor, ME, USA), resulting in offspring that is either *Hif-2α* knockout (KO) or wildtype (WT). Please note, that the WT litteremates, which were used as control animals, are not fully wildtypic as they still carry the floxed *Hif-2α* gene.

The following annotations for the specific genotypes were used subsequently:
Hif-2α $^{fl/fl}$ x NesCre $^{-/-}$ - **WT**
Hif-2α $^{fl/fl}$ x NesCre $^{+/-}$ - **HIF-2α KO**

In general, mice were kept in groups in *Sealsafe NEXT Type II blue line* cages under specific hygienic conditions at 20 °C and a 12 h day and night rhythm at the central animal facility, University Hospital Essen, according to German law for animal welfare. Standard rodent pellets and drinking water were given ad libitum and nesting material and housing was provided. For the environmental enrichment study (2.2.6), enriched mice were kept in T4 rat cages during the course of the experiment. Animal breeding was approved by the State Agency for Nature, Environment and Consumer Protection of North Rhine-Westphalia under the file number 84-02.04.2016.A173.

All cell culture experiments were performed using primary cells generated from the above-mentioned mice, with detailed protocols provided under 2.2.1. The generation of primary hippocampal neurons out of E15.5 – E17.5 embryos was permitted by the by the State Agency for Nature, Environment and Consumer Protection of North Rhine-Westphalia under the file number 81-02.04.2019.A409.

2.1.2. Machines and devices

Table 2.1: Used machines and devices and their manufacturer.

Device/machine	Manufacturer
Anaesthesia device Trajan 808	Dräger
Analytical balance PioneerTM PA64	Ohaus Europa
Aperio ScanScope® CS2	Leica
Autoclave Systec VX-100	Systec GmbH & Co. KG
Axiovert 200M Inverted Fluorescence Microscope	Carl Zeiss Microscopy GmbH
Benchtop centrifuge Heraeus Fresco 21	Thermo Scientific
Benchtop centrifuge Labofuge 400R, function line	Heraeus Instruments
Benchtop micro centrifuge 5415R, refrigerated	Eppendorf
Benchtop micro centrifuge 5420	Eppendorf
Benchtop micro centrifuge Biofuge fresco	Heraeus Instruments
Benchtop mini centrifuge	Biozym
BioDoc-It™ Imaging System + benchtop UV transilluminator	UVP
Cell culture hood HERA Safe	Heraeus Instruments
CFX96 Touch Real-Time PCR Detection System	Bio-Rad Laboratories, Inc.
Cryo console EC 350-2	Thermo Scientific
Electrophoresis power supply Power Pac 200 & 300	Bio-Rad Laboratories, Inc.
Epoch™ Microplate Spectrophotometer (Take3 plate)	BioTek
Exhaust pump	Vacuumbrand GmbH & Co. KG
FusionFX7	Vilber
Homogenizer	Polytron
Incubator Hera cell	Heraeus Instruments
Inverted Microscope for cell culture CK40	Olympus
Inverted Microscope for cell culture DMi1	Leica
InvivO2 400 Hypoxia Workstation	Baker Ruskinn
Magnetic stirrer Rotilabo® MH 15 with heater	Carl Roth GmbH & Co. KG
Microwave MW2700	Exquisit
Mini-PROTEAN® Tetra Cell electrophoresis cell	Bio-Rad Laboratories, Inc.
Monochrom thermal printer P91E	Mitsubishi
Orbital shaker	ELMI

Paraffin embedding station EG1150H	Leica
Perfusor E	B. Braun
pH/mV meter pH900	Presica
Platform wave shaker Polymax 1040 (5° tilt angle)	Heidolph Instruments GmbH & Co. KG
Precision balance 572	Kern
Rotary microtome Microm HM 340E	Thermo Scientific
Stereo-zoom microscope OZL 456	KERN & Sohn
Thermal cycler 5333 MasterCycler	Eppendorf
Thermal cycler Biometra TOne	Analytik Jena
Thermal cycler Techne® Prime	Cole Parmer
Thermoshaker TM130-6	HLC BioTech
Tilt/roller mixer RS-TR 05	PHOENIX Instrument
Tissue dehydration machine	RWW Medizintechnik
Tissue floatation bath TFB 45	MEDITE Medical GmbH
Trans-Blot Turbo Transfer System	Bio-Rad Laboratories, Inc.
Transmission electron microscope (TEM) 1400plus	JEOL GmbH
VIP ECO ultra-low temperature freezer	PHCbi, PHC Corporation of North America
Vortex-genie 2	Scientific Industries
Water bath	GFL

2.1.3. Consumables and plastic ware

Table 2.2: Used consumables and plastic ware and their manufacturer.

Consumable/plastic ware	**Manufacturer/Provider**
96-well PCR plate full skirt LP transparent	Sarstedt
96-well skirted PCR plate, clear PP	AZENTA Life Sciences
BD Eclipse™ needle (20G x 1 1/2 TW	Becton Dickinson
BD Plastipak™ syringe, 1 ml	Becton Dickinson
Beakers (different sizes)	Schott AG
Biosphere® LowRet FilTip (2.5 µl, 20 µl, 100 µl, 1000 µl)	Sarstedt
Capillary pipette tips (200 µl)	Biozym Scientific GmbH
Cell scraper with two-position blade (size S and M)	Sarstedt
CryoPure tube 1.6 ml	Sarstedt
Embedding cassettes	Carl Roth GmbH & Co. KG

Environmental Enrichment accessories: Mouse Igloo® + activity wheel Fast Trac Mouse Swings, single Mouse mezzanine Polycarbonate tunnels™ (rat size and mouse size) + wire for hanging-up Aspen bricks (M) Mouse Hut™ Crawl Ball™	ZOONLAB GmbH
Falcon tube, 15 ml/50 ml	Sarstedt
Forceps Dumont no. 5, extra fine, straight | 2-1033	neoLab
Forceps with non-slip grip, type 2AG-SA, 120 mm long, straight, round | 1-1042	neoLab
Forceps with non-slip grip, type 2G-SA, 115 mm long, straight, fine | 1-1041	neoLab
Forceps with non-slip grip, type 5G-SA, 110 mm long, straight, extra fine | 1-1045	neoLab
Glass Pasteur pipettes (145 mm/225 mm)	Brand®
Glass staining trough	
Micro scissors	
Micro tube 1.5 ml	Sarstedt
Microscope cover glasses (Ø 18 mm)	Paul Marienfeld GmbH & Co. KG
Microscope slides (Menzel Gläser - SUPERFROST PLUS)	ThermoScientific
Microscope slides SuperFrost® Plus	R. Langenbrinck GmbH
Microtome blades A35 & S35	Feather®
Mini-PROTEAN Combs, 15-well, 1.5 mm, 40 µl Casting Stand Casting Frame Casting Stand Gaskets Mini Cell Buffer Dams Gel Releasers	Bio-Rad Laboratories, Inc.
Neubauer hemocytometer	Becton Dickinson GmbH
NucleoSpin® RNA purification kit	Macherey-Nagel GmbH
Paraffin wax	McCormick Scientific
Parafilm® M	Bemis
PCR Seal Clear adhesive film	4tidue
PCR tube 0.2 ml 8-Strip	STARLAB International GmbH
Pipette tips (20 µl, 200 µl, 1000 µl)	Sarstedt
Polyvinylidene fluoride (PVDF) blotting membrane 0.2 µl	PeqLab
RT^2 First Strand Kit	Qiagen
RT^2 Profiler™ PCR Array Mouse Synaptic Plasticity	Qiagen
SafeSeal micro tube (0.5/1.5/2 ml)	Sarstedt
SafeSeal SurPhob tips (20 µl, 100 µl)	Biozym

Serological pipettes (5 ml, 10 ml, 25 ml)	Greiner Bio-One
Stainless steel histology mold	
Tissue culture dish (Ø 100 mm)	Sarstedt
Tissue culture dish EASY GRIP (Ø 35 mm, Ø 60 mm)	Corning, Inc.
Tissue culture flasks (T75)	Sarstedt
Tissue culture plate (12-well)	Sarstedt
Whatman® gel blotting paper, Grade GB003	Sigma-Aldrich

2.1.4. Chemicals, reagents and solutions

Table 2.3: Used chemicals, reagents, supplements and enzymes and their manufacturer.

Chemical/reagent	Manufacturer
10x Taq Reaction Buffer	Biozym
4′,6-diamidino-2-phenylindole (DAPI)	AppliChem
Acetic acid	AppliChem
Agarose	PanReac AppliChem
Ammonium persulfate (APS)	Bio-Rad Laboratories, Inc.
B-27™ Plus Supplement (50x)	Gibco™
Blue S´Green qPCR 2x Mix	Biozym Scientific GmbH
Boric acid	Carl Roth GmbH & Co. KG
Bovine pancreatic deoxyribonuclease I (DNAse I)	Worthington
Bovine serum albumin (BSA)	SERVA Electroph. GmbH
Bromphenol blue	Sigma-Aldrich
Cresyl Violet acetate	Sigma-Aldrich
Cytosine ß-D-arabinofuranoside (AraC)	Sigma-Aldrich
D-(+)-Glucose-solution	Sigma-Aldrich
Denatured alcohol	University hospital Essen
deoxynucleotide triphosphates (dNTPs): dATP, dGTP, dCTP, dTTP	Promega
Diethyl pyrocarbonate (DEPC) BioChemica	AppliChem
Dimethyl sulfoxide (DMSO)	Sigma-Aldrich
DNA ladder 100bp plus	AppliChem
Entellan®	Merck
Ethanol (EtOH) absolute	Honeywell International, Inc.
Ethidium bromide solution, 0.07%	AppliChem
Fetal calf serum (FCS)	Sigma-Aldrich
GlutaMAX™ Supplement	Gibco™

Glycerin	Sigma-Aldrich
Glycerol for molecular biology, >99%	Sigma-Aldrich
GoTaq G2 polymerase	Promega
GoTaq reaction buffer (5X)	Promega
Guanidinium thiocyanate (GTC)	Carl Roth GmbH & Co. KG
Hanks' balanced salt solution (HBSS), no calcium, no magnesium, no phenol red	Gibco™
Hematoxylin	Merck
Hibernate™-E Medium	Gibco™
Hydrochloric acid (HCl), fuming, ≥37%	Sigma-Aldrich
Isoflurane CP® 1 ml/ml	CP-Pharma
Isopropanol	AppliChem
Laminin from Engelbreth-Holm-Swarm murine sarcoma basement membrane	Sigma-Aldrich
L-Glutamine	Invitrogen
MEM Eagle w: EBSS, w: 2 mM L-Glutamine, w: 1 mM Sodium pyruvate, w: NEAA, w: 1.5 g/L NaHCO3	PAN-Biotech
M-MLV reverse transcriptase	Promega
M-MLV RT reaction buffer (5X)	Promega
Mowiol	Calbiochem, Merck
N,N,N′,N′-Tetramethylethylenediamine (TEMED)	Sigma-Aldrich
Neurobasal™ Plus Medium	Gibco™
Nonidet® P40 (NP40)	AppliChem
Normal goat serum (NGS)	Sigma-Aldrich
PageRuler™ Prestained Protein Ladder, 10 bis 180 kDa	Thermo Scientific
Papain suspension	Worthington
Penicillin/streptavidin (P/S), 10000 U/mL	Invitrogen
Phenol	AppliChem
Phenol:chloroform:isoamyl alcohol mixture	AppliChem
Poly-D-lysine hydrobromide (PDL)	Sigma-Aldrich
Poly-L-ornithine hydrobromide (PORN)	Sigma-Aldrich
Proteinase inhibitor (PI) (Complete Mini, EDTA-free)	Sigma-Aldrich
Reagent A and B (DC protein assay)	Bio-Rad Laboratories, Inc.
Restore™ PLUS Western Blot Stripping Buffer	Thermo Scientific
ROTI®Histofix 4%	Carl Roth GmbH & Co. KG
Rotiphorese® NF-Acrylamide/Bis solution, 30% (29:1)	Carl Roth GmbH & Co. KG
RT² First Strand Kit	Qiagen

RT² Profiler™ PCR Array Mouse Synaptic Plasticity	Qiagen
RT² SYBR Green qPCR Mastermix	Qiagen
Skimmed milk powder	University hospital Essen
Sodium acetate (NaOAc)	Sigma-Aldrich
Sodium chloride (NaCl)	Sigma-Aldrich
ß-Mercaptoethanol	Merck
SuperSignal™ West Femto Maximum Sensitivity Substrate	Thermo Scientific
Taq DNA Polymerase, 5 U/µl	Biozym
Trans-Blot Turbo 5x Transfer Buffer	Bio-Rad Laboratories, Inc.
Tris(hydroxymethyl)-aminomethane (Tris)	AppliChem
Tris-EDTA, pH 8.0	Sigma-Aldrich
Triton X-100	Sigma-Aldrich
Trypan blue solution, 0.4%	Gibco™
Trypsin-EDTA (0.5% / 10X)	Gibco™
Tween® 20	Carl Roth GmbH & Co. KG
Xylol	Carl Roth GmbH & Co. KG

2.1.5. Buffers and media

Table 2.4: Used buffers and media and their compositions.

Buffer/solution/media	Composition
APS, 10%	150 mg APS in 1.5 ml dH_2O
AraC stock solution	5 mM in dH_2O, sterile filtered
Blocking solution (Western Blot)	5 % skimmed milk powder in TBS-T
Borate buffer, 150 mM, pH 3.0	Boric acid in dH_2O
Cresyl violet solution, 0.1%	0.2 g cresyl violet powder in 200 ml deionized H_2O
Culture medium (astrocytes)	MEM Eagle 10% FCS 1% P/S 2 mM L-glutamine 0.6% glucose
Culture medium (neurons)	Neurobasal™ Plus 2% B-27™ Plus Supplement 1% P/S 1% GlutaMAX™ Supplement
DEPC water/H_2O	0.1% DEPC in dH_2O
Digestion solution (astrocytes)	MEM Eagle 30 U/ml papain

	0.5 mg/ml L-cysteine 80 µg/ml DNAse I
Digestion solution (neurons)	Preparation medium 30 U/ml papain 0.5 mg/ml L-cysteine 80 µg/ml DNAse I
Freezing medium (astrocytes)	Culture medium (astrocytes) 10% FCS 10% DMSO
GTC solution (4M)	4 M GTC 250 mM NaOAc 0.75% β-mercaptoethanol in DEPC water
Laminin stock solution	250 µg/ml in sterile PBS
Lower buffer (4x, SDS-PAGE), pH 8.8	1.5 M Tris-Base 13.8 mM SDS in dH_2O
Mowiol	5 g Mowiol 20 ml PBS 10 ml Glycerol (100%)
NaOAc (2M), pH 4.0	2 M NaOAc in DEPC-H_2O
NaOAc (3M), pH 5.2	3 M NaOAc in DEPC-H_2O
NaOH, 50 mM	1 M NaOH in dH_2O
PBS (10x), pH 7.4	137 mM NaCl 2.7 mM KCl 10 mM Na_2HPO_4 2 mM KH_2PO_4 in dH_2O Dilute 1:10 in deionized H_2O for 1x PBS solution.
PBS/A (immunofluorescence)	1x PBS 0.1% BSA
PBS/T (immunofluorescence)	1x PBS 0.3% Triton-X-100
PBT1 (immunofluorescence)	1x PBS 1% BSA 0.1% Triton-X-100
PDL stock solution	1 mg/ml PDL in sterile dH_2O
PORN stock solution	0.5 mg/ml PORN in 150 mM sterile borate buffer
Preparation medium (neurons)	HBSS (w/o calcium, magnesium & phenol red) 0.6% glucose
Protein lysis buffer	20 mM Tris pH 7.5 150 mM NaCl 1% NP40 5 mM EDTA in dH_2O Add 10% PI before use

Running buffer (10x, SDS-PAGE)	250 mM Tris-Base 1.92 M Glycine 35 mM SDS in dH_2O
SDS buffer (4x)	100 mM Tris pH 6.8 4% SDS 10% β-mercaptoethanol 0.025% Bromphenol blue 20% Glycerol
TAE buffer (1x), pH 8.0	40 mM Tris 0.11% Acetic acid 1 mM EDTA
TBS (10x), pH 7.6	200 mM Tris-Base 1.37 M NaCl in dH_2O Dilute 1:10 in deionized H_2O for 1x TBS solution.
TBS-T	TBS (1x) 0.05 % Tween® 20
Tris-HCl, 1 M	7.9 g Tris in 50 ml HCl
Upper buffer (4x, SDS-PAGE), pH 6.8	500 mM Tris-Base 13.8 mM SDS in dH_2O

2.1.6. Antibodies

Table 2.5: Antibodies used for Western Blot.

Target/name	Host species	Dilution	Company
Anti-Mouse IgG (Fab specific) - Peroxidase	Goat, polyclonal	1:10000	Sigma-Aldrich
Anti-Rabbit IgG (whole molecule) - Peroxidase	Goat, polyclonal	1:10000	Sigma-Aldrich
BDNF	Rabbit, monoclonal	1:2000	abcam
HIF-1α, C-Term	Rabbit, polyclonal	1:500	Cayman Chemical
HIF-2α, ep190b	Mouse, monoclonal	1:500	Novus Biologicals
α-Tubulin	Mouse, monoclonal	1:500	Santa Cruz Biotechnology, Inc.

All antibodies for Western Blotting were diluted in 5% skimmed milk in TBS-T (blocking solution).

Table 2.6: Antibodies used for immunocytochemistry.

Target/name	Host species	Dilution	Company
Alexa Fluor® 488 Goat Anti-Mouse IgG (H+L)	Goat, polyclonal	1:200	Thermo Scientific
Alexa Fluor® 568 Goat Anti-Mouse IgM (µ chain)	Goat, polyclonal	1:200	Thermo Scientific
Alexa Fluor® 568 Goat Anti-Rabbit IgG (H+L)	Goat, polyclonal	1:200	Thermo Scientific
AlexaFluor® 488 Goat Anti-Rabbit IgG (H+L)	Goat, polyclonal	1:200	Thermo Scientific
Glial Fibrillary Acidic Protein (GFAP)	Mouse, monoclonal	1:200	Merck, Millipore
ß-Tubulin III	Rabbit, polyclonal	1:200	Sigma-Aldrich
Synapsin1	Mouse, monoclonal	1:200	Synaptic Systems GmbH

All antibodies for immunocytochemistry were diluted in PBT1 + 1:200 NGS.

2.1.7. Oligonucleotides / primers

Table 2.7: Used oligonucleotides and primers.

Name	Target gene	Sequence	Product length
Adam10	*ADAM Metallopeptidase Domain 10*	5' TCATGGGTCTGTCATTGATGGA 3' TCAAAAACGGAGTGATCTGCAC	195 bp
Adcy1	*Adenylate Cyclase 1*	5' TTGGCAAGTTCGATGAGTTAGC 3' GGCGTGATCCGTCTTAGGC	110 bp
Adcy8	*Adenylate Cyclase 8*	5' CAGCTACCGAGGGGTCATTTT 3' ACGTTCATCACTACCTCCGATT	120 bp
Adora1	*Adenosine A1 Receptor*	5' GGCCACAGACCTACTTCCAC 3' CCACAGCAATAGCAAGCAGAG	96 bp
Adora2a	*Adenosine A2a Receptor*	5' GCAATAGCCAAGAGGCTGAAGA 3' GCCATCCCATTCGCCATCA	122 bp
Akt1	*AKT Serine/Threonine Kinase 1*	5' ATGAACGACGTAGCCATTGTG 3' TTGTAGCCAATAAAGGTGCCAT	116 bp
Arc	*Activity Regulated Cytoskeleton Associated Protein*	5' TTGGTAAGTGCCGAGCTGAG 3' ACGTAGCCGTCCAAGTTGTT	145 bp
Bdnf	*Brain Derived Neurotrophic Factor*	5' TCATACTTCGGTTGCATGAAGG 3' AGACCTCTCGAACCTGCCC	137 bp
bIII Tubulin	*Class III ß-Tubulin (Tubb3)*	5' TTTTCGTCTCTAGCCGCGTG 3' GATGACCTCCCAGAACTTGGC	100 bp

Camk2a	*Calcium/Calmodulin Dependent Protein Kinase II Alpha*	5’ GTCAGTCAAGCCGGTTCTCC 3’ TTAGGCTGGGAACTAGGGCT	105 bp
Camk2g	*Calcium/Calmodulin Dependent Protein Kinase II Gamma*	5’ TCCGCCCGAGATCATCAGAA 3’ GGTAACAAGGTCAAACACGAGG	132 bp
Cdh2	*Cadherin 2*	5’ AGCGCAGTCTTACCGAAGG 3’ TCGCTGCTTTCATACTGAACTTT	101 bp
Cebpb	*CCAAT Enhancer Binding Protein Beta*	5’ GCCGCCTTATAAACCTCCCG 3’ GGCCACTTCCATGGGTCTAAA	168 bp
Cebpd	*CCAAT Enhancer Binding Protein Delta*	5’ AGAACCCGCGGCCTTCTAC 3’ GTCGTACATGGCAGGAGTCG	106 bp
Cnr1	*Cannabinoid Receptor 1*	5’ AAGTCGATCTTAGACGGCCTT 3’ TCCTAATTTGGATGCCATGTCTC	123 bp
Collybistin	*Arhgef9 = CDC42 guanine nucleotide exchange factor (GEF) 9*	5’ CGGAGCGCCATTACATCAAG 3’ GGGATCATCATTGTTGTACTGCT	185 bp
Creb1	*CAMP Responsive Element Binding Protein 1*	5’ CAGCCACAGATTGCCACATT 3’ GATAACTGATGGCTGGGCCG	147 bp
Crem	*CAMP Responsive Element Modulator*	5’ ATGTCTTGAAAATCGTGTGGCT 3’ TGGCAATAAAGGTCTTTGAGGG	87 bp
Dap4	*= Dlgap4, DLG Associated Protein 4*	5’ GGCCATGATCAACAGGTCCG 3’ CCTCTGCGGTTGTAGACTCG	97 bp
Dbn1	*Drebrin*	5’ CAGGTTTGAACAGGAACGGAT 3’ TGGTCACCAAAGATAGACTGCT	168 bp
Egr1	*Early Growth Response 1*	5’ CAGTCCCATCTACTCGGCTG 3’ TGTGGAAACAGATAGTCAGGGAT	180 bp
EpoR	*Erythropoietin Receptor*	5’ CTGAGTGTGTTCTGAGCAACC 3’ CACTCCAGAATCCGCTGAAG	96 bp
Erk1	*Extracellular signal-regulated kinase 1*	5’ TCCGCCATGAGAATGTTATAGGC 3’ GGTGGTGTTGATAAGCAGATTGG	248 bp
Gfap	*Glial fibrillary acidic protein*	5’ TTGCTGGAGGGCGAAGAAAA 3’ GCTTTTGCCCCCTCGGATCT	78 bp
Gphn	*Gephyrin*	5’ GGTGGGACTATATCGGCATACA 3’ CCCCGTTCCTCCAGTTGTTAATA	120 bp
Grin2a	*Glutamate [NMDA] receptor subunit epsilon-1, NMDAR2A*	5’ ACGTGACAGAACGCGAACTT 3’ TCAGTGCGGTTCATCAATAACG	100 bp
Grin2b	*Glutamate [NMDA] receptor subunit epsilon-2, NMDAR2B*	5’ CTGTCATGCTCAACATCATGGA 3’ GCGGATCTTGTTCACGAAGTC	98 bp
Grin2c	*Glutamate receptor, ionotropic, NMDA2C (epsilon 3)*	5’ GGGATCTGCCATAACGAGAAG 3’ GCACTGAGTGTCGAAGTTTCCA	157 bp
Hif-1α	*Hypoxia inducible factor 1, alpha subunit*	5’ CTGTTAGGCTGGGAAAAGTTAGG 3’ ACCTTCATCGGAAACTCCAAAG	228 bp
Hif-2α KO	*Hif-2α exon 2*	5' AGGAGACGGAGGTCTTCTATGA 3’ ACAGGAGCTTATGTGTCCGA	126 bp
Il1b	*Interleukin 1 Beta*	5’ TTCAGGCAGGCAGTATCACTC 3’ GAAGGTCCACGGGAAAGACAC	75 bp
Inhba	*Inhibin Subunit Beta A*	5’ GGGGAGAACGGGTATGTGGA 3’ CCTGACTCGGCAAAGGTGAT	104 bp

Junb	*Jun-B oncogene*	5’ TCACGACGACTCTTACGCAG 3’ CCTTGAGACCCCGATAGGGA	125 bp
Kif17	*Kinesin Family Member 17*	5’ ACAACGAGATCGCCTACCC 3’ AGTCCCTGCATGGTGAAAGAC	109 bp
Map2k1	*=Mek1, Mitogen-Activated Protein Kinase Kinase 1*	5’ GAGTGCAACTCCCCGTACATC 3’ TTCTCCCGAAGATAGGTCAGG	191 bp
Mbp	*Myelin Basic Protein*	5’ CCCCAGAGCTGGTGCTTTTA 3’ GAGAACTCCTGCAGTCCCAC	97 bp
Mmp9	*Matrix metallopeptidase 9*	5’ GCGTCGTGATCCCCACTTAC 3’ CAGGCCGAATAGGAGCGTC	88 bp
Nestin, control	Internal control	5’ CTAGGCCACAGAATTGAAAGATCT 3’ GTAGGTGGAAATTCTAGCATCATCC	324 bp
Nestin, transgene	*Cre* recombinase	5’ GCGGTCTGGCAGTAAAAACTATC 3’ GTGAAACAGCATTGCTGTCACTT	100 bp
Ngfr	*Nerve Growth Factor Receptor*	5’ TGCCGATGCTCCTATGGCTA 3’ CTGGGCACTCTTCACACACTG	133 bp
Nlgn1	*Neuroligin 1*	5’ GGAACGCCACTCAGTTTGCT 3’ TTGGACGTATGATGAAACCACAT	119 bp
Nrgn	*Neurogranin*	5’ TCCAAGCCAGACGACGATATT 3’ CACACTCTCCGCTCTTTATCTTC	127 bp
Ntf3	*Neurotrophin 3*	5’ GGAGTTTGCCGGAAGACTCTC 3’ GGGTGCTCTGGTAATTTTCCTTA	117 bp
Olig2	*Oligodendrocyte transcription factor 2*	5’ TCCCCAGAACCCGATGATCTT 3’ CGTGGACGAGGACACAGTC	90 bp
Oligo-dT’s		TTT TTT TTT TTT TTT	
Pcdh8	*Protocadherin 8*	5’ GTGAGGGATGTAAACGACCAC 3’ CGGCTAGGCGTACACTCTG	154 bp
Psd95	*= Dlg4, Discs Large MAGUK Scaffold Protein 4*	5’ TCCGGGAGGTGACCCATTC 3’ TTTCCGGCGCATGACGTAG	83 bp
ribProt	*Ribosomal protein S16*	5’ AGATGATCGAGCCGCGC 3’ GCTACCAGGGCCTTTGAGATGGA	163 bp
Rpl13a	*60S Ribosomal Protein*	5’ GACCACCATCCGCTTTTTCTT 3’ CTGTGAAGGCATCAACATTTCTG	250 bp
Snap25	*Synaptosomal nerve-associated protein 25*	5’ ATCCGCAGGGTAACAAATGATG 3’ CGGAGGTTTCCGATGATGC	83 bp
Syn1	*Synapsin 1*	5’ CCC AGC TCA ACA AAT CCC AGT 3’ TCA CCT CGT CCT GGC TAA GG	90 bp
Th	*Tyrosine hydroxylase*	5’ TCTCCTTGAGGGGTACAAAACC 3’ ACCTCGAAGCGCACAAAGT	151 bp
Vegf	*Vascular Endothelial Growth Factor A*	5’ ACTGGACCCTGGCTTTACTG 3’ ACTTGATCACTTCATGGGACTTCT	99 bp
Vegfr2	*Vascular endothelial growth factor receptor 2*	5’ TTCACAGTCGGGTTACAGGC 3’ TCTCACAATTCTTCGGCCCC	209 bp
Wnt7a	*Wnt family member 7A*	5’ GACAAATACAACGAGGCCGT 3’ GGCTGTCTTATTGCAGGCTC	207 bp

Primers were solved in Tris-EDTA to a stock concentration of 200 µM. As a final working concentration used in PCRs, stock primers were furthermore diluted 1:10 in Tris-EDTA to a concentration of 20 µM and stored at 4 °C. Primers were sufficient in a standard PCR with an annealing temperature of 60 °C, 30 cycles or in a qPCR with an annealing temperature of 60 °C, 40 cycles, unless stated otherwise.

2.1.8. Software

Table 2.8: Used software and its purpose.

Name and version	Purpose	Company/provider
Aperio ImageScope 12	Image processing	Leica
CFX Manager Software 3.1	qPCR data processing	Bio-Rad Laboratories, Inc.
EM Report 1.0	TEM images preview and converting	
Excel 2016	Data analysis	Microsoft
FIJI / ImageJ 1.53t	Image processing and analysis	Open source / public domain
FusionCapt	Western Blot detection	Vilber
GraphPad PRISM® 9	Statistics / Figure creation	GraphPad Software, Inc.
PowerPoint 2016	Figure creation	Microsoft
ZEN 3.1 blue edition	Fluorescence microscopy	Carl Zeiss Microscopy GmbH

2.2. Methods

2.2.1. Cell culture

All cell culture was performed with primary cells generated from WT or HIF-2α KO mice. Standard incubation took place at 37 °C and 5% CO_2 and ambient oxygen levels in a standard cell culture incubator.

For studying synapses and synapse-associated processes, a neuron-astrocyte co-culture was conducted, as astrocytes promote neuronal growth and survival through secretion of different factors. The protocol established for this study is based on Jones' *et al.* (2012) sandwich approach where astrocytes and neurons are spatially separated through plating them on individually compartments. This allows for the precise analysis of the different cell types without mixing of the culture. Due to lab-specific differences in for example laboratory equipment and the used mouse strain, the protocols differ slightly for instance in timing of the culture and media composition. A schematic overview of the procedure is depicted in Figure 2.1.

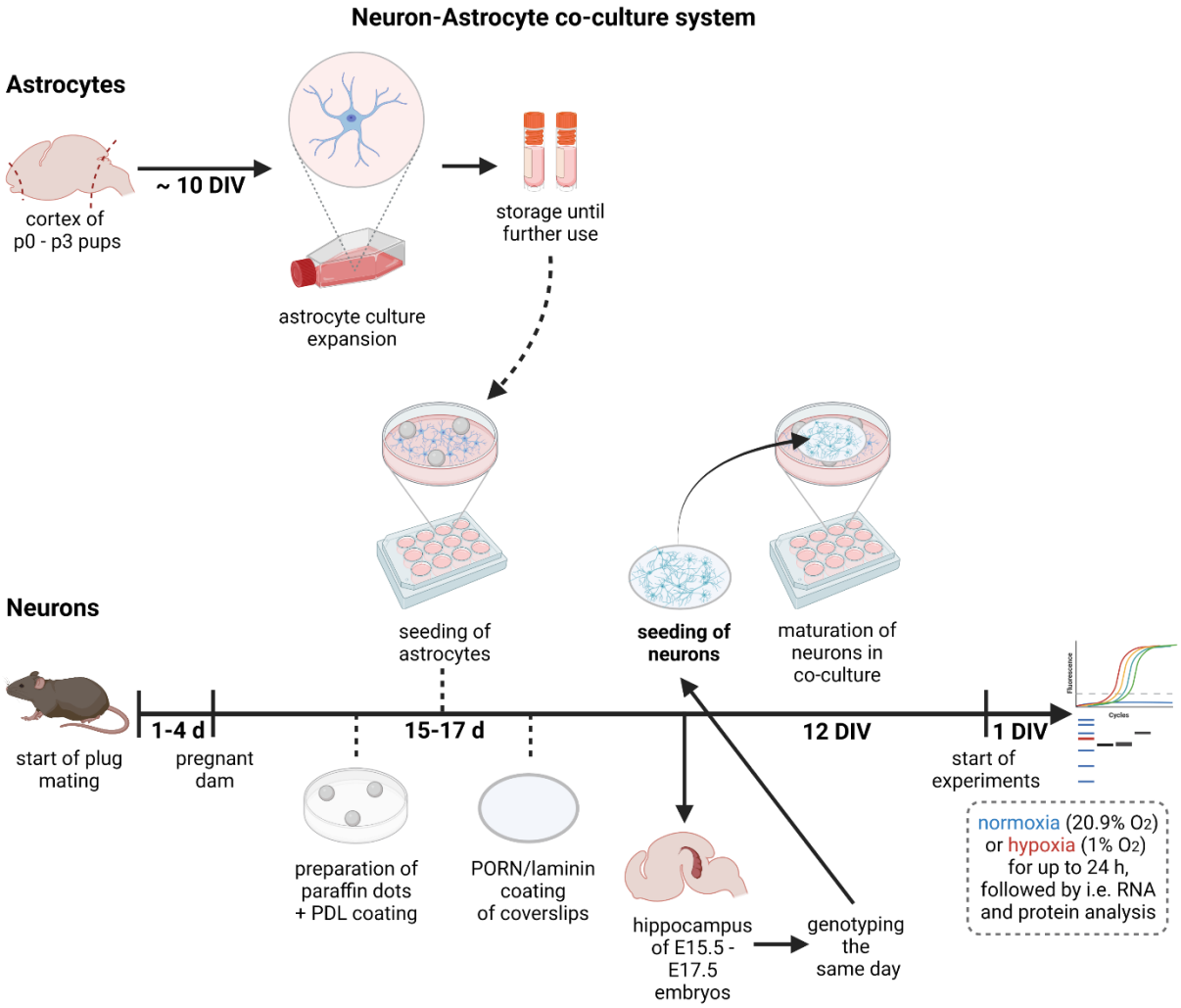

Figure 2.1: Schematic overview of the neuron-astrocyte co-culture system.

For the neuron-astrocyte co-culture, WT or HIF-2α KO cortical astrocytes that were obtained in advance were plated on PDL-coated 12-well plates provided with paraffin dots. Hippocampal WT or HIF-2α KO neurons freshly obtained from E15.5 – E17.5 embryos were plated on coated coverslips that were transferred on top of the astrocytes, with the paraffin dots serving as spacers. Neurons matured in this sandwich approach for 12 days in vitro (DIV) before starting of NOX/HOX experiments with following RNA and protein analysis. Figure created with BioRender.com.

2.2.1.1. Isolation and culture of cortical astrocytes

For convenient purposes, astrocytes were isolated in advance, stored at -80 °C and thawed when needed, which simplified the timing for the co-culture with neurons. For isolation of cortical astrocytes, p0 - p2 mouse pups were decapitated with sharp scissors and the head was opened. A piece of tail was taken for genotyping. The brain was carefully removed and put in cold MEM. The hemispheres were separated, the meninges removed and the cortices dissected with help of a stereo zoom microscope using fine forceps. Cortices of one pup each were transferred to a 2 ml tube containing cold MEM on ice and cut into small pieces using scissors.

Under a cell culture hood, excess MEM medium was carefully removed by pipetting and 1 ml digestion solution containing Papain enzyme was added. Digestion took place for 30 min at 37 °C in a water bath whilst occasionally flicking the tube. Afterwards, the digestion solution was carefully removed by pipetting and the digestion stopped by adding 1 ml of astrocyte culture medium on top. Tissue pieces were triturated carefully with 1000 µl tips until a homogenous suspension was obtained. The solution was transferred to a falcon tube provided with 10 ml of astrocyte culture medium and centrifuged for 5 min at 1000 rpm. The supernatant was removed and the cell pellet resuspended in 1 ml astrocyte culture medium. The cell suspension originated of each pup was finally transferred to an own T75 flask containing 11 ml of astrocyte culture medium. Cells were incubated under standard cell culture conditions. Three to four days after plating, the cells were washed with PBS to remove cell debris and provided with fresh medium. Half of the medium was changed every four to five days until a dense monolayer was reached after about ten days. As astrocytes display contact inhibition, incubation was extended for one or two more days until all flasks that were generated out of different pups were fully dense before the cells were stored at -80 °C.
Some publications mention an additional step of several hours of shaking off glia cells and oligodendrocytes of the astrocyte layer in order to improve purity of the culture. Here, preliminary experiments showed no overall improvement in purity and this step was therefore skipped in the protocol established for this study.

2.2.1.2. Freezing of cortical astrocytes

When the T75 flask containing astrocytes was completely confluent for up to three days, cells were collected and stored at -80 °C. For this, the culture medium was discarded and the cells washed once in 37 °C warm PBS. Cells were detached with 2 ml Trypsin at 37 °C for ~5 min until full detachment was achieved. The trypsinization process was stopped by addition of 8 ml culture medium and the cell suspension was transferred into a 15 ml tube. After centrifugation for 5 min at 1000 g and room temperature (RT), the supernatant was discarded and the cell pellet suspended in 3 ml of freezing medium. Then, the cell suspension was split to three cryo vials with 1 ml each and incubated on ice for 5 min for slow cooling of the cells. Cryo vials were then transferred to -80 °C in a polystyrene box overnight (ON) and then stored permanently at -80 °C in plastic boxes until further use.

2.2.1.3. Preparation of paraffin dots, PDL coating and seeding of cortical astrocytes for co-culture

Frozen astrocytes were thawed and plated out 7 – 8 days before isolation of neurons to reach a good confluence when starting the co-culture with neurons. Beforehand, wax dots were

prepared in 12-well plates that later served as spacers between the astrocytes in the 12-well plate and the neurons on coverslips on top.
For preparation of wax spacers, paraffin droplets were heated up in a glass beaker with a magnetic stir bar on a hot plate until the paraffin was completely melted. A 1 ml syringe provided with a 20G cannula was warmed up in the hot paraffin before taking up ~100 µl of the paraffin. Three paraffin dots of comparable size were placed in each well of the 12-well plate in a triangle form with adequate distance between dots and the wall of the well, so that a coverslip can later be placed on top. Before paraffin leftovers started to cool down in the syringe, it was placed back into the warm beaker and new paraffin was taken up. If the syringe was blocked by solid paraffin, a fresh syringe was prepared. For convenience, the preparation of paraffin dots was performed under non-sterile conditions. Subsequently, they were UV-radiated for 15 min in a cell culture bench for sterilization and afterwards wrapped in foil and stored at RT until needed.

One day or directly before thawing of astrocytes, the 12-well plates containing paraffin dots were coated with poly-D-lysine (PDL). For this, a 1 mg/ml PDL stock solution was diluted 1:100 to a 10 µg/ml working solution in sterile dH_2O. 450 µl PDL working solution per well were incubated at 37 °C for 1 – 2 h. Solution was aspirated and the wells washed 2x with sterile PBS for 5 min each. Afterwards, plates were completely dried and directly used or wrapped in parafilm and stored at 4 °C for up to one week.
Thawed astrocytes exhibiting the same genotype (so either WT or HIF-2α) originated from different pups were pooled and seeded out together. Thawing took place at 37 °C in a water bath until only a small frozen pellet was visible. Then, cells were quickly transferred into 15 ml falcon tubes containing 10 ml astrocyte culture medium. To remove DMSO, cells were centrifuged at 1000 rpm for 5 min and the pellet resuspended in 2 ml fresh medium. Cells were counted using a Neubauer advanced hemocytometer. If cell numbers were too low, additional aliquots of astrocytes were thawed and pooled with the other cells. 1 ml of astrocyte culture medium per well was pipetted to the PDL-coated 12-well plate containing the paraffin dots and 50000 astrocytes were seeded per well. When astrocytes were quite confluent, half of the medium was exchanged with fresh one.

2.2.1.4. PORN/laminin coating, isolation of hippocampal neurons and co-culture with astrocytes

Round coverslips (⌀ 18 mm) were steam sterilized and stored in glass bottles. Two days before isolation of neurons, the coverslips were prepared with a poly-L-ornithine hydrobromide (PORN)/laminin coating. For this, coverslips were transferred into 12-well plates. A PORN

stock solution of 0.5 mg/ml was diluted 1:33 in sterile PBS to a working solution of 15 µg/ml. Coverslips were coated with 400 µl of the PORN working solution for 5 h at 37 °C. Next, the solution was aspirated and the coverslips washed with sterile PBS 3x 5 min. A laminin stock solution of 250 µl/ml was diluted 1:50 in sterile PBS to a working solution of 5 µg/ml. Coverslips were coated with 400 µl of the laminin working solution ON at 37 °C. Next, the solution was aspirated and the coverslips washed with sterile PBS 3x 5 min. The coverslips were stored in PBS at 4 °C until isolation of neurons the next day.

WT and HIF-2α KO hippocampal neurons were extracted from E15.5 – E17.5 embryos. Three pairings were used for a timed pregnancy, with checking for vaginal plugs of the female mice by the animal caretakers for up to four days before the mating was ended. The occurrence of a plug was timed as E0.5. On the day of dissection, the dam that showed the clearest signs for pregnancy was used first and if enough embryos were present, the other mice were spared. For removal of embryos, the pregnant dam was quickly sacrificed by cervical dislocation, disinfected and the abdominal cavity opened with sharp scissors. The uterus containing the embryos was removed and placed in a 10 cm dish containing cold PBS on ice. For each embryo, the placenta was removed using small forceps and the embryo removed from the remaining sac. The embryo was decapitated and the head placed in a new dish containing cold PBS for washing. When all heads were collected, they were transferred into separate 6 cm dishes containing cold preparation medium (HBSS w/o calcium, magnesium and phenol red + 0.6% glucose) and stored on ice.
Using a stereo zoom dissecting microscope, the head of the embryo was anchored with forceps and the skin layer and skull pieces were carefully removed using second fine forceps and microdissection scissors. The forceps were carefully angled under the brain and the brain removed from the skull. The two hemispheres were separated from the midbrain and from each other. Remaining leftover tissue was transferred into 0.5 ml tubes containing 300 µl of 50 mM NaOH for genotyping. For both hemispheres, the meninges were removed using one forceps while the other one anchored the tissue. Caution was taken to not have the hippocampus attached to the meninges. After meninges were removed properly, the hippocampus was detached from the cortex by plucking with fine forceps. Hippocampi of both hemispheres were carefully transferred into a 2 ml tube with a hole in the lid and containing 500 µl of HibernateE medium. When hippocampi of all embryos were collected this way, the tubes were stored at 4 °C for the duration of a genotyping PCR (2.2.2.5). HibernateE is a CO_2-independent medium that can be used for storage of neuronal tissue under ambient CO_2 levels for up to 48 h without significant loss of cell viability.

During the tissue incubation for the following genotyping PCR, the astrocytes were prepared for the co-culture. For this, the astrocyte culture medium was aspirated and the cells washed once with sterile PBS. Then, 1.5 ml of neuronal culture medium was pipetted onto the astrocytes for preconditioning of the medium.

When the genotyping process was finished, the seeding of neurons continued. For this, the excess HibernateE medium was carefully removed with a 1000 µl pipette and the tissue digested with 1 ml digestion buffer containing Papain for 15 min at 37 °C in an incubator of water bath. Tubes were flicked occasionally to ensure that all tissue is in contact with the enzyme. In the meantime, 750 µl/well of the preconditioned astrocyte medium was transferred from the astrocytes to the 12-well plates containing the PORN/laminin-coated coverslips that were prepared in advance and stored at 37 °C in the incubator.
After the digestion process, the digestion buffer was carefully removed using a 1000 µl pipette and the tissue washed 2x with 1 ml neuronal culture medium + 1% FCS. Care was taken to avoid bubble formation and the tissue was allowed to set down between the washing steps. Finally, the hippocampi were triturated carefully in culture medium w/o FCS using a 1000 µl pipette until a homogenous cell suspension was achieved. Cells were counted using a Neubauer advanced hemocytometer and 40.000 neurons were plated per coverslip. Please note, that neurons of individual embryos were not pooled but seeded separately. Cells were thereby already plated in a scheme that fits to the planned experiment, so that i.e. for sample collection at different time points, these cells were all seeded on the same plate for collection of each RNA and protein samples in duplicates. Neurons were let to set down for 1 - 2 h at 37 °C. Finally, coverslips with the neurons facing upwards were transferred to the 12-well plates containing the astrocytes and wax spacers using forceps. The remaining 750 µl of preconditioned medium were also transferred back to the co-culture.

The neuron-astrocyte co-culture was maintained for 12 days before start of the experiments like NOX/HOX incubation. On day 4 and 7, the medium was partly changed (300 µl/well were taken out and 400 µl/well of fresh neuronal culture medium was provided). On day 4, the medium was furthermore provided with 5 µM cytosine ß-D-arabinofuranoside (AraC), a DNA replication inhibitor, to curb glial overgrowth. On day 11, a final change of medium took place (900 µl/well were taken out and 1000 µl of fresh neuronal culture medium was provided) before starting the experiment the next day.

2.2.2. Gene expression analysis

2.2.2.1. RNA isolation from hippocampal neurons (kit-extraction)

Before cell lysis, coverslips containing hippocampal neurons were transferred into a new well of a 12-well plate and washed with PBS once. This transfer allows the separate harvesting of the two different cell types of the co-culture (neurons and astrocytes). Neurons were then lysed in 350 µl GTC solution, scraped off the coverslip and transferred into a 2 ml tube. If cells had been incubated under hypoxic conditions, all lysis steps were performed in the hypoxic chamber. Tubes were collected on ice and stored at -20 °C until proceeding with RNA isolation. RNA was isolated using the NucleoSpin® RNA purification kit (Macherey-Nagel, user manual version June 2015 / Rev. 17) with omission of the DNAse step. Besides, because of low RNA yield, RNA was eluted twice in a total volume of 25 µl RNAse-free H_2O.

Concentration and purity of the isolated RNA was assessed by an Epoch™ Microplate Spectrophotometer using 2 µl of undiluted RNA sample. A 260 nm/280 nm absorption ratio of 1.7 - 2.2 was accepted as a good RNA quality. The RNA was then stored at -80 °C until further use.

2.2.2.2. RNA isolation from cortical astrocytes and tissue (phenol-chloroform-extraction)

Astrocytes were washed with PBS and lysed in 700 µl GTC solution. Cells were than scraped off the well and transferred into a 2 ml tube. If cells had been incubated under hypoxic conditions, all lysis steps were performed in the hypoxic chamber. Tubes were collected on ice and stored at -20 °C until proceeding with RNA isolation.

For brain tissue, the tissue stored at -80 °C was quickly transferred on ice. 350 µl ice-cold GTC solution was pipetted into the tube containing the tissue and the brain was then shredded using a Polytron homogenizer. Between each new tissue and as a final step, the homogenizer was washed two times in deionized H_2O and one time in DEPC-H_2O. Tissue lysates were collected on ice and centrifuged at 6000 rpm and 4 °C for 5 min. The supernatant containing the RNA was transferred into a new 2 ml tube and topped up with another 350 µl of GTC solution for a final volume of 700 µl. Samples were stored at -20 °C or were directly used for RNA isolation.

RNA of astrocytes or brain tissue was isolated by phenol-chloroform extraction. For this, after thawing at room temperature (RT), samples were acidified by adding 70 µl of 2 M sodium acetate (NaOAc), pH 4.0. Next, 500 µl phenol and 350 µl phenol:chloroform:isoamyl alcohol mixture was added and vortexed until a milky yellow suspension was formed. If this was not the case, 100 µl of additional phenol:chloroform:isoamyl alcohol mixture was added and the

suspension vortexed again. The mixture was incubated on ice for 60 min, followed by centrifugation at 13.200 rpm, 4 °C for 35 min for separation of the two phases. The upper aqueous phase containing the RNA was carefully transferred into a new 1.5 ml tube that was prepared with 600 µl isopropanol in advance. Samples were vortexed and stored at -20 °C ON. Next day, samples were directly centrifuged for 30 min at 13.200 rpm and 4 °C. The supernatant was discarded and the formed pellet air-dried for 60 min to evaporate remaining phenol. Next, 300 µl GTC solution and 500 µl isopropanol was added, samples vortexed and frozen away at -20 °C ON for precipitation of RNA.

Next day, samples were centrifuged for 30 min at 13.200 rpm and 4 °C. The supernatant was discarded and the pellet air-dried for 5 min. 500 µl 75% EtOH (in DEPC-H_2O) was added, the samples vortexed and incubated for 15 min at RT. After that, samples were centrifuged again for 30 min at 13.200 rpm and 4 °C. Supernatant was discarded and the pellet air-dried again for 60-90 min until completely dry.

As final step, the RNA pellet was dissolved in RNAse-free H_2O (13 µl for astrocytes, 40 µl for brain tissue) by vortexing and heating the solution for max. 10 min at 60 °C.

Concentration and purity of the isolated RNA was assessed by an Epoch™ Microplate Spectrophotometer using 2 µl of undiluted RNA sample. A 260 nm/280 nm absorption ratio of 1.7 - 2.2 was accepted as a good RNA quality. If RNA concentration of brain tissue was too high for proper measurement, RNA was further diluted in RNAse-free H_2O until a concentration of <1000 ng/µl was achieved. The RNA was then stored at -80 °C until further use.

2.2.2.3. Complementary DNA (cDNA) synthesis

For analysis of gene expression levels, obtained RNA samples need to be transcribed into complementary DNA (cDNA) with help of a reverse transcriptase.

Table 2.9: RNA mix for cDNA synthesis.

RNA mix components	Amount/volume per sample
RNA	
astrocytes	300 ng
neurons	300 ng
brain tissue (hippocampus)	400 ng
brain tissue (cortex)	800 ng
brain tissue (hemispheres, P3, P20, adult)	500 ng
Oligo-dT's	2.5 µl
dH_2O	Fill up to 12 µl total volume

First, equal amounts of total RNA were mixed with oligo-dT's and dH_2O (Table 2.9) and incubated at 68 °C for 10 minutes. If the sample concentration was too low to achieve the desired amounts of transcribed RNA, the highest possible volume of RNA (9.5 µl) was mixed with the oligo-dT's without further addition of dH_2O.

Table 2.10: Reaction mix for cDNA synthesis.

Reaction mix component	Volume per sample
M-MLV RT reaction buffer (5X)	5 µl
dNTPs (2.5 mM each, 10 mM in total)	5 µl
dH_2O	2.5 µl
M-MLV reverse transcriptase (200 u/µl)	0.5 µl

After 5 min of cooling down on ice, the RNA mix was then combined with 13 µl of the reaction mix (Table 2.10) and incubated in a thermal cycler using the following program (Table 2.11) for cDNA synthesis.

After completion of the program, the success of cDNA synthesis was verified by standard polymerase chain reaction (PCR, 2.2.2.4) for a housekeeping gene (= HKG, here: *ribosomal protein* or *Rpl13a*). The synthesized cDNA was then stored at 4 °C for short-term and subsequent use, or for long-term storage at -20 °C.

Table 2.11: Protocol for cDNA synthesis.

Temperature	Time	Step
45 °C	90 min	Accumulation of oligo-dT primers
52 °C	30 min	cDNA synthesis
95 °C	15 min	DNA denaturation

2.2.2.4. Polymerase chain reaction (PCR)

The polymerase chain reaction (PCR) is a method for exponential amplification of DNA by use of specific primers that flank the desired gene sequence to be amplified and a polymerase that synthesizes the complementary DNA during a series of cycles of different temperatures. With help of a PCR, even tiny amounts of template DNA can thereby be amplified and detected.

The PCR product can later be visualized in an agarose gel with help of DNA-intercalating dyes such as ethidium bromide.

Table 2.12: Reaction mix for PCR.

Component (stock concentration)	Volume per sample	Final concentration
GoTaq reaction buffer (5X)	5 µl	1x
dNTPs (2.5 mM each, 10 mM in total)	2 µl	0.2 mM each
5’ and 3’ primer (20 µM)	0.5 µl each	0.4 µM each
dH_2O	17 µl	
GoTaq G2 polymerase (5 U/µl)	0.05 µl	0.01 u/µl

For a PCR, 24.5 µl of reaction mix containing the polymerase, its reaction buffer, dNTPs and the gene specific primers, was mixed with 0.5 µl of template DNA (Table 2.12).

For each PCR, a negative control containing water instead of template DNA was furthermore added for verification of purity of the reagents.

Depending on the research question, different primers were used that are listed in 2.1.7. All PCRs were thereby carried out with an annealing temperature of 60 °C.
After mixing the DNA template with the PCR mix in a 0.2 ml PCR tube, samples were transferred into a thermal cycler and the PCR program depicted in Table 2.13 was run.

Table 2.13: Standard PCR program.

Temperature	Time	Step	
95 °C	3 min	Initial denaturation of DNA	
95 °C	60 sec	Denaturation of DNA	x30
60 °C	60 sec	Annealing of primers	
72 °C	60 sec	Elongation	
72 °C	10 min	Final elongation	

Then, 20 µl of the synthesized PCR product and an appropriate DNA ladder for comparison were separated by agarose gel electrophoresis according to its size in a 2% agarose gel containing 0.08% ethidium bromide. Run was carried out at 120 V for 20 min and the DNA visualized and compared to the DNA ladder using UV light in a gel documentation system.

Here, the standard PCR was mainly used for genotyping of mice, testing of specificity and annealing temperature of new primers and for verification of proper cDNA synthesis.

2.2.2.5. Genomic DNA (gDNA) isolation and genotyping PCR

For genotyping of mice, genomic DNA (gDNA) was extracted from tissue. For this, ear tissue of mice was used for both identification of the mice as well as tissue samples for gDNA isolation. The ear tissue was collected in tubes containing 300 µl of 50 mM NaOH and incubated at 95 °C, 400 rpm in a thermoshaker. Afterwards, 30 µl of 1 M Tris-HCl was added, samples mixed and spun at 11.000 rpm for 1 min. These pre-processed samples were used as templates in a genotyping PCR and stored long-term at 4 °C.

The genotyping PCR is a standard PCR (2.2.2.4) checking for the insertion of Cre recombinase by using two primer sets, one serving as internal control and one for checking of the transgene insertion. In contrary to PCRs using cDNA, for genotyping PCR 22.5 µl PCR reaction mix were combined with 2.5 µl gDNA. The internal control gives an amplicon of 324 bp size, the transgene with Cre recombinase insertion a product of 100 bp. The assay thereby does not distinguish hemizygous from homozygous transgenic animals.

2.2.2.6. Quantitative PCR (qPCR)

The quantitative PCR (qPCR) is an extension to a normal PCR where after each cycle of denaturation, annealing and elongation, a fluorescence signal is measured directly in real-time. The intensity of the signal is thereby dependent on the amount of DNA, making it possible to draw conclusions about the initial amount of target DNA in the sample. There are two common methods for detection of DNA: one is with help of sequence-specific reporter probes, the other one with help of unspecific fluorescent dyes that intercalate into double-stranded DNA. In this study, the second option is used.

By measuring cDNA content, which is directly linked to mRNA levels, it is possible to quantify levels of gene expression of a specific gene of interest in comparison to housekeeping genes that are used for normalization.

Table 2.14: Reaction mix for qPCR.

Component (stock concentration)	Volume per duplicate	Final concentration
Blue S´Green qPCR Mix (2x)	12 µl	1x
5' and 3' primer (20 µM)	0.5 µl each	0.42 µM
Deionized H_2O	11 µl	

For each qPCR, 9.5 µl of qPCR reaction mix were combined with 0.5 µl of cDNA sample in a 96-well PCR plate in technical duplicates. The qPCR reaction mix was pipetted according to Table 2.14. Furthermore, a non-template negative control with dH_2O instead of cDNA was pipetted.

The plate was firmly sealed, vortexed and centrifuged at 1000 g for up to 1 min, before starting the qPCR program depicted in Table 2.15 on the CFX96™ Real-Time System from Bio-Rad. Melting curve analysis was performed to assess the specificity of amplification.

Table 2.15: qPCR program.

Temperature	Time	Step	
95 °C	2 min	Initial denaturation	
95 °C	5 sec	Denaturation	x40
60 °C	30 sec	Annealing / Elongation	
		Plate read	
65 °C - 95 °C (+ 1 °C inc.)	5 sec/step	Melting curve analysis	

For analysis of qPCR results, the 2^-ΔCt (cycle of threshold) method was used. The automatically calculated thresholds of the CFX manager software were manually changed to

300, as depending on the set-up, different genes were on one plate or samples of different plates were combined in the following analysis. The Ct values of the genes of interest were normalized to a constitutively expressed housekeeping gene (*rP* or *Rpl13a*) as reference.
As samples from the NOX/HOX experiments were generated in duplicates, these values were averaged. Experimental data from different experiments were pooled and the fold change values of treated groups were calculated and compared to control groups that were internally normalized to a fold change of 1.

2.2.2.7. RT² Profiler™ PCR Array

Qiagen RT^2 Profiler™ PCR arrays are designed for the rapid analysis of gene expression of a focused panel of genes related to different research topics or pathways in 96-well or 384-well format. First, the RNA needs to be transcribed into cDNA using the RT^2 First Strand Kit that is optimized for subsequent use with the Profiler™ PCR Array. For the environmental enrichment study, a total of 1000 ng of pooled RNA of either WT or HIF-2α KO mice was transcribed into cDNA according to the protocol provided For the brain development study, a total of 500 ng of pooled RNA of either three WT or three HIF-2α KO mice was further processed.
Next, the array for *Mouse Synaptic Plasticity* was performed for WT and HIF-2α KO samples in a specific qPCR according to the protocol provided. Plates were thereby covered with the commonly used adhesive film and not the caps provided with the kit.
Analysis took place via the Qiagen Data Analysis online tool according to the handbook *RT2ProfilerDataAnalysisHandbook v3.5.* The automatic normalization method from HKG panel was chosen together with a Ct cut-off at <37.

2.2.3. Immunocytochemistry

Immunocytochemistry is an antibody-based staining technique for the detection and localization of specific proteins or other antigens in cell cultured or individually obtained cells. A target-specific primary antibody is either directly labelled with a fluorophore or reporter enzyme, or detected by a secondary, species-specific antibody that binds to the primary antibody.
For visualization by fluorescence microscopy, cells were seeded on glass coverslips and grown to confluence under standard incubation conditions. For immunocytochemistry of intracellular proteins, cells were then fixed prior to staining. For this, medium was removed and the cells washed twice with PBS. Cells were fixed in 4% ROTI®Histofix for 10 min and then washed two times in PBT1. As for intracellular staining the antibodies need to enter the cells, cells were then permeabilized using 0.3% Triton X-100 in PBS for 10 min at RT, followed by a wash step in PBT1. Then, unspecific binding was blocked with 10% normal goat serum (NGS)

in PBT1 for 60 min at RT. Without washing, cells were then incubated with the respective primary antibody (Table 2.6) diluted in PBT1 + 1:200 NGS at 4 °C ON. The next day, primary antibody was washed off two times with PBS/A. Next, secondary antibody (diluted in PBT1 + 1:200 NGS) incubation took place for 1 h at RT in the dark. Secondary antibody was then washed off two times with PBS. For staining of nuclei, cells were incubated in DAPI (1:10000 in PBS) for 5 min at RT. After two additional washing steps with PBS, coverslips were finally embedded upside-down in Mowiol on object slides and dried ON in the dark. For long-term storage, object slides were stored at 4 °C in the dark.

2.2.4. Protein analysis

2.2.4.1. Cell lysis and protein extraction

Before cell lysis, coverslips containing hippocampal neurons were transferred into a new well of a 12-well plate and washed once with ice-cold PBS. This transfer allows the independent harvesting of the two different cell types of the co-culture. Astrocytes were washed with ice-cold PBS as well. Neurons and astrocytes were then lysed independently in 65 µl protein lysis buffer, scraped off the coverslip and transferred into a 1.5 ml tube. If cells had been incubated under hypoxic conditions, all lysis steps were performed in the hypoxic chamber on a cold plate for minimizing protein degradation. Tubes were collected on ice and incubated for 20 min, followed by 5 min of centrifugation at 5000 rpm, 4 °C to spin down the cellular debris. The supernatant containing the proteins was transferred into a new 1.5 ml tube and 5 µl were taken into another tube for measuring total protein content of the respective sample. Protein samples were stored at -80 °C.

2.2.4.2. Protein concentration analysis

In order to load and evaluate equal amounts of protein in Western Blot analysis, quantification of total protein content in the samples was performed with the DC protein colorimetric assay from BioRad. This modified method is based on the Lowry method and depends on a copper-based Biuret reaction resulting in a purple-blue color formation that directly correlates with the protein content of the sample. For comparison of protein amounts, a bovine serum albumin (BSA) standard series ranging from 0.1 mg/µl to 25 mg/µl was used. 5 µl of BSA standard and protein sample were diluted 1:10 in dH_2O and pipetted in duplets into a 96-well flat bottom plate. For blanking, dH_2O was used. 10 µl reagent A and 75 µl reagent B were pipetted on top and incubated for 5 min at RT with occasional shaking of the plate. Finally, the absorbance was measured on an Epoch™ Microplate Spectrophotometer at 700 nm and protein concentrations were calculated using the BSA standard as reference.

2.2.4.3. SDS-PAGE and Western Blotting

Western Blotting is an immunological method for protein analysis in order to detect specific proteins of interest in a sample or tissue with help of specific antibodies. For this, protein lysates first need to be separated according to their molecular weights by a sodium dodecyl sulfate-polyacrylamide gel electrophoresis (SDS-PAGE), followed by transfer of the separated proteins to a nitrocellulose or polyvinylidene fluoride (PVFD) membrane where then specific antigen-antibody interactions take place and can be visualized.

Here, 20 µg-30 µg total protein lysate was mixed 1:4 with 4x sodium dodecyl sulfate (SDS) buffer and heated up to 95 °C for 10 min for denaturation. After a quick centrifugation, samples and 10 µl of protein ladder were loaded onto a 1.5 mm thick polyacrylamide gel containing 15 pockets. A discontinuous SDS-PAGE system was used consisting of a 7.5% separating gel with a 5% stacking gel on top. For the exact gel composition, see Table 2.16.

Table 2.16: Composition of stacking and separation gel of a SDS-PAGE.

Component	Stacking gel (5%)	Separation gel (7.5%)
Acrylamide/Bis solution, 30%	0.83 ml	2.5 ml
4x Upper buffer, pH 8.8	1.25 ml	-
4x Lower buffer, pH 6.8	-	2.5 ml
dH_2O	2.92 ml	5 ml
APS, 10%	50 µl	100 µl
TEMED	5 µl	10 µl

The aperture was filled up with running buffer and the SDS-PAGE was performed at 80 V until the dye front of the 4x SDS buffer reached the end of the gel.

Next, the proteins were transferred to a PVDF membrane using a semi-dry Western Blotting approach following the protocol from Bio-Rad (Trans-Blot® Turbo™ Transfer System). First, the membrane was activated in EtOH for 1 min and, together with the blotting paper, soaked in transfer buffer. For the transfer, three layers of blotting paper, the PVDF membrane, the gel containing the samples and three layers of blotting paper were placed as a sandwich into the Western Blot cassette of the transfer device and remaining air bubbles squeezed out. The transfer was carried out using the default program for one 1.5 mm gel per cassette (10 min, 1.3 V), followed by a cooling phase at 4 °C for 10 min. For large proteins of interest, another transfer phase of 6 min, 1.3 V followed.

Afterwards, the membrane was incubated in blocking solution (5% skimmed milk in TBS-T) for 1 h at RT to minimize unspecific binding of primary antibodies. In order to detect antibodies of different molecular weights simultaneously, the membrane was then cut horizontally with a sharp scalpel into smaller fragments. The location of the cut thereby depends on the molecular weight of the proteins of interest and should be at a sufficient distance to any possible antibody signal. Next, primary antibodies (Table 2.5) were diluted in blocking solution and the membrane parts incubated ON at 4 °C while shaking.

The day after, the membrane parts were washed 3x 5 min in TBS-T, followed by incubation with the respective secondary antibody for 1 h at RT while shaking. All secondary antibodies were diluted 1:10000 in blocking solution. Next, membranes were washed again 3x 5 min in TBS-T. Finally, the membrane parts were developed in SuperSignal™ West Femto Maximum Sensitivity Substrate for 2 min and the chemiluminescence of the bound secondary antibody detected using a FusionFX7 machine.
Signal intensities of target bands were assessed with FIJI software and normalized in relation to a housekeeping gene for semi-quantitative quantification.
If necessary, membranes were washed 3x 5 min in TBS-T afterwards and antibodies stripped off the membrane by 30 min incubation in stripping buffer, followed by another 3x 5 min wash in TBS-T. After blocking again for 1 h at RT while shaking, incubation with another primary antibody may take place according to the same protocol. This may be an option if two proteins of interest have a similar molecular weight but should be evaluated on the same membrane.
For storage, membranes were put in plastic, wrapped in aluminum foil and stored at -20 °C.

For semi-quantification of proteins, the intensity values of the protein bands of the protein of interest and the HKG were quantified using FIJI/ImageJ's gel analysis tool. Then, the lane normalization factor for each sample was calculated as the observed signal of the HKG for the corresponding lane divided by the highest observed HGK signal on the blot. With this factor, the signals of the target proteins were normalized as the intensity of the each sample divided by its corresponding lane normalization factor. With these resulting normalized values further calculations and quantifications took place according to the experimental design and research question.

2.2.5. Transmission electron microscopy analysis

2.2.5.1. Perfusion, fixation, cutting and embedding of brain tissue

Transmission electron microscopy (TEM) can be used to visualize specimens at a very high magnification by use of a high voltage electron beam. In contrast to standard light microscopy, the wavelength of an electron can be much shorter than of visible light and thereby electron microscopy can be used for magnifications up to 2.000.000x with a very high resolution of up to 0.1 nm. This allows the visualization of very small structures inside a cell, for example mitochondria or synapses.
For standard TEM, the samples like tissue specimens need to undergo a specific preparation protocol for generation of ultrathin slices, including trans-cardiac perfusion of the mouse.
For this, the final fixation solution containing 2.5% glutaraldehyde, provided by the Imaging Center Essen (IMCES), was prepared under a fume hood according to the IMCES protocol

and stored on ice. A perfusor was prepared with a 20 ml syringe + butterfly containing the fixation solution. Next, the mouse was slowly narcotized by isoflurane with help of an anesthetic machine, kindly provided by AG Ferenz, with an O_2 flow rate of 4 l/min and isoflurane dosage of 4 vol% and finally overdosed with isoflurane for euthanasia. The mouse was pinned on polystyrene, disinfected, the chest opened, the right heart ventricle cut open and the left ventricle perfused with around 10 ml of the fixation solution at a flow rate of 5 ml/min, until all blood was washed out. After fixation, the mouse was decapitated and the whole brain removed and transferred into a dish containing fixation solution. The bulb and cerebellum were removed and the hemispheres separated. Two millimeter of the upper cortex were cut away with a sharp scalpel for generation of a cutting edge for later orientation and the hemispheres were transferred into separate falcon tubes containing fixation solution.
For blinded analysis, at this time-point, the samples were pseudonymized by random labeling with numbers instead of mice name and genotype. The samples were transferred to the IMCES electron microscopy unit and stored at 4 °C until further processing the next day.

IMCES staff performed further fixation, staining, embedding and cutting processes.
Briefly, samples were directly glued with liquid glue onto plates in sagittal orientation for vibratome sectioning of 200 µm thick slices. Slices were collected in 12-well plates and three sections per sample were identified where the hippocampus and dentate gyrus were clearly visible. Similar sections for all samples/hemispheres were chosen. Out of this slices, a smaller part containing the region of interest (hippocampus) was cut out with a sharp scalpel. These probes were further osmium stained and embedded in Epon by IMCES staff according to their standard protocols.

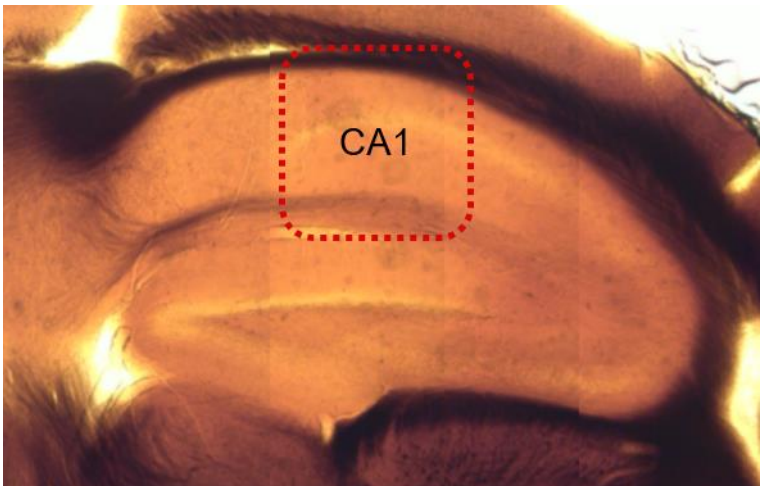

Figure 2.2: Region of interest for electron microscopy analysis.
The Stratum radiatum of the CA1 region of the hippocampus was chosen for EM analysis. Before ultra-thin sectioning, the Osmium stained and Epon embedded sections were further cut to the area and size depicted by the red square.

Before generation of ultra-thin slices, the samples were further cut down to the CA1 region of the hippocampus containing the Stratum radiatum region of interest, as depicted in Figure 2.2. Then, 200 nm and 60 nm ultra-thin sections were cut with a diamond blade on an ultra-microtome and placed onto TEM copper grids. Partly, slices also underwent post-contrastation for better imaging with the electron microscope.

2.2.5.2. Image acquisition

Post-contrasted, 60 nm thick slices were imaged with the transmission electron microscope JEOL 1400plus, a TVIPS TemCam-F416 CMOS camera and the EM-Menu 4.0 extended software at an acceleration voltage of 120 kV.

First, the nucleus layer of the Stratum pyramidalis was searched and based on that the Stratum radiatum identified. Images were acquired around one comb away from the nucleus layer inside the Stratum radiatum. Four overview images were taken at 250x magnification for each mouse and the position saved in the software. Then, three more detailed images at 2000x magnification in each of the 250x images were created and the position saved. Finally, six images in each of the 2000x images were taken at a final magnification of 12000x while carefully avoiding same areas. A report .pdf was generated with the EM Report 1.0 software to get a visual overview of all acquired images and the specifications like name, magnification, exposure time and scale bar for each image in one document.

2.2.5.3. Image analysis

Images were acquired as 16-bit TIFF format and batch-converted into 8-bit format via ImageJ/FIJI software. Brightness and contrast was auto-adjusted for better visualization of the synapses and saved as new images.

For analysis of synapses, different parameters were chosen. In general, only synapses that showed a clear pre-synaptic compartment containing synaptic vesicles, dendritic cleft and post-synaptic compartment were analyzed. The post-synaptic density (PSD) was analyzed at 12.000x magnification for length of the PSD/synaptic cleft contact zone as well as area of the PSD. For this, the contact zone of the PSD was measured with the freehand line tool and saved in the ROI manager, followed by encircling the whole PSD with the freehand selection tool and saving it in the ROI manager. This was performed for all properly oriented synapses for each image. Finally, length and area were assessed by the “measure” command in the ROI manager and data exported to Excel for analysis and quantification.

Additionally to the PSD, the width of the synaptic cleft was measured. For this, for each synapse, the width was measured at three different points using the straight line tool and saved in the ROI manager. Data was exported to Excel for analysis. Triplicates were thereby averaged. Labeled synapses were saved in an image overlay to enable backtracking of the data.

The overall abundance of synapses as well as the appearance of multiple-spine or perforated synapses was assessed with the images at 2000x magnification. Multiple-spine synapses exhibit two or more dendrites at the same pre-synaptic vesicle pool, whereas perforated synapses show two or more separated PSDs of the same post-synapse, reaching to the same

pre-synaptic vesicle pool. For analysis, in each image, five 5x5 squares were extracted (one in each corner and one in the middle) and saved as new images labeled with -1, -2, -3, -4 and -5 to have smaller sections for analysis. For each of these squares, the overall abundance of synapses, the amount of perforated synapses and the amount of multiple-spine synapses were counted using the multi-point tool. The numbers were copied to Excel for data analysis.
At the end of all analyses, samples were de-anonymized and results pooled according to their genotype.

2.2.6. Environmental enrichment study

An environmental enrichment (EE) study was conducted to enhance neurogenesis and synaptic plasticity in WT and HIF-2α KO mice, in comparison to their standard housed littermates (depicted in Figure 2.3).

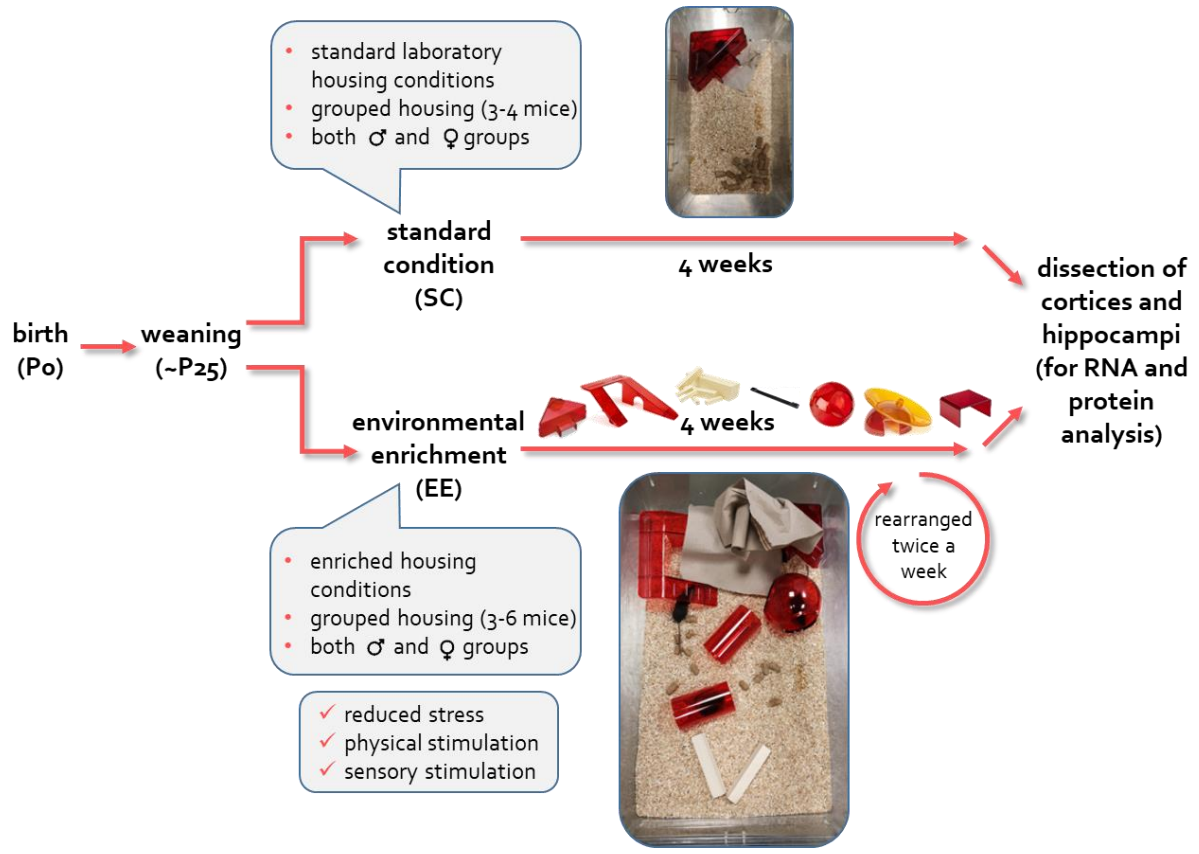

Figure 2.3: Environmental enrichment study design.

For enhancement of neuro- and synaptogenesis, one weaned group of WT and HIF-2α KO mice was housed under environmentally enriched (EE) conditions, where the mice are provided with different toys and objects in enlarged cages. The control group was housed under standard housing conditions (SC). After four weeks of housing, the cortices and hippocampi were dissected for RNA and protein analysis.

Our protocol was adapted from Novkovic and colleagues (2015) where a variety of different tools and toys was placed in enlarged cages of group-housed mice and changed on a regular basis to provide new stimulation for four weeks in total. Enriched and standard housing groups

were separated according to their gender and the study was started after weaning of the mice around 25 days (d) of age. For each housing condition, both female and male groups were used. Mice were further on housed in two groups of 3-6 mice (depending on litter size and gender distribution). One group stayed under standard housing conditions (SC) in standard cages with nesting material and a small house provided. Cages were changed regularly by animal caretakes and food and water was provided *ad libitum*. The second, enriched group was housed in larger T4 rat cages. For keeping both groups in the same room, the T4 cages were thereby not connected to the HEPA-filtered air flow system but stayed under normal room air and were exchanged and cleaned if necessary. The cages were provided with the same bedding, housing and food as the standard group. In addition, the enriched group was provided with different toys and objects that were exchanged and rearranged two times a week over a course of four weeks. Toys and objects were cleaned frequently with water during the course of the experiment as well as autoclaved at the end of the experiment.

For changing the objects, mice were transferred into a standard cage while the T4 cage was newly equipped. For each independent experiment, the objects and toys were exchanged in the same manner according to the following scheme:

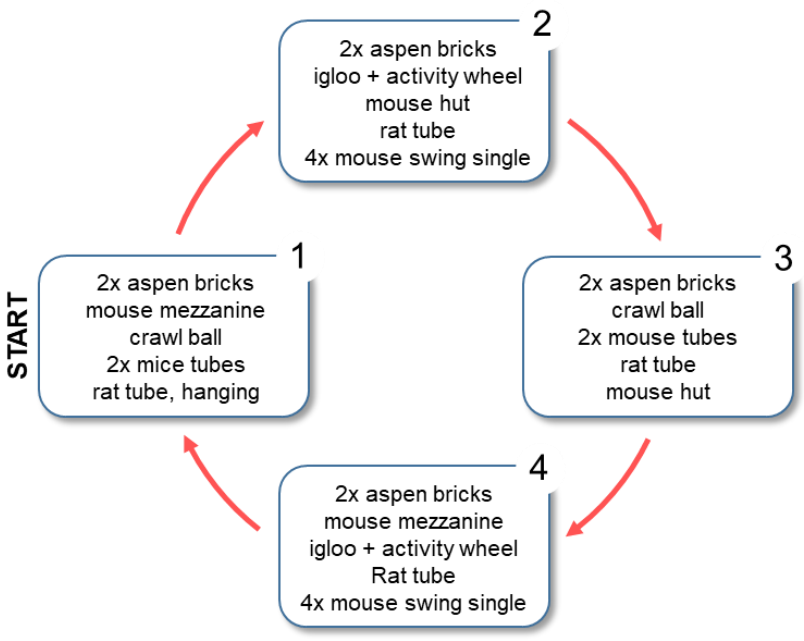

Figure 2.4: Scheme of cage equipment for environmental enrichment. WT and HIF-2α KO mice were housed for four weeks under enriched conditions. For this, cages were provided with different toys and objects that were rearranged twice a week in a specific manner. After two weeks, the arrangement was repeated.

Four altered arrangements of objects and toys were used that were changed twice a week, therefore after two weeks, the whole course was repeated starting with arrangement 1.

After four weeks, the brains of the mice of the standard and enriched housing were dissected and cortices and hippocampus used for further RNA and protein analysis. At this point of time, mice were furthermore genotyped.

2.2.7. Brain tissue analysis

2.2.7.1. Dissection of brain hemispheres, cortices and hippocampi

For analysis of brain and hippocampus development *in vivo*, the brains of mice of different age were dissected. P3 mice were thereby sacrificed by decapitation, P20 and adult mice by cervical dislocation. The skull was opened and the whole brain carefully removed. The brain was washed in PBS briefly and cut in half along the hemispheres with a sharp scalpel. One part of the brain was transferred into a plastic cassette or Falcon tube for organ fixation. The other half of the brain was transferred into a 2 ml tube, put into liquid nitrogen for shock freezing and stored at -80 °C until further processing for RNA analysis.

For the environmental enrichment study, mice were sacrificed by cervical dislocation. The head was cut off with large scissors and the skull opened. The whole brain was carefully removed, submerged briefly in Hank's balanced salt solution (HBSS, without calcium and magnesium) and transferred into a 60 mm petri dish containing ice-cold HBSS. The brain hemispheres were separated using a scalpel and after removal of the midbrain, the cortices and hippocampi of both hemispheres were dissected under a stereo zoom microscope using fine forceps. If possible, meninges were removed. The cortices and hippocampi were transferred into 2 ml tubes and put into liquid nitrogen for shock freezing. Tissue was then stored at -80 °C until further processing for RNA and protein analysis.

2.2.7.2. Shredding of brain tissue for RNA and protein analysis

Organs and tissue were stored at -80 °C in 2 ml tubes. For further processing of brain tissue for RNA analysis, the organs were put on ice and 350 µl 4 M GTC solution was pipetted directly on top. Organs were then shredded using a tissue homogenizer until the organ was fully disintegrated. The homogenizer was washed 2x with deionized H_2O and 1x with DEPC-H_2O before and in-between sample processing. The lysate was put back on ice for 10 min and then centrifuged for 5 min at 5000 rpm. The supernatant of the lysate was transferred into a new 2 ml tube and was either stored at -20 °C or the RNA was directly isolated using phenol-chloroform extraction.

For protein analysis, samples were processed as for RNA analysis with following differences: samples were processed in 200 µl protein lysis buffer instead of 4 M GTC solution and the homogenizer was washed 3x in deionized H_2O instead of DEPC-H_2O.

After centrifugation and transfer of the supernatant, 5 µl of the protein lysate was used for determination of protein concentration and the final lysates were stored at -80 °C until further use.

2.2.7.3. Tissue fixation, dehydration and embedding

For (immune-)cytochemistry, organs or tissue need to be dehydrated and embedded in paraffin wax for sectioning with a microtome.

Table 2.17: Protocol for tissue sample dehydration.

Solution	Time
70% EtOH	50 min
96% EtOH	50 min
96% EtOH	50 min
100% EtOH	50 min
100% EtOH	60 min
Xylol	40 min
Xylol	40 min
Xylol	40 min
Paraffin wax	70 min at 58 °C
Paraffin wax	150 min at 62 °C

First, organs and tissue need to be fixed to preserve them from decay and autolysis. Brain tissue was immersed in 4% formaldehyde at 4 °C for one to four days depending on the tissue size. After fixation, the tissue was dehydrated in increasing concentrations of EtOH to enable embedding with paraffin, which is water-insoluble. Before embedding, the alcohol was cleared by Xylol incubation, which was then replaced by the molten paraffin. Table 2.17 depicts the exact incubation times used in an automated dehydration machine. Samples were then stored at room temperature or directly transferred to the embedding station to obtain blocks for tissue sectioning. During the embedding process, the sample tissue or organ is surrounded by an embedding medium, here molten paraffin, using a stainless steel mold of appropriate size with plastic cover. On a cold plate, the paraffin solidifies, thereby giving stability to the tissue and allowing for sectioning with a microtome. The brain hemispheres were oriented with the cut surface facing downwards, resulting in sagittal sections beginning in the middle of the brain. Sample blocks were stored at RT.

2.2.7.4. Tissue cutting and serial sectioning

For morphometrically analyses of hemispheres of P3, P20 and adult WT and KO mice, serial sectioning was performed to make sure that the later analyzed areas are in similar sections of the brain and therefore comparable. First, new blocks were trimmed on a rotary microtome connected with a tissue flotation bath in 20 µm steps until the hippocampus became apparent. Then, samples were cut into 5 µm thick slices in ribbons of six. For mounting, slices were first carefully transferred into the 60 °C hot flotation bath where the slices stretched for around 30 sec until most wrinkles in the tissue disappeared. Then, pairs of two were mounted onto SUPERFROST PLUS objects slides while taking care of the exact order of the slices. Before starting with the next ribbon, 2 x 20 µm trimming took place. In addition, the first slice of each newly started ribbon had to be discarded due to compression of the tissue. Objects slides were numbered in ascending order and trimming between slides marked with a “+”. Tissue was cut like this until the hippocampus started to appear in the lower area of the hemisphere as well.

Slides were dried ON and stored at RT. For following Nissl staining and analysis of morphometrical parameters of the hippocampus, slides of the serial sectioning were taken that exhibited a similar area of the brain, starting with the ribbon where the midbrain is not visible for the first time. Then, a slide from each ribbon was taken until that slide where the hippocampus is not visible anymore. This resulted in 6-8 slides for P3 mice and 8-12 slides for P20 and adult mice with 200 µm distance in between that were Nissl stained and analyzed.

2.2.7.5. Nissl staining

Nissl staining is a histological staining technique based on binding of specific basic dyes like Cresyl violet or Toluidine blue to negatively charged RNA or DNA. It is mainly used in neurosciences for staining of neuronal structures, especially the nucleus and rough endoplasmic reticulum (= Nissl substance) of the neuronal bodies.

For Nissl staining of brain tissue, all incubation steps were performed at RT. Slides were first incubated for 10 min in Xylol , followed by 5 min incubation in a second Xylol bath for extraction of the paraffin. Next, a descending alcohol series was used for hydrophylization of the tissue, which is 5 min 100% EtOH, 3 min 90% EtOH, 3 min 70% EtOH, followed by a short dip in deionized H_2O. Then, samples were incubated for 3 min in 0.1% Cresyl violet solution and staining was stopped by rinsing the slides thoroughly in deionized H_2O. Differentiation of the staining was performed for 1 min in 200 ml 90% EtOH + two drops of pure acetic acid out of a 1000 µl pipette. Tissue was dehydrated by 2 min incubation in 90% EtOH without acetic acid, followed by 2 min incubation in 100% EtOH. Slides were finally incubated in two different Xylol baths for 5 min each before they were covered with a coverslip, using Entellan as mounting medium. After drying ON, slides were scanned with an Aperio ScanScope® CS2 at 20x magnification.

2.2.7.6. Analysis of hippocampal tissue

Nissl-stained brain tissue of three different age cohorts (P3, P20 and adult) of WT and HIF-2α KO mice was analyzed for different parameters based on Li *et al.* (2021).

For analysis with FIJI, the .svs images were first converted to .stacked-tiff images using the Aperio ImageScope software. The hyperstack image was then reduced to a one RGB layer image and saved as standard .tiff.

First, an analysis of the general structure of the hippocampus over different serial sections was performed by contour analysis using FIJI. For this, the contour of the hippocampus was traced manually using the freehand selection tool and filled in with black color for better visualization.

The second analysis focused on the hippocampus in more detail. With the straight-line tool, the thickness of the cell layers of three different regions, namely CA1, CA3 and dentate gyrus

(DG) was measured in triplicates and averaged. Furthermore, with the rotated rectangle tool, a 150px x 150px square was laid into each region and the cell density/field of view (FOV) measured with the multi-point tool counting all cell nuclei. Due to the differentiation state of the hippocampal cells of P3 mice, the cell density count was not possible for this age cohort.
Please note that during the analysis the genotype stage of the respective sample remained unknown, thereby preventing a possible bias of the results.

2.2.8. Statistics

All statistical analysis was performed using GraphPad PRISM® 9. Data was tested for normal distribution by Anderson-Darling and D'Agostino-Pearson omnibus tests. If necessary, data underwent log-transformation (Y=log(Y)) to reach normality before further statistical analyses. Statistics was then implemented into the graph of the un-transformed data. For pairwise comparison with only one variable, like the electron microscopy analysis, the analysis of Nissl staining and the gene expression analysis of brain tissue of adult, P20 and P3 mice, an unpaired, two-tailed t-test was performed. A two-way ANOVA was applied to data sets with two independent categorical variables in the experimental set-up, combined with the recommended multiple-comparisons test (Tukey or Šidák correction). In case of the environmental enrichment analyses for gene expression and protein levels, a two-way ANOVA/main effects only model was used in combination with Tukey's multiple comparisons test. For the analysis of cell culture experiments, a mixed effects model, with matched values (rising from the same animal) stacked in subcolumns, was used in order to minimize effects of high intra-individual differences. This mixed model uses a compound symmetry covariance matrix and is fit using Restricted Maximum Likelihood (REML). In the absence of missing values, this method gives the same P values and multiple comparisons tests as repeated measures ANOVA. In the presence of missing values (missing completely at random), the results can be interpreted like repeated measures ANOVA. A full model with a Geisser-Greenhouse correction was used, followed by multiple comparisons analysis for time of hypoxia and genotype with the appropriate test (Dunnett, Tukey or Šidák correction). For a more specific analysis on effects of genotypes, cell types were pooled according to their identical genotype and analyzed in a separate mixed effects model to test for either effects of the genotype of the respective cell population or if the genotype of the other co-cultured cell type had an influence. All data is shown as mean ±/ or + standard deviation (SD) as indicated in the figure legends. P-values < 0.05 are considered statistically significant with $p < 0.05$ = */#, $p < 0.01$ = **/##, $p < 0.001$ = ***/### and $p < 0.0001$ = ****/####. Asterisks (*) are used for comparison between genotypes, hashs (#) for comparison of the same genotype between different experimental conditions.

3. RESULTS

3.1. Functions of cerebral HIF-2α in vivo

3.1.1. Brain development and synapse formation in WT and HIF-2α KO mice

Numerous studies showed that brain development of mice and other rodents is not completed with birth but continues at postnatal stages, thereby showing differences depending on the specific brain area. Brain morphology, differentiation or maturation of specific cell types and gene expression profiles are constantly changing until brain development reaches a steady-state in adulthood (for reviews, see Chen *et al.*, 2017; Dillman and Cookson, 2014; Semple *et al.*, 2013; Thion and Garel, 2017). Leu *et al*. (2021) showed in an in vitro model using murine neurospheres and oxygen-glucose deprivation (OGD) positive effects of HIF-2α on neural differentiation and cell migration and that even under normoxic conditions, migration is restricted in HIF-2α KO cells, indicating a potential role for HIF-2α in brain development. This was in line with the previous work from Kleszka *et al.* (2020) showing an effect on neuronal development and synapse-associated processes in vivo.

The study presented here therefore aimed to investigate the effect of HIF-2α on different developmental stages of the brain of WT and HIF-2α KO mice.

For this, brain tissue of three days old (P3), twenty days old (P20) and adult (> 8 weeks) mice was collected and used for gene expression and histological analyses. P3 was chosen as a time-point of an early developmental stage where, amongst others, cortical and hippocampal synaptogenesis and synapse formation is about to accelerate, while neurogenesis is decreasing. Synaptic maturation and cell myelination peaks around P20, thereby choosing this time-point as a state of synaptic development after activation of sensory inputs (opening of eyes, interacting with the environment), followed by reduced synaptic density levels in adult animals due to synaptic pruning (Lohmann and Kessels, 2014; Thion and Garel, 2017).

3.1.1.1. Morphological analysis of the hippocampus of P3, P20 and adult WT and HIF-2α KO mice

Kleszka *et al.* (2020) previously reported a loss of pyramidal neurons and reduced thickness of the retrosplenial cortex layer in adult HIF-2α KO mice and reduced gene expression levels of genes associated to synapse formation and function. They furthermore found behavioral deficits of the HIF-2α KO animals in for example the back/white box test and Novel Object Recognition test. While their study mainly focused on cortical analyses on these mice, not much is known about effects of HIF-2α on the hippocampus, although the hippocampus is important for learning and memory and resembles a very synapse-dense region that can be

used as a study system of synaptic transmission and plasticity through for example electrophysiological measurements. Furthermore, hippocampal neurons resemble a convenient in vitro cell culture system for studying neurological processes.
As the focus of the presented study is to investigate a potential role of HIF-2α in synaptic transmission, here the morphology of the hippocampus of P3, P20 and adult WT and HIF-2α KO mice was assessed. For this, serial sections of the brain were Nissl-stained and analyzed for different morphological parameters (see 2.2.7.6).

First, the general shape and morphology of the hippocampus was compared with help of a contour analysis where the hippocampus was traced manually and dyed black for better visualization. For each mouse, comparable starting slides were chosen that resemble a similar area of the brain and up to five sectional planes with 200 µm distance in between were used for the contour analysis. Figure 3.1 depicts representative images.
At all ages, WT and HIF-2α KO mice showed comparable macroscopic morphological features and no visible developmental defects or retardations of the hippocampus. Additionally, the overall macroscopic morphology of the whole brain appeared comparable between both genotypes and at all developmental stages.

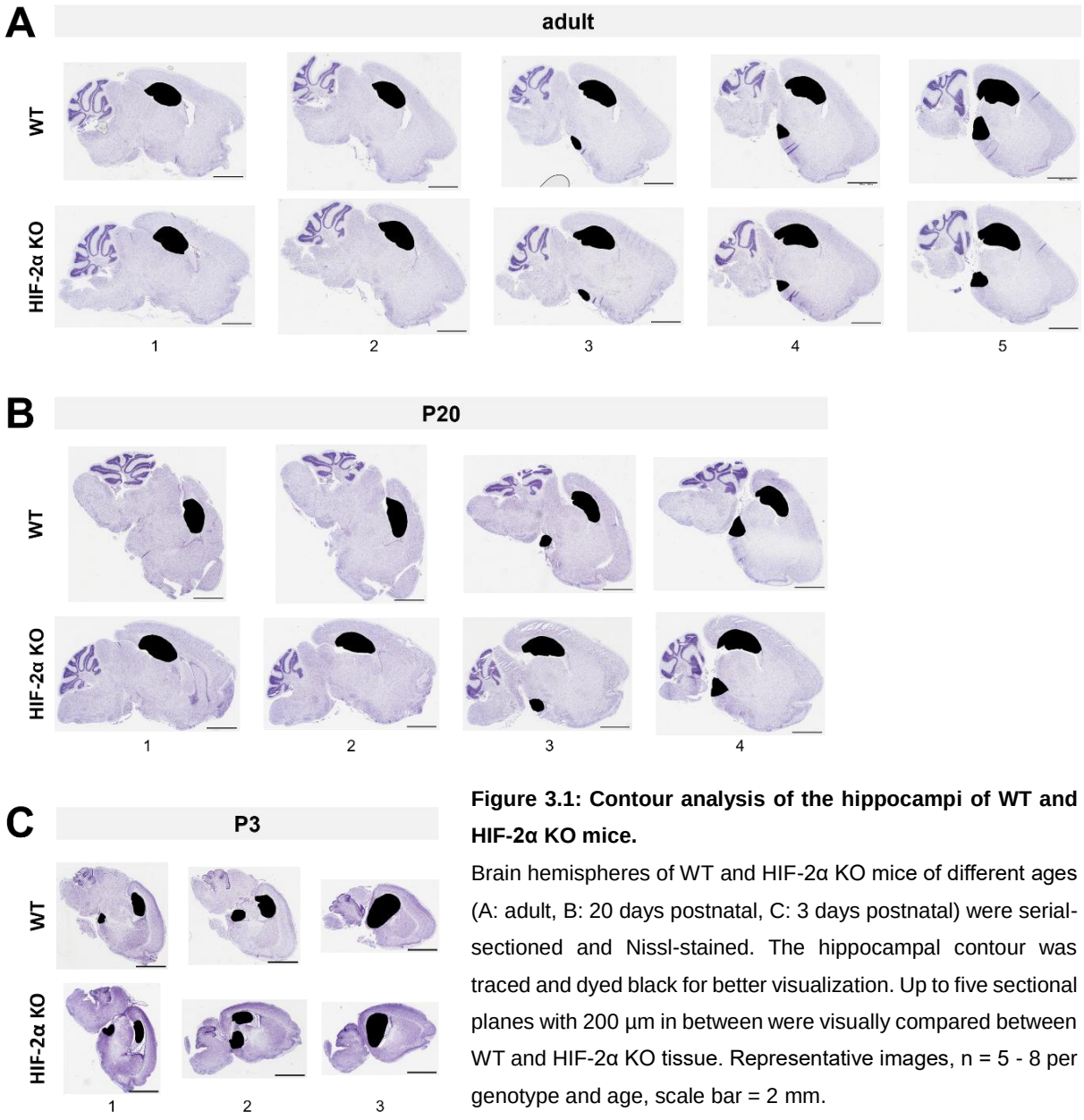

Figure 3.1: Contour analysis of the hippocampi of WT and HIF-2α KO mice.

Brain hemispheres of WT and HIF-2α KO mice of different ages (A: adult, B: 20 days postnatal, C: 3 days postnatal) were serial-sectioned and Nissl-stained. The hippocampal contour was traced and dyed black for better visualization. Up to five sectional planes with 200 µm in between were visually compared between WT and HIF-2α KO tissue. Representative images, n = 5 - 8 per genotype and age, scale bar = 2 mm.

As there were no macroscopically visible differences between the two genotypes, a more detailed analysis of the hippocampus, especially the CA1, CA3 and dentate gyrus (DG) regions, which are part of the trisynaptic circuit of the hippocampus, was performed. Here, the thickness of each layer and the cell density per field of view (FOV) was measured and counted as depicted in Figure 3.2 A. Please note that due to the differentiation status of the cells in P3 mice, it was not possible to count individual cells for the cell density analysis (for comparison with the other age stages, see Figure 3.2 B). Therefore, for P3 mice, only the thickness of the cell layer was measured.

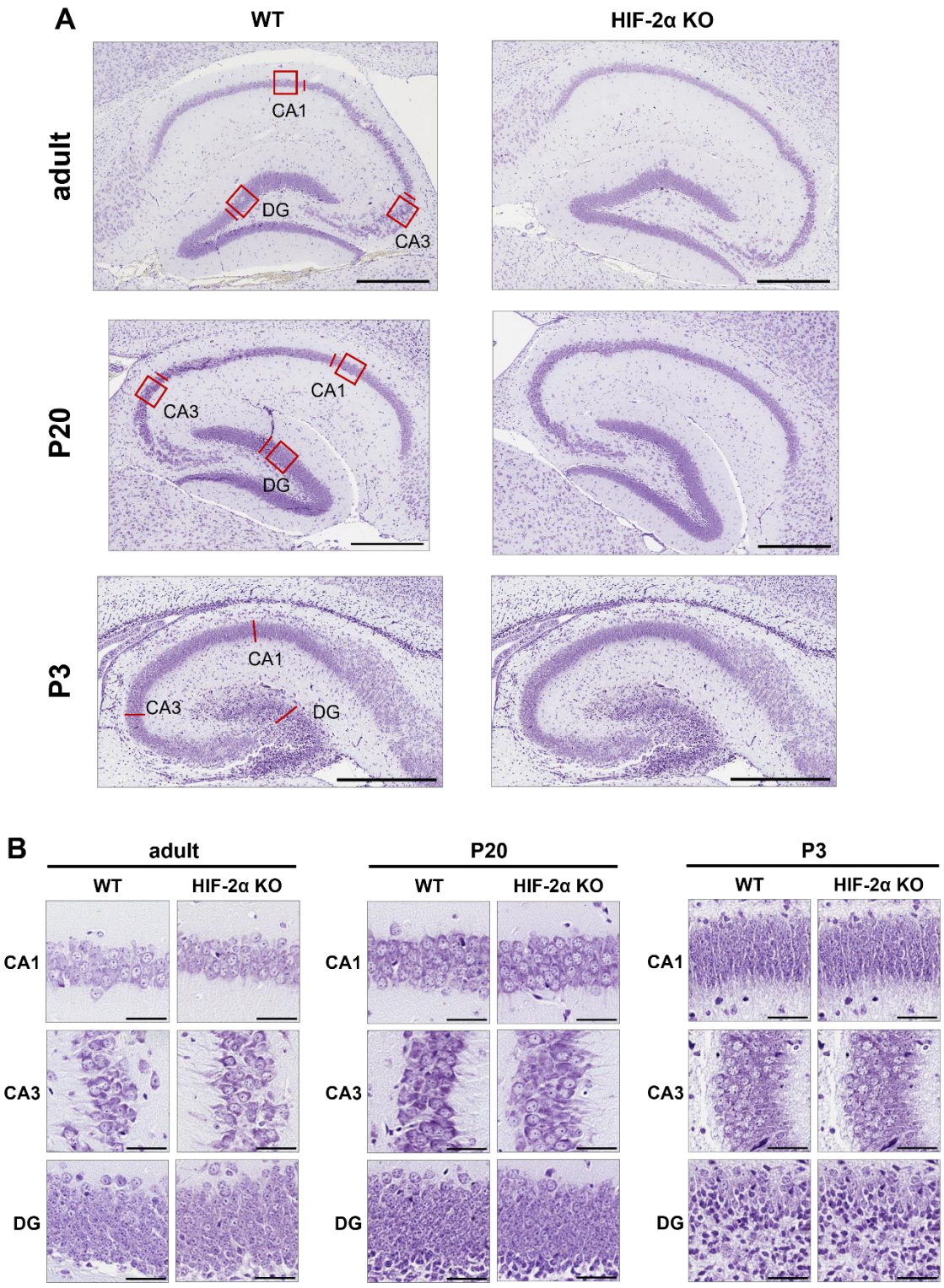

Figure 3.2: Analysis parameters and overview of Nissl-stained hippocampi of WT and HIF-2α KO mice.
Brain hemispheres of WT and HIF-2α KO mice of different ages (adult, P20 = 20 days postnatal, P3 = 3 days postnatal) were serial-sectioned and Nissl-stained.
A: Representative images of WT and HIF-2α KO hippocampal tissue for all three stages of age. Analysis parameters are depicted in red (line = thickness of layer, square = field of view for cell density analysis) for three different regions of the hippocampus (CA1, CA3 and dentate gyrus = DG). Scale bar = 500 µm.
B: Representative images of the hippocampal CA1, CA3 and DG regions in more detail. Scale bar = 50 µm.

Figure 3.3 shows the results for the thickness of the nuclei layers as length in µm for each hippocampal region at all different ages. For all conditions, both genotypes (WT and HIF-2α KO) exhibited comparable results independent of age or hippocampal region.

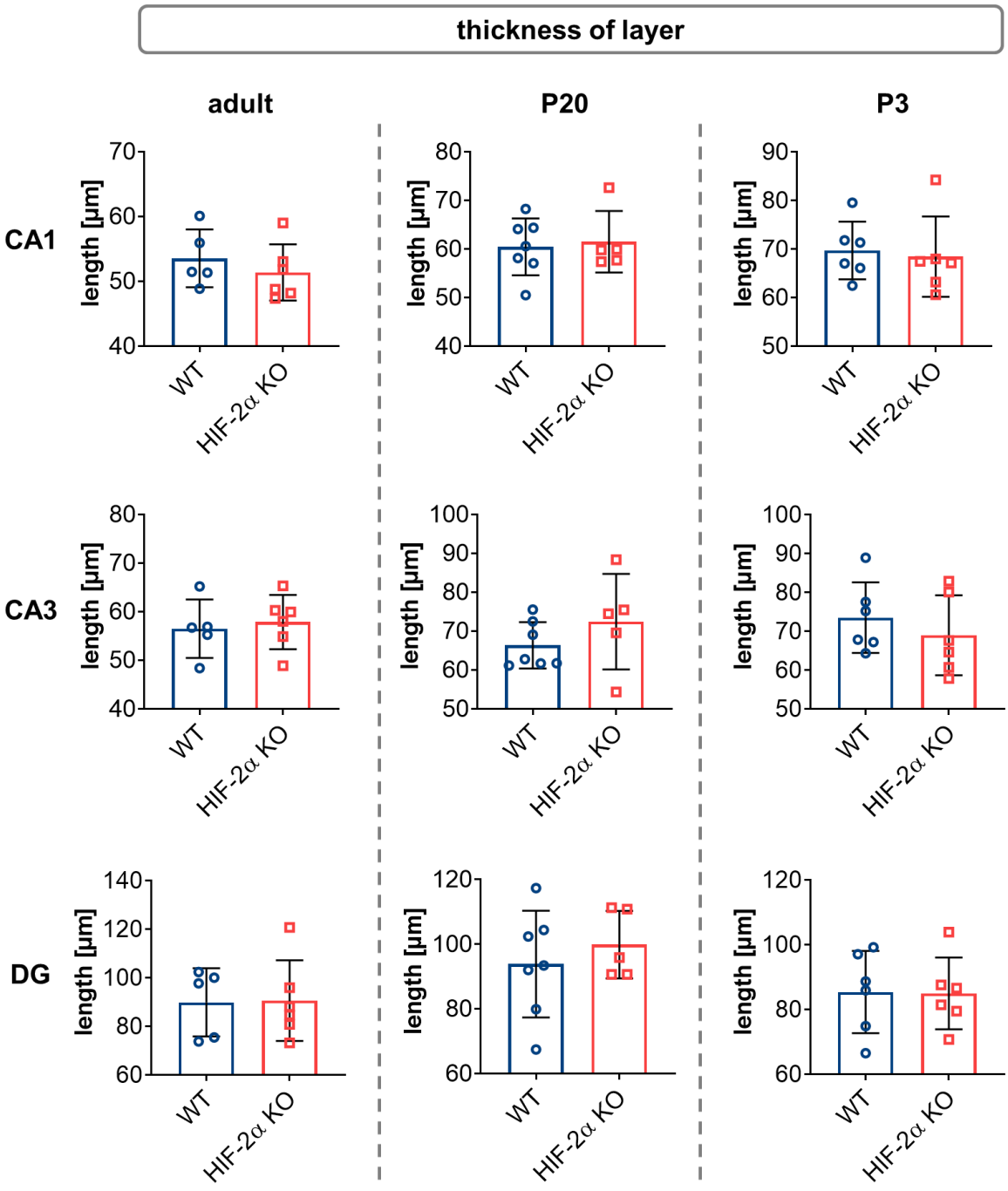

Figure 3.3: Thickness of CA1, CA3 and DG hippocampal layers of WT and HIF-2α KO mice.
Brain hemispheres of WT and HIF-2α KO mice of different ages (adult, P20 = 20 days postnatal, P3 = 3 days postnatal) were serial-sectioned and Nissl-stained. The thickness of the nuclei layer of the CA1, CA3 and DG regions was measured as length in µm for both genotypes at all ages. Mean ± SD, n = 5 - 7 per genotype and age.

The same was observed for the cell density of the CA1, CA3 and DG regions for the analyzed ages (adult and P20) with no significant differences between the two genotypes, as depicted in Figure 3.4.

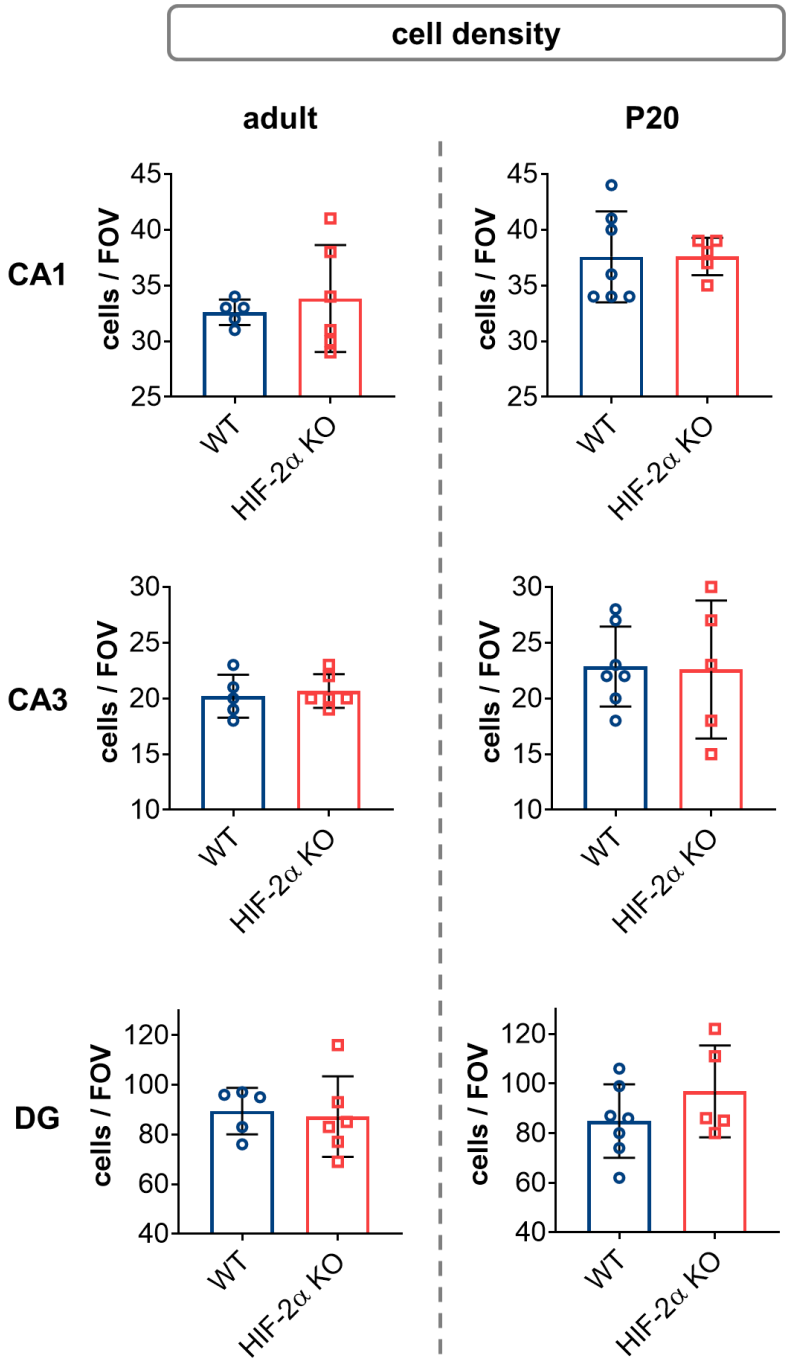

Figure 3.4: Cell density of CA1, CA3 and DG hippocampal layers of WT and HIF-2α KO mice.
Brain hemispheres of WT and HIF-2α KO mice of different ages (adult, P20 = 20 days postnatal) were serial-sectioned and Nissl-stained. The density of the nuclei layer of the CA1, CA3 and DG regions was measured as cells/field of view (FOV) for both genotypes. Mean ± SD, n = 5 - 7 per genotype and age.

As the tissue was serial-sectioned, a second section of the hippocampus was analyzed that was located more medial. This second analysis ensured reproducibility of the results in different layers of the tissue. Again, both genotypes presented similar results for thickness of layer (Supplementary Figure 6.6) and cell density (Supplementary Figure 6.7) for all tested ages. Only the length and cell density may differed between the two analyses itself, as the size and shape of the hippocampus of course changes between the different analyzed sections.

3.1.1.2. Quantitative analysis of synapse-associated genes in the brain of P3, P20 and adult WT and HIF-2α KO mice

Besides the analysis of the morphology of the brain tissue with focus on the hippocampus, this study furthermore investigated the gene expression status of synapse-related or (potentially) HIF-2α-related genes in the brain tissue. To get an overview, a RT^2 profiler PCR array for 84 different genes related to synaptic plasticity was performed using RNA extracted from the hemispheres of adult WT and HIF-2α KO mice.

The heat map in Figure 3.5 depicts the changes in gene expression of HIF-2α KO mice as fold change values in comparison to WT animals. A fold change of ± 1.7 or higher was considered as potentially relevant for further examination. Five genes (*Grip1, Inhba, Junb, Mmp9, Ngfr*) were down-regulated and five genes showed a slight up-regulation in HIF-2α KO compared to WT mice (*Akt1, Cebpb, Grin2c, Kif17, Ntf3*).

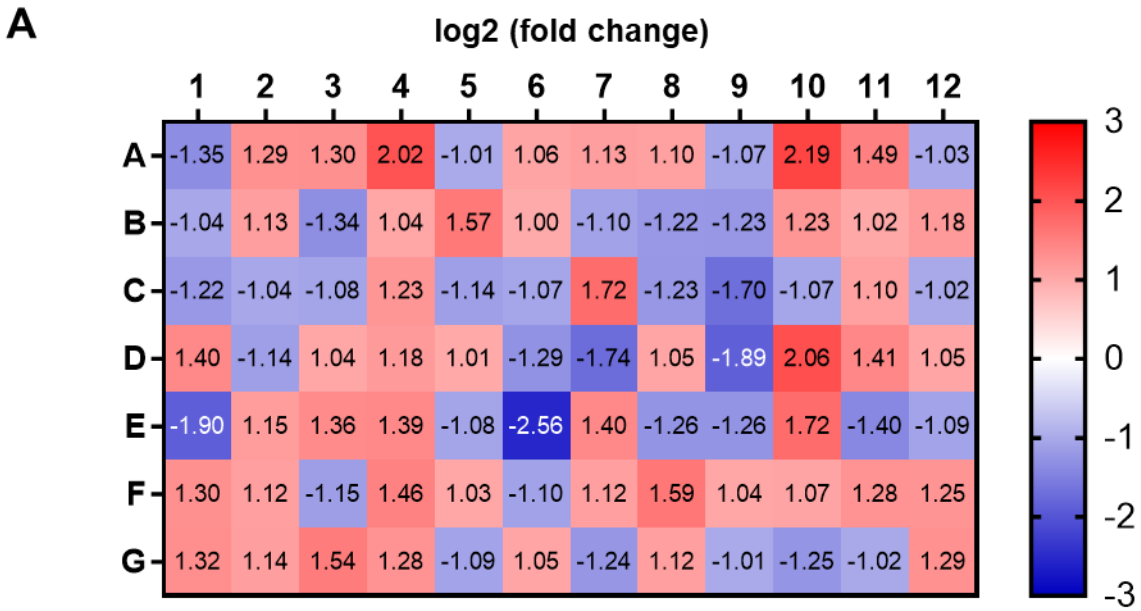

Continuation of figure on next page.

B

	1	2	3	4	5	6	7	8	9	10	11	12
A	*Adam10*	*Adcy1*	*Adcy8*	*Akt1*	*Arc*	*Bdnf*	*Camk2a*	*Camk2g*	*Cdh2*	*Cebpb*	*Cebpd*	*Cnr1*
B	*Creb1*	*Crem*	*Dlg4*	*Egr1*	*Egr2*	*Egr3*	*Egr4*	*Ephb2*	*Fos*	*Gabra5*	*Gnai1*	*Gria1*
C	*Gria2*	*Gria3*	*Gria4*	*Grin1*	*Grin2a*	*Grin2b*	*Grin2c*	*Grin2d*	*Grip1*	*Grm1*	*Grm2*	*Grm3*
D	*Grm4*	*Grm5*	*Grm7*	*Grm8*	*Homer1*	*Igf1*	*Inhba*	*Jun*	*Junb*	*Kif17*	*Klf10*	*Mapk1*
E	*Mmp9*	*Ncam1*	*Nfkb1*	*Nfkbib*	*Ngf*	*Ngfr*	*Nos1*	*Nptx2*	*Nr4a1*	*Ntf3*	*Ntf5*	*Ntrk2*
F	*Pcdh8*	*Pick1*	*Pim1*	*Plat*	*Plcg1*	*Ppp1ca*	*Ppp1cc*	*Ppp1r14a*	*Ppp2ca*	*Ppp3ca*	*Prkca*	*Prkcg*
G	*Prkg*	*Rab3a*	*Rela*	*Reln*	*Rgs2*	*Rheb*	*Sirt1*	*Srf*	*Synpo*	*Timp*	*Tnf*	*Ywhaq*

Figure 3.5: RT^2 profiler PCR array for synaptic plasticity of brain hemispheres of adult WT and HIF-2α KO mice.

Brain hemispheres of adult WT and HIF-2α KO mice were dissected and the tissue used for gene analysis of synapse-associated genes.

A: Heat map of the results of the RT^2 profiler PCR array. Results are depicted as fold change values (see legend on the right) of HIF-2α KO animals in comparison to the WT controls. Positive values greater than 1 resemble a gene induction while negative values resemble a reduced gene expression with the fold-regulation as the negative inverse of the fold-change.

B: Corresponding gene map.

The expression of the genes that showed a difference between WT and HIF-2α KO adult brain tissue (see Figure 3.5) was further verified in a standard qPCR using primers for the respective genes (Figure 3.6).

Overall, there were no significant changes in gene expression levels between WT and HIF-2α KO samples. Moreover, not even the tendencies that were found in the array (down-regulation, Figure 3.6 A / up-regulation, Figure 3.6 B) were reproducible for all genes. *Ngfr* for example, which showed a down-regulation of -2.56 in the array, was rather induced in the standard qPCR with a fold change of 2.92 in HIF-2α KO mice compared to the WT controls. The same was seen for the other potentially down-regulated genes like *Inhba*, *Junb* and *Mmp9,* which all instead showed a tendency to be up-regulated.

Kif17 on the other hand, which showed an up-regulation of 2.06 in the array, was rather reduced in the standard qPCR with a fold change of 0.72. *Akt1*, *Cebpb* and *Grin2c* also did not show the same up-regulation as the array in the standard qPCR. Only *Ntf3*, that was up-regulated in the array by a fold change of 1.72 showed almost the same values in the standard qPCR with a fold change of 2.03.

Taken together, the results of the RT^2 profiler PCR array could not be verified by standard qPCR and no significant differences between the two genotypes were visible.

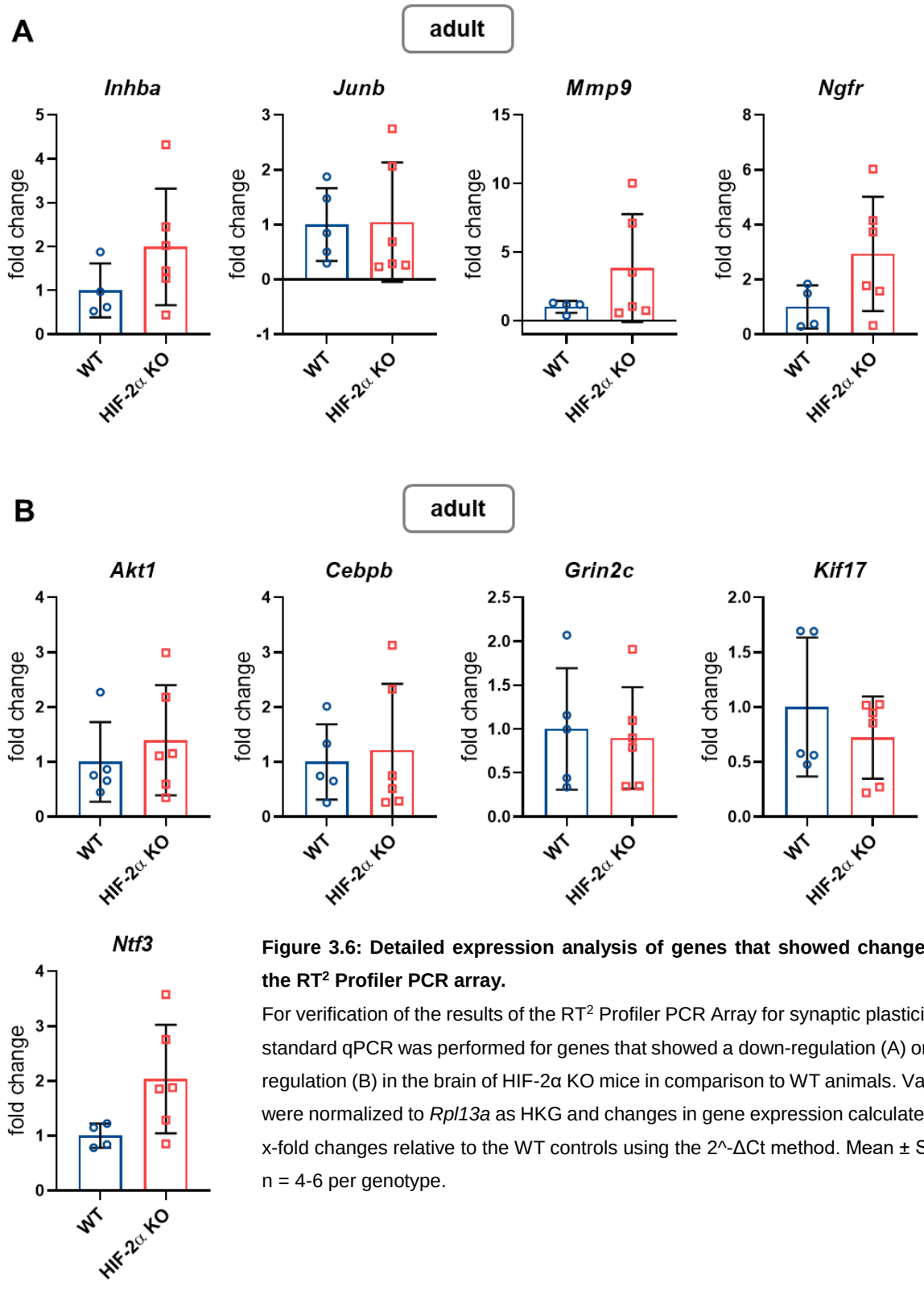

Figure 3.6: Detailed expression analysis of genes that showed changes in the RT² Profiler PCR array.

For verification of the results of the RT² Profiler PCR Array for synaptic plasticity, a standard qPCR was performed for genes that showed a down-regulation (A) or up-regulation (B) in the brain of HIF-2α KO mice in comparison to WT animals. Values were normalized to *Rpl13a* as HKG and changes in gene expression calculated as x-fold changes relative to the WT controls using the 2^-ΔCt method. Mean ± SD, n = 4-6 per genotype.

3.1.1.3. Quantitative analysis of (potentially) HIF-2α-associated genes in the brain of P3, P20 and adult WT and HIF-2α KO mice

As there were no major changes in the array-based gene expression levels between adult WT and HIF-2α KO mice (see Figure 3.6), these genes were not tested further in the P3 and P20

mice. Instead, expression levels of other brain- or synapse-associated genes that already showed a normoxic down-regulation in adult HIF-2α KO mice (*Synapsin*) and in an in vitro neurosphere approach (*Synapsin* and *Dap4*) (Kleszka *et al.,* 2020) were assessed in all three age cohorts. By looking at three different developmental stages of the mice (P3, P20, adult), the presented study aimed to see at which state the effect was already visible, thereby having a closer look at the timed function of HIF-2α in brain and synapse development.

For all age stages, *Synapsin*, which is located at the pre-synapse, expression remained without significant differences between both genotypes. For post-synaptically expressed *Dap4*, the expression showed no significant differences in adult and P20 mice, but was significantly up-regulated in P3 mice with a fold change of 1.46 (Figure 3.7).

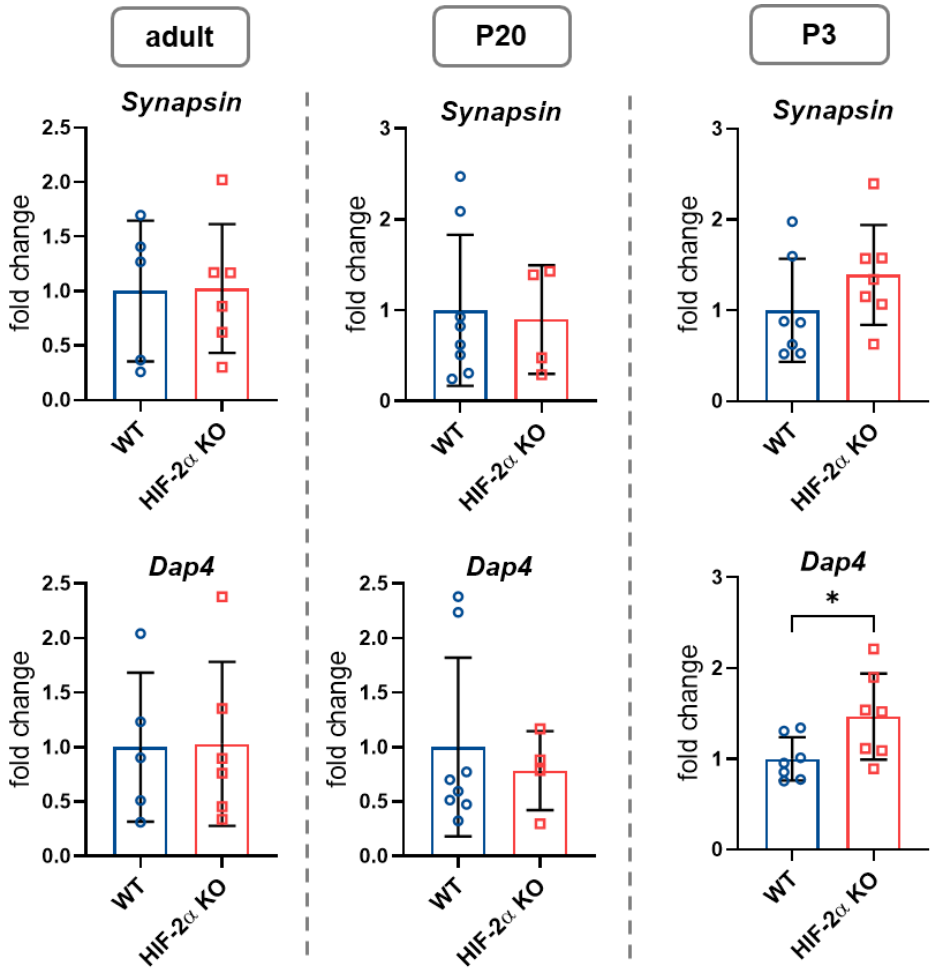

Figure 3.7: Expression analysis of (potentially) HIF-2α-associated genes in brain tissue of WT and HIF-2α KO mice.

Brain hemispheres of WT and HIF-2α KO mice of different ages (adult, P20 = 20 days postnatal, P3 = 3 days postnatal) were analyzed by qPCR for its gene expression status of pre-synaptic *Synapsin* and post-synaptic *Dap4.* Reduced expression levels in adult HIF-2α KO mice and neurospheres were already reported for these genes before (Kleszka *et al.*, 2020). Values were normalized to *Rpl13a* as HKG and changes in gene expression calculated as x-fold changes relative to the WT controls using the 2^-ΔCt method. Mean ± SD, unpaired t-test, $p < 0.05$ = *, n = 4-8 per genotype.

In addition, Kleszka *et al.* (2020) examined the cell-type specific marker expression of astrocytes, neurons and oligodendrocytes and found a significant down-regulation of the neuronal marker *bIII Tubulin* and oligodendrocyte marker *Mbp* in HIF-2α KO brain tissue. Leu and colleagues furthermore reported a reduced number of neurons and increased number of astrocytes in HIF-2α KO cells in a neurosphere differentiation assay under OGD conditions (Leu *et al.*, 2021), leading altogether to the assumption that HIF-2α has potential effects on brain and neuronal development.

Therefore, cell-type specific marker genes were analyzed in the adult, P20 and P3 brain hemispheres of WT and HIF-2α KO mice (Figure 3.8). The neuronal marker gene *bIII Tubulin* and the oligodendrocyte marker *Olig2* showed a significant up-regulation in P3 HIF-2α KO animals (with a fold change of 1.42 and 1.59, respectively) while the astrocyte marker *Gfap* remained constantly expressed between the two genotypes. In P20 mice, a significant up-regulation was still visible for *Olig2* (with a fold change of 3.22), while the other two marker genes showed no significant differences. Finally, in adult animals, the expression levels of all three marker genes (*Gfap*, *bIII Tubulin* and *Olig2*) showed no significant differences anymore (Figure 3.8).

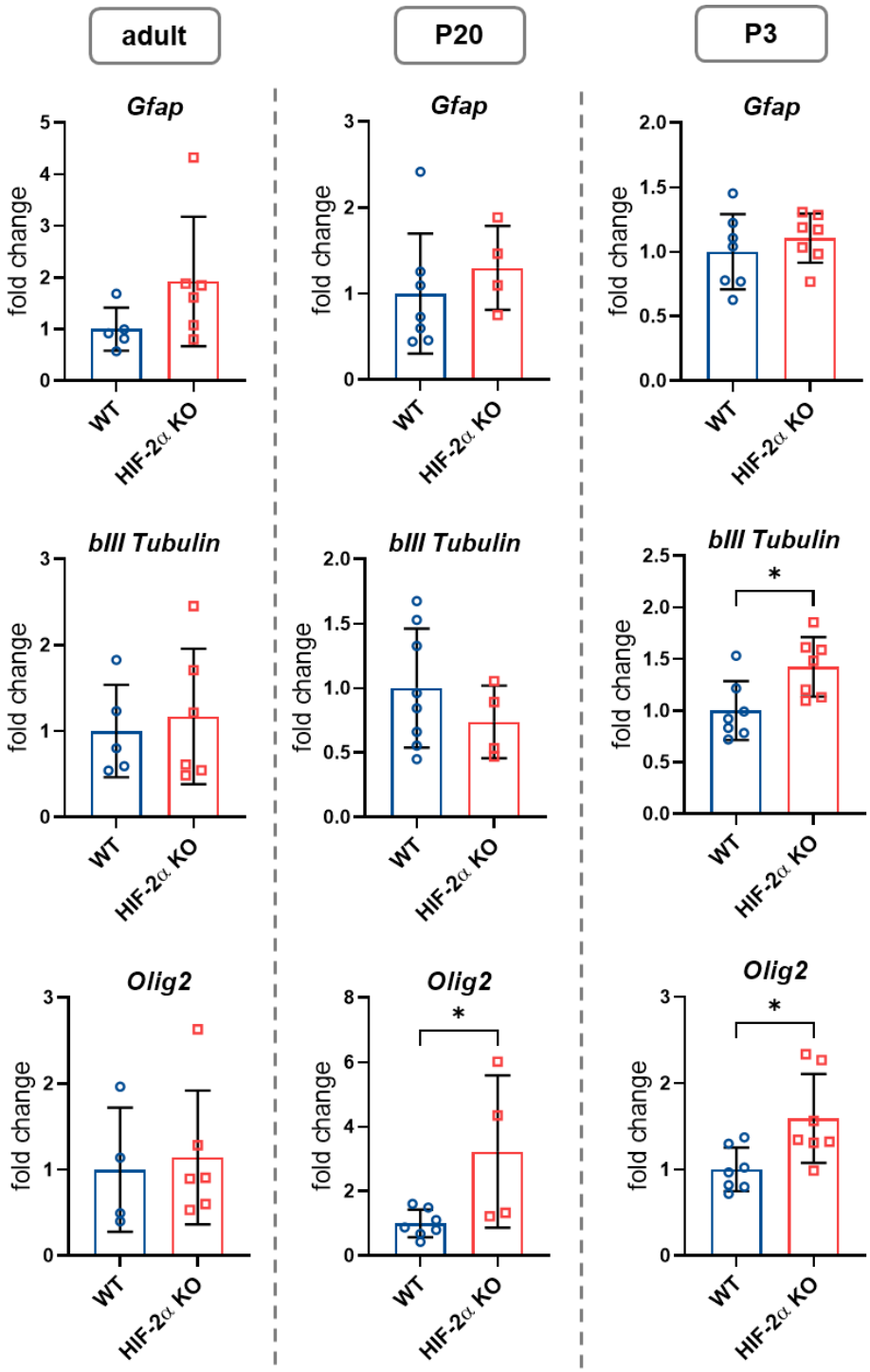

Figure 3.8: Expression analysis of cell-type specific markers in brain tissue of WT and HIF-2α KO mice. Brain hemispheres of WT and HIF-2α KO mice of different ages (adult, P20 = 20 days postnatal, P3 = 3 days postnatal) were analyzed by qPCR for cell-type specific genes for astrocytes (*Gfap*), neurons (*bIII Tubulin*) and oligodendrocytes (*Olig2*). Values were normalized to *Rpl13a* as HKG and changes in gene expression calculated as x-fold changes relative to the WT controls using the 2^-ΔCt method. Mean ± SD, unpaired t-test, $p < 0.05$ = *, n = 4-8 per genotype.

In addition, the expression of other potential target genes of HIF-2α at synapses was analyzed (Figure 3.9).

Adenosine is one of many metabolites whose production is increased under hypoxia and several studies proved interactions between the HIF pathway and adenosine receptor family. Adora1 and Adora2a are part of the adenosine receptor family, which functions through adenosine binding and cAMP as second messenger and has a variety of functions in for example tissue adaptation under energy depletion or ischemic/hypoxic conditions (for review, see Liu and Xia, 2015; Poth *et al.*, 2013). *Adora2a* for instance was shown to be an angiogenic target of HIF-2α in human pulmonary endothelial cells, although the same study did not see this effect in mouse-derived endothelial cells (Ahmad *et al.*, 2009).

In this study, the expression of *Adora1* and *Adora2a* was assessed and no significant differences were found between WT and HIF-2α KO mice at all stages of age (Figure 3.9)

Furthermore, expression levels of *Th*, the rate-limiting enzyme in catecholamine biosynthesis, were evaluated, as several studies reported a correlation of hypoxia/HIF and TH levels, as mentioned earlier (1.3.2). Here, the expression levels of *Th* remained constant between WT and HIF-2α KO mice at all developmental stages (Figure 3.9).

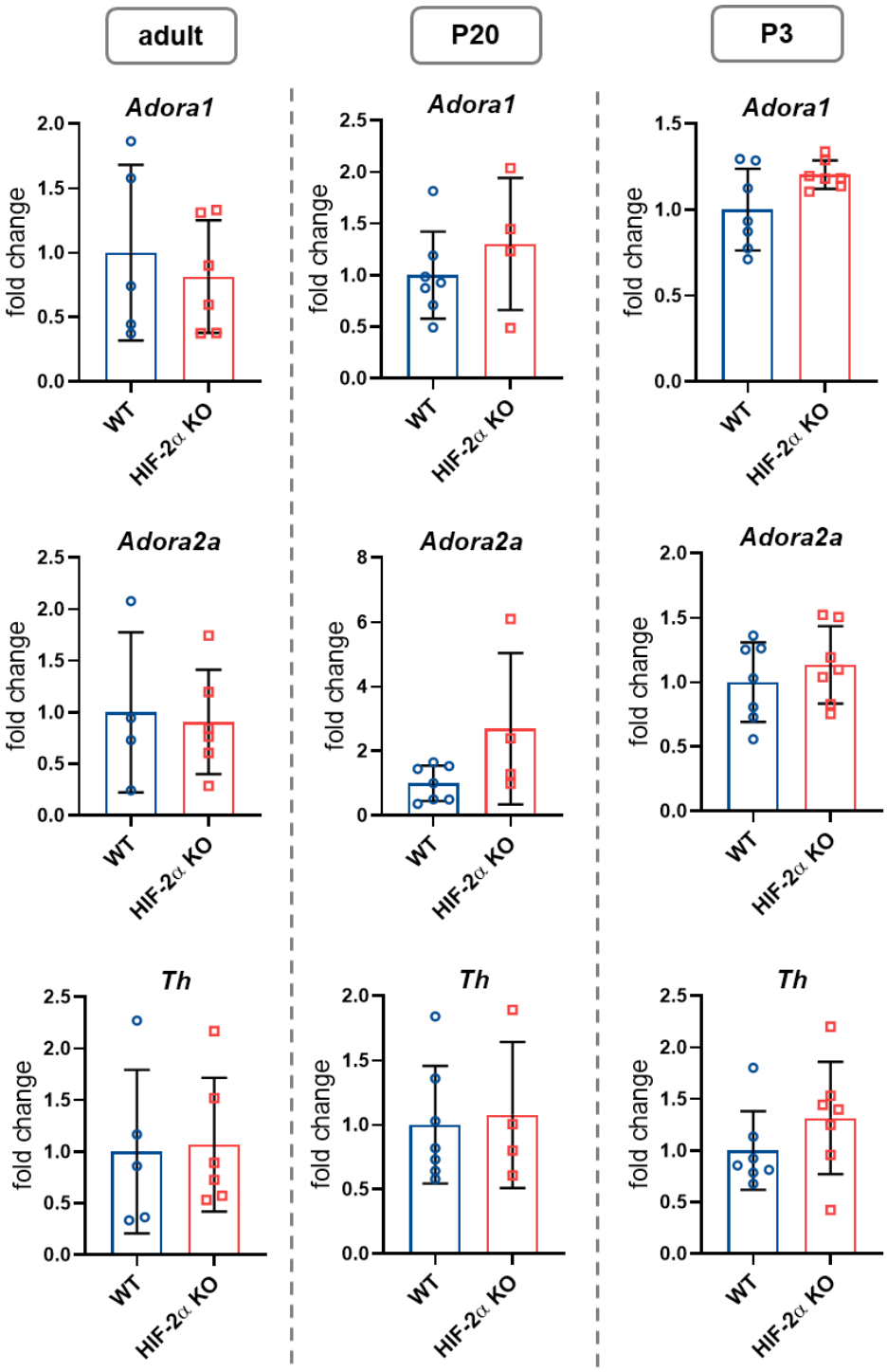

Figure 3.9: Expression analysis of potential targets of HIF-2α in brain tissue of WT and HIF-2α KO mice. Brain hemispheres of WT and HIF-2α KO mice of different ages (adult, P20 = 20 days postnatal, P3 = 3 days postnatal) were analyzed by qPCR for their gene expression status of potential target genes (adenosine A1 and A2a receptors = *Adora1*, *Adora2a*, tyrosine hydroxylase = *Th*) of HIF-2α. Values were normalized to *Rpl13a* as HKG and changes in gene expression calculated as x-fold changes relative to the WT controls using the 2^-ΔCt method. Mean ± SD, unpaired t-test, $p < 0.05$ = *, n = 4-7 per genotype.

Expression analysis of additional genes that have important functions at the synapse and during synaptic development led to similar results as for the genes described above. For some genes, there was a significant up-regulation in three days old HIF-2α KO mice that was diminished at later stages. Genes that showed this pattern were: *Collybistin* (brain specific guanine nucleotide exchange factor shown to interact with Gephyrin (Kins *et al.*, 2000)), *Gphn* itself (Gephyrin; structural protein at inhibitory synapses), *Wnt7a* (member of the Wnt/β-catenin signaling pathway in the brain), *Dbn1* (Drebrin; cytoplasmic actin-binding protein which functions in neuronal growth), *Nlgn2* (Neuroligin2; post-synaptic cell-adhesion molecule of inhibitory synapses), *Nlgn3* (Neuroligin3; post-synaptic cell-adhesion molecule of excitatory and inhibitory synapses) and *Nrxn3* (Neurexin3; pre-synaptic cell-adhesion molecule) as seen in Supplementary Figure 6.1, Figure 6.2, Figure 6.3, Figure 6.4 and Figure 6.5.

The expression of other genes remained comparable at all times in both genotypes for the following tested genes: *Grin2c* (subunit of ionotropic glutamate NMDA receptor), *Psd95* (Post-synaptic density protein 95; scaffolding protein at excitatory synapses), *Snap25* (Synaptosomal-associated protein, 25kDa; component of the trans-SNARE complex), *Bdnf* (Brain derived neutrophic factor; growth facztor), *Nlgn1* (NEUROLIGIN1; post-synaptic cell adhesion molecule at excitatory synapses), *Nrxn1* (NEUREXIN1, pre-synaptic cell adhesion molecule), *Nrxn2* (NEUREXIN2; pre-synaptic cell-adhesion molecule), also depicted in Supplementary Figure 6.1, Figure 6.2, Figure 6.3, Figure 6.4 and Figure 6.5.

3.1.2. Ultrastructure of hippocampal synapses of WT and HIF-2α KO mice

Kleszka *et al*. (2020) described reductions in the expression of PSD-associated genes in HIF-2α KO neurospheres in vitro but found no differences in the ultrastructure of synapses in the cortices of the mice with the respective genotype in vivo. As it was furthermore shown that HIF-2α KO mice exhibit deficits in learning and memory, here, the ultrastructure of synapses of the hippocampus was resolved by standard transmission electron microscopy (TEM). The stratum radiatum of the CA1 region was chosen for analysis as this suprapyramidal region contains for example CA3 to CA1 Schaffer collaterals that are connected to short-term and long-term synaptic plasticity. Furthermore, the synapses of the Schaffer collaterals serve as a typical type of excitatory glutamatergic synapses that can be referred to as a standard synapse in research (Bin Ibrahim *et al.*, 2022; Neves *et al.*, 2008).

By eye, both WT and HIF-2α KO mice exhibited a similar synaptic structure with no visible defects or differences (Figure 3.10 A). Depending on the orientation of the synapse, the pre-synaptic vesicular pool, the synaptic cleft and the PSD zone were clearly visible.
Thus, to get a more detailed look at possible differences between the two genotypes, parameters such as the abundance of multiple-spine or perforated synapses, the width of the synaptic cleft and the length, area and thickness of the PSD zone were quantified. Analysis parameters are depicted in Figure 3.10 B and C.

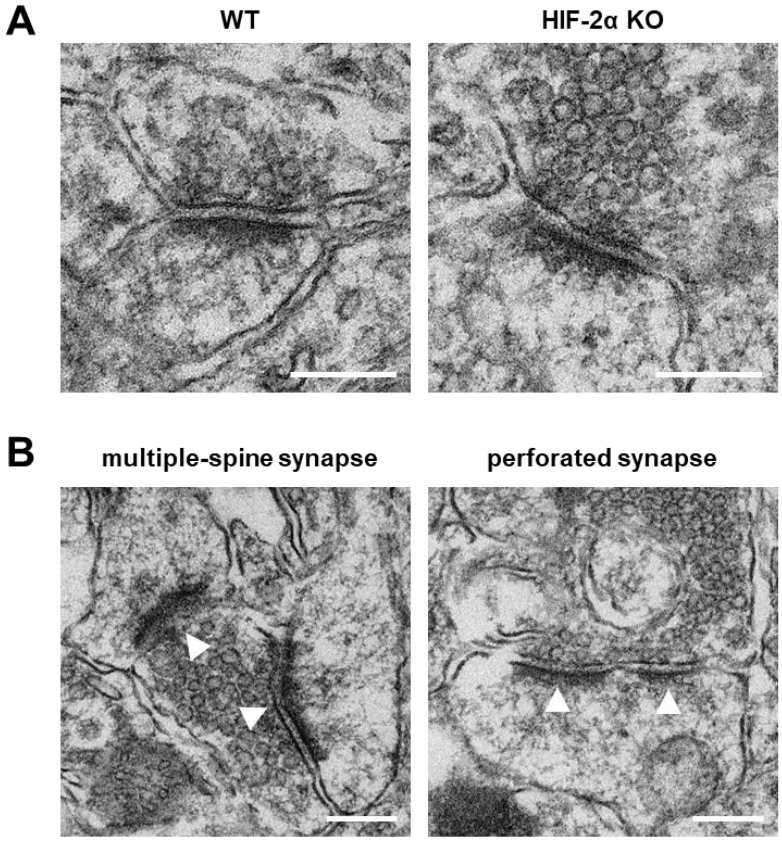

Continuation of figure on next page.

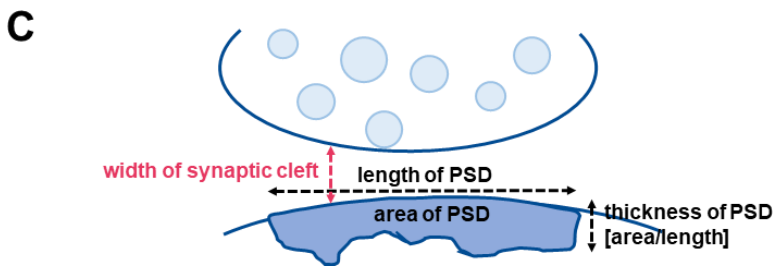

Figure 3.10: Overview of the TEM-analyzed synapses of WT and HIF-2α KO mice and the analysis parameters.

A: An example of a typical hippocampal synapse of WT and HIF-2α KO mice that was used for analysis. Note the clearly visible vesicle pool, synaptic cleft and PSD zone. Scale bar = 0.2 µm.

B: Examples for multiple-spine synapses (with two or more dendrites reaching to the same pre-synaptic vesicle pool, white arrowheads) and perforated synapses (showing a discontinuous PSD, white arrowheads). Scale bar = 0.2 µm.

C: Scheme of the analysis parameters at one single synapse. The width of the synaptic cleft, the length of the PSD and the area of the PSD was analyzed. The thickness of the PSD was calculated as the ratio between area and length.

Overall, the PSD length and area (Figure 3.11 A, B) were similar between WT and HIF-2α KO mice, whereas the average thickness of the PSD zone was significantly reduced in HIF-2α KO animals (Figure 3.11 C). Please note that the thickness is calculated as the quotient of area/length, thereby leading to an exponentiation of smaller differences. Furthermore, HIF-2α KO mice showed a significantly shorter distance of the synaptic cleft with a width of 19.07 µm in WT animals and 16.52 µm in HIF-2α KO animals (Figure 3.11 D). When looking at the overall occurrence and shape of the hippocampal synapses, the synapse density (number of synapses per area) was constant between the two genotypes (Figure 3.11 E) and the abundance of multiple-spine and perforated synapses was similar (Figure 3.11 F).

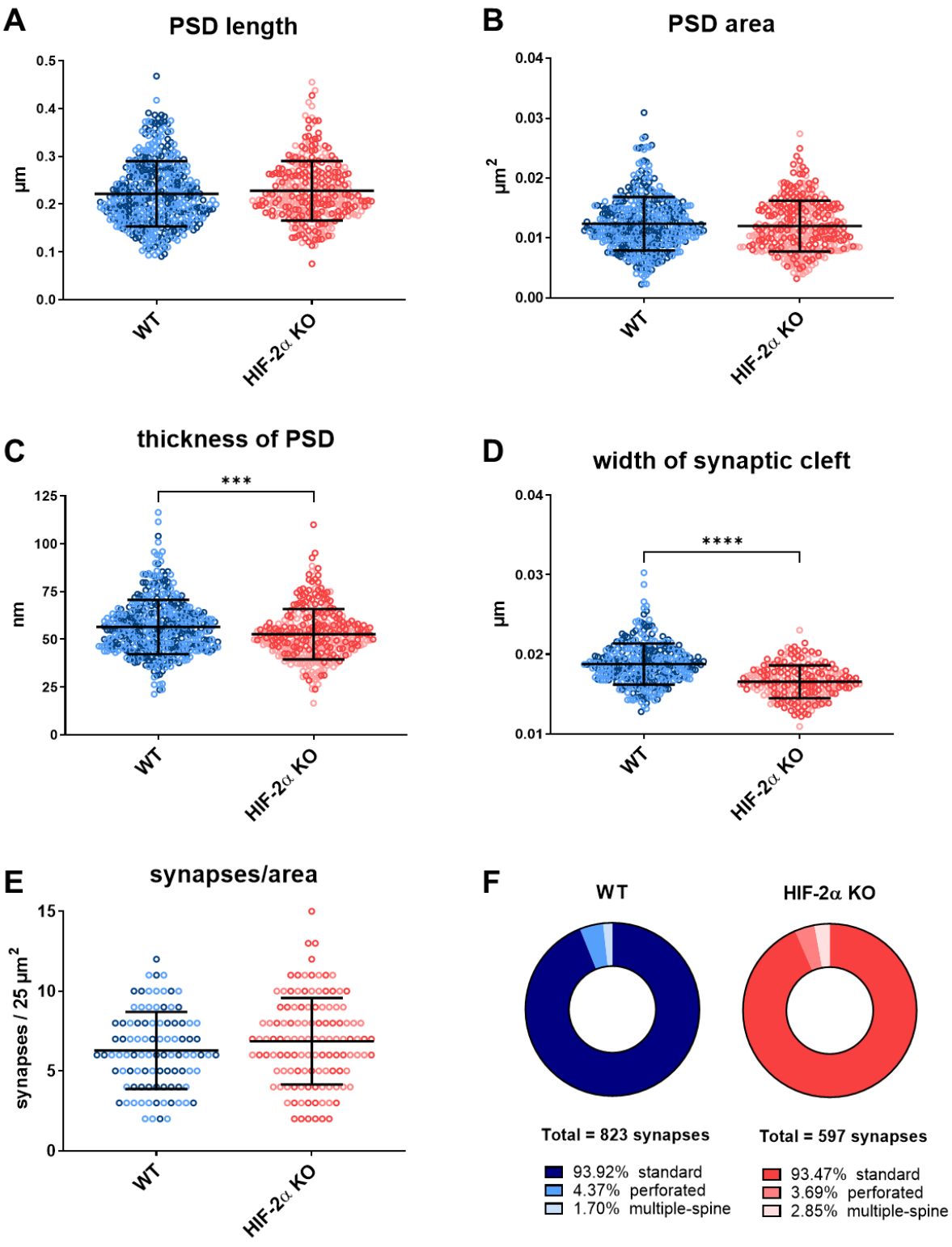

Figure 3.11: Analysis of hippocampal synapses of adult WT and HIF-2α KO mice.

Hippocampal synapses of the stratum radiatum of the CA1 region were visualized by standard TEM. PSD length (A), PSD area (B), thickness of PSD (C), width of the synaptic cleft (D), synapses per area (E) and the abundance of perforated and multiple-spine synapses (F) in comparison to standard synapses were analyzed. Mean ± SD, $p < 0.05$ = *, $p < 0.01$ = **, $p < 0.001$ = ***, $p < 0.0001$ = ****, n = 2 per genotype, illustrated by the color scheme (blue/light blue and red/light red).

3.1.3. Effects of environmental enrichment on WT and HIF-2α KO mice

Behavioral studies showed deficits in HIF-2α KO mice especially in terms of learning and memory and the dynamics of synapses under normoxic, oxygen-independent conditions (Kleszka *et al.*, 2020). To enhance a possible effect of HIF-2α on synapse-associated processes even under normoxia, an environmental enrichment study was conducted. Amongst others, environmental enrichment is known for its neurological effects, for example on brain morphology or expression of genes regulating neuronal structure, synaptic signaling and brain plasticity (Bayne, 2018; Rampon *et al.*, 2000). This study therefore aimed to enhance brain activity through enriched housing (EE = environmentally enriched) in WT and HIF-2α KO animals in contrast to their standard housed (SC = standard condition) littermates. After 4 weeks, cortices and hippocampi of the animals were used for further gene expression and protein analysis.

3.1.3.1. Quantitative analysis of synapse-associated genes in the cortex and hippocampus of enriched and standard housed WT and HIF-2α KO mice

First, to get an impression of potential changes in gene expression levels regarding synaptic plasticity, a RT^2 profiler PCR array for 84 different genes related to synaptic plasticity was performed for the hippocampus of environmentally enriched WT and HIF-2α KO animals, as the strongest impact was expected under these conditions.

The heat map in Figure 3.12 depicts the changes in gene expression of HIF-2α KO mice as fold change values in comparison to their WT littermates. A fold change of ± 2 or higher was chosen as potentially relevant for further examination. Two genes (*Ngfr* and *Pcdh8*) were down-regulated whereas several genes showed a moderate to very strong up-regulation (*Adam10*, *Adcy1*, *Adcy8*, *Akt1*, *Arc*, *Bdnf*, *Camk2a*, *Camk2g*, *Cdh2*, *Cebpb*, *Cebpd*, *Cnr1*, *Creb1*, *Crem*, *Dlg4/Psd95*, *Egr1*, *Inhba*, *Kif17*).

These genes were further considered for verification in a standard qPCR. In addition to the hippocampal tissue, the standard qPCR was also performed with the cortex samples of these animals.

A

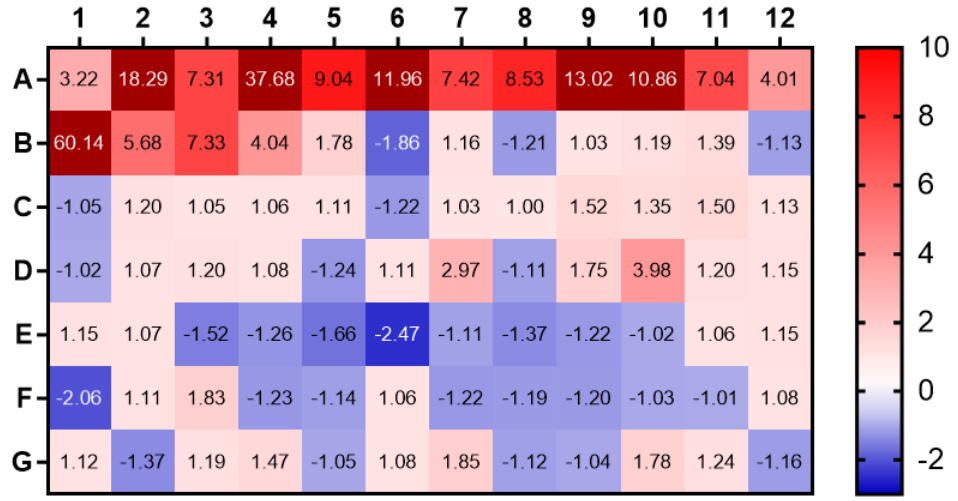

B

	1	2	3	4	5	6	7	8	9	10	11	12
A	*Adam10*	*Adcy1*	*Adcy8*	*Akt1*	*Arc*	*Bdnf*	*Camk2a*	*Camk2g*	*Cdh2*	*Cebpb*	*Cebpd*	*Cnr1*
B	*Creb1*	*Crem*	*Dlg4*	*Egr1*	*Egr2*	*Egr3*	*Egr4*	*Ephb2*	*Fos*	*Gabra5*	*Gnai1*	*Gria1*
C	*Gria2*	*Gria3*	*Gria4*	*Grin1*	*Grin2a*	*Grin2b*	*Grin2c*	*Grin2d*	*Grip1*	*Grm1*	*Grm2*	*Grm3*
D	*Grm4*	*Grm5*	*Grm7*	*Grm8*	*Homer1*	*Igf1*	*Inhba*	*Jun*	*Junb*	*Kif17*	*Klf10*	*Mapk1*
E	*Mmp9*	*Ncam1*	*Nfkb1*	*Nfkbib*	*Ngf*	*Ngfr*	*Nos1*	*Nptx2*	*Nr4a1*	*Ntf3*	*Ntf5*	*Ntrk2*
F	*Pcdh8*	*Pick1*	*Pim1*	*Plat*	*Plcg1*	*Ppp1ca*	*Ppp1cc*	*Ppp1r14a*	*Ppp2ca*	*Ppp3ca*	*Prkca*	*Prkcg*
G	*Prkg*	*Rab3a*	*Rela*	*Reln*	*Rgs2*	*Rheb*	*Sirt1*	*Srf*	*Synpo*	*Timp*	*Tnf*	*Ywhaq*

Figure 3.12: RT² profiler PCR array for synaptic plasticity of the hippocampus of environmentally enriched WT and HIF-2α KO mice.

WT and HIF-2α KO mice were housed under enriched conditions for 4 weeks and the hippocampal tissue used for gene analysis of synapse-associated genes.

A: Heat map of the results of the RT² profiler PCR array. Results are depicted as fold change values (see legend on the right) of HIF-2α KO animals in comparison to the WT controls. Positive values greater than 1 resemble a gene induction while negative values resemble a reduced gene expression with the fold-regulation as the negative inverse of the fold-change.

B: Corresponding gene map.

In total, all differences in gene expression that were identified with the RT^2 profiler array using RNA from hippocampal EE tissue could not be verified by single qPCRs.

There was no difference between the two genotypes in expression of genes that showed a very high up-regulation (Figure 3.13), a high up-regulation (Figure 3.14), a moderate up-regulation (Figure 3.15) or a down-regulation (Figure 3.16) in the RT^2 profiler array. Only the *Kif17* expression (Figure 3.15) differed significantly in EE HIF-2α KO hippocampal tissue, though not as moderately up-regulated like in the array, but instead down-regulated. Furthermore, the SC mice also showed no differences in hippocampal gene expression between the two genotypes. In addition, the expression of these genes in the cortex of the WT and HIF-2α KO mice remained similar between the two genotypes.

An overall effect of the housing condition, independent of the genotype of the mice, was visible as a significant down-regulation for some genes especially in the hippocampus, for example for *Cdh2* (Figure 3.13), *Adcy8*, *Camk2a*, *Camk2g*, *Psd95* (Figure 3.14) and *Pcdh8* (Figure 3.16). In the cortex, EE led to a significant down-regulation of *Cepbd* (Figure 3.14), *Crem* (Figure 3.15), *Ngfr* and *Pcdh8* (Figure 3.16) in comparison to SC housing.

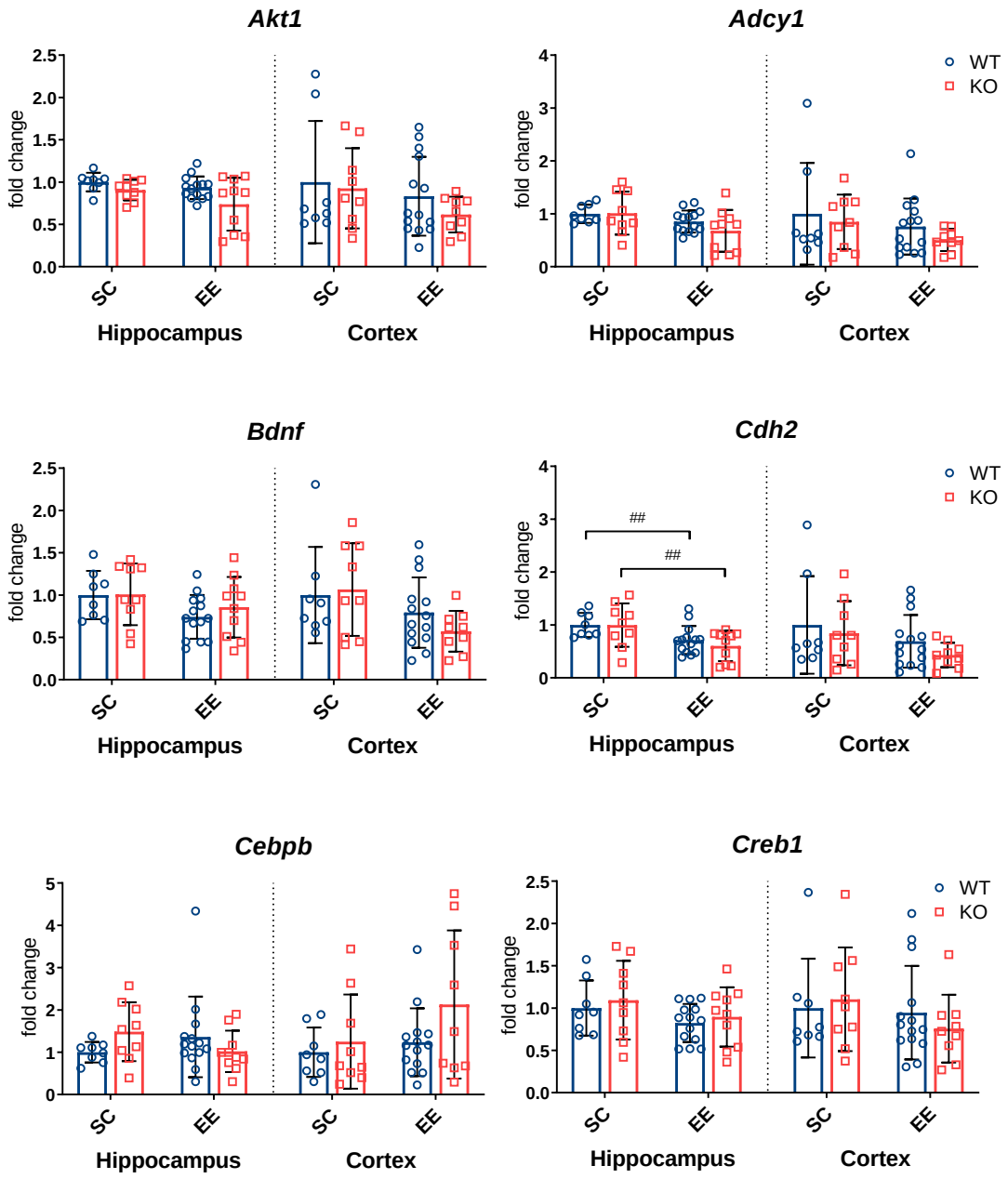

Figure 3.13: Detailed expression analysis of genes that were very highly up-regulated in the RT² Profiler PCR array.

For verification of the results of the RT² Profiler PCR Array for synaptic plasticity, a standard qPCR was performed for genes that showed a very high up-regulation in the hippocampus of environmentally enriched (EE) HIF-2α KO mice in comparison to their WT littermates. Additionally, cortical gene expression was tested. Values were normalized to *ribProt* as HKG and changes in gene expression calculated as x-fold changes relative to the respective tissue of standard housed (SC = standard condition) WT animals using the 2^-ΔCt method. Mean ± SD, $p < 0.01$ = ## between different housing conditions, n = 8-14 per genotype.

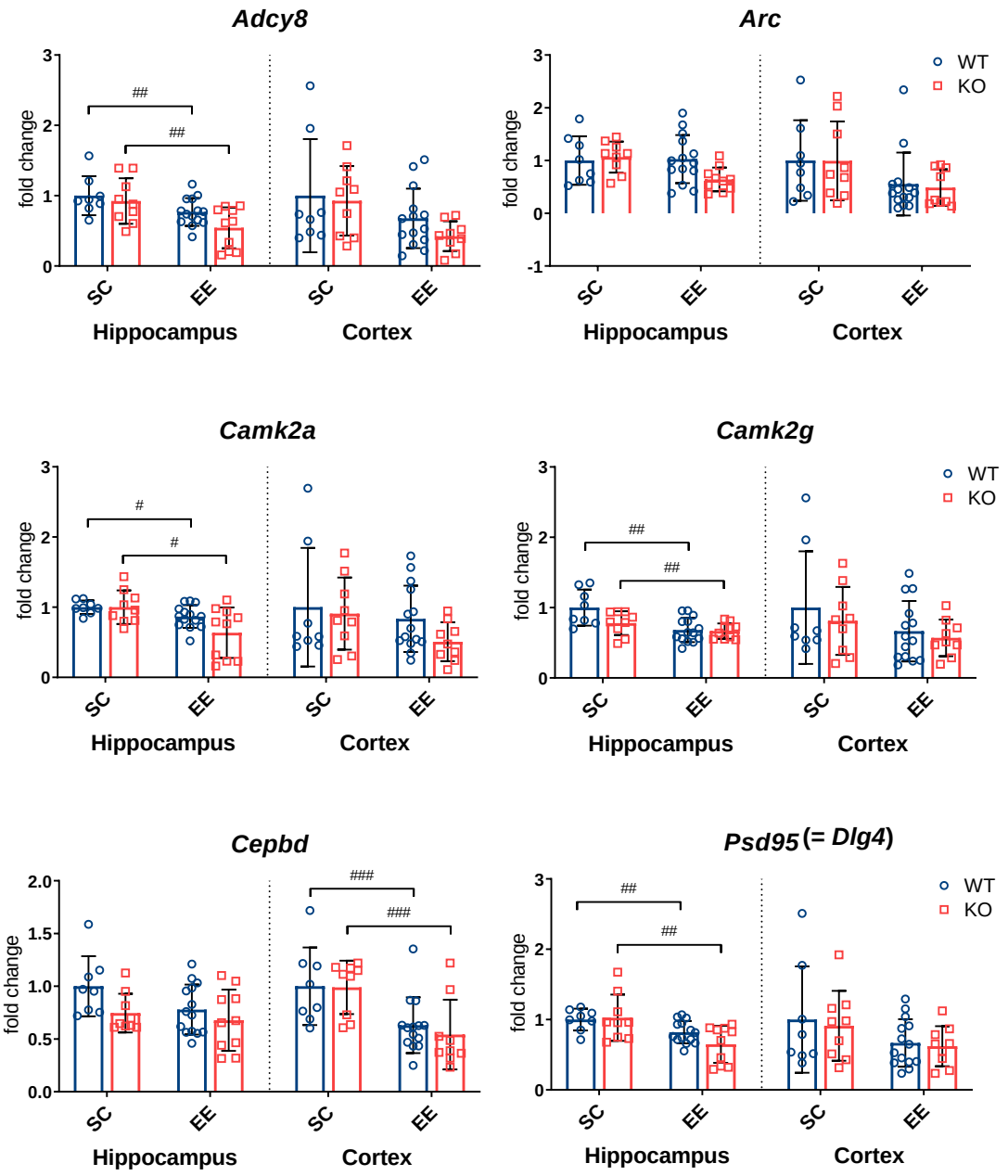

Figure 3.14: Detailed expression analysis of genes that were highly up-regulated in the RT² Profiler PCR array.

For verification of the results of the RT² Profiler PCR Array for synaptic plasticity, a standard qPCR was performed for genes that showed a high up-regulation in the hippocampus of environmentally enriched (EE) HIF-2α KO mice in comparison to their WT littermates. Additionally, cortical gene expression was tested. Values were normalized to *ribProt* as HKG and changes in gene expression calculated as x-fold changes relative to the respective tissue of standard housed (SC = standard condition) WT animals using the 2^-ΔCt method. Mean ± SD, $p < 0.05$ = #, $p < 0.01$ = ##, $p < 0.001$ = ### between different housing conditions, n = 8-14 per genotype.

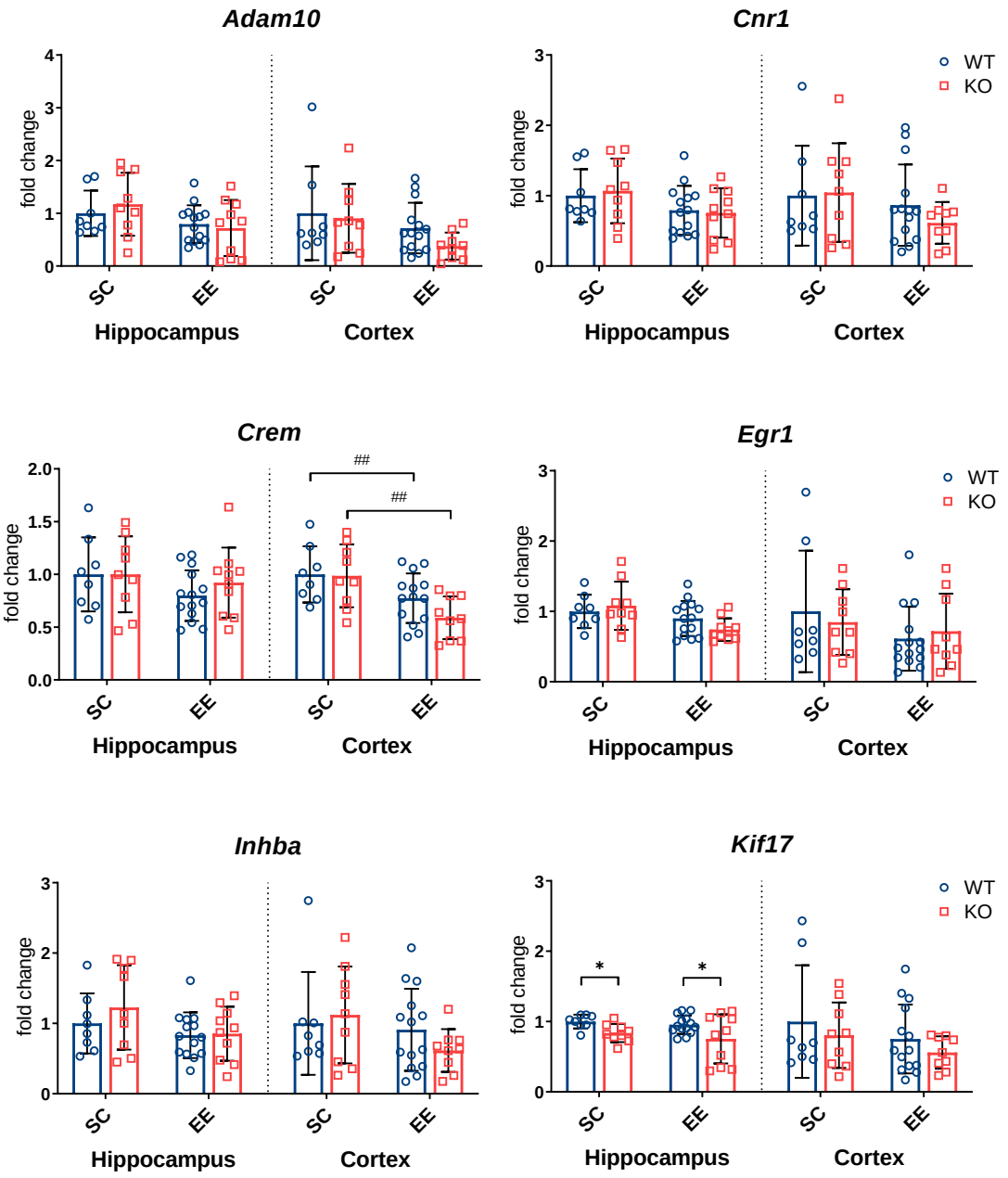

Figure 3.15: Detailed expression analysis of genes that were moderately up-regulated in the RT² Profiler PCR array.

For verification of the results of the RT² Profiler PCR Array for synaptic plasticity, a standard qPCR was performed for genes that showed a moderate up-regulation in the hippocampus of environmentally enriched (EE) HIF-2α KO mice in comparison to their WT littermates. Additionally, cortical gene expression was tested. Values were normalized to *ribProt* as HKG and changes in gene expression calculated as x-fold changes relative to the respective tissue of standard housed (SC = standard condition) WT animals using the 2^-ΔCt method. Mean ± SD, $p < 0.05$ = * between genotypes, $p < 0.01$ = ## between different housing conditions, n = 8-14 per genotype.

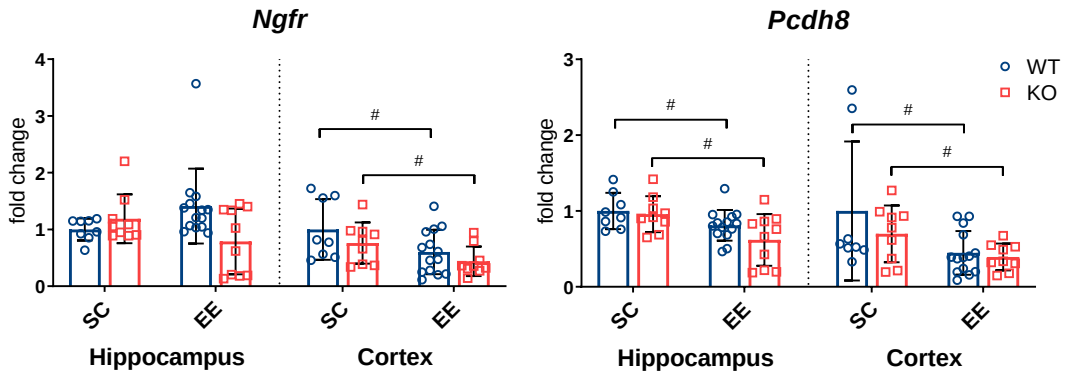

Figure 3.16: Detailed expression analysis of genes that were down-regulated in the RT² Profiler PCR array. For verification of the results of the RT² Profiler PCR Array for synaptic plasticity, a standard qPCR was performed for genes that showed a down-regulation in the hippocampus of environmentally enriched (EE) HIF-2α KO mice in comparison to their WT littermates. Additionally, cortical gene expression was tested. Values were normalized to *ribProt* as HKG and changes in gene expression calculated as x-fold changes relative to the respective tissue of standard housed (SC = standard condition) WT animals using the 2^-ΔCt method. Mean ± SD, $p < 0.05$ = # between different housing conditions, n = 8-14 per genotype.

3.1.3.2. Quantitative analysis of HIF-2α-associated genes in the cortex and hippocampus of enriched and standard housed WT and HIF-2α KO mice

As there were no visible differences between the two genotypes, the HIF-2α KO efficiency in the hippocampal and cortical tissue of SC and EE housed mice was re-validated (Figure 3.17) to verify the stability of the KO. For both tissues and housing conditions there was a significant difference in the expression of *Hif-2α* exon 2, which is part of the sequence that is supposed to be cut-out in the KO animals. Thus, the HIF-2α KO mice had a sufficient KO efficiency.

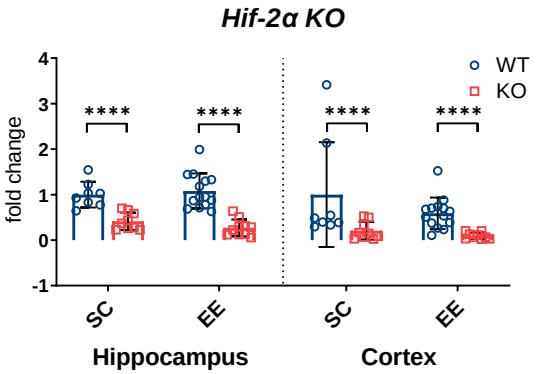

Figure 3.17: HIF-2α KO efficiency in hippocampal and cortical tissue of SC and EE housed mice. WT and HIF-2α KO mice were housed under enriched (EE) and standard housing (SC) conditions for 4 weeks and the hippocampal and cortical tissue used for gene expression analysis. Here, the HIF-2α KO efficiency was validated. Values were normalized to *ribProt* as HKG and changes in gene expression calculated as x-fold changes relative to the respective tissue of SC housed WT animals using the 2^-ΔCt method. Mean ± SD, $p < 0.0001$ = **** between genotypes, n = 8-14 per genotype.

Next, neuronal and synapse-associated genes were analyzed that have been reported to be down-regulated in the cortex of standard housed HIF-2α KO mice (Kleszka *et al.*, 2020) to assess, whether enrichment would enhance these effects. Strikingly, the effects were not visible in this study. Independent of tissue and housing condition, the gene expression of *Synapsin*, *Nrgn*, *Mbp* and *Dap4* remained constant between the two genotypes. Furthermore, the housing condition itself also showed no effect on gene expression levels in hippocampus and cortex (Figure 3.18).

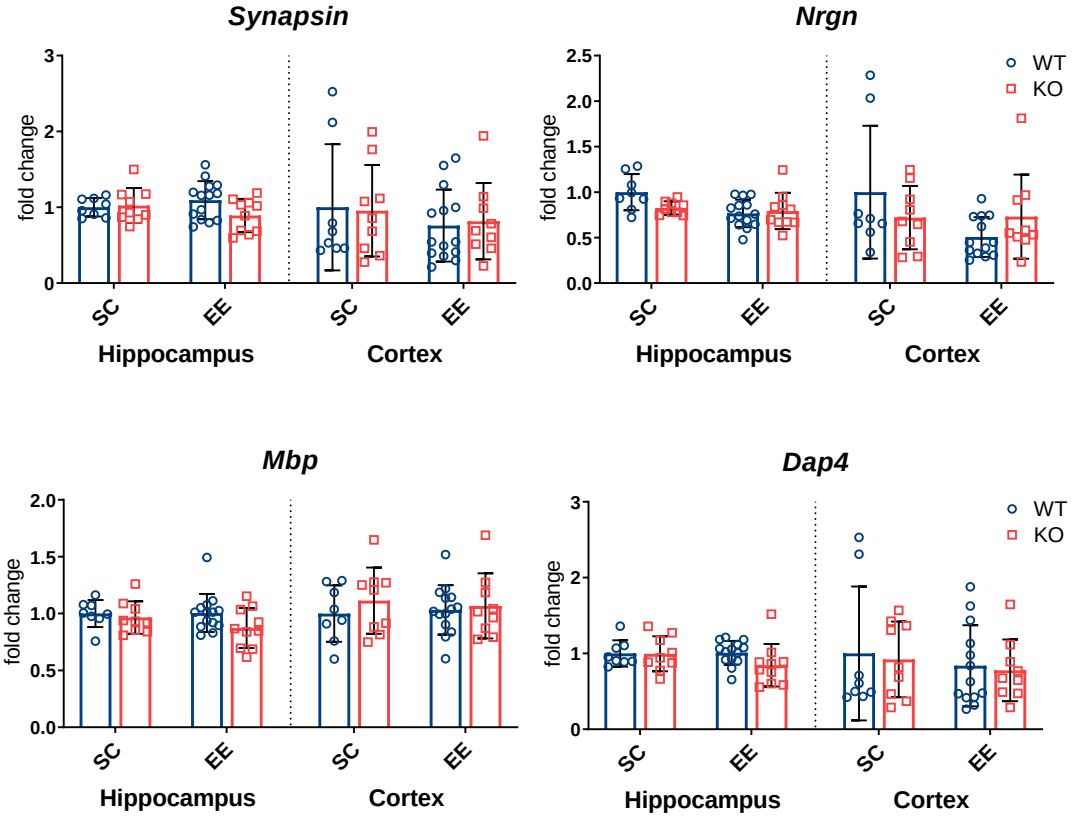

Figure 3.18: Expression analysis of additional neuronal and synapse-associated genes in hippocampal and cortical tissue of SC and EE housed WT and HIF-2α KO mice.

WT and HIF-2α KO mice were housed under enriched (EE) and standard housing (SC) conditions for 4 weeks and the hippocampal and cortical tissue used for gene analysis. Gene expression of *Synapsin*, *Nrgn*, *Mbp* and *Dap4* was assessed by qPCR. Values were normalized to *ribProt* as HKG and changes in gene expression calculated as x-fold changes relative to the respective tissue of SC housed WT animals using the 2^-ΔCt method. Mean ± SD, n = 8-14 per genotype.

In addition, gene expression was analyzed for genes that are directly or potentially connected to HIF-2α, like *Vegf*, *EpoR*, *Map2k1*, *IL1b*, *Adora1* and *Adora2a* (see 1.3.2).

When comparing WT with HIF-2α KO mice, only the expression of hippocampal *Adora2a* was significantly down-regulated in SC as well as EE housed HIF-2α KO animals (Figure 3.19). The other analyzed genes showed no differences between the genotypes. Furthermore, EE

housing led to a significant down-regulation of *Vegf* and *Map2k1* in the hippocampus as well as *Map2k1* and *IL1b* in the cortex, independent of the genotype of the mice.

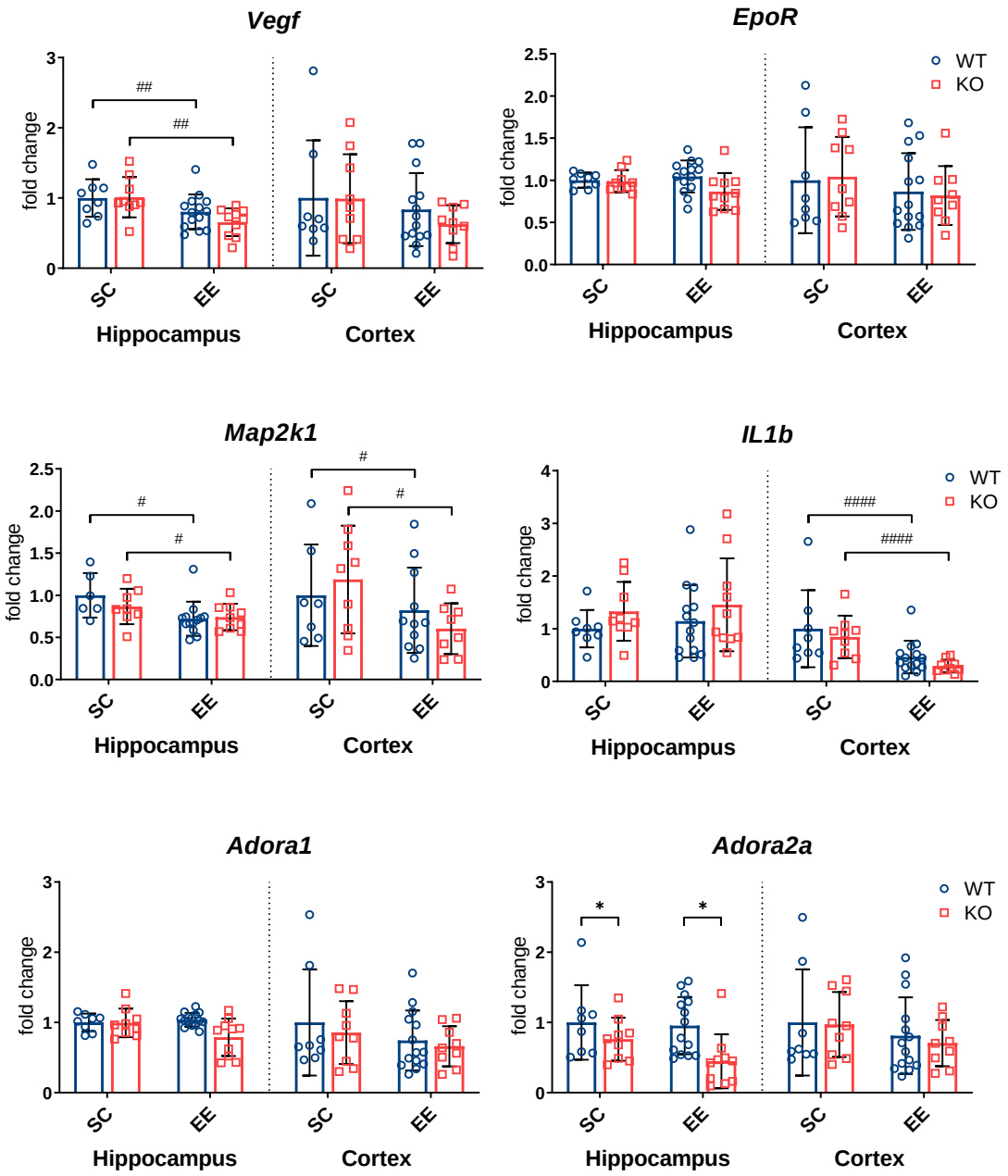

Figure 3.19: Expression analysis of (potentially) HIF-2α-associated genes in hippocampal and cortical tissue of SC and EE housed WT and HIF-2α KO mice.

WT and HIF-2α KO mice were housed under enriched (EE) and standard housing (SC) conditions for 4 weeks and the hippocampal and cortical tissue used for gene analysis. Gene expression of HIF-2α-associated genes as well as potential HIF-2α target genes was assessed by qPCR. Values were normalized to *ribProt* as HKG and changes in gene expression calculated as x-fold changes relative to the respective tissue of SC housed WT animals using the 2^-ΔCt method. Mean ± SD, $p < 0.05$ = *, $p < 0.01$ = **, $p < 0.001$ = ***, $p < 0.0001$ = **** (* = between genotypes, # = between housing conditions), n = 8-14 per genotype.

3.1.3.3. BDNF content in the cortex and hippocampus of enriched and standard housed WT and HIF-2α KO mice

As mentioned earlier (1.3.2), BDNF is a growth factor with important functions in synaptic transmission and plasticity and studies showed interactions between hypoxia and BDNF. BDNF is also associated to environmental enrichment with studies showing a correlation between EE and BDNF gene or protein expression, although there are also other studies that show no effects at all, as reviewed by Barros *et al.* (2019).

Although this study found no changes on gene expression levels of *Bdnf* (Figure 3.13), the protein levels of mature BDNF and its precursor form (proBDNF) were examined by Western Blotting in the hippocampus (Figure 3.20) and cortex (Figure 3.21) of the SC and EE housed WT and HIF-2α mice, to examine a potential correlation of BDNF, EE and HIF-2α.

When looking on protein levels of proBDNF in the hippocampus, both WT and HIF-2α KO SC housed mice showed a similar protein abundance. Furthermore, EE housing had no significant effect on proBDNF expression for both genotypes, although there was a trend to higher proBDNF levels in the HIF-2α KO mice. The BDNF form was significantly up-regulated in EE housed animals, independent of their genotype (Figure 3.20 B). Summarized, in the hippocampus, there was an effect of housing condition on BDNF abundance, but no differences were explored between WT and HIF-2α KO mice.

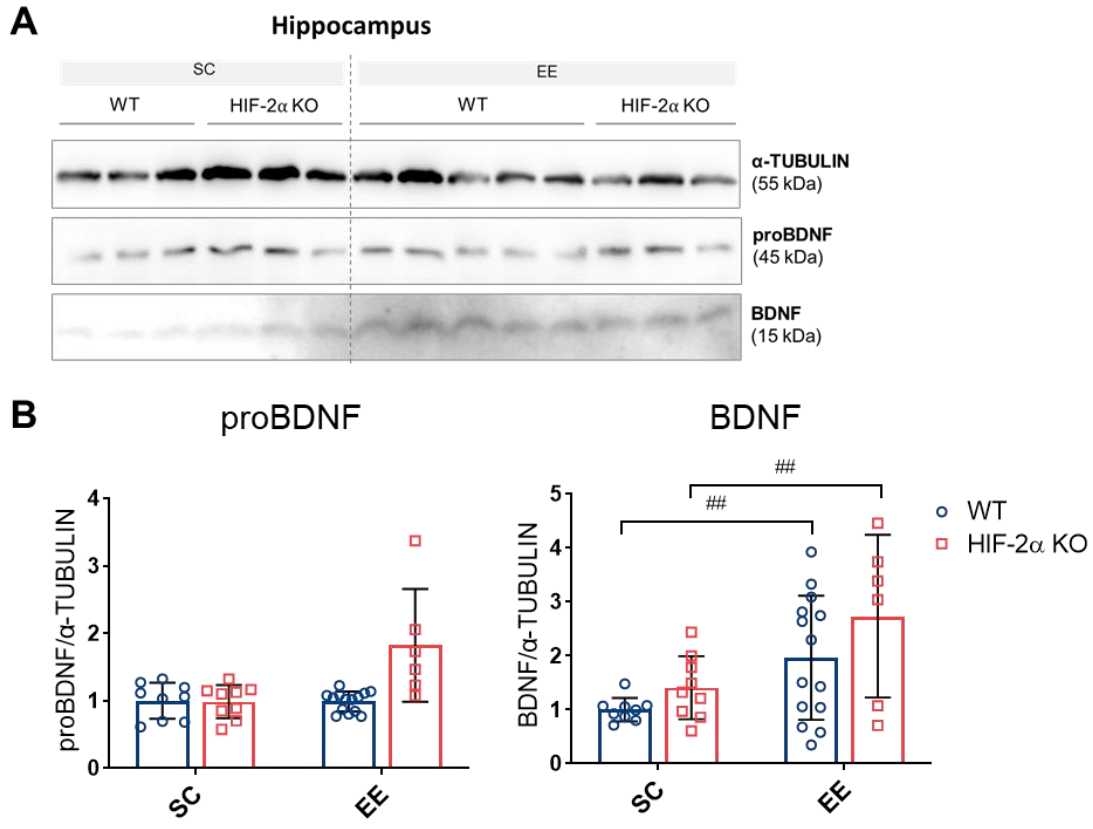

Figure legend on next page.

Figure 3.20: proBDNF and BDNF content in the hippocampus of SC and EE housed WT and HIF-2α KO mice.

WT and HIF-2α KO mice were housed under enriched (EE) and standard housing (SC) conditions for 4 weeks and the hippocampal tissue was analyzed for its proBDNF (45 kDa) and BDNF (15 kDa) protein content by Western Blotting. α-TUBULIN (55 kDa) served as a loading control, 30 µg total protein lysate were used.

A: Representative image of the Western Blot.

B: Calculated x-fold protein levels for proBDNF and BDNF, internally normalized to α-TUBULIN and compared to the SC/WT condition. Mean ± SD, p < 0.01 = ## between housing conditions, n = 6-14 per genotype.

In the cortex, no significant changes of proBDNF and BDNF were detected by Western Blotting. Protein levels remained constant independent of genotype and housing condition (Figure 3.21).

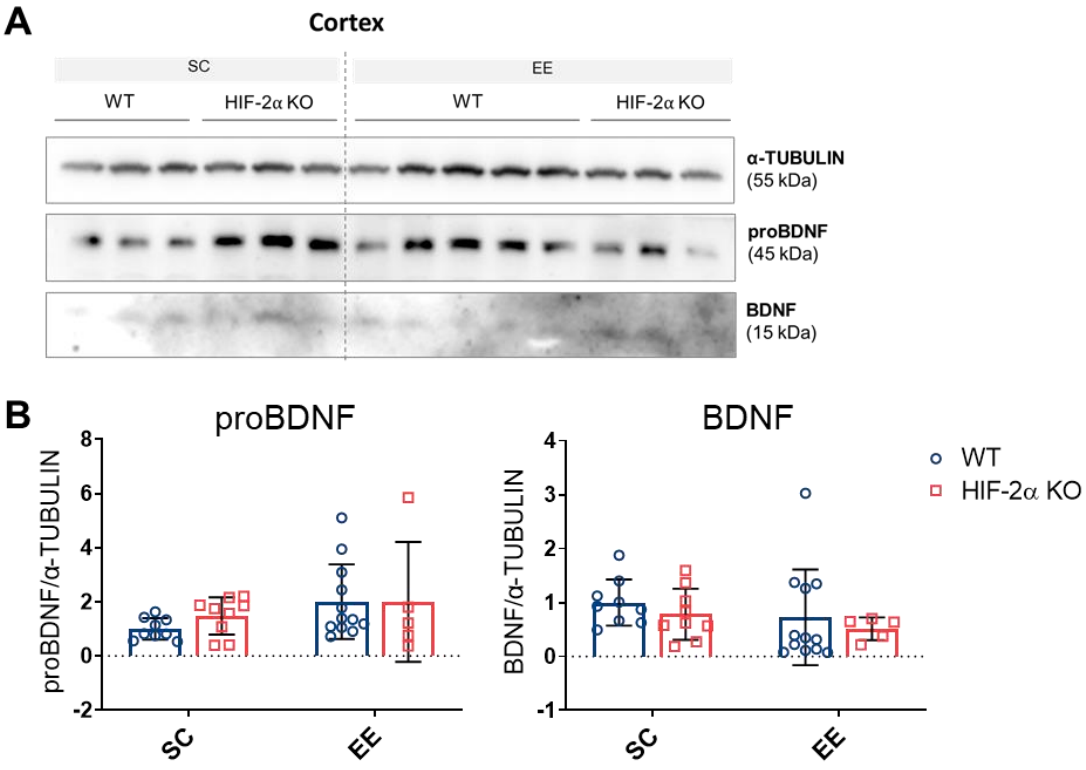

Figure 3.21: proBDNF and BDNF content in the cortex of SC and EE housed WT and HIF-2α KO mice.

WT and HIF-2α KO mice were housed under enriched (EE) and standard housing (SC) conditions for 4 weeks and the cortical tissue was analyzed for its proBDNF (45 kDa) and BDNF (15 kDa) protein content by Western Blotting. α-TUBULIN (55 kDa) served as a loading control.

A: Representative image of the Western Blot.

B: Calculated x-fold protein levels for proBDNF and BDNF, internally normalized to α-TUBULIN and compared to the SC/WT condition. Mean ± SD, p < 0.01 = ## between housing conditions, n = 5-12 per genotype.

3.2. Functions of cerebral HIF-2α in vitro

The in vivo analyses of WT and HIF-2α KO mice and tissues were mainly based on the observation that HIF-2α was stabilized in brain tissue even under normoxic conditions and that the mice showed differences in for example behavior or cell development depending on their genotype (Kleszka *et al.*, 2020). Nevertheless, as the HIF family is the main regulator of the cellular adaptation to hypoxia, the impact of HIF-2α on neurons and synapses in particular also needs to be evaluated under hypoxic conditions. For better handling and manipulation and in terms of the 3R (reduction, refinement, replacement) principle in animal research, this research question was further addressed in an in vitro approach.

In this study, a co-culture model was used where the two cell types of interest, astrocytes and neurons, remain in spatial distance. This enables the growing of a rather pure culture instead of a combination of different cell types, as for example in a neurosphere culture system. The co-culture approach allows for a better study of synapses and synapse-associated processes in contrast to for example brain developmental processes, where neurospheres resemble a better system.

For the co-culture, primary hippocampal WT or HIF-2α KO neurons that were isolated from mice with the respective genotype were co-cultured with cortical WT or HIF-2α KO astrocytes in different genotypic combinations (WT neurons/WT astrocytes, WT neurons/KO astrocytes, KO neurons/WT astrocytes, KO neurons/KO astrocytes) under normoxic (NOX, 21% oxygen) or hypoxic (HOX, 1% oxygen) conditions. With these combinations, possible cell-type specific effects can be identified. Astrocytes thereby not only serve as a feeder layer through secretion of growth factors and extracellular matrix proteins, but also have an important role in promoting neuronal survival and synapse formation (Jones *et al.*, 2012). Further studies also indicate that the neuronal response to hypoxia may also be regulated through paracrine effects of astrocytes (Vangeison *et al.*, 2008; Vangeison and Rempe, 2009), which further supports the use of this culture model.

3.2.1. Establishment of a neuron-astrocyte co-culture system under normoxic and hypoxic conditions

There are diverse protocols for generation of a primary neuron culture system that differ in for example coating reagent of dishes, media composition, digestion buffer used for tissue digestion, additional treatment with AraC to curb glial proliferation, or if astrocytes are used as a feeder layer or not.

As the culture system used in this study was not implemented in the research group before, the hippocampal neuronal culture first needed to be established for this study. Various parameters were tested and assessed in pre-tests to find optimal conditions for the generation

of a reproducible neuron-astrocyte co-culture. The used optimal approach and parameters are thereby specifically working for the used mouse strain, plastic ware, consumables, culture conditions etc. and may be different for other labs.

In this study, the planned experiments ought to be performed with mature neurons that already finished synaptogenesis and exhibited fully developed synaptic connections, to first look for effects of HIF-2α on mature synapses. When looking at the literature that investigated the development and synapse formation of hippocampal neurons of mice and rats, spontaneous synaptic events were found as early as 4 days in vitro (DIV) and first excitatory synapses were found at 7 DIV. Altogether, most reports conclude that fully mature synapses, i.e. that dispose of a clear pre- and post-synaptic compartment, can be found from 10-12 DIV onward, while peaking after 2 - 3 weeks of culture (Basarsky *et al.*, 1994; Grabrucker *et al.*, 2009). This study therefore used 12 DIV as starting point of the final experiments. Therefore, all establishment processes and testing were also performed up to ~ 15 DIV, as the culture was expected to be definitely stable up to this time-point.
Parameters tested and determined are depicted in Figure 3.22 and the detailed final protocol can be found in the materials and methods section, 2.2.1.

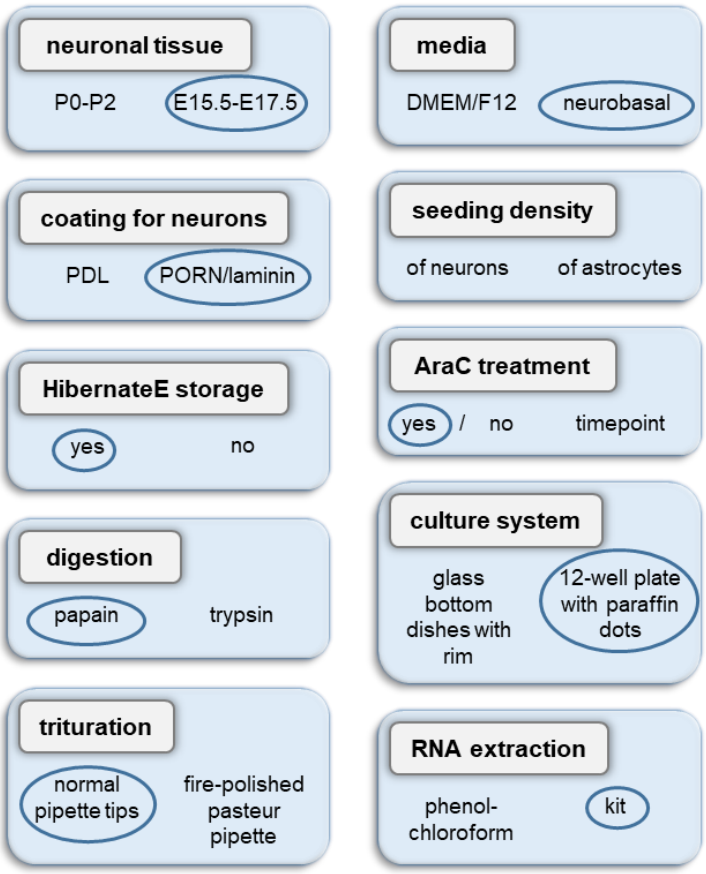

Figure 3.22: Tested parameters for optimization of a neuron-astrocyte co-culture system.
For establishment of a neuron-astrocyte co-culture, different parameters (origin of neuronal tissue, coating reagent, storage conditions for short-term storage, digestion buffer for hippocampus, trituration method, media composition, optimal seeding density of neurons and astrocytes, treatment of cells with AraC, used plastic ware and RNA extraction method for neurons) were tested. The final parameters are encircled in blue and a detailed method description can further be found in the materials & methods section.

Amongst others, the optimal coating method for the coverslips onto which the neurons were seeded needed to be assessed. Most protocols use either PDL or a PORN/laminin coating. Both were tested in combination with different seeding densities of neurons (Figure 3.23). For both PDL and PORN/laminin coating, neurons settled down and started to mature and form axons and dendrites after one day. However, the PDL coating resulted in more poorly attached and dead cells than with the PORN/laminin coating. This tendency was further intensified with ongoing time and clearly visible after 7 DIV and 14 DIV (Figure 3.23). Furthermore, different seeding densities of the neuronal cells were tested. Seeding 100.000 cells on PORN/laminin coated coverslips resulted in too dense cultures where cells started clustering and overgrew each other after 14 DIV. In contrast, 50.000 cells seeded under the same conditions formed a dense dendritic network where individual cells were still distinguishable. Therefore, the lower seeding density was chosen.

Please note that this initial trial experiments were performed with a slightly larger coverslip than the final experiments, therefore for the final experiments the seeding density of neurons was further reduced to 40.000 cells per coverslip.

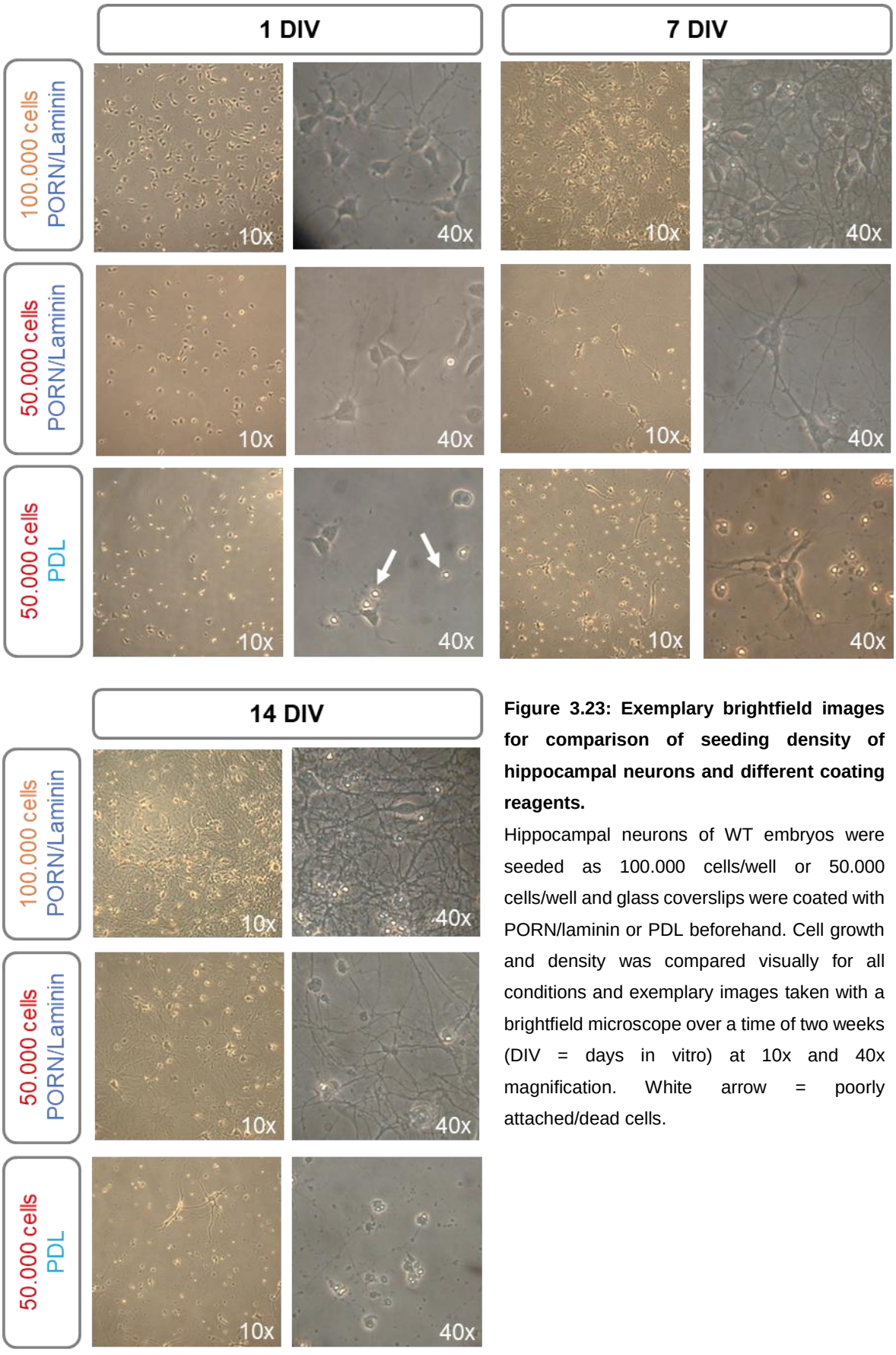

Figure 3.23: Exemplary brightfield images for comparison of seeding density of hippocampal neurons and different coating reagents.

Hippocampal neurons of WT embryos were seeded as 100.000 cells/well or 50.000 cells/well and glass coverslips were coated with PORN/laminin or PDL beforehand. Cell growth and density was compared visually for all conditions and exemplary images taken with a brightfield microscope over a time of two weeks (DIV = days in vitro) at 10x and 40x magnification. White arrow = poorly attached/dead cells.

Besides the analysis of cellular appearance and morphology by brightfield microscopy, the specificity of the cell types was furthermore verified by immunocytochemistry.

For this, neurons and astrocytes were plated on spatially separated glass coverslips and incubated as co-culture under NOX conditions until neurons fully matured. Then, coverslips were separated and both populations were stained individually for different cell-type specific markers such as bIII-TUBULIN (microtubules) and SYNAPSIN (synapses) for neurons and GFAP (intermediate filament) for astrocytes. Figure 3.24 shows representative images of the neuron and astrocyte staining. As shown, the neuron compartment indeed mostly features neuronal cells with clearly visible cell bodies, dendritic branches and synapses. The astrocyte compartment primarily features GFAP-positive cells that resemble astrocytes. Therefore, the culture indeed consists of the desired cell types.

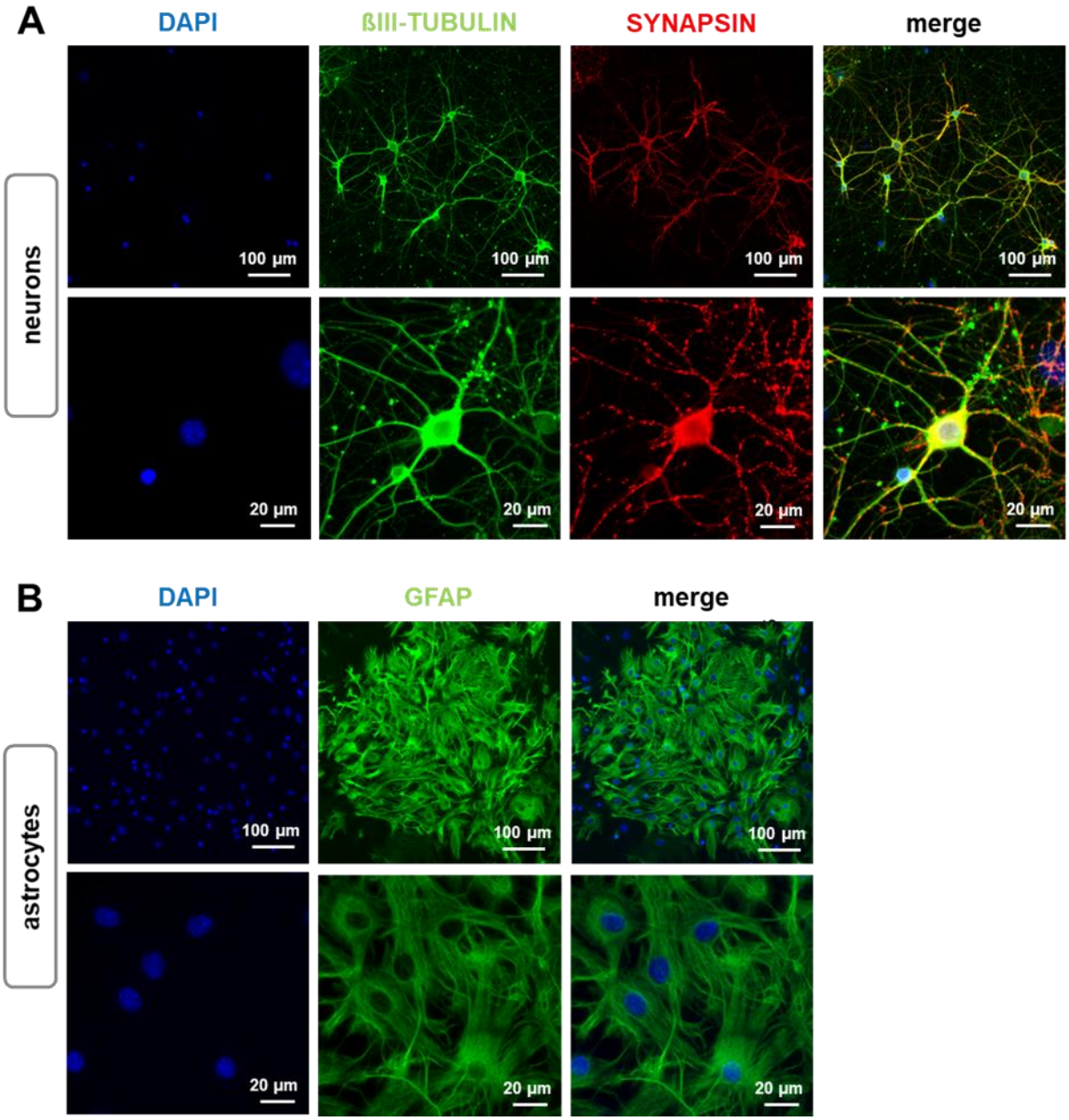

Figure legend on next page.

Figure 3.24: Immunofluorescence staining of neurons and astrocytes.
Hippocampal neurons and cortical astrocytes were grown in a co-culture system in spatial distance until neurons were fully mature, followed by immunocytochemistry for cell type-specific markers. Depicted are single channels and merged channels, scale bars are as indicated.
A: Representative images of the neuronal culture, stained with DAPI (nuclei), ßIII TUBULIN (microtubules, neuron-specific) and SYNAPSIN (synapses).
B: Representative images of the astrocyte culture, stained with DAPI and GFAP (intermediate filament, mainly astrocyte-specific).

Please note that both cell cultures are not completely pure as the cells were generated out of whole tissue and the domination of a specific cell type is mainly achieved through specific coating and media composition. Especially the astrocyte compartment tends to be overgrown by microglia, which is tried to be prevented through AraC treatment at 4 DIV.

The establishment process for the neuron-astrocyte co-culture was mostly performed using WT neurons. Of course, after optimal culture conditions were implemented, the maturation of neurons was also monitored in HIF-2α KO cells, as seen in Figure 3.25. HIF-2α KO neurons thereby showed a similar appearance as WT neurons, with attached cells and dendrite formation as early as 1 DIV and well-formed dendritic networks over a time course of 14 DIV. By eye, no difference was observed between WT and HIF-2α KO neuronal growth under standard normoxic conditions.

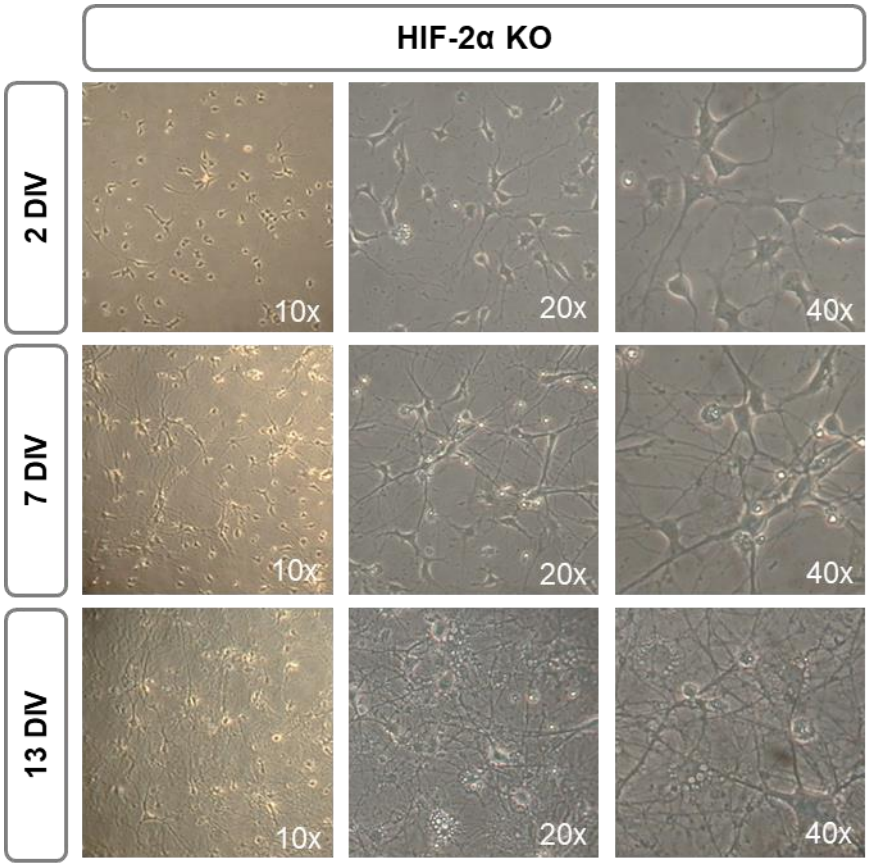

Figure 3.25: Exemplary brightfield images of maturing hippocampal HIF-2α KO neurons.
Hippocampal neurons of HIF-2α KO embryos were seeded in a neuron-astrocyte co-culture system and neuronal growth and maturation monitored over 13 DIV (days in vitro). Exemplary images were taken at 10x, 20x and 40x magnification.

All testing and optimization was performed under standard cultivation conditions with ambient oxygen concentrations. However, further experiments were planned to be performed under hypoxic conditions as well, which are known to lead to changes in neuronal activity, metabolism or even neuronal cell death.

Therefore, it was tested how the neurons cope with 1% oxygen (HOX) for up to 48 h in comparison to neurons that maintained at NOX conditions. By looking at the morphology of the cells in a brightfield microscope at the end of the incubation time, morphological changes were visible in terms of reduced or degenerated dendrites that appeared more frizzy, although the general neuronal architecture was still intact (Figure 3.26).

These results suggest that 1% HOX incubation is sufficiently tolerated by the neurons, especially as the following experiments were conducted with only 24 h instead of longer hypoxic incubation.

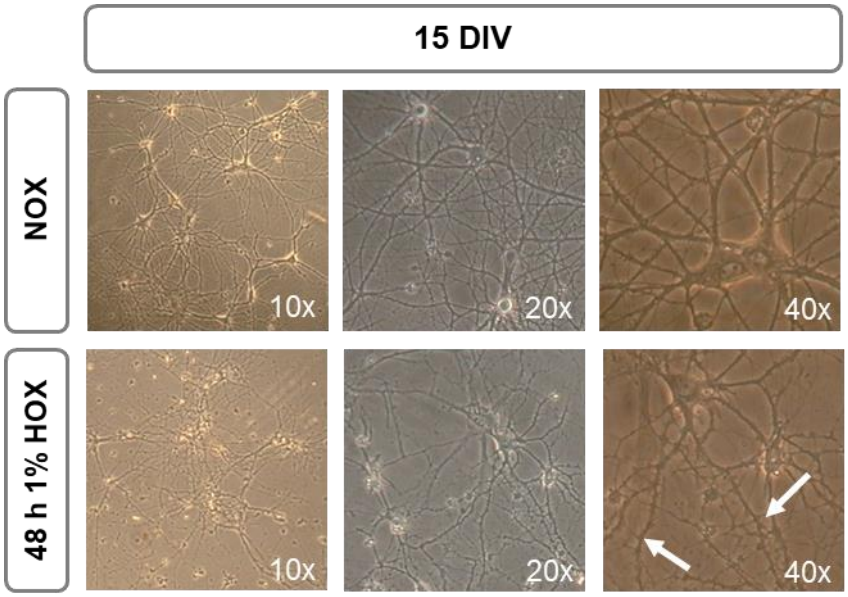

Figure 3.26: Exemplary brightfield images of WT neurons under normoxic or hypoxic incubation.
Hippocampal neurons of WT embryos were seeded in a neuron-astrocyte co-culture system and grown for 13 DIV (days in vitro) under normoxic (NOX) conditions. Then, cells were split into 48 h of further NOX incubation or 48 h of incubation with 1% oxygen (= hypoxia/HOX). Exemplary brightfield images were taken at 10x, 20x and 40x magnification at the end of the incubation time. White arrows = degenerated dendrites.

Please note that the neuron-astrocyte co-culture is still sensitive and the survival and maturation of the neurons is also depending on for example the quality of the seeded astrocytes, the researcher performing the experiments, the coating efficiency or some other stress factors. The quality of each culture was therefore always checked by brightfield microscopy before experiments were performed. One problem that could occur was clustering and aggregation of neurons (as depicted in supplementary Figure 6.8), which was independent of the neuronal or astrocytic genotype and can be a sign of poor coating or other stress factors.

A final important factor for establishing a working neuron-astrocyte co-culture system was the generation of RNA samples out of these cells. It was incidentally shown in different independent experiments, that neuronal RNA of sufficient quality could not be extracted via the standard phenol-chloroform extraction used in the research group (Figure 3.27). Every attempt to generate cDNA using this RNA samples failed. On the contrary, neuronal RNA extracted using a commercial kit from Macherey & Nagel was suitable for successful generation of cDNA. For corresponding astrocytes that were in co-culture together with the respective neurons, both isolation methods worked fine, which served as a control that the observed problems were indeed specific for neurons.

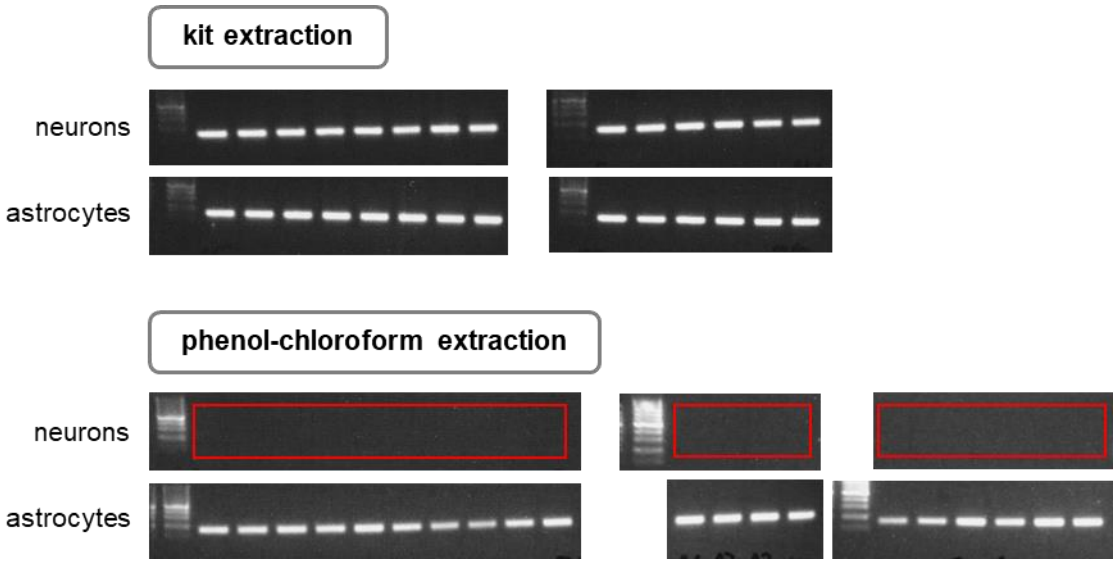

Figure 3.27: Neuron and astrocyte cDNA analysis of kit-extracted or phenol-chloroform-extracted RNA samples.

RNA of neurons and astrocytes was either isolated with a kit or by phenol-chloroform extraction and transcribed into cDNA by reverse transcription. The efficiency of cDNA synthesis was verified by standard PCR using a HKG, followed by separation in an agarose gel electrophoresis and visualization with UV light. The neuron and corresponding astrocyte samples are vertically aligned and belong to the same culture dish. Red squares = missing signals of neuronal cDNA after phenol-chloroform extraction of RNA.

3.2.2. Establishment of an experimental set-up and induction of hypoxic target genes in neurons and astrocytes

After successful establishment of the neuron-astrocyte co-culture, the next step was to investigate on the hypoxic response in these cell types, as the experiments were also planned to be performed under hypoxic conditions.

Astrocytes play a crucial role in regulation of the homeostasis of the central nervous system and in regulation of oxidative stress responses. It is also known that under hypoxia, astrocytes secrete for example VEGF and EPO (for review, see Vangeison and Rempe, 2009). A trial

experiment was performed to test under which oxygen concentrations and over which time course cortical astrocytes react with an upregulation of hypoxic target genes. Therefore, WT neurons and WT astrocytes were co-cultivated for 12 DIV and subsequently split into three different cultures that were incubated under normoxic (21% O_2), mild hypoxic (10% O_2) and hypoxic (1% O_2) conditions for 72 h. RNA samples were collected at different time points and expression of the hypoxia-inducible target genes *Vegf* and *Phd3* was analyzed in the WT astrocytes by qPCR (Figure 3.28).

At 10% oxygen levels, the astrocytes showed no induction of hypoxia-related genes in total. Only a slight induction of *Vegf* expression was visible at 1 h of 10% HOX incubation that was not longer observed at the later time points. *Phd3* gene expression showed no induction at all at 10% O_2. When looking at incubation with 1% oxygen, a high induction was seen for both *Vegf* and *Phd3* expression that peeked at 48 h for *Vegf* with a fold change of 6.6 and at 24 h for *Phd3* with a fold change of 9.1. For both genes, the beginning induction of the gene expression was seen after 4 h of incubation whereas 72 h of 1% HOX led to almost basal levels of *Vegf* and *Phd3* again.
In summary, 10% oxygen was not sufficient to initiate a hypoxic response in WT astrocytes whereas 1% oxygen levels led to an increase in hypoxic target genes, with the response finished after 72 h.

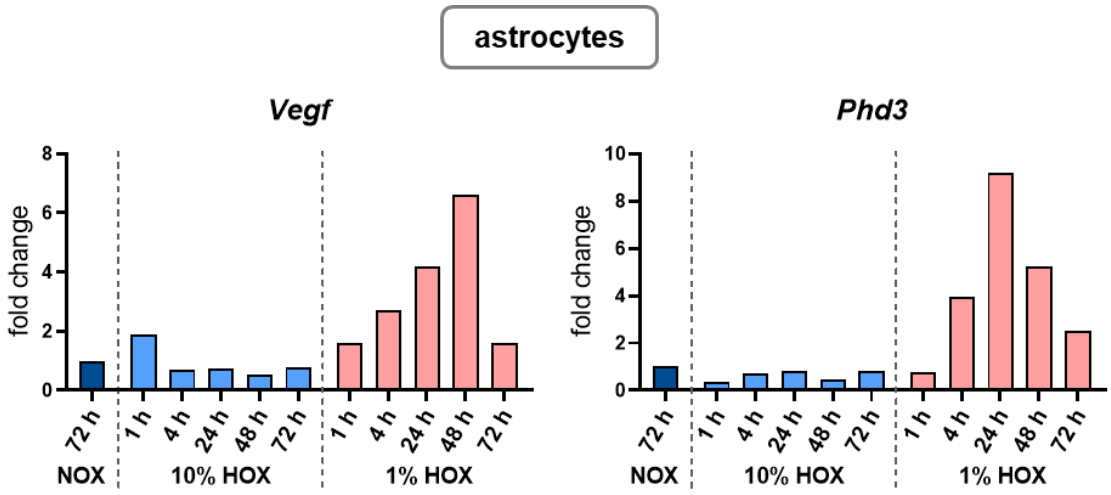

Figure 3.28: Pilot experiment for the expression of hypoxic target genes in astrocytes at different O_2 levels. A neuron-astrocyte co-culture was cultured for 12 DIV under standard conditions before splitting the culture up to more normoxic (NOX, 21% O_2), 10% O_2 or 1% O_2 (hypoxia = HOX) incubation for up to 72 h. RNA samples were collected for WT astrocytes at different time points. The expression of the hypoxia-inducible target genes *Vegf* and *Phd3* was assessed by qPCR. Values were normalized to *Rpl13a* as HKG and changes in gene expression calculated as x-fold changes relative to the 72 h NOX control sample using the 2^-ΔCt method.

Next, the time course of the hypoxic response of both astrocytes and neurons was studied in more detail for 1% oxygen levels. As the astrocytic reaction to 1% oxygen was diminished after 72 h of incubation (Figure 3.28), here time points up to 48 h were examined and additional time points at the beginning of hypoxic response were analyzed.

Again, WT astrocytes showed a robust hypoxic response in terms of up-regulation of the target genes *Vegf*, *Phd2* and *Phd3* (Figure 3.29 A). *Vegf* expression was significantly induced after 4 h of incubation with fold changes around 40 while at later time points, expression stayed on a constant level with a more or less 20-fold induction. *Phd2* expression increased gradually up to its highest and significant peak at 24 h of hypoxia (fold change 4.7) whereas *Phd3* up-regulation started slightly earlier and reached the first significant difference to normoxic control levels after 4 h. *Phd3* expression thereby peaked at 6 h of hypoxic incubation and slowly decreased from that time on, while still being significantly up-regulated at the end of the time course.

As the WT neuronal induction was tested in only one pilot experiment, no statistical analysis was performed here. Therefore, only the general trend in the expression of *Vegf*, *Phd2* and *Phd3* in neurons was observed (Figure 3.29 B). *Vegf* expression was first increased after 4 h of HOX, peaked at 6 h with a fold change of 3.2 and then gradually decreased until reaching basal levels again after 48 h HOX. Changes in *Phd2* and *Phd3* expression were first observed after 6 h HOX and kept constant levels up to the 48 h of hypoxic incubation. *Phd2* expression was up-regulated by a maximum fold change of 2.05 and *Phd3* with a fold change of 2.6.

Especially *Phd3* and *Vegf* up-regulation was more prominent in astrocytes compared to neurons. Nevertheless, both cell types reacted to the 1% hypoxic incubation through up-regulation of hypoxia target genes, especially in the first 24 h of incubation. In addition, as ongoing hypoxic incubation is not beneficial for neuronal and astrocytic survival, the following experiments focus on the first 24 h of hypoxic response, starting with the analyses from 4 h HOX onward.

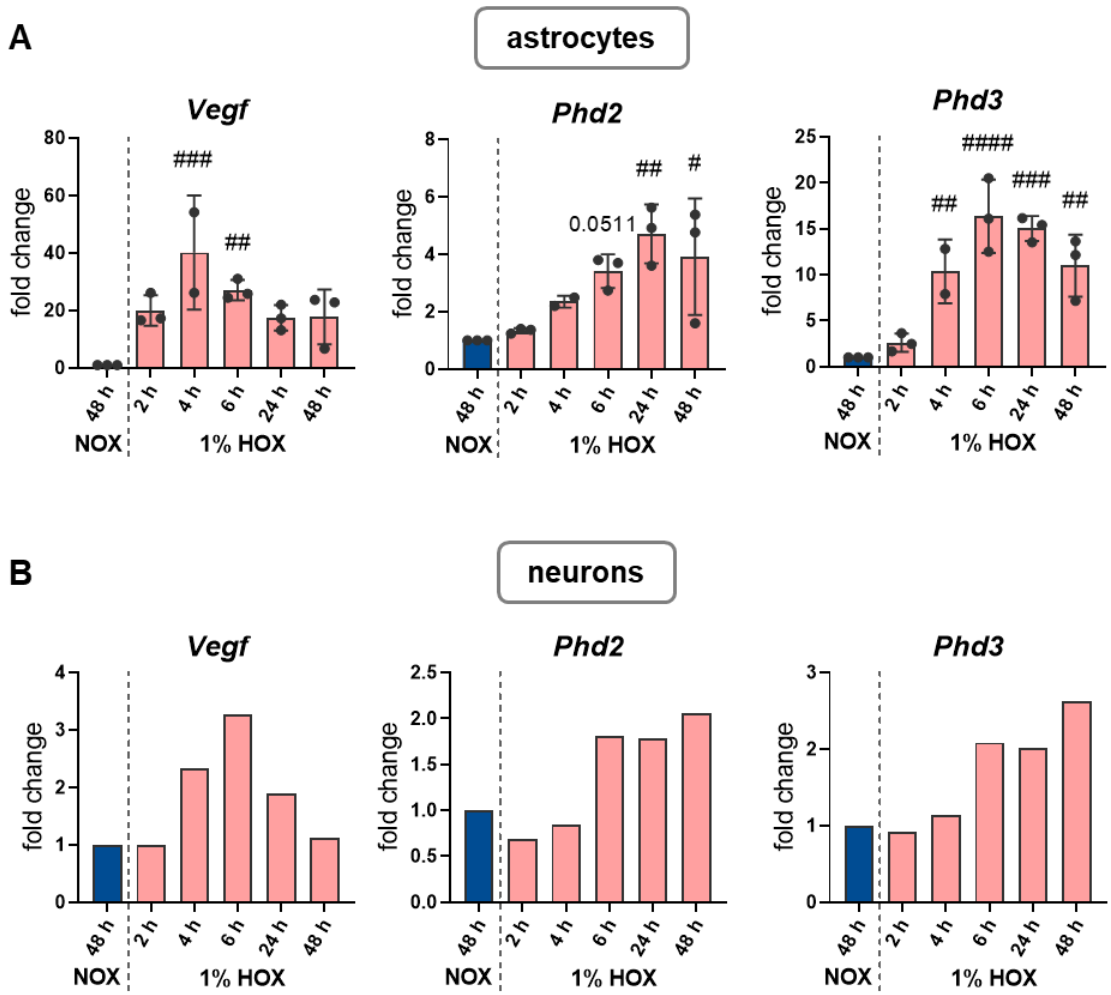

Figure 3.29: Timed expression of hypoxic target genes in astrocytes and neurons at 1% O_2.

A neuron-astrocyte co-culture was cultured for 12 DIV under standard conditions before splitting the culture for normoxic (NOX, 21% O_2) or hypoxic (HOX, 1% O_2) incubation for up to 48 h. RNA samples were collected at different time points and the expression of hypoxia-inducible target genes like *Vegf*, *Phd2* and *Phd3* was assessed by qPCR. Values were normalized to *Rpl13a* as HKG and changes in gene expression calculated as x-fold changes relative to the 48 h NOX control sample using the 2^-ΔCt method.

A: Expression in WT astrocytes. Mean ± SD, $p < 0.05$ = #, $p < 0.01$ = ##, $p < 0.001$ = ### and $p < 0.0001$ = #### to the 48 h NOX control, n = 3.

B: Expression in WT neurons, n = 1.

3.2.3. HIF-2α KO efficiency in neurons and astrocytes under NOX and HOX conditions

WT and HIF-2α KO neurons were co-cultured with WT or HIF-2α KO astrocytes in four different combinations (WT neurons + WT astrocytes, HIF-2α KO neurons + WT astrocytes, WT neurons + HIF-2α KO astrocytes, HIF-2α KO neurons + HIF-2α KO astrocytes). This enables to look for both effects of the genotype of the neurons itself but also on effects of the genotype of the astrocytes on the neurons. After 12 DIV of normoxic incubation, the different co-cultures

were incubated at 1% HOX for 24 h and RNA and protein samples of both neurons and astrocytes were collected separately in duplicates at 0 h (= NOX control), 4 h, 8 h and 24 h. Therefore, the independent analysis of the different cell populations was possible. The analyzed cell type is always depicted on top of the figures and furthermore indicated in bold letters in the figure legend.

First, the HIF-2α KO efficiency was analyzed in both cell types by expression analysis of the *Hif-2α exon 2*. In total, the expression in both astrocytes (Figure 3.30 A) and neurons (Figure 3.30 B) remained constant over the 24 h of HOX incubation. Furthermore, HIF-2α KO astrocytes exhibited a significant down-regulation of *Hif-2α exon 2* at all time-points compared to WT astrocytes that were in co-culture with genotypic identical neurons as the HIF-2α KO astrocytes. When looking at the neurons, HIF-2α KO neurons also showed a good overall KO efficiency. For neurons in co-culture with WT astrocytes, the down-regulation of *Hif-2α exon 2* in the HIF-2α KO neurons was visible, though not statistically significant, whereas for neurons in co-culture with HIF-2α KO astrocytes, the HIF-2α KO efficiency was statistically significant. As the astrocytes and neurons are initially seeded out in different 12-well plates and at different time-points, a possible interference of the astrocytic WT genotype on the outcome of the neuronal KO efficiency was ruled out. In summary, the HIF-2α KO efficiency was good and sufficient for both astrocytes and neurons.

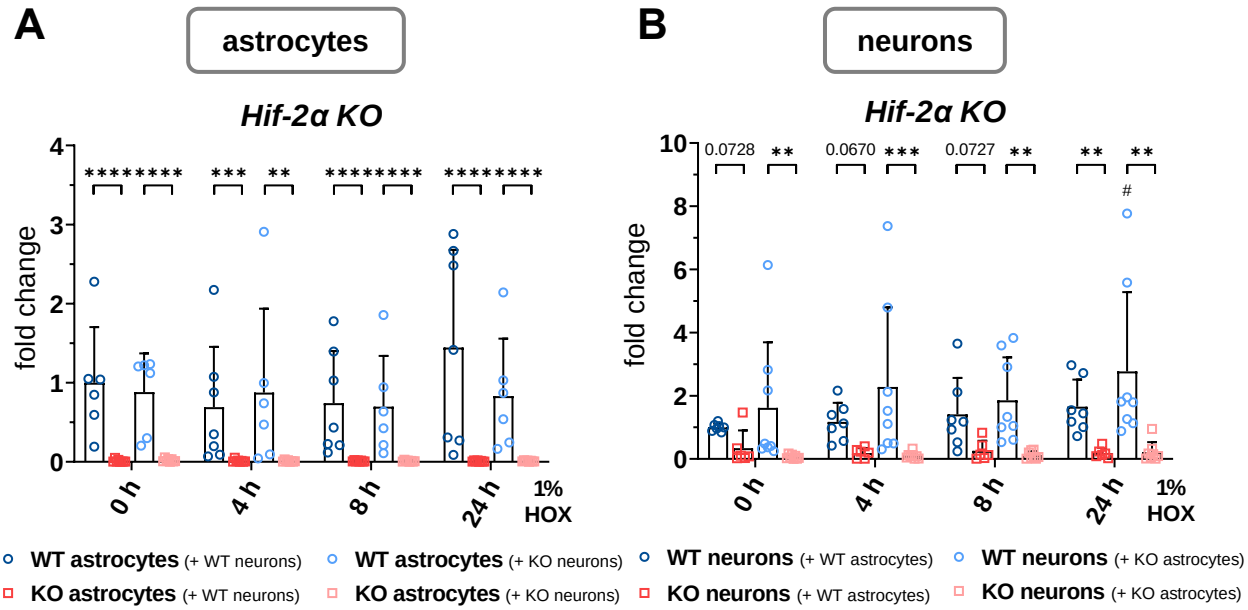

Figure 3.30: HIF-2α KO efficiency in neurons and astrocytes under NOX and HOX conditions.
Combinations of WT/HIF-2α hippocampal neurons and WT/HIF-2α KO astrocytes were co-cultured for 12 DIV under normoxic (NOX, 21% O_2) conditions, followed by hypoxic incubation (HOX, 1% O_2) for 24 h. RNA samples were collected at 0 h (NOX control), 4 h, 8 h and 24 h of hypoxia. HIF-2α KO efficiency was assessed in astrocytes (A) and neurons (B) by qPCR. Values were normalized to *ribProt* as HKG and changes in gene expression calculated as x-fold changes relative to the 0 h control of WT neurons + WT astrocytes using the 2^-ΔCt method. Mean + SD, $p < 0.01$ = **, $p < 0.001$ = *** and $p < 0.0001$ = ****, n = 6 - 8 in 3 independent experiments per genotype combination.

3.2.4. Stability of neuronal and astrocytic marker expression over the experimental time course

The NOX/HOX experiments were conducted after 12 DIV, when most neurons were fully developed. To validate that possible changes in expression levels of certain genes over the time of hypoxia are indeed hypoxia-related and not due to further developmental processes of the neurons independent of hypoxia, a part of the co-culture was also maintained for additional 24 h of NOX incubation and RNA and protein samples collected. For both astrocytes and neurons, the expression of certain markers was then analyzed for changes over the time course.

For astrocytes, the expression of *Gfap* remained stable between 0h NOX and 24 h NOX for all combinations of the co-culture approach. Furthermore, there were no differences between WT and HIF-2α KO astrocytes (Figure 3.31 A).

For neurons (Figure 3.31 B), the general neuronal marker *bIII Tubulin* was analyzed, which showed a constant expression between WT and HIF-2α KO neurons, independent of the co-cultured astrocytic genotype. After 24 h of incubation, an induction in *bIII Tubulin* expression was seen for the WT neurons/KO astrocytes combination, but overall, expression remained stable over time. In addition, the expression of synapse-associated genes of both pre- (*Synapsin*) and post-synaptic (*Nrgn* = Neurogranin, *Psd95*, *Gphn* = Gephyrin) compartments were analyzed - *Psd95* thereby as a component of excitatory synapses, *Gphn* of inhibitory synapses. For all tested genes, the expression remained constant between 0 h NOX and 24 h NOX for all tested co-culture combinations. Although no significant differences of the expression levels between WT and HIF-2α KO neurons itself were visible, the astrocytic genotype appears to have an influence on the *Nrgn* expression of neurons, as neurons of both genotypes showed a tendency to express higher levels of *Nrgn* when co-cultured with HIF-2α KO astrocytes.

In summary, astrocytes and neurons were stable over the time of the NOX/HOX experiments and potential changes in expression levels are mainly effects of hypoxia and not time in general.

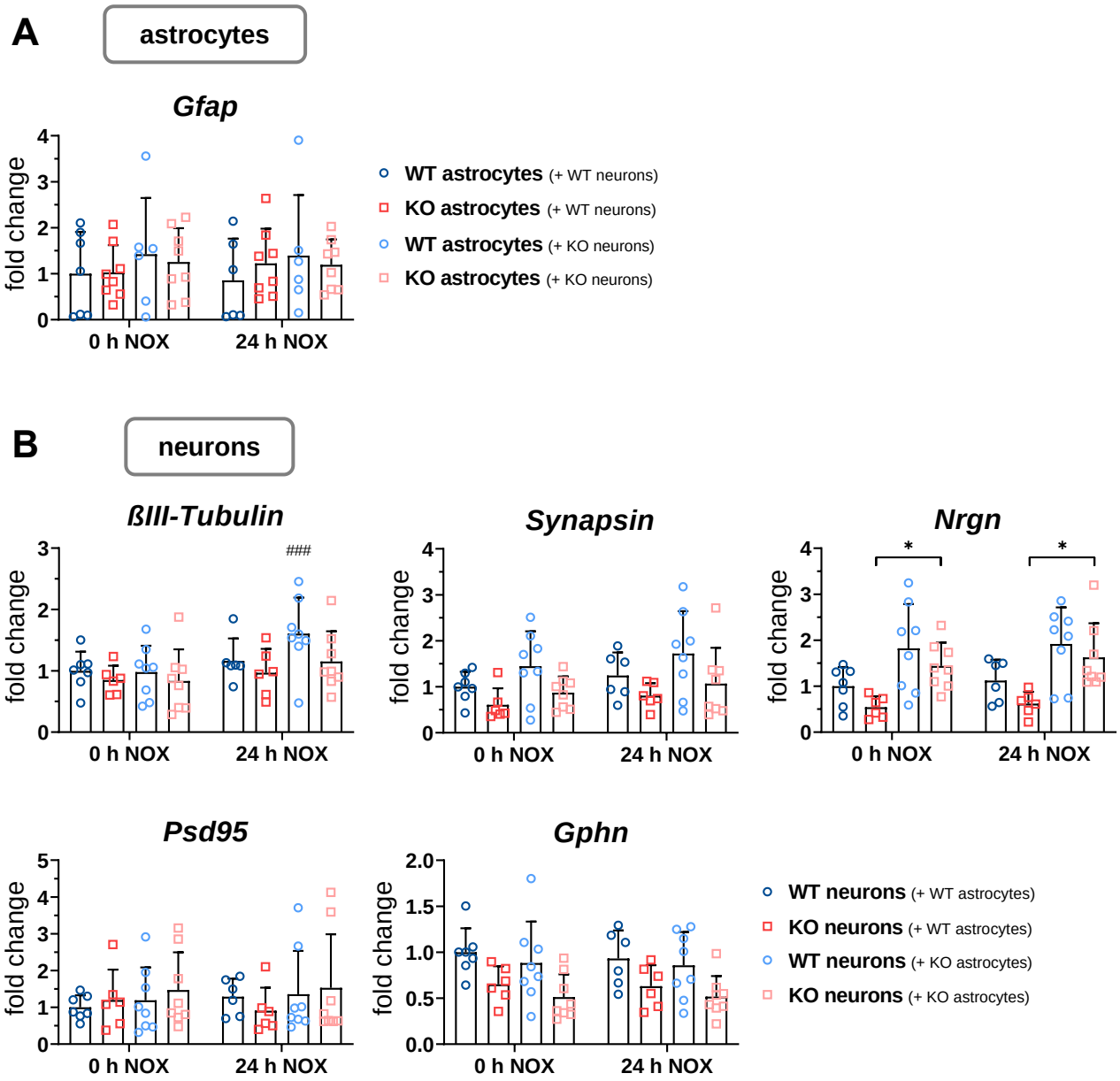

Figure 3.31: Stability of gene expression levels for astrocytic and neuronal markers under normoxic culture conditions.

Combinations of WT/HIF-2α hippocampal neurons and WT/HIF-2α KO astrocytes were co-cultured for 12 DIV under normoxic (NOX, 21% O_2) conditions. For comparison with cells that then underwent 24 h of hypoxic incubation (1% O_2), control cells also stayed in NOX for additional 24 h. RNA samples were collected at beginning (0 h) and end (24 h) of experiment and the expression of selected marker genes was assessed by qPCR for both astrocytes (A) and neurons (B). Values were normalized to *ribProt* as HKG and changes in gene expression calculated as x-fold changes relative to the 0 h control of WT neurons + WT astrocytes using the 2^-ΔCt method. Mean + SD, $p < 0.05$ = * between genotypes, $p < 0.001$ = ### to the respective 0 h time point, n = 6 - 8 in 3 independent experiments per genotype combination.

3.2.5. Quantitative analysis of synapse-associated and hypoxia-inducible genes in WT and HIF-2α KO astrocytes under HOX conditions

Next, the expression of hypoxia-inducible target genes was analyzed in WT and HIF-2α KO astrocytes (Figure 3.32 A). For better comparison, the layout of the graph was changed so the hypoxic up-regulation inside one co-culture combination over time and an overall effect of astrocyte genotype is better visualized. Both WT and HIF-2α KO astrocytes showed a significant up-regulation of *Vegf*, *Epo*, *Phd2* and *Phd3* over the 24 h of hypoxic incubation in comparison to the 0 h starting point. The highest induction of gene expression was seen for *Vegf* and *Phd3* (both with over 10-fold induction), whereas *Epo* expression was induced up to 5-fold and *Phd2* expression up to 10-fold. The up-regulation of all tested hypoxia target genes was still persistent at 24 h HOX or even peaked after 24 h as seen for the expression of *Phd2*. The neuronal genotype did not affect the expression levels in the astrocytes, but the astrocytes themselves showed significant differences between WT and HIF-2α KO cells. HIF-2α KO astrocytes showed an overall significantly diminished up-regulation of *Vegf* and *Epo* in comparison to WT cells. The *Vegf* expression in WT astrocytes reached for example induction levels of up to 25-fold for single samples whereas the highest induction in KO cells was 11.95-fold. This indicates a partial HIF-2α-dependent expression of both genes. There seems to be a similar tendency for *Phd3* expression, although the differences were not statistically different. The *Phd2* up-regulation, on the other hand, was overall significantly higher in the HIF-2α KO astrocytes compared to the WT cells, thereby showing an opposite effect in comparison to *Vegf* and *Epo* expression.

Overall, the differences between WT and HIF-2α KO astrocytes in *Vegf* and *Epo* could also be the result of a temporally delayed hypoxic response. As the up-regulation of target genes was still persistent after 24 h, it is unknown if for example *Vegf* expression in KO astrocytes would later also reach induction levels comparable to the WT astrocytes. On the other hand, *Phd2* induction was initially stronger in HIF-2α KO astrocytes which speaks against a sole delay.

Furthermore, the expression levels of *Gfap* were compared (Figure 3.32 B). The genotype of neither neurons nor astrocytes had an influence on *Gfap* expression in astrocytes. Only the hypoxic incubation itself showed an effect, as for all co-culture combinations there was a (sometimes significant) down-regulation of *Gfap* after 24 h of HOX.

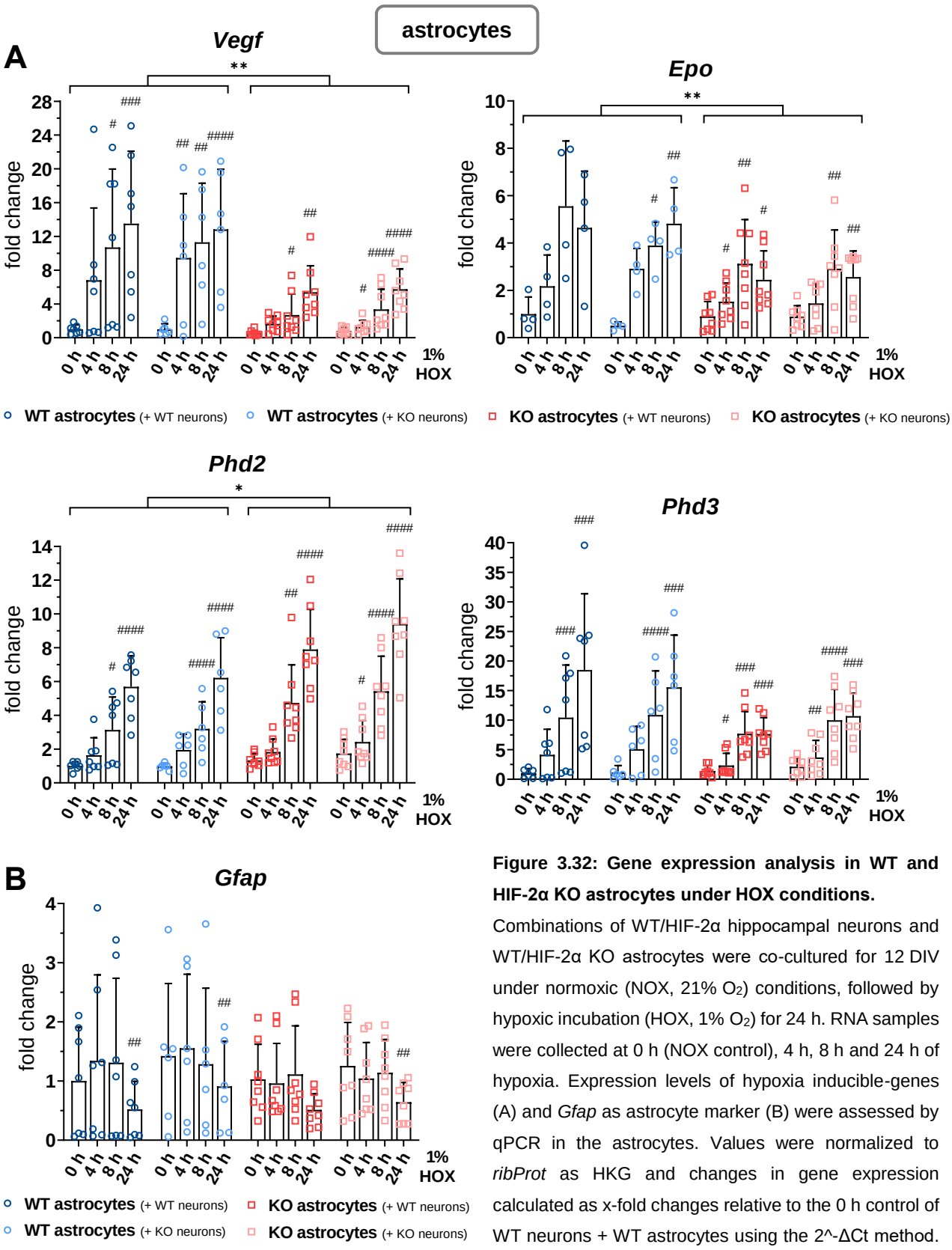

Figure 3.32: Gene expression analysis in WT and HIF-2α KO astrocytes under HOX conditions.

Combinations of WT/HIF-2α hippocampal neurons and WT/HIF-2α KO astrocytes were co-cultured for 12 DIV under normoxic (NOX, 21% O_2) conditions, followed by hypoxic incubation (HOX, 1% O_2) for 24 h. RNA samples were collected at 0 h (NOX control), 4 h, 8 h and 24 h of hypoxia. Expression levels of hypoxia inducible-genes (A) and *Gfap* as astrocyte marker (B) were assessed by qPCR in the astrocytes. Values were normalized to *ribProt* as HKG and changes in gene expression calculated as x-fold changes relative to the 0 h control of WT neurons + WT astrocytes using the 2^-ΔCt method. Mean + SD, $p < 0.05$ = *, $p < 0.01$ = **, $p < 0.001$ = *** and $p < 0.0001$ = ****, * between astrocyte genotype as indicated, # compared to the 0 h control of the same co-culture combination. n = 6 - 8 in 3 independent experiments per genotype combination.

As mentioned earlier (1.3.2), the adenosine signaling system is important for synaptic function and adenosine receptors on both neurons and astrocytes might correlate with HIF functions. Therefore, expression levels of two main adenosine receptors of the CNS were assessed (Figure 3.33). Altogether, *Adora1* expression levels were not up-regulated under hypoxic conditions, but, if at all, rather down-regulated - this being even significant for the KO astrocytes/WT neurons combination after 24 h of hypoxic incubation. The expression levels of *Adora1* were furthermore comparable between the different astrocytic genotypes, although the results of HIF-2α KO astrocytes exhibited an overall higher standard deviation.

Adora2a expression was significantly induced under hypoxic conditions, especially after 8 h and 24 h of incubation. No differences were seen for WT and HIF-2α KO astrocytes and the neuronal genotype did not affect the astrocytic *Adora2a* expression further.

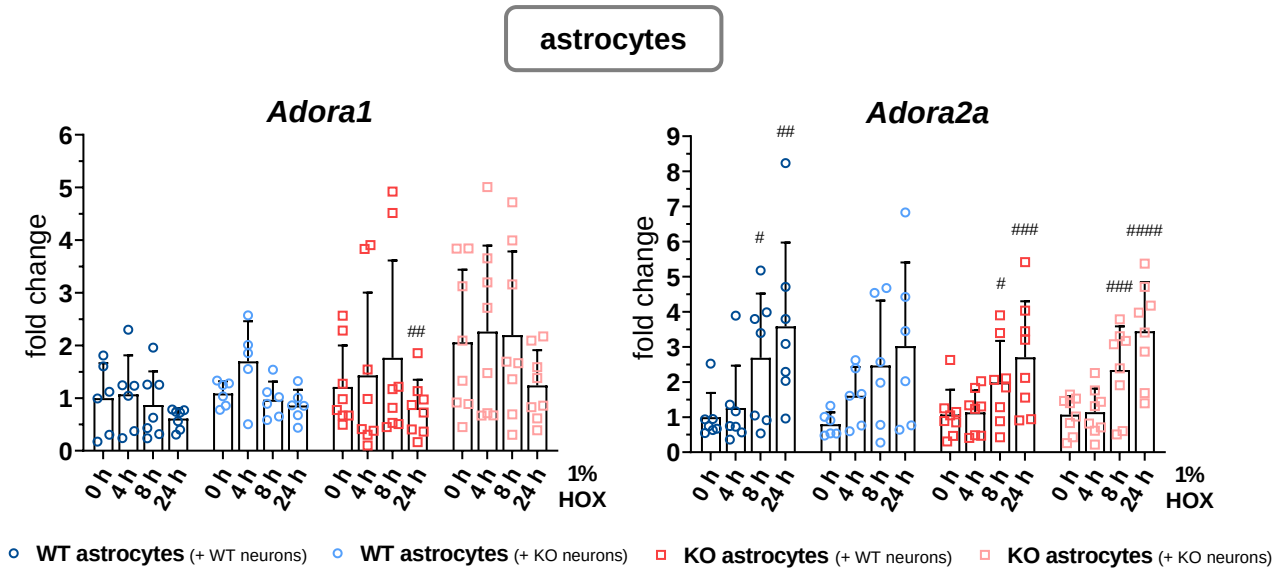

Figure 3.33: Gene expression analysis of adenosine receptors in WT and HIF-2α KO astrocytes under HOX conditions.

Combinations of WT/HIF-2α hippocampal neurons and WT/HIF-2α KO astrocytes were co-cultured for 12 DIV under normoxic (NOX, 21% O_2) conditions, followed by hypoxic incubation (HOX, 1% O_2) for 24 h. RNA samples were collected at 0 h (NOX control), 4 h, 8 h and 24 h of hypoxia. Expression levels of the adenosine receptors *Adora1* and *Adora2a* were assessed by qPCR in the astrocytes. Values were normalized to *ribProt* as HKG and changes in gene expression calculated as x-fold changes relative to the 0 h control of WT neurons + WT astrocytes using the 2^-ΔCt method. Mean + SD, $p < 0.05$ = #, $p < 0.01$ = ##, $p < 0.001$ = ### and $p < 0.0001$ = ###, compared to the 0 h control of the same co-culture combination. n = 6 - 8 in 3 independent experiments per genotype combination.

3.2.6. HIF-1α and HIF-2α protein and gene levels in WT and HIF-2α KO astrocytes under HOX conditions

As the WT and HIF-2α KO astrocytes showed differences in the induction of hypoxic target genes, the protein levels of HIF-1α and HIF-2α were analyzed by Western Blotting. This was done to test if the stabilization of the HIF proteins over the hypoxic time course was different due to potential changes in regulatory feedback-loops or compensatory mechanisms in the HIF-2α KO astrocytes.

Figure 3.34 shows exemplary images of the Western Blot membranes as well as the semi-quantitative analysis of HIF-1α and HIF-2α levels for both WT (A) and HIF-2α KO (B) astrocytes in co-culture with either WT or HIF-2α KO neurons.

WT astrocytes showed a significant induction of HIF-2α protein, which was still high after 24 h of HOX incubation. On the contrary, HIF-1α levels remained stable over the hypoxic time course. Interestingly, HIF-1α levels were already present at the 0 h HOX time-point, indicating that the astrocytes, which are at the bottom of the co-culture sandwich approach, might exhibited a mild hypoxia even under 21% atmospheric oxygen levels. Nevertheless, the HOX target gene induction was still significant in the astrocytes at 1% O_2 (Figure 3.32) suggesting that they still showed a higher hypoxic response when cultured under hypoxic cell culture conditions.

A similar result was seen for the HIF-1α levels of the HIF-2α KO astrocytes. Again, HIF-1α protein was detectable even at NOX conditions and the protein levels did barely rise over the hypoxic time course for HIF-2α KO astrocytes that had been co-cultured with WT neurons. Interestingly, an induction of HIF-1α protein levels was seen for HIF-2α KO astrocytes that had been in co-culture with HIF-2α KO neurons.

Although the HIF2-2α KO astrocytes lack a functional version of HIF-2α, as the DNA binding domain is eliminated in the KO variant, it might still be detectable by Western Blotting, depending on the antigen epitope that is detected by the used antibodies. Here, the HIF-2α protein levels of the HIF-2α KO astrocytes remained at a low amount and did not rise significantly with ongoing hypoxia although there was also a tendency for an up-regulation in the HIF-2α KO astrocytes that had been co-cultured with HIF-2α KO neurons.

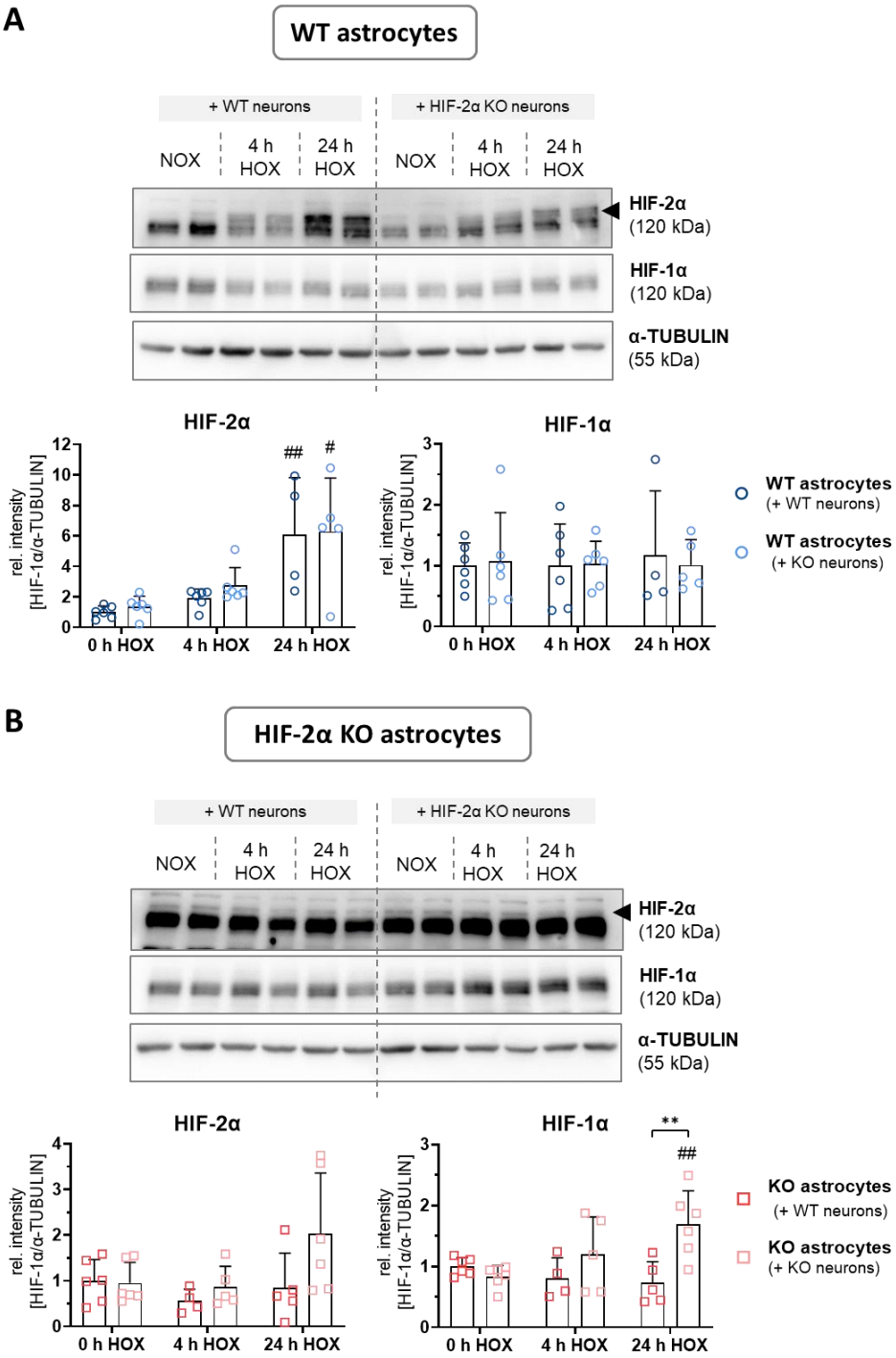

Figure 3.34: Western Blot analysis for HIF-1α and HIF-2α in WT and HIF-2α KO astrocytes under HOX conditions.

Combinations of WT/HIF-2α hippocampal neurons and WT/HIF-2α KO astrocytes were co-cultured for 12 DIV under normoxic (21% O_2) conditions, followed by hypoxic incubation (HOX, 1% O_2) for 24 h. Protein samples were collected at 0 h (control), 4 h and 24 h of hypoxia. HIF-1α and HIF-2α levels were analyzed by Western Blotting in the WT astrocytes (A) and HIF-2α KO astrocytes (B) and relative intensities were normalized to α-TUBULIN as HKG. Mean + SD, $p < 0.05$ = * and $p < 0.01$ = **, * between genotype, # compared to the 0 h control of the same co-culture combination. n = 4 - 8 in 3 independent experiments per genotype combination. Black arrowhead = height of the HIF-2α signal.

In addition to the Western Blot analysis of HIF proteins, gene expression of *Hif-1α* was assessed in the WT and HIF-2α KO astrocytes (Figure 3.35). Expression levels of *Hif-1α* in WT astrocytes did not change significantly during HOX incubation whereas HIF-2α KO astrocytes showed a significant up-regulation after 8 h of HOX incubation when incubated with WT neurons and after 8 h and 24 h of HOX incubation when incubated with HIF-2α KO neurons.This induction of gene expression over time correlates to the higher HIF-1α levels in the HIF-2α KO astrocytes (+ KO neurons) after 24 h of HOX incubation, which was seen in the Western Blot (Figure 3.34 B).

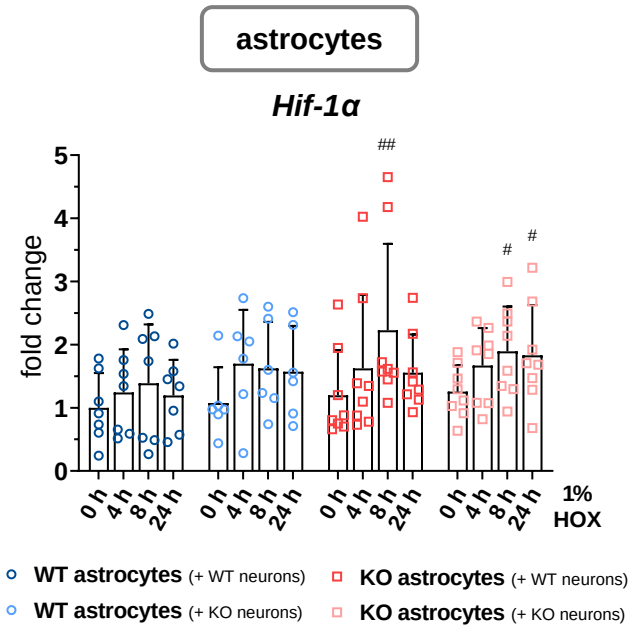

Figure 3.35: Hif-1α expression in WT and HIF-2α KO astrocytes under HOX conditions.
Combinations of WT/HIF-2α hippocampal neurons and WT/HIF-2α KO astrocytes were co-cultured for 12 DIV under normoxic (NOX, 21% O_2) conditions, followed by hypoxic incubation (HOX, 1% O_2) for 24 h. RNA samples were collected at 0 h (NOX control), 4 h, 8 h and 24 h of hypoxia. Expression levels of *Hif-1α* were assessed by qPCR in the astrocytes. Values were normalized to *ribProt* as HKG and changes in gene expression calculated as x-fold changes relative to the 0 h control of WT neurons + WT astrocytes using the 2^-ΔCt method. Mean + SD, $p < 0.05$ = # and $p < 0.01$ = ##, compared to the 0 h control of the same co-culture combination. n = 6 - 8 in 3 independent experiments per genotype combination.

3.2.7. Quantitative analysis of hypoxia-inducible genes in WT and HIF-2α KO neurons under HOX conditions

In addition to the gene expression analysis of hypoxia-inducible genes in astrocytes, the hypoxic response was furthermore studied in the WT and HIF-2α KO neurons of the respective cultures. Overall, both WT and HIF-2α KO neurons showed a significant induction of the hypoxia target genes *Vegf*, *Phd2* and *Phd3* and only a slight tendency for induction of *Epo* (Figure 3.36).

Besides a significant difference in gene expression of *Vegf* between WT neurons (+ KO astrocytes) and KO neurons (+ KO astrocytes) at 8 h of hypoxia, no differences between the two neuronal genotypes were observed and the hypoxic response followed a comparable kinetic and strength. The up-regulation of *Vegf*, *Phd2* and *Phd3* was still persistent at 24 h

HOX or even peaked after 24 h in case of *Phd2* and *Phd3* for all tested co-culture combinations.

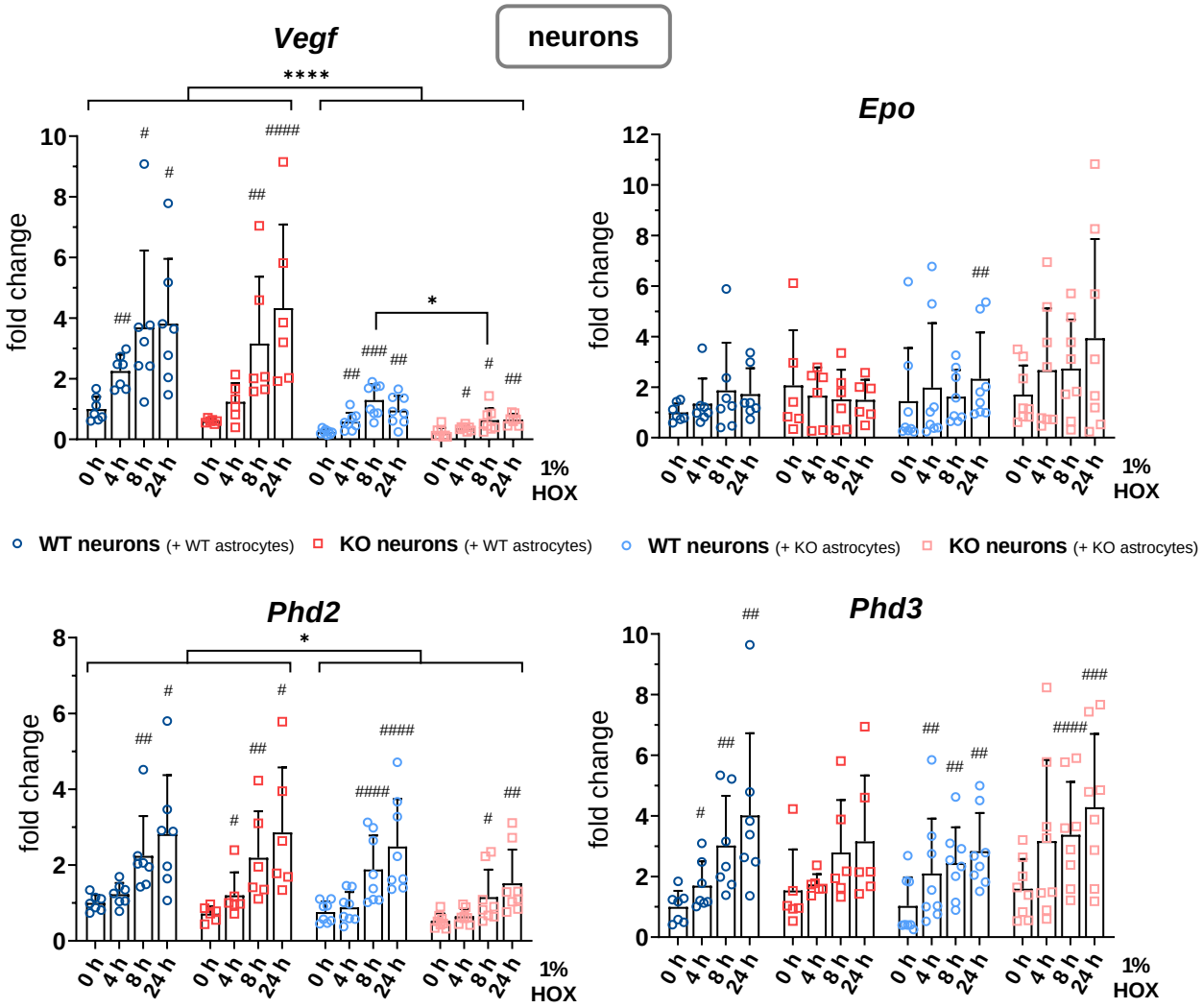

Figure 3.36: Gene expression analysis of hypoxia target genes in WT and HIF-2α KO neurons under HOX conditions.

Combinations of WT/HIF-2α hippocampal neurons and WT/HIF-2α KO astrocytes were co-cultured for 12 DIV under normoxic (NOX, 21% O_2) conditions, followed by hypoxic incubation (HOX, 1% O_2) for 24 h. RNA samples were collected at 0 h (NOX control), 4 h, 8 h and 24 h of hypoxia. Expression levels of hypoxia-inducible genes were assessed by qPCR in the neurons. Values were normalized to *ribProt* as HKG and changes in gene expression calculated as x-fold changes relative to the 0 h control of WT neurons + WT astrocytes using the 2^-ΔCt method. Mean + SD, $p < 0.05$ = *, $p < 0.01$ = **, $p < 0.001$ = *** and $p < 0.0001$ = ****, * between neuronal genotype as indicated, # compared to the 0 h control of the same co-culture combination. n = 6 - 8 in 3 independent experiments per genotype combination.

While seeing no effect of the neuronal genotype on the astrocytic hypoxia response (Figure 3.32), the opposite was observed for the neuronal hypoxia response (Figure 3.36). Here, the genotype of the astrocytes affected the gene expression of *Vegf* and *Phd2* in the neurons. Although still significantly induced over time in comparison to the 0 h control, the up-regulation of *Vegf* was significantly diminished in neurons that had been in co-culture with HIF-2α KO

astrocytes in comparison to neurons in co-culture with WT astrocytes. The same was seen for *Phd2* expression, although not as strongly as for *Vegf*. This suggests that astrocytes indeed affect and modulate neuronal adaptation mechanisms through paracrine effects and that astrocytic HIF-2α might be involved in this process.

3.2.8. Quantitative analysis of neuron- and synapse-associated genes in WT and HIF-2α KO neurons under HOX conditions

Kleszka *et al.* (2020) not only observed significant reductions in the expression of *bIII Tubulin*, *Nrgn* and *Synapsin* in vivo in the cortices of HIF-2α KO mice, but also found diminished expression levels of *Synapsin* and *Dap4* in HIF-2α KO neurospheres, where differentiating neurospheres were challenged with 1% O_2 and 0.2% O_2 for up to 72 h .

The expression of these genes was therefore also tested in the WT and HIF-2α KO neurons of the neuron-astrocyte co-cultures (Figure 3.37). In case of *bIII Tubulin*, *Synapsin* and *Dap4*, all co-culture combinations showed comparable expression levels at all tested time-points of hypoxic incubation. Whereas *bIII Tubulin* and *Synapsin* expression furthermore was constant over time, a slight decrease in *Dap4* expression was seen after 24 h of hypoxia, although this change was not statistically significant.

Nrgn gene expression showed a stronger reduction under prolonged hypoxia, with significant changes for WT neurons (+ KO astrocytes) and KO neurons (+ KO astrocytes), when comparing HOX cultured neurons with the respective 0 h control. Furthermore, the astrocytic genotype also seemed to influence the *Nrgn* expression as overall, *Nrgn* was significantly higher expressed in neurons that were co-cultured with HIF-2α KO astrocytes compared to neurons in co-culture with WT astrocytes.

Altogether, the high differences of *Synapsin* and *Dap4* expression in HIF-2α KO cells compared to WT cells that had been found in neurospheres were not visible in the single cell population co-culture model and neuronal HIF-2α did not influence the expression of these genes under NOX nor HOX conditions.

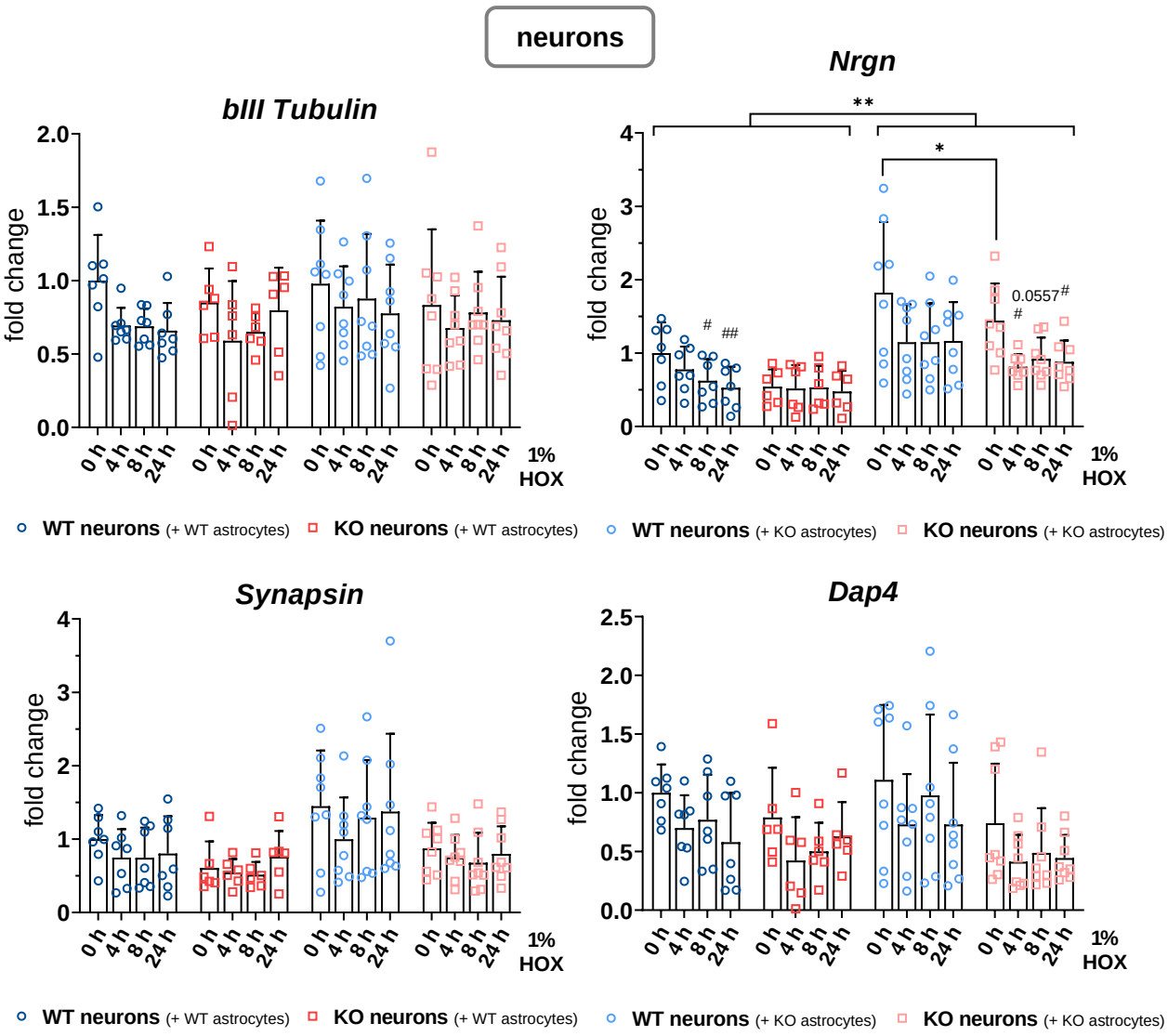

Figure 3.37: Gene expression analysis of potential HIF-2α-dependent neuronal genes in WT and HIF-2α KO neurons under HOX conditions.

Combinations of WT/HIF-2α hippocampal neurons and WT/HIF-2α KO astrocytes were co-cultured for 12 DIV under normoxic (NOX, 21% O_2) conditions, followed by hypoxic incubation (HOX, 1% O_2) for 24 h. RNA samples were collected at 0 h (NOX control), 4 h, 8 h and 24 h of hypoxia. Expression levels of neuronal and synapse-associated genes were assessed by qPCR in the neurons. Values were normalized to *ribProt* as HKG and changes in gene expression calculated as x-fold changes relative to the 0 h control of WT neurons + WT astrocytes using the 2^-ΔCt method. Mean + SD, $p < 0.05$ = *, $p < 0.01$ = **, * between neuronal genotype as indicated, # compared to the 0 h control of the same co-culture combination. n = 6 - 8 in 3 independent experiments per genotype combination.

Furthermore, the expression level of *Bdnf* growth factor was analyzed (Figure 3.38), which was also analyzed in the cortex and hippocampus of enriched and standard housed WT and HIF-2α KO mice in the environmental enrichment study. Under hypoxic conditions, the *Bdnf* expression in both WT and HIF-2α KO neurons was decreasing, with sometimes significant changes after 24 h of hypoxia compared to the 0 h controls. On the other hand, HIF-2α KO astrocytes had an beneficial effect on the *Bdnf* expression in neurons, independent of the neuronal phenotype, as the overall basal expression levels of *Bdnf* were higher in neurons co-cultured with HIF-2α KO astrocytes already at the beginning of the experiment.

Wnt7a expression was also slightly induced under hypoxia in neurons that were co-cultured with HIF-2α KO astrocytes whereas the overall basal levels were significantly reduced in comparison to neurons that were co-cultured with WT astrocytes. *Wnt7a* levels were assessed as it is associated with functions in for example progenitor cell and neuronal differentiation (Hirabayashi *et al.*, 2004; Lie *et al.*, 2005; Qu *et al.*, 2013) but also synaptic formation, maintenance or transmitter release (Ahmad-Annuar *et al.*, 2006; Lucas and Salinas, 1997).

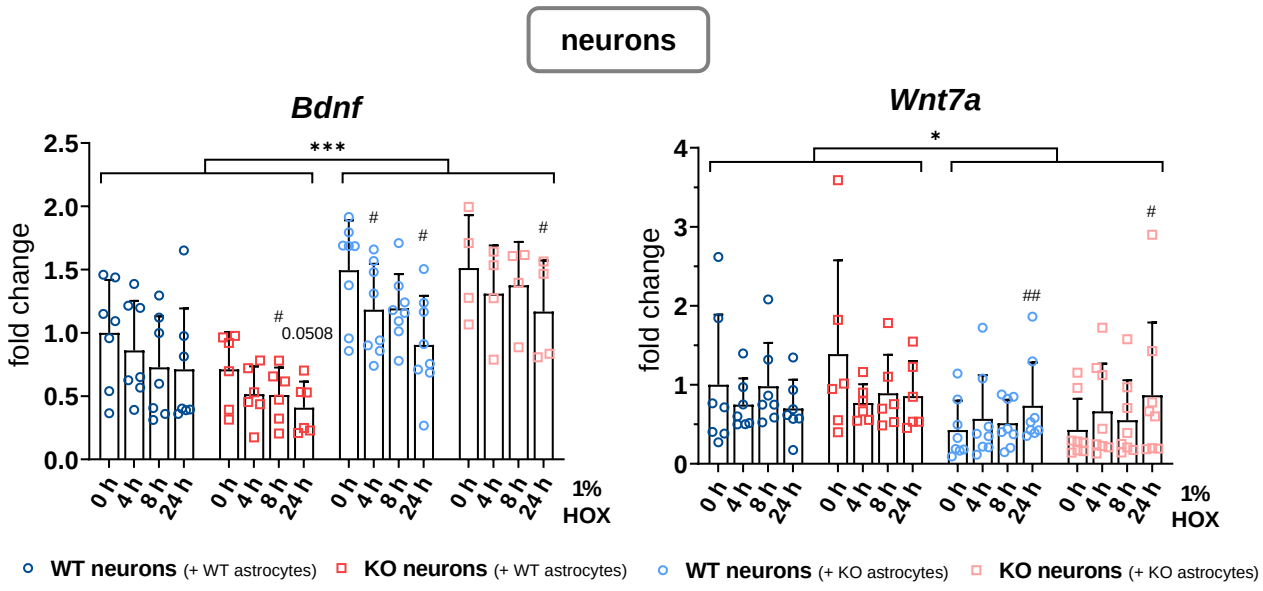

Figure 3.38: Gene expression analysis of *Bdnf* and *Wnt7a* in WT and HIF-2α KO neurons under HOX conditions.

Combinations of WT/HIF-2α hippocampal neurons and WT/HIF-2α KO astrocytes were co-cultured for 12 DIV under normoxic (NOX, 21% O_2) conditions, followed by hypoxic incubation (HOX, 1% O_2) for 24 h. RNA samples were collected at 0 h (NOX control), 4 h, 8 h and 24 h of hypoxia. Expression levels of growth factor *Bdnf* and Wnt signaling molecule *Wnt7a* were assessed by qPCR in the neurons. Values were normalized to *ribProt* as HKG and changes in gene expression calculated as x-fold changes relative to the 0 h control of WT neurons + WT astrocytes using the 2^-ΔCt method. Mean + SD, $p < 0.05$ = *, $p < 0.01$ = ** and $p < 0.001$ = ***, * between neuronal genotype as indicated, # compared to the 0 h control of the same co-culture combination. n = 6 - 8 in 3 independent experiments per genotype combination.

Next, it was assessed, whether HIF-2α may influence scaffolding proteins and their expression in a different way depending on excitatory or inhibitory synapse functioning (Figure 3.39). Genes that function at excitatory synapses like *Gphn* as a major scaffolding protein and facilitator of GABAergic receptor recruitment, or *Collybistin* as an adaptor protein for the formation of GEPHYRIN clusters, showed a trend for a decreased expression under hypoxic conditions (Figure 3.39 A). In addition, both genes seemed to be less expressed in HIF-2α KO neurons compared to WT neurons and the co-culture with HIF-2α KO astrocytes even seemed to boost this down-regulation.

An up-regulatory effect of HIF-2α KO astrocytes on neurons similar to the regulation of *Bdnf* expression (Figure 3.38) was seen for the expression of the excitatory post-synaptic scaffolding protein *Psd95* (Figure 3.39 B). Here, instead of having higher basal levels already at 0 h that are reduced under hypoxia, it seems to be more an up-regulation of *Psd95* under prolonged hypoxic conditions.

NLGN1 has been shown to interact with PSD95 (Irie *et al.*, 1997). Here, the expression of *Nlgn1* is not altered based on the genotype of the astrocytes nor through hypoxia (Figure 3.39 B). The same was seen for the pre-synaptic *Snap25* (Figure 3.39 C).

Taken together, a HIF-2α KO in astrocytes seems to influence the expression of scaffolding-associated genes belonging to inhibitory synapses in neurons in a negative manner, whereas the expression of genes belonging to excitatory synapses is increased when HIF-2α is knocked down in astrocytes.

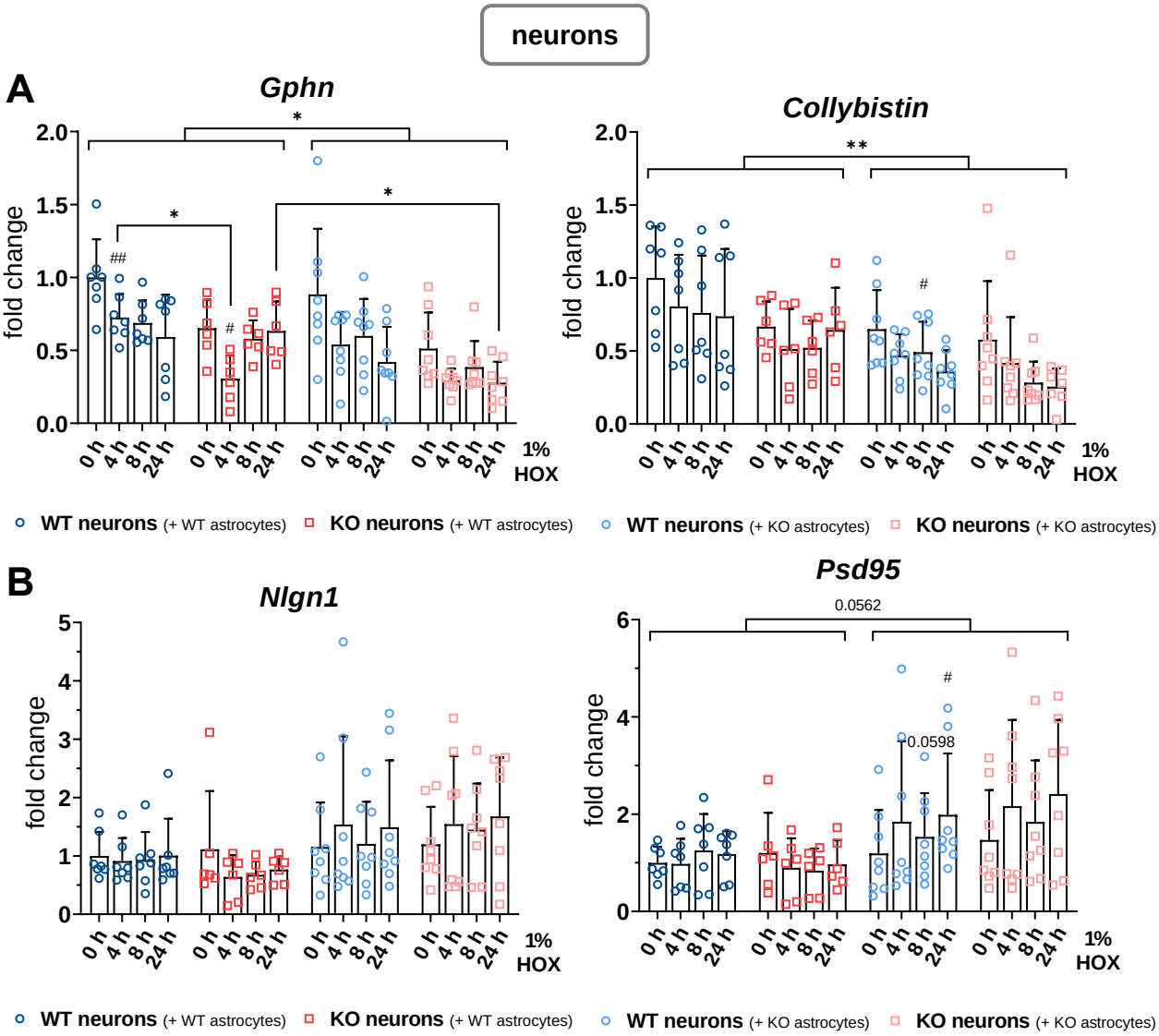

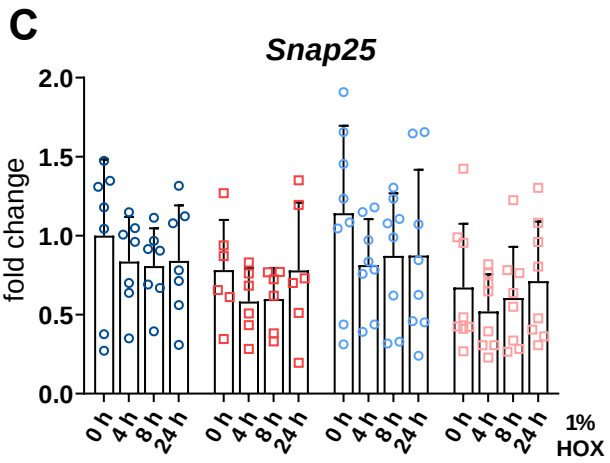

A: Expression of post-synaptic genes of inhibitory synapses (*Gphn* = Gephyrin, *Collybistin* = Cdc42 Guanine Nucleotide Exchange Factor 9).

B: Expression of post-synaptic genes of excitatory synapses (*Nlgn1* = Neurologin 1 and *Psd95* = Post-synaptic density protein 95).

C: Expression of pre-synaptic *Snap25*.

Figure 3.39: Gene expression analysis of neuronal and synapse-associated genes in WT and HIF-2α KO neurons under HOX conditions.

Combinations of WT/HIF-2α hippocampal neurons and WT/HIF-2α KO astrocytes were co-cultured for 12 DIV under normoxic (NOX, 21% O_2) conditions, followed by hypoxic incubation (HOX, 1% O_2) for 24 h. RNA samples were collected at 0 h (NOX control), 4 h, 8 h and 24 h of hypoxia. Expression levels of neuronal and synapse-associated genes were assessed by qPCR in the neurons. Values were normalized to *ribProt* as HKG and changes in gene expression calculated as x-fold changes relative to the 0 h control of WT neurons + WT astrocytes using the 2^-ΔCt method. Mean + SD, $p < 0.05$ = *, $p < 0.01$ = ** and $p < 0.001$ = ***, * between neuronal genotype as indicated, # compared to the 0 h control of the same co-culture combination. n = 6 - 8 in 3 independent experiments per genotype combination.

An additional gene panel was examined for genes important for receptor signaling and calcium channeling (Figure 3.40). Like for the astrocytes, the expression levels of adenosine receptors *Adora1* and *Adora2a* were analyzed, as there are already published correlations between HIFs and adenosine receptors in different cell types. Overall, the HIF-2α KO in neurons did not influence the expression of *Adora1* and *Adora2a* whereas a HIF-2α KO in astrocytes seemed to affect neuronal expression of *Adora1* and *Adora2a* in a paracrine manner: neurons in co-culture with HIF-2α KO astrocytes had a tendency to increase the expression of these receptors under prolonged hypoxia. On the contrary, the expression levels of the receptors remained constant over time when neurons were co-cultured with WT astrocytes (Figure 3.40 A). A similar effect was seen for the expression of the glutamate receptors *Grin2a* and *Grin2b* of excitatory synapses (Figure 3.40 B). Here, the HIF-2α KO astrocytes also promoted the expression of these receptors in the neurons, independent of the neuronal HIF-2α status. Prolonged hypoxia furthermore increased the expression of *Grin2a* and *Grin2b* in both WT and HIF-2α KO neurons whereas neurons in co-culture with WT astrocytes did not enhance receptor expression over time.

When looking at the expression of *Cacna1a*, a subunit of the voltage gated calcium channel at the pre-synapse that was shown to be strongly induced by HIF-2 in embryonic kidney cells (Wang *et al.*, 2005), no significant differences between WT and HIF-2α KO neurons were visible in this experimental set-up. Hypoxia itself also let to no induction of *Cacna1a* expression (Figure 3.40 C).

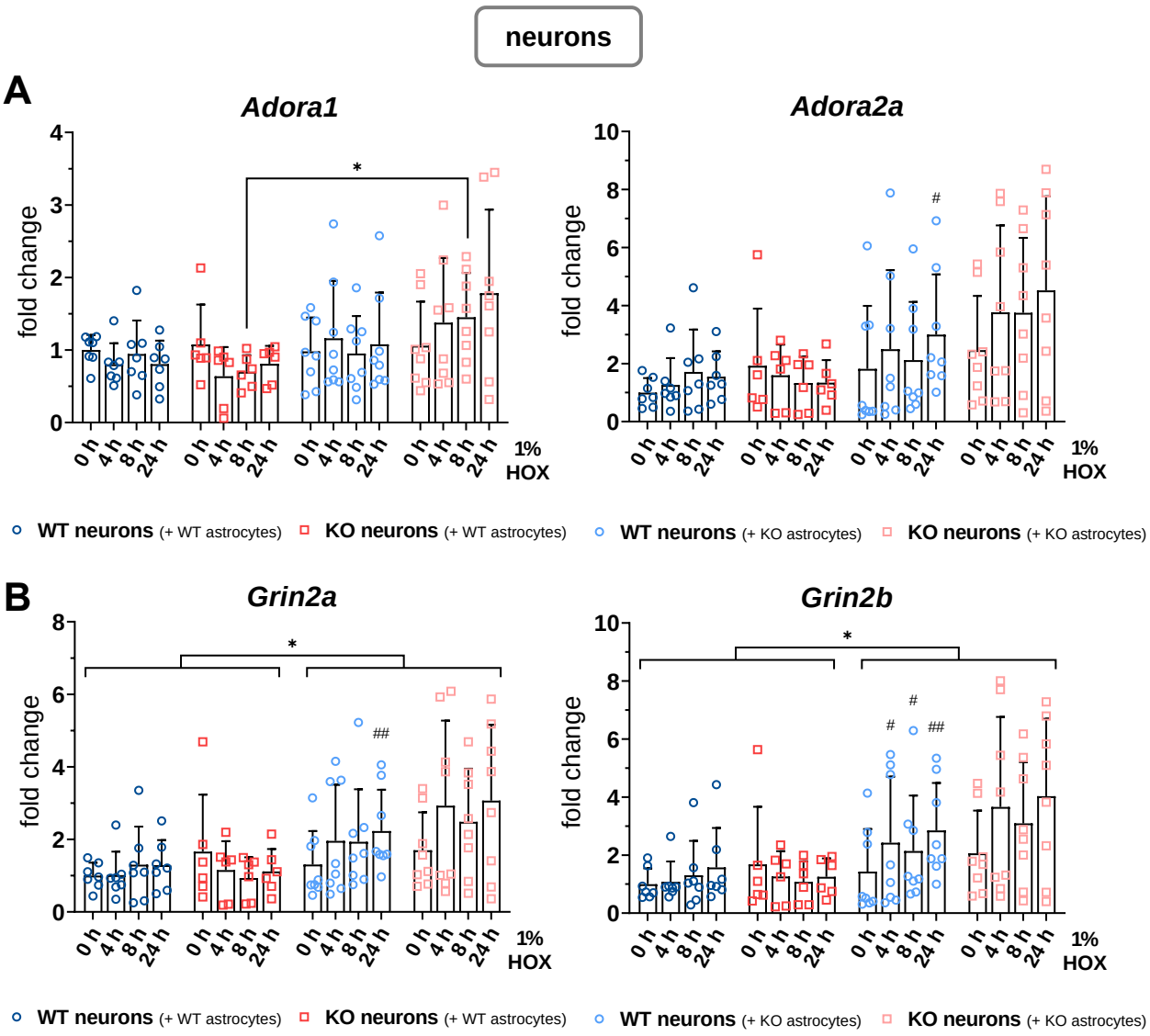

A: Expression of adenosine receptors *Adora1* and *Adora2a*.

B: Expression of glutamate receptors *Grin2a* and *Grin2b*.

C: Expression of voltage-gated calcium channel subunit *Cacna1a*.

Figure 3.40: Gene expression analysis of neuronal and synapse-associated genes in WT and HIF-2α KO neurons under HOX conditions.

Combinations of WT/HIF-2α hippocampal neurons and WT/HIF-2α KO astrocytes were co-cultured for 12 DIV under normoxic (NOX, 21% O_2) conditions, followed by hypoxic incubation (HOX, 1% O_2) for 24 h. RNA samples were collected at 0 h (NOX control), 4 h, 8 h and 24 h of hypoxia. Expression levels of genes important for neuronal signaling were assessed by qPCR in the neurons. Values were normalized to *ribProt* as HKG and changes in gene expression calculated as x-fold changes relative to the 0 h control of WT neurons + WT astrocytes using the 2^-ΔCt method. Mean + SD, $p < 0.05$ = * and $p < 0.01$ = **, * between neuronal genotype as indicated, # compared to the 0 h control of the same co-culture combination.

n = 6 - 8 in 3 independent experiments per genotype combination.

Figure 3.41 depicts the expression of some additional genes of special interest. First, the expression of two genes of the MAPK/ERK signaling pathway (*Map2k1* and *Erk1*) was analyzed (Figure 3.41 A), as recent studies showed that HIF-2α affects the MAPK/ERK signaling pathway in primary cilia of neurons and loss of HIF-2α decreased the expression of *Mek1/2* and *Erk1/2* (Leu *et al.*, 2023). In the neurons of the neuron-astrocyte co-culture, the HIF-2α KO neurons (+ WT astrocytes) showed a significant decreased *Map2k1* (Mek1) expression at 0 h and 4 h time-points while the effect was no longer visible at later time-points. Also, the expression in HIF-2α KO neurons (+ KO astrocytes) had a tendency to lower compared to the WT neurons, although this difference was not significant. In general, the HIF-2α KO astrocytes furthermore significantly decreased the expression levels of *Map2k1* in both neuronal genotypes.

For *Erk1* expression, a decrease in WT neurons (+ WT astrocytes) was observed, while for the other co-culture combinations no significant differences in expression levels were observed.

Furthermore, the expression levels of the VEGF receptor *Vegfr2* and of the EPO receptor (*EpoR*) were analyzed (Figure 3.41 B). As the *Vegf* expression in both WT and HIF-2α neurons was influenced by the astrocytic genotype, it was of interest, if the VEGF receptor was also affected by the astrocytes, as VEGFR2 is part of the HIF/VEGF/VEGFR axis. No significant differences were found when comparing the different co-culture combinations regarding their genotypes. Furthermore, *Vegfr2* was slightly induced in WT neurons (+ KO astrocytes) after 8 h and 24 h of hypoxia and HIF-2α KO neurons (+ KO astrocytes) showed a similar tendency. Neurons in co-culture with WT astrocytes showed no visible hypoxic induction.

EpoR was significantly higher expressed in neurons that had been in co-culture with HIF-2α KO astrocytes. WT neurons thereby showed a slight induction under HOX conditions.

Lastly, the expression of *Hif-1α* was assessed (Figure 3.41 C). Although predominantly post-translationally regulated under hypoxia, there are also oxygen-independent stimuli like lipopolysaccharide, angiotensin II or ROS levels that can affect HIF translation through for example the proteinkinase C pathway in macrophages or vascular smooth muscle cells (Page *et al.*, 2002; Ziello *et al.*, 2007). Here, *Hif-1α* gene expression showed a slightly down-regulation in WT neurons and seemed to be more stable in HIF-2α KO neurons during the HOX incubation. In addition, in co-culture with HIF-2α KO astrocytes the expression levels of *Hif-1α* in neuronal cells was rather reduced.

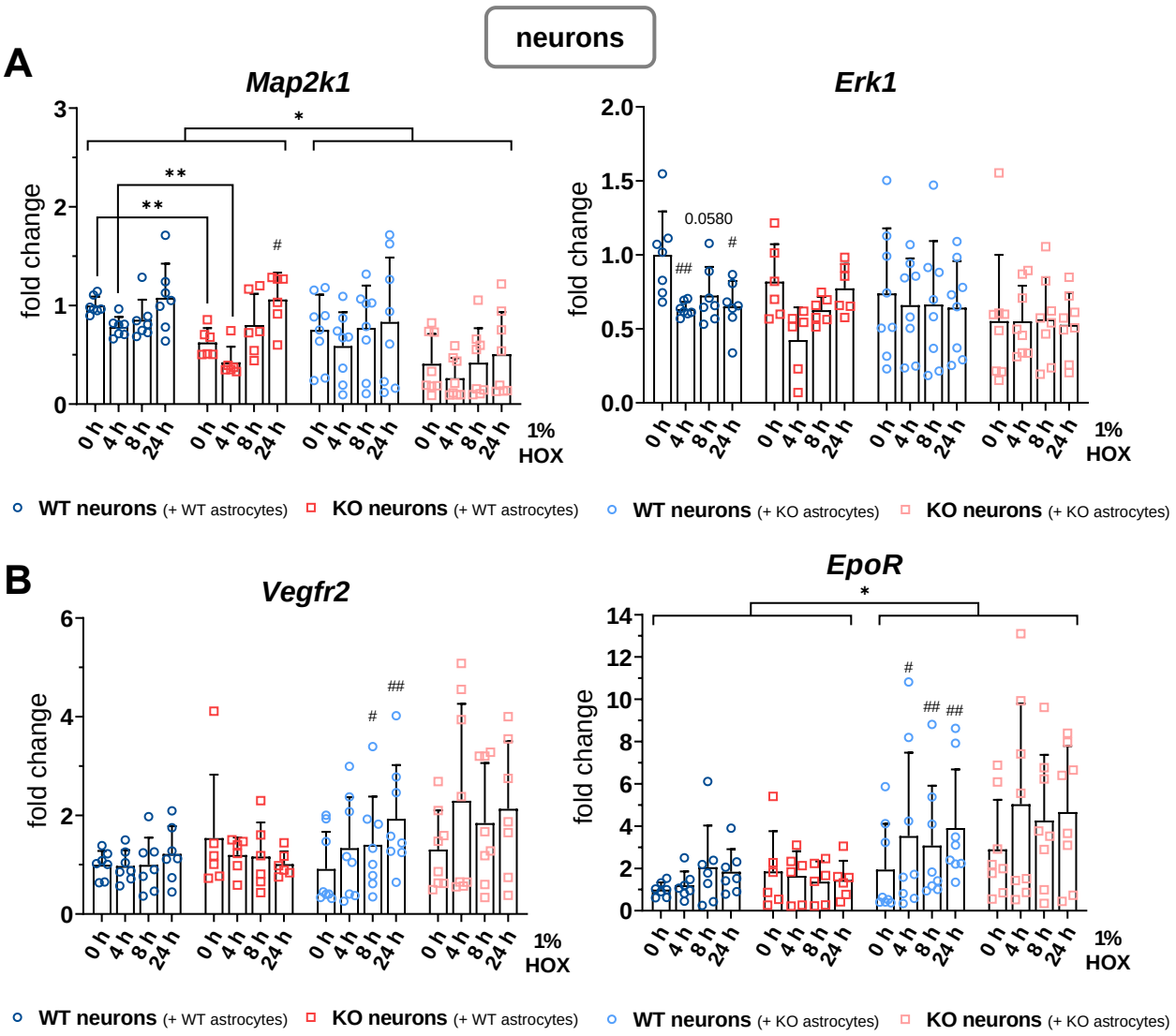

A: Expression of genes of the MAPK/Erk pathway.

B: Expression of hypoxia-related receptors *Vegfr2* and *EpoR*.

C: Expression of *Hif-1α*.

Figure 3.41: Gene expression analysis of further genes of interest in WT and HIF-2α KO neurons under HOX conditions.

Combinations of WT/HIF-2α hippocampal neurons and WT/HIF-2α KO astrocytes were co-cultured for 12 DIV under normoxic (NOX, 21% O_2) conditions, followed by hypoxic incubation (HOX, 1% O_2) for 24 h. RNA samples were collected at 0 h (NOX control), 4 h, 8 h and 24 h of hypoxia. Expression levels of different genes were assessed by qPCR in the neurons. Values were normalized to *ribProt* as HKG and changes in gene expression calculated as x-fold changes relative to the 0 h control of WT neurons + WT astrocytes using the 2^-ΔCt method. Mean + SD, $p < 0.05$ = *, $p < 0.01$ = ** and $p < 0.001$ = ***, * between neuronal genotype as indicated, # compared to the 0 h control of the same co-culture combination.

n = 6 - 8 in 3 independent experiments per genotype combination.

4. DISCUSSION

Overall, the study presented here aims to deepen the understanding of HIF-2 functions in the normoxic and hypoxic brain, with special regards to synapse-associated processes. As HIF-2α was found to be stabilized in the brain even under normoxia in mice (Kleszka *et al.*, 2020), one part of the study dealt with functions of cerebral HIF-2α in vivo under normoxic conditions. In a second part, an in vitro culture system of murine neurons and astrocytes with either wild-typical or knocked-out HIF-2α was used for conducting experiments under hypoxic conditions.

4.1. Aspects of brain development in neonatal (P3), juvenile (P20) and adult WT and HIF-2α KO mice

HIF-2α is already known to be an important player for different developmental aspects such as vascularization during embryonic development and tumorigenesis, or through modulation of stem cells. Different HIF-2α knockout models thereby showed divergent, but severe phenotypical effects (Befani and Liakos, 2018; Covello *et al.*, 2006). Recent studies of a conditional *Hif-2α* KO in neural stem cells furthermore showed a potential role of HIF-2α during brain development, migration of stem cells and synapse-associated gene expression (Kleszka *et al.*, 2020). Here, the effect of HIF-2α on different developmental stages of the brain of WT and HIF-2α KO mice with a focus on hippocampal development and synapse architecture (see 3.1.1) was assessed by histological staining, electron microscopy and gene expression analysis in three days old (P3), 20 days old (P20) and adult (> 8 weeks) mice

4.1.1. WT and HIF-2α KO mice exhibit a similar hippocampal development

Altogether, the hippocampus of WT and HIF-2α KO mice exhibited similar morphological characteristics and developed without any visible defects or retardations at all tested stages of development (P3, P20 and adult). This was assessed by Nissl staining and analysis of morphological parameters like the shape of the hippocampus, the thickness of the nuclei layer of the hippocampal regions CA1, CA3 and DG and the cellular density in these layers. Although pyramidal neurons were reduced in the retrosplenial cortex of HIF-2α KO animals (Kleszka *et al.*, 2020), this was not the case for the pyramidal neurons of the CA1 and CA3 region in the hippocampus of these mice. In the DG, the main cellular layer containing granule cells also showed no differences between WT and HIF-2α KO mice.

Therefore, when looking for effects of HIF-2α on brain development, it is important to consider area-specific differences and distinguish them from global effects.

4.1.2. The width of the synaptic cleft is reduced in the Stratum radiatum of adult HIF-2α KO mice

In the Stratum radiatum, most synapses occur on spines and are of glutamatergic origin. In total, studies showed that over 90% of synapses are excitatory and only a small portion is inhibitory (Megias *et al.*, 2001; Racca *et al.*, 2000). The analysis of the present study did not distinguish between excitatory and inhibitory capability or synapses of different sub-types. Though based on the general percentage of glutamatergic, excitatory synapses, it is most likely that the results obtained in this study are mainly based on this type of synapse. When looking at the ultrastructure of the synapses in the Stratum radiatum of the CA1 hippocampal region of adult mice, the overall synapse morphology showed no obvious deficits between WT and HIF-2α KO animals. Length and thickness of PSD zone were similar, as well as the occurrence of specific types of synapses like perforated or multiple-spine synapses. The synapse density per area was constant between the two genotypes, which correlates with the Nissl staining of nuclei in the same area where also no difference of cellular density was visible.

The synaptic cleft, the interspace between the pre- and post-synaptic membrane, contains released or re-trafficking neurotransmitters, as well as various adhesion molecules originating from the pre- or post-synaptic site, like Cadherins, Neurexins or Neuroligins, collectively referred to as *synaptic cell adhesion molecules* (Missler *et al.*, 2012). Interestingly, HIF-2α KO mice exhibited a significantly reduced width of the synaptic cleft (16.52 nm in HIF-2α KO animals, 19.07 nm in WT animals). The width of a standard chemical synapse is on average around 20 nm. Rat cortical synapses, for instance, showed synaptic clefts of 20-30 nm distance (Gray, 1959; Palay, 1956). In a more recent mouse study of synaptic and cellular changes induced by the schizophrenia susceptibility gene G72, the width of the synaptic cleft in the analyzed mice was 18 nm on average (Posfai *et al.*, 2016). In a human study of synaptic changes over age, the synaptic cleft width remained constant around 20 nm between people of different ages ranging from 45 years up to 84 years (Adams, 1987). Altogether, studies showed that the synaptic cleft is rather stable during development and different osmotic or physiological manipulations and seems to be determined by the synaptic cell adhesion molecules scaffolding the cleft. Furthermore, changes in synaptic cleft width are susceptible for measurement errors due to the small range of change and limited image resolution.

There are many theoretical models, for instance different Monte Carlo simulations, which analyze the kinetics of synaptic receptor currents and synaptic transmission under different parameters, one parameter being the synaptic cleft width (Savtchenko *et al.*, 2000; Savtchenko and Rusakov, 2007; Wahl *et al.*, 1996). In theory, a narrow synaptic cleft increases the local neurotransmitter concentration and therefore enhances receptor activation and synaptic

strength. On the other hand, narrowing the synaptic cleft could lead to reduced receptor currents (Savtchenko and Rusakov, 2007). If the composition of synaptic adhesion molecules differs between HIF-2α KO and WT mice, resulting in changes in synaptic cleft appearance and if this difference has a functional effect on synaptic strength at all, needs further investigation. Besides, only adult mice were used for analysis so far. As HIF-2α may have transient effects during development, it is of interest to look for the synaptic ultrastructure and tested parameters at other developmental stages as well.

Of note, researching on and identifying proteins of the synaptic cleft is rather challenging by the lack of suitable methods for distinguishing between synaptic cleft components or components of the neighboring membranes or extracellular matrix (Burch *et al.*, 2017).

4.1.3. Differences in expression of cerebral genes are mainly found in neonatal mice and resolve during adulthood

Kleszka *et al.* (2020) found a reduced cortical expression of *Nrgn* and *Syn1*, both associated to synaptic functions, in tissue of HIF-2α KO mice under normoxic conditions. For identification of further potentially changed genes, a commercially available profiler PCR array was performed regarding synaptic plasticity-associated genes in these mice. Unfortunately, the promising candidates of the array that were differentially expressed between adult HIF-2α KO and WT mice were not altered when verifying the results in single qPCR analysis. The array used pooled RNA samples and was analyzed with help of an online tool provided by the manufacturer. The subsequent testing of individual samples via qPCR followed by an analysis method implemented in our working group is thereby more accurate and should be considered as more reliable. Overall, adult WT and HIF-2α KO mice exhibited a similar expression profile of the array-based analyzed genes.

As HIF-2α seems to take part in brain development and migration and differentiation of stem cells (Kleszka *et al.*, 2020; Leu *et al.*, 2021), the expression of different promising genes of interest was further on assessed in the aforementioned different age cohorts (P3, P20 and adult) of the WT and HIF-2α KO mice. This ensures a better insight into a possibly age-dependent function of HIF-2α during brain and synapse development.

The analysis was, amongst others, performed for genes that already showed a normoxic down-regulation in adult HIF-2α KO mice (Kleszka *et al.*, 2020). Unexpectedly, the reduced expression levels described before could not be verified in this study. Adult mice showed no differences in the expression levels of the synapse-associated genes *Synapsin* and *Dap4* or the neuronal marker gene *bIII-Tubulin*. When adding the P3 and P20 age cohorts to the analysis, a rather opposite effect is observed on gene expression levels. Especially at P3, HIF-2α KO mice showed an up-regulation of genes like *Dap4*, *bIII-Tubulin* and the

oligodendrocyte marker *Olig2* - an effect that is mostly diminished at P20 and completely gone in the adult animals where gene expression levels were equal between both genotypes.
Kleszka *et al.* (2020) analyzed the gene expression levels only in the cortices of the animals whereas here, a whole hemisphere was used. Therefore, the differences in the studies might be due to different expression levels in specific brain regions.

In addition, none of the tested potential HIF-2α target genes (*Adora1*, *Adora2a* and *Th*, see 1.3.2) showed a correlation to a HIF-2α knockout, independent of the age of the tested animals. Therefore, at least under normoxic conditions and during brain development, HIF-2α does not modify the overall expression of these genes in the brain.
However, in HIF-2α KO mice, in comparison to WT mice, other neuron- and synapse-associated genes were up-regulated in the P3 age cohort, while the differences in expression levels were no longer detectable in the adult animals. These up-regulations seems to be mainly found in genes associated with inhibitory synapses, especially at the post-synaptic compartment, namely *Gephyrin*, *Collybistin*, *Neurexin3*, *Neuroligin2* and *Neuroligin3*.
Gephyrin is a scaffolding protein at inhibitory synapses that plays a critical role in the synaptic localization and concentration of glycine receptors and major GABA receptor subtypes by anchoring these receptors to the plasma membrane, thereby facilitating important functions for inhibitory synaptic transmission and long-term potentiation. Its analogue at excitatory synapses is PSD95 (Choii and Ko, 2015). In 2000, it was shown that a brain-specific guanine exchange factor, Collybistin, is required for the clustering of Gephyrin itself to the post-synaptic membrane by binding both Gephyrin and membrane lipids (Kins *et al.*, 2000). Furthermore, both proteins interact with Neuroligin2, a post-synaptic cell-adhesion molecule that forms a connection with Gephyrin using a conserved cytoplasmic motif and acts as a specialized activator for Collybistin, which, in turn, guides the tethering of the inhibitory post-synaptic scaffold to the cell membrane (Poulopoulos *et al.*, 2009). Together, they create a framework that clusters inhibitory post-synaptic receptors, thus forming a functional inhibitory synapse. Although Neurexin3, a synaptic cell-adhesion molecule located at the pre-synapse mainly interacts with different binding partners of excitatory synapses, there is also evidence that Neurexin3 promotes post-synaptic differentiation at inhibitory synapses by binding to Neuroligin2 (Zhang *et al.*, 2023). Neurexin3 is furthermore believed to have a critical role during early development of Alzheimer's disease. Higher concentrations of Neurexin3 and Neuroligin2 have been observed in the cerebrospinal fluid of individuals in the preclinical stage of Alzheimer's disease. These elevated levels may contribute to the upregulation of GABA receptors, which in turn can influence information transmission at inhibitory synapses, as well as synaptic plasticity, learning, and memory processes, thereby promoting the progression of Alzheimer's disease (Lleo *et al.*, 2019; Zhang *et al.*, 2023).

Neuroligin3, which was also up-regulated in P3 HIF-2α KO mice, is also present in both excitatory and inhibitory synapses (Budreck and Scheiffele, 2007).
Although there were also genes up-regulated that in most instances take part in excitatory synaptic functioning, like *Wnt7a* and *Drebrin,* the majority of excitatory synapse-associated genes showed no changes in expression between the neonatal WT and HIF-2α KO animals.
For instance, this was seen when looking at receptor-clustering complexes similar to the Neuroligin2/Gephyrin/Collybistin complexes of inhibitory synapses. Neuroligin1 for example is important for clustering of NMDA receptors through interactions with the Gephyrin-analog PSD95 and Neurexin1 (Barrow *et al.*, 2009; Giannone *et al.*, 2013).
In summary, a HIF-2α KO seems to affect the expression of certain genes at early neonatal development and younger ages, whereas this effect is resolved during adulthood. The changes in expression levels are furthermore preferably found in genes associated with functions at inhibitory synapses, indicating a function of HIF-2α in regulation of the proportion of excitatory and inhibitory synapses during early development.

For a more in-depth analysis of changes in certain gene clusters, RNA sequencing (RNAseq) would be beneficial to assess the transcriptome in a high-throughput approach.
It should be considered that gene expression analysis here is not distinguishing between different brain areas or even cell types, as RNA samples of whole hemispheres were evaluated. Therefore, it is not possible to conclude, whether changes of gene expression are due to a different expression status in the cells itself or whether the total number of cells expressing the gene of interest has changed. Therefore, in case of for example *bIII-Tubulin* and *Olig2* expression that were up-regulated in HIF-2α KO animals in the P3 population, it is not possible to conclude whether the number of neurons and oligodendrocytes in the tissue has changed or if the transcription of the genes itself was up-regulated in the single cells. A change in cellular composition was already shown by immunocytochemical stainings in differentiating HIF-2α KO neurospheres, where bIII-TUBULIN+ neuronal cells were diminished and the number of oligodendrocytes was constant after 72 h of differentiation under normoxic conditions. However, the authors attributed this observation to changed migration capabilities of the cells out of the neurosphere (Kleszka *et al.*, 2020).
The exact proportions of cell types in the brain tissue can be assessed by flow cytometry analysis with specific antibody markers for distinct cell populations like neurons, astrocytes and oligodendrocytes. Through specific gating and quantification of the total amount of cells, the percentage of each cell type in the analyzed tissue can be determined and compared between WT and HIF-2α KO mice. However, sample preparation of brain tissue for flow cytometry has some difficulties and limitations especially with tissue dissociation, as neurons are rather susceptible to enzymatically or mechanical stress (Martin *et al.*, 2017; Trujillo *et al.*,

2021). Therefore, companies already developed special brain and neuronal dissociation kits for optimal tissue preparation. This approach was, however, beyond the scope of this study.

It was already shown that HIFs can function in a region- or even cell-type specific manner (see 1.3.1), highlighting the need for even more precise analyses of individual brain compartments or cells. In the study presented, this was further enabled in the environmental enrichment study, where cortices and hippocampi were analyzed independently, as well as in the in vitro co-culture model were analysis of single cell types, namely neurons and astrocytes, was accomplished.

4.2. Effects of environmental enrichment on a cerebral HIF-2α KO

Behavioral experiments revealed that adult HIF-2α KO mice exhibit specific impairments in learning and memory, as well as the expression of synapse-associated genes even under physiological oxygen conditions (Kleszka *et al.*, 2020). This study aimed to accentuate these results through implementation of an environmental enrichment (EE) study in adult animals. After weaning, HIF-2α KO mice and their WT littermates were thereby housed under either environmentally enriched conditions or in standard housing conditions (SC) for four weeks and gene expression analyses were conducted afterwards. EE housed mice had enlarged space and different toys and objects for sensory input, which has been shown to enhance neurogenesis and synaptic plasticity in these animals (Bayne, 2018; Rampon *et al.*, 2000).

4.2.1. Environmental enrichment does not enhance differences in gene expression levels in the cortex and hippocampus between HIF-2α KO and WT mice

After the EE and SC housing phase, cortices and hippocampi of the WT and HIF-2α KO mice were analyzed. To get an overview of potential genes of interest, a commercially available PCR array for synaptic plasticity was carried out. The array showed several differentially expressed genes between pooled RNA samples of the cortices of EE housed WT and HIF-2α KO mice. Unfortunately, similar to the array used in the brain developmental study, these results could not be verified by the following single qPCR analysis. As mentioned earlier, the analysis of individual samples by qPCRs is more trustworthy than the results of the array. Further on, single qPCRs were not only performed for the cortices of the EE housed animals but also for SC housing, as well as for the hippocampi under both housing conditions.

Adora2a and *Kif17* were both significantly down-regulated in the hippocampus of HIF-2α KO mice, but not in the cortex. EE housing had no effect on expression levels. KIF17 is a member of the kinesin-2 family of plus-end directed microtubule-based motor proteins and is important for carrying cargo across microtubules from cell bodies exclusively to dendrites. Known cargos of KIF17 are for example NR2B, a subunit of the glutamergic NMDA receptor, and potassium Kv4.2 channels - both implicated in synaptic transmission, learning and memory (Wong-Riley and Besharse, 2012). Literature research did not reveal any connections to the hypoxia/HIF pathway so far. *Adora2a*, on the contrary, is one of the potentially HIF-2α associated genes (see 1.3.2). Rombo *et al.* showed that in the hippocampus, Adora2a facilitates excitatory glutamatergic Schaffer collateral synapses to CA1 pyramidal cells, but not to GABAergic inhibitory interneuron (Rombo *et al.*, 2015). While this study reported no difference in *Adora2a* expression in the whole hemisphere during brain development analysis, the more detailed analysis of different tissues now showed a diminished expression in the hippocampus of adult HIF-2α KO mice, indicating again area- or even cell-type specific effects of a HIF-2α knockout. In total, all of the other analyzed genes showed no changes in expression levels between the HIF-2α KO and WT mice in neither cortex nor hippocampus. Furthermore, EE housing did not enhance any differences between the two genotypes.

4.2.2. Environmental enrichment does not induce overall neuro- and synaptogenesis on gene level

Besides the absence of differences between WT and HIF-2α KO mice in the expression levels of most of the tested genes, the EE housing condition itself did not show inducing effects at all, based on expression analysis of genes related to synaptic plasticity.

Most of the tested genes showed a similar expression between EE and SC housing in both hippocampus and cortex. Other genes were down-regulated under EE conditions, some of them only in the hippocampus (like *Cdh2* = Cadherin2*,* a calcium-dependent cell-adhesion molecule*; Adcy8* = Adenylyl cyclase type 8; and *Psd95*), some in the cortex (like *Crem* = cAMP responsive element modulator, and *Ngfr* = nerve growth factor receptor) and some in both hippocampus and cortex (*Pcdh8* = *Proto-Cadherin 8*; and *Map2k1* = mitogen-activated protein kinase 1). Overall, no consistency between certain gene groups was cognizable regarding tissue-specific alterations. Furthermore, the reductions, although significantly different, were rather small in fold change levels, highlighting the need for further analyses. For example, behavioral studies testing for recognition memory or spatial learning memory are suitable to investigate positive effects of environmental enrichment on these parameters.

In general, the trend for a rather decreased gene expression under EE conditions in comparison to SC conditions was unexpected. The idea of enhancing neuro- and

synaptogenesis by EE conditions fueled the expectation of induction in the expression of genes related to synaptic plasticity. Of note, the expected alterations depend on the specific function of the gene. In an array-based gene expression study of mice which were subjected to environmentally enrichment for different periods of time, genes related to neuronal signaling rather showed an increased gene expression, whereas genes related to proteases or cell death rather showed a decreased expression profile in the cortex of these animals (Rampon *et al.*, 2000).

Overall, the missing induction of genes related to synaptic plasticity might also be due to the temporal setup of the study. Mice were kept under enriched and standard conditions for four weeks. This might have been too long to see effects on RNA levels, as by the end of the study, gene expression might have already returned to normal levels due to adaption. For instance, Nithianantharajah *et al.* (2004) reported an induction of SYNAPTOPHYSIN protein levels in animals that had been enriched for 30 days by Western Blot and sandwich ELISA. However, Heinla *et al.* (2015) did not see an induced expression of Synaptophysin when analyzing the hippocampus of mice kept under enriched conditions for seven weeks. Furthermore, Rampon *et al.* (2000) showed in their analyses that gene expression levels can change over the time of enrichment. For instance, *Psd95* expression was induced 7-fold in two days enriched mice, whereas in seven days enriched mice, the induction was only 2.3-fold.

Brain-derived neutrophic factor (BDNF), which belongs to the family of neutrophins, is considered as a key protein for synaptic plasticity processes, brain development and cognitive performance like learning and memory (Miranda *et al.*, 2019). In general, *Bdnf* is widely expressed in the central nervous system. Transcription is regulated by several promoters, which govern the expression tissue-specific and in response to activity. Highest levels of *Bdnf* in the brain have been found in hippocampal neurons (Timmusk *et al.*, 1993).

Several studies reported a positive correlation between BDNF protein levels or *Bdnf* gene expression and environmental enrichment, as reviewed by Barros *et al.* (2019), making BDNF a marker to control for the efficiency of environmental enrichment. In addition, BDNF exerts a crucial role in facilitating and enhancing cognitive improvement and functional performance in behavioral studies or LTP/LTD measurements of environmentally enriched animals (Cao *et al.*, 2014; Dandi *et al.*, 2018; Gutierrez-Vera *et al.*, 2022; Heinla *et al.*, 2015; Novkovic *et al.*, 2015; Sun *et al.*, 2010).

Here, expression levels of *Bdnf* were analyzed by qPCR as well as protein levels by Western Blotting. As BDNF is secreted as a precursor form (proBDNF) with sometimes opposing effects (reviewed in Lu *et al.*, 2005; Martinowich *et al.*, 2007), levels of both BDNF and proBDNF were assessed to also look for potential effects on the conversion of proBDNF to BDNF.

On transcriptional level, the expression of *Bdnf* remained equal between SC and EE conditions in both hippocampus and cortex. Besides, no difference was detectable between WT and HIF-2α KO mice. This was also seen for protein levels of proBDNF and BDNF in the cortex of the mice. Levels of both forms remained constant between SC and EE condition and no significant difference was observed between WT and HIF-2α KO mice, indicating that the enrichment had no influence on cortical activity in these animals. When looking at the hippocampus, BDNF levels were significantly higher under enriched conditions for both WT and HIF-2α KO mice in comparison to SC conditions, whereas proBDNF levels remained constant. Thus, EE induced BDNF levels in the hippocampus of both WT and HIF-2α KO mice, indicating a positive effect of EE on brain activity in the hippocampus. This is consistent with literature, as BDNF is predominantly expressed in the hippocampus and most studies that investigated and found up-regulations of BDNF also analyzed hippocampal tissue, where synaptic plasticity and LTP is extremely active. Interestingly, the levels of proBDNF did not decrease with increasing levels of BDNF, although BDNF is generated from proBDNF by proteolytic cleavage. Cao *et al.* (2014) analyzed the levels of proBDNF and BDNF in rat hippocampal tissue and found similar results, although the proBDNF levels in their study exhibited at least a tendency for down-regulation. As BDNF has a positive effect on brain activity and proBDNF a rather depressing effect, the up-regulation of BDNF should nevertheless outreach possible functions of proBDNF. As the *Bdnf* expression was constant between SC and EE conditions, the increased levels of BDNF rather depend on post-transcriptional regulation.
In total, results regarding BDNF are not always consistent, depending on the analyzed brain tissue, the method used (such as gene expression analysis, Western Blotting or immunohistochemistry) or the overall study design. Barros *et al.* (2019) comprehensively summed up research regarding BDNF and EE, the results and the limitations of the respective study.

In general, diverse protocols for environmental enrichment have been published but a gold standard for conducting this kind of studies has not been developed until to date. Protocols differ in the duration of enrichment (short-term vs long-term, hours vs. days vs. weeks), the equipment provided and age of the tested animals. Therefore, when comparing results of such studies it is important to look for the exact procedure of the particular study. Here, the phase of environmental enrichment seems to be either too long or too short to observe changes in gene expression levels. Future studies should focus on changes on protein levels and behavioral experiments. As BDNF levels were constant in the cortex but up-regulated in the hippocampus, further analyses should also address changes in the hippocampus, as effects of EE seem to be more prominent in this tissue.

4.3. Effects of a HIF-2α KO on neurons and astrocytes in vitro under hypoxic conditions

For the functional analysis of HIF-2α on neuronal and synaptic processes under hypoxic conditions, a neuron-astrocyte co-culture model was successfully implemented for this study. Murine hippocampal neurons and cortical astrocytes of either WT or HIF-2α KO genotypic origin were co-cultured, although in spatial distance from each other. Thus, the separate analysis of for example RNA or protein content over 24 h of hypoxic (1% O_2) incubation was possible for both cell types, allowing for the analysis of cell-type specific effects of HIF-2α. This was further achieved by using different genotypic combinations of the co-culture (WT neurons + WT astrocytes, KO neurons + WT astrocytes, WT neurons + KO astrocytes, KO neurons + KO astrocytes). The neuron-astrocyte co-culture thereby resembles a favorable in vitro system for the study of (tripartite) synaptic functions in contrast to for example neurospheres that are more suitable for analysis of brain developmental processes.

Both cell populations exhibited an efficient knockout of HIF-2α under both NOX and HOX conditions. As the *Hif-2α exon 2* is permanently deleted on gene level in neural stem cells and not for example transiently silenced RNA interference, the sufficient and stable knockout in the differentiated neurons and astrocytes over the duration of the experiments was expectable.

4.3.1. Hypoxic response of WT and HIF-2α KO astrocytes

4.3.1.1. The hypoxic response in astrocytes is not influenced by neuronal HIF-2α

Overall, when incubated under hypoxic conditions, the astrocytes intensively responded to the reduced oxygen levels through up-regulation of hypoxia target genes like *Vegf* and *Epo*. In addition, the gene expression of the oxygen sensors and negative regulators of the hypoxia pathway such as *Phd2* and *Phd3* was significantly induced.

Thereby, the up-regulation of target genes in astrocytes was independent of the neuronal genotype of the respective co-culture. A HIF-2α KO in neurons did not influence the hypoxic response of the astrocytes at all. This was not unexpected, as astrocytes are mainly thought to interact and support neuronal survival and synaptic functions through paracrine effects such as the secretion of growth factors, energy metabolites or gliotransmitters (Jones *et al.*, 2012; Vangeison and Rempe, 2009), but not vice versa - at least in terms of hypoxic responses or oxidative stress. Nevertheless, neurons are able to interact with astrocytes in a bidirectional way at the tripartite synapse through for example secretion of neurotransmitters that can be re-uptaken by astrocytes.

4.3.1.2. *Epo* and *Vegf* are target genes of HIF-2α in astrocytes

Although both WT and HIF-2α KO astrocytes showed a significant up-regulation of *Vegf* and *Epo* gene expression under 1% oxygen, the induction was significantly lower in HIF-2α KO astrocytes compared to WT astrocytes. This indicates a HIF-2α-dependent regulation of these genes. A HIF-2α-dependent regulation of *Epo* expression has already been described by Chavez and colleagues in 2006 using an in vitro cell culture model (2006). Data of Weidemann *et al.* (2009) further indicate a HIF-2α-dependent regulation of EPO production in a mouse model of an astrocyte-specific HIF-2α knockout, although they also found a contribution of HIF-1α, at least in the absence of HIF-2α. Therefore, our findings are in line with previous reports and confirm *Epo* as a HIF-2α specific target gene in astrocytes.

Leu *et al.* (2021) did not observe this HIF-2α-dependency in a HIF-2α KO neurosphere model of OGD (with 0.2% oxygen and no glucose, for up to 4 h). However, neurospheres resemble a pool of different cell types, including neurons, astrocytes and oligodendrocytes therefore potentially masking the astrocyte-specific effects. Furthermore, although the authors used an enhanced oxygen deprivation with only 0.2% O_2, they only incubated the cells for 4 h of OGD. This was probably not long enough to see the effects of HIF-2α depletion on *Epo* expression, as in this study, the *Epo* induction was still ongoing at 8 h and 24 h of hypoxia.Interestingly, the study of Chavez *et al.* (2006) reported a HIF-1α dependency of *Vegf* expression in astrocytes, although in the study presented here, *Vegf* expression is even more prominently reduced in HIF-2α KO astrocytes than *Epo*. Similar results were seen in a murine hepatocyte model based on von-Hippel-Lindau protein knockout mice, where Rankin *et al.* (2008) suggested that HIF-2α dominantly regulates hepatic *Vegf* expression. Nevertheless, it was already mentioned that functions of HIF-1 and HIF-2 are to some extent tissue- and cell type-specific. For instance, in MCF-7 cells, a human breast cancer cell line, HIF-1α primarily contributed to hypoxia-induced *Vegf* expression, whereas in the same study, HIF-2α primarily contributes to constitutive *Vegf* expression in renal carcinoma cells (Carroll and Ashcroft, 2006). In the neurosphere approach from Leu *et al* (2021), a reduced *Vegf* expression was furthermore correlated to the HIF-2α KO.

Conclusively, further research needs to address the question, if *Vegf* expression in astrocytes is indeed predominantly HIF-2α-specific as it was shown for the present study.

It is worth mentioning that the hypoxic up-regulation of *Vegf* and *Epo* was not completely eliminated, but only significantly reduced in the HIF-2α KO astrocytes. Therefore, it seems as the hypoxic up-regulation might be triggered, at least partly, by other compensatory mechanisms, for example higher preference of HIF-1α for these genes. These results also fit with the findings of Weidemann *et al.*, as mentioned above. Moreover, HepG2 cells (human

liver cancer cell line) with HIF-2α depletion showed a reciprocal increase of HIF-1α, due to enhanced HIF-1α translation (Schulz *et al.*, 2012).

4.3.1.3. *Phd2* expression is increased in HIF-2α KO astrocytes compared to WT astrocytes

HIF prolyl hydroxylases (PHDs) act as important regulators of the HIF pathway. The activity of PHDs relies on their ability to hydroxylate specific proline residues within the oxygen-dependent degradation domain (ODD) of HIF-α subunits. PHDs have relatively low oxygen affinities and sense oxygen in physiologically relevant concentrations. Therefore, especially PHD2 is considered as the main cellular oxygen sensors in cells (Ivan and Kaelin, 2017). Additionally, PHD2 and PHD3 are target genes of HIFs itself, therefore resembling a negative feedback loop on HIF activation in order to precisely coordinate and limit overshooting hypoxia response or upon re-oxygenation (D'Angelo *et al.*, 2003).

In astrocytes, *Phd3* induction was much higher than *Phd2* induction in comparison to the normoxic basal levels and *Phd3* levels were comparable between both genotypes. This is consistent with for example results of Rosiewicz *et al.* (2023) where in different hypoxic astrocyte cell lines *Phd3* was more induced than *Phd2*.

PHD2 is reported to be more abundantly expressed and translated, especially under normoxic conditions and is thought to be the main initial regulator of hypoxia response (Rabie *et al.*, 2011). However, the abundance of PHD enzymes is in general tissue-specific as proven in an elegant study of Appelhoff *et al.* (2004) using different cell lines. They furthermore saw, that PHD3 was often significantly higher induced under hypoxia than PHD2, although this was not the case for all tested cell lines. Taken together, the higher induction of *Phd3* fits to other studies.

Interestingly, whereas *Phd3* levels were comparable between both genotypes, *Phd2* induction was significantly higher in HIF-2α KO astrocytes compared to WT astrocytes.

Especially HIF-1α is attributed to bind to the HRE of *Phd2* and induce the feedback mechanism (D'Angelo *et al.*, 2003). To assess, if the higher *Phd2* levels in HIF-2α KO astrocytes were because of an increase in HIF-1α to compensate for the loss of HIF-2α, protein abundance and gene expression of HIF-1α was investigated in Western Blot and qPCR.

Though gene expression of HIF-1α was not significantly different in HIF-2α KO astrocytes compared to WT astrocytes, the overall expression seemed to be slightly induced in the HIF-2α KO astrocytes during prolonged hypoxia. Furthermore, HIF-1α protein levels of HIF-2α KO astrocytes were moderately induced during the hypoxic incubation. Upon visual inspection, HIF-1α seemed to be more abundant in HIF-2α KO astrocytes compared to WT astrocytes

although a direct quantification was not possible as samples were analyzed on different membranes of the Western Blot. Taken together, the reduced *Phd2* expression in HIF-2α KO astrocytes could indeed be to a compensatory higher induction of HIF-1α on both gene and protein level.

Unexpectedly, both WT and HIF-2α KO astrocytes already showed HIF-1α protein accumulation at normoxic conditions and especially for WT astrocytes, HIF-1α levels did not further increase under hypoxic conditions. In contrast, HIF-2α was substantially induced in the WT astrocytes. Nevertheless, the astrocytes responded to 1% of oxygen through up-regulation of target genes. Therefore, the normoxic astrocytes probably only exhibited some sort of mild hypoxia due to the culture condition where the neuronal coverslip is on top of the astrocyte compartment, thereby reducing the surface exposed to the surrounding air. In addition, HIF-1 is rather thought to act on acute and short hypoxia in first minutes and hours whereas HIF-2 gets stabilized under prolonged and severe hypoxia after some hours up to a day, as proven in different cell types (Jaskiewicz *et al.*, 2022; Koh and Powis, 2012; Serocki *et al.*, 2018).

4.3.1.4. Adora2a, but not Adora1, is a hypoxia target gene in astrocytes, though independent of HIF-2α

Adora1 and Adora2a are the main adenosine receptors in the brain and function, amongst others, in regulating neurotransmission. While both receptors are G-protein coupled, the downstream intracellular second messenger pathways differ. Adora1 activation leads to a decrease in intracellular cAMP and therefore inhibition of synaptic activity while Adora2a activation increases intracellular cAMP levels, leading to enhanced synaptic activity (Liu and Xia, 2015).

Adora2a is not considered as a standard hypoxia target gene such as *Vegf*, *Epo* or *Glut-1*. Adenosine signaling and synthesis itself are increased under hypoxia or energy depletion, when adenosine serves as a main signaling molecule for the adaptation of cells to acute stress conditions. In the literature, one finds inconsistent results regarding the hypoxic induction of Adora2a and it remains unclear whether HIF-1 or HIF-2 is the main driver of this induction. Whereas both gene and protein levels of Adora2a were induced under hypoxic conditions (as proven by Western and Northern Blotting) and even in a HIF-2α-specific manner in human lung microvascular endothelial cells, the same study reported no hypoxic induction of *Adora2a* expression in pulmonary mouse-derived endothelial cells at all (Ahmad *et al.*, 2009). Kong *et al.* (2006), in turn, reported a HIF-1α-mediated up-regulation of *Adora2a* in human microvascular endothelial cells. In addition, *Adora2a* levels were significantly induced in murine retinal endothelial cells during the hypoxic phase of a mouse model of oxygen-induced

retinopathy, in contrast to *Adora1*, *Adora2b* and *Adora3*. The same study found identical results in hypoxic human primary retinal microvascular endothelial cells and showed that HIF-2α is mainly responsible for the Adora2a up-regulation (Liu *et al.*, 2017). Expression of *Adora2a* was furthermore increased in hypoxic (1% O_2) patient-derived chronic lymphocytic leukemia cells (Serra *et al.*, 2016).
Herein, *Adora2a*, but not *Adora1*, expression was significantly induced in astrocytes under hypoxic incubation for all tested co-culture combinations. However, although being a hypoxia target gene in murine astrocytes, the induction was independent of HIF-2α.

Overall, in the hypoxic or ischemic brain, adenosine acts through the Adora1 and Adora2a receptors as a rather neuroprotective agent. For instance, activation of Adora1 receptor leads to a reduction in neuronal activity by inhibiting the release of neurotransmitters such as glutamate, GABA and acetylcholine. This decrease in neurotransmitter release helps to conserve energy and prevent further cellular damage during hypoxia and glutamate-induced excitotoxicity. Adora1 also influences potassium channels, reducing neuronal excitability, which helps to maintain cellular ionic balance during periods of oxygen deprivation (Liu and Xia, 2015). Additionally, stimulation of Adora2a has neuroprotective effects by promoting cerebral blood flow and inducing vasodilation through its activation in brain endothelial cells. Increased blood flow can help to deliver more oxygen and nutrients to the affected brain regions, minimizing the extent of hypoxic damage. Furthermore, Adora2a activation leads to the inhibition of inflammatory processes. On the other hand, Adora2a inactivation as well showed neuroprotective effects through for example inhibition of glutamate release, which represents a contradictory role of Adora2a activation or inactivation both resulting in neuroprotection. This diverse role may depend on different stages of pathological processes or the pre-dominantly activated cell types (Chen *et al.*, 2014; Liu and Xia, 2015).

Adenosine also acts as a modulator of astrocytic function, although the precise mechanisms are unknown yet. In astrocytes, Adora1 is responsible for inducing an immunosuppressive response and Adora1 activation decreases astrocyte proliferation and astrogliosis (Agostinho *et al.*, 2020). Adora1 further helps to protect astrocytes from cell death, as shown in different studies using hypoxic or OGD incubation (Bjorklund *et al.*, 2008; Ciccarelli *et al.*, 2007).
In contrast, Adora2a activation can lead to transcriptional disruption and facilitates astrocyte proliferation and reactive gliosis, which was shown in reactive astrocytes in vitro. Moreover, astrocytic Adora2a plays a role in regulating synaptic transmission by controlling glutamate release and uptake. Glutamate can be increased in the extracellular compartment, which involves modulating the levels of glutamate transporters like GLT-1 and the activity of Na^+/K^+-ATPase (all reviewed in Agostinho *et al.*, 2020; Boison *et al.*, 2010 and Lopes *et al.*, 2021).

These functions might also be enhanced through the up-regulated *Adora2a* expression in the astrocytes as seen in this study.

4.3.1.5. The hypoxic up-regulation of target genes is more prominent in astrocytes than in neurons

When comparing the degree of induction of hypoxia target genes in terms of fold changes between astrocytes and neurons, it is noticeable that the induction in astrocytes was substantially higher when compared to the induction in neurons. Whereas astrocytes show an induction in the expression of *Vegf* up to 14-fold, *Phd2* up to 8-fold and *Phd3* up to 17-fold, *Vegf* expression in neurons is only induced up to 4-fold, *Phd2* up to 3-fold and *Phd3* up to 4-fold. Of note, these results are just showing the induction of gene expression compared to the normoxic controls in the specific cell population. It is not a quantification of the levels of total mRNA transcripts, therefore the basal expression levels of for example *Vegf* could already be substantially different between neurons and astrocyte. However, Chavez *et al.* (2006) reported similar results on gene expression levels when incubating neurons and astrocytes under 0.5% hypoxia or under oxygen-glucose deprivation (OGD) for 24 h. They furthermore measured secreted EPO and VEGF levels by ELISA and total levels of both were significantly lower in neuronal-conditioned medium than in astrocyte-conditioned medium.

Neurons are notably susceptible to oxygen shortage because of their high energetic demand, so it is possible that their basal expression levels of genes crucial for survival and cellular homeostasis under difficult environmental conditions are already higher than in astrocytes.

In addition, neurons extremely rely on the support of astrocytes also in terms of energy and nutrient provision and neuronal survival. VEGF, for example, has been shown to exert direct neurotrophic effects in neurons but also indirectly through secretion by astrocytes (Rosenstein *et al.*, 2010). Furthermore, the secretion of EPO or other growth factors from astrocytes can modulate neuronal survival during ischemic events (Ruscher *et al.*, 2002).

Therefore it is possible that the intense VEGF and EPO secretion of hypoxic astrocytes exceeds the need of the neurons for an own intensified production under hypoxic conditions and astrocytes indeed support neurons through trophic mechanisms.

4.3.2. Hypoxic response of WT and HIF-2α KO neurons

4.3.2.1. The expression of hypoxia target genes *Vegf*, *Phd2* and *Phd3* is not HIF-2α-dependent in neurons

Overall, when incubated under hypoxic conditions neurons significantly responded to the reduced oxygen levels, as proven by up-regulation of the hypoxia target gene *Vegf*. As mentioned in the introduction, VEGF thereby not only serves as a pro-angiogenic factor for

recruitment of endothelial cells, but also exhibits functions in direct neuroprotection. In addition, the gene expression of the oxygen sensors and negative regulators of the hypoxia pathway *Phd2* and *Phd3* was significantly induced. Therefore, the neurons responded to the hypoxic conditions, which verifies the used experimental set-up.

In contrast to astrocytes, neurons showed no significant induction of the expression of *Epo* under hypoxic conditions although a slight increase was seen for neurons incubated with HIF-2α KO astrocytes. In addition, *EpoR*, the respective EPO receptor, was slightly induced in neurons co-cultured with HIF-2α KO astrocytes, but not with WT astrocytes. In general, *Epo* and *EpoR* are known to be expressed in both astrocytes and neurons and studies showed inductions in both cell types under hypoxic conditions, although astrocytes seem to be the main source of brain-derived EPO (for review, see Noguchi *et al.*, 2007), which was verified in this study. Furthermore, in contrast to astrocytes, *Adora2a* expression was not induced in neurons incubated with WT astrocytes.

Whereas in the astrocytes, *Vegf* and *Epo* induction seems to be mainly HIF-2α dependent, this was not seen for the hippocampal neurons in this study. Both WT and HIF-2α KO neurons showed a similar induction of all hypoxia target genes. This again perfectly indicates the cell-type specific functions of HIF-2α. Therefore, precise research is necessary when treatment options of for example ischemic stroke or neural disorders are developed.

4.3.2.2. The up-regulation of neuronal *Vegf* and *Phd2* depends on the HIF-2α status of astrocytes

Though neuronal HIF-2α had no direct effect on the expression of hypoxia target genes in the neurons itself, as WT and HIF-2α KO neurons exhibited a similar up-regulation of *Vegf*, *Phd2* and *Phd3*, a significant impact of the HIF-2α status of the astrocytes on the neuronal expression was observed in this study. The *Vegf* and *Phd2* basal expression and induction under hypoxia in both WT and HIF-2α KO neurons was significantly lower for neurons incubated with HIF-2α KO astrocytes in comparison to incubation with WT astrocytes.

When reconsidering the results from astrocytic hypoxic induction, the HIF-2α KO in astrocytes led to a significantly lower induction of *Vegf* and *Epo*, and a higher induction of *Phd2* in the HIF-2α KO astrocytes. Methodically, neurons are first seeded out and settled down on coverslips in a different compartment separated from the astrocytes, before the coverslips were transferred on top of the astrocytes. Thus, a possible interference in the gene expression results of the neurons due to intermixed astrocytes is ruled out.

This difference in *Vegf* and *Phd2* expression leads to the assumption that a HIF-2α loss in astrocytes changes the astrocytic hypoxia answer in such way, that neuronal expression and neuronal response to hypoxia are affected indirectly or in a paracrine manner. It was shown in

this study and others, that astrocytes are neurotrophic and have a higher hypoxic response than neurons. As this response is diminished in HIF-2α KO astrocytes, one can speculate that maybe the neuronal response to hypoxia is enhanced as a compensatory mechanism and more VEGF is produced by the neurons to act as a neuroprotective agent in an autocrine manner. In fact, the opposite is the case, at least in term of expression of hypoxia target genes. As the neuronal hypoxic response is diminished upon loss of HIF-2α in astrocytes, the neurons showed a compensatory significantly induced *EpoR* expression when co-cultured with HIF-2α KO astrocytes. Likewise, VGFR2, a VEGF receptor, showed a tendency for higher expression levels.

Thus, neurons do not respond to the diminished VEGF and EPO levels secreted by HIF-2α KO astrocytes with an up-regulation of *Vegf* or *Epo* itself, but with an up-regulation of the respective receptors under prolonged hypoxia, resulting in a higher susceptibility for lower extracellular VEGF and EPO levels.

Both EPO and VEGF have potent neuroprotective properties in vivo and in vitro. It is known that for example during ischemia the secretion of EPO or other growth factors by astrocytes can modulate the capacity of neurons to survive ischemic stress (Ruscher *et al.*, 2002). EPO regulates these effects through binding to its receptor, EpoR, which activates different pathways resulting in a decrease in apoptosis, expression of miRNAs regulating the apoptotic process, oxidative stress and neuroinflammation, as well as an increase in neuroprotective actions like synaptic plasticity, neurogenesis and autophagy, mostly through the EpoR/PI3K/Akt and EpoR/MAPK pathway (Rey *et al.*, 2019). In HIF-2α KO experiments Chavez *et al.* (2006) additionally identified that astrocyte-derived EPO, taken from conditioned medium of hypoxic astrocytes, protected neurons exposed to OGD, while conditioned medium of HIF-2α KO astrocytes did not show these protective effects. Therefore, HIF-2α-dependent factors secreted by astrocytes can affect the survival of neurons exposed to oxygen-glucose deprivation in a paracrine manner. However, the effects were only evaluated based on viability assays and no further analysis of the modulation of intracellular signaling pathways inside the neurons were performed. VEGF acts through different VEGF receptors, for example VEGFR2, a tyrosine kinase, or Neuropilin1, and VEGF was shown to be a neuroprotective factor in many studies. Thereby, VEGF has a dual neurotrophic role in either directly affecting neurons or indirectly through effects mediated by astrocytes or other glial cells (Rosenstein *et al.*, 2010). The VEGF/VEGF receptor axis regulates the activity of several downstream kinases like Phosphokinase C or the PI3K-Akt pathway leading to overall effects on cell proliferation, migration, survival and vascular permeability (Apte *et al.*, 2019)

When a loss of functional HIF-2α dampens the hypoxic response in astrocytes, less VEGF or EPO is secreted into the extracellular compartment, leading to reduced effects of both on

regulating cellular responses and adaptation mechanisms of neurons to hypoxia. In addition, there might be other factors changed in the astrocytes due to a HIF-2α KO besides the reduced expression of *Vegf* and *Epo*, which have not been deciphered in this study and may be the main reason for the diminished neuronal response to hypoxia.
The neurons thereby do respond to hypoxic stimuli on their own, as the hypoxic induction of gene expression is not completely eliminated. But overall, the HIF pathway in neurons appears to be less sensitive and weaker, and further enhancement of the neuronal intrinsic adaptation to hypoxia requires additional support by paracrine factors secreted by astrocytes.

Besides *Vegf*, also *Phd2* expression in neurons was dependent on the HIF-2α status of the astrocytes and was significantly lower in neurons co-cultured with HIF-2α KO astrocytes. *Phd3* expression thereby remained unaffected by the astrocytic HIF-2α status.
This study already showed that the expression of *Phd2* and *Phd3* is not HIF-2α-dependent in neurons themselves. Furthermore, astrocytes also showed no tendency for a HIF-2α regulated gene expression of these two genes.
As mentioned before, PHDs are important regulators and suppressors of the HIF pathway. Prolonged hypoxia and HIF activation thereby enhance PHD abundance as *Phd* genes are targets of HIFs themselves, therefore regulating their own activation in a negative feedback loop. When co-cultured with HIF-2α KO astrocytes, the neurons are only minimally stimulated by for example VEGF and EPO secreted by the astrocytes. Therefore, the neurons themselves probably have no demand for further negative regulation of their own hypoxia response.
As mentioned before, PHD2 is reported to be the most abundant form in the brain (Rabie *et al.*, 2011) and is also considered as the key oxygen sensor especially under normoxic conditions. Furthermore, PHD2 seems to preferably interact with HIF-1α while PHD3 seems to predominantly affect HIF-2α under hypoxic conditions (Appelhoff *et al.*, 2004), although this must always be viewed in the complete cellular context. Under normoxic conditions for example, PHD2 appears to act equally on both HIF-1 and HIF-2 (Berra *et al.*, 2003; Wielockx *et al.*, 2019). In the brain, it was shown that a neuron-specific PHD2 KO reduces brain injury in a mouse model of transient cerebral ischemia (Kunze *et al.*, 2012) and improves ischemic stroke recovery in a HIF-dependent manner (Li *et al.*, 2016).
Therefore, the lower levels of *Phd2* in neurons co-cultured with HIF-2α KO astrocytes compared to co-culture with WT astrocytes may lead to and enhance a positive outcome on the neurons, as the astrocytic neuroprotective effects are diminished.

4.3.2.3. Neuronal HIF-2α is not important for expression of genes associated with synaptic formation and function

One major part of this study was to address the question if HIF-2α abundance in neurons is correlated with gene expression associated to synaptic formation and function. For this, the expression of genes related to different functional panels was investigated for all cultured genetic combinations of neurons and astrocytes. Furthermore, potential HIF-2α target genes based on literature were assessed.

Tested genes included general neuronal markers like *bIII-Tubulin*, the universal growth factor *Bdnf*, genes associated with excitatory or inhibitory synapse formation, genes associated to the pre- and post-synapse and genes of subunits of synaptic receptors. In total, no significant differences were found in expression levels of those genes between WT and HIF-2α KO neurons. Furthermore, no new hypoxia-inducible target genes were identified. Gene expression rather stayed stable or had a tendency for down-regulation, for example *Nrgn, Dap4, Gphrn, Collibystin* and *Bdnf* expression, over the hypoxic time-course. This is in line with common knowledge that hypoxic responses of neurons include a decline in synaptic signaling, usually a result of changes in anaerobic metabolism. This serves as a protection mechanism of neurons in the challenging hypoxic environment (Mukandala *et al.*, 2016), although a BDNF overexpression was also contributed with neuroprotective effects in different studies such as hypoxic-ischemic brain injury (Chen *et al.*, 2013; Turovskaya *et al.*, 2020; Wang *et al.*, 2006).

Surprisingly, gene expression of *Synapsin*, *Dap4* and *Nrgn* was comparable between WT and HIF-2α KO neurons. In these genes, Kleszka *et al.* (2020) reported affected expression levels in HIF-2α KO tissue and cells in vivo and in vitro. Whereas the neurosphere system used by Kleszka and colleagues (2020) is a mixture of different cell types that differentiated out of neural stem cells (NSC), the culture used here is indeed a pure neuronal culture. Therefore, effects on gene transcription level are solely based on changes in the neuronal phenotype. It might be that the reduced expression levels of for example *Synapsin* and *Dap4* in HIF-2α KO neurospheres are not based on changes in expression levels of the neuron subpopulation itself, but that the overall number of neurons is diminished in HIF-2α KO neurospheres. Indeed, in the study of Kleszka *et al.* this was the case for normoxic conditions as visualized by immunocytochemical stainings for different cell type-specific markers. However, the authors discussed this as a result of impaired migration capabilities due to HIF-2α loss and not due to differences in overall differentiation of NSCs into neurons (Kleszka *et al.*, 2020). In addition, Kleszka *et al.* investigated effects of HIF-2α KO during longer times of hypoxia with 24 h, 48 h and 72 h time-points and the differences became more prominent at later stages of hypoxic incubation. Here, effects of HIF-2α KO were assessed in the first 24 h of hypoxia.

Yet, as the system used in this study is methodically more suitable for the research question of this study, it is more likely that neuronal HIF-2α does not influence synapse-associated gene expression itself. Nevertheless, indirect effects of HIF-2α on gene expression in neurons are possible, as discussed in the following chapter. Therefore, the differences seen by Kleszka *et al.* might also be due to indirect effects resulting from HIF-2α-dependent changes of other cell types in the neurospheres.

Taken together, neuronal HIF-2α is not important for the transcription of synapse-associated genes in the neurons themselves, neither under normoxic nor under hypoxic conditions.

4.3.2.4. The HIF-2α status of astrocytes affects the neuronal expression of genes associated with synaptic function and hypoxic adaptation

A HIF-2α KO in neurons did not lead to any detectable changes in the expression of different synapse-associated genes. On the contrary, the HIF-2α KO in astrocytes had a significant impact on gene expression levels in the neurons related to different functions in synaptic signaling and hypoxic adaptation. Figure 4.1 summarizes the genes that were expressed at either higher or lower levels in neurons of both genotypes when co-cultured with HIF-2α KO astrocytes compared to co-cultivation with WT astrocytes.

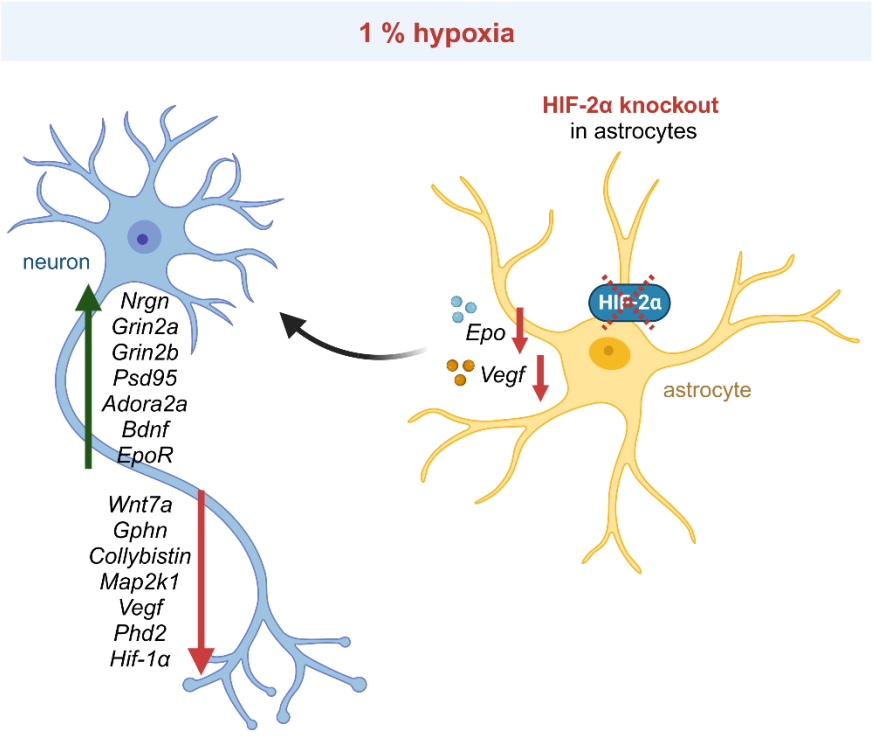

Figure 4.1: Altered gene expression in both WT and HIF-2α KO neurons + HIF-2α KO astrocytes.
Under hypoxic incubation, neurons of both genotypes (WT and HIF-2α KO) showed an altered gene expression when co-cultured with HIF-2α KO astrocytes, compared to co-culture with WT astrocytes. HIF-2α KO astrocytes themselves exhibited a significant down-regulation of *Epo* and *Vegf* gene levels. Green arrow = up-regulation, red arrow = down-regulation. Created with BioRender.com.

The differences in expression levels of *Vegf* and *Phd2* were already discussed (4.3.2.2).
Considering the cellular functions of the gene products, it is apparent that genes associated with excitatory synapses are higher expressed while genes associated with inhibitory synapses showed a reduced expression in the neurons when co-cultured with HIF-2α KO astrocytes.
Neurogranin (*Nrgn*) is a Calmodulin-binding protein mainly located in dendritic spines of excitatory synapses. It is mainly found post-synaptically where it senses Ca^{2+} influx through NMDA receptors. By determining Calmodulin availability, Neurogranin regulates synaptic plasticity and function and is attributed to enhance and fine-tune LTP (Zhong *et al.*, 2011). Recent studies furthermore link Neurogranin abundance to synaptic dysfunction in Alzheimer's, making it a potential biomarker for this disease (Agnello *et al.*, 2021).
Grin2a and Grin2b are subunits of the NMDA receptor, the glutamate-gated ion channels typically found in the membrane of the post-synaptic compartment. During ischemia or traumatic brain injury, especially Grin2b-containing receptors are excessively activated and contribute to glutamate-induced excitotoxicity (Paoletti *et al.*, 2013).
PSD95 is a post-synaptic scaffolding protein important for clustering NMDA and AMPA receptors at the post-synapse and has been shown to interact with for example Grin2b and Grin2c. Through increasing the local density of important receptors and channels, PSD95 plays an important role in synaptic plasticity and the stabilization of synaptic changes during long-term potentiation (Coley and Gao, 2018).
The adenosine-receptor Adora2a is furthermore predominantly expressed on glutamatergic excitatory pre- and post-synapses and enhances glutamate release as well as NMDA receptor activation, regulating the induction and expression of LTPs and LTDs (Chen *et al.*, 2014). Although the *Adora2a* expression between co-culturing neurons with HIF-2α KO astrocytes or WT astrocytes was not significantly different, there was a tendency for up-regulation of *Adora2a* in the neurons co-cultured with HIF-2α KO astrocytes especially under prolonged hypoxia. Therefore, neuronal *Adora2a* expression seems to be dependent on the astrocytic HIF-2α status. However, *Adora2a* expression in the astrocytes themselves was independent of the astrocytic HIF-2α status, as *Adora2a* gene levels were induced under hypoxia in both WT and HIF-2α KO astrocytes.
Bdnf expression was higher in neurons co-cultured with HIF-2α KO astrocytes too. However, similar to when co-cultured with WT astrocytes, the expression over the hypoxic time course rather decreased. Instead, the basal expression was already much higher under NOX conditions. BDNF is a growth factor with multiple and complex functions in the nervous system, for example through interaction with the glutamate-releasing system. The existence of a proBDNF form with sometimes opposing effects additionally increases the complexity of BDNF signaling. BDNF signaling pathway involves the binding to the TrkB receptor, which activates different intracellular signaling cascades like the PI3K/Akt or MAPK pathway (as

comprehensively reviewed by Kowianski *et al.*, 2018). Therefore, functions of BDNF always have to be discussed depending on the different cellular compartments, pathways activated and at which physiological or pathophysiological conditions BDNF function is assessed. Because of the complex regulation and function of BDNF, reasons for the higher expression in neurons in co-culture with HIF-2α KO astrocytes are difficult to assess without further experiments.

The induction of *EpoR* expression, especially under longer hypoxic incubation, is potentially the result of neuronal adaptation to the reduced expression of *Epo* in the HIF-2α KO astrocytes. When less EPO is present in the synaptic cleft that serve in a neuroprotective manner, an up-regulation of the EPO receptor in the neurons increases the possibility of EPO-EPO receptor interaction.

Besides genes that showed an up-regulation in neurons co-cultured with HIF-2α KO astrocytes, some genes also showed down-regulations under these conditions (Figure 4.1). As a reminder, Gephyrin and Collybistin are part of a framework of different proteins that cluster post-synaptic receptors like glycine or major GABAergic receptors at inhibitory synapses. In the in vitro experiments, the HIF-2α KO in astrocytes indirectly led to lower expression levels of these genes in neurons. *Gphn* and *Collybistin* gene levels in general were rather decreased over the time of hypoxic incubation in all culture combinations. These findings support research of Hwang and colleagues (2018) who focused on the alterations of inhibitory synapses following hypoxic injury in terms of compositional changes of inhibitory neuron-related proteins and the formation of inhibitory synapses. Hwang *et al.* could show that during hypoxia, the expression of numerous inhibitory neuron-related proteins are reduced such as glutamate decarboxylase enzymes important for synthesis of GABA and Gephyrin clusters at the PSD zone. The results in the study presented here extend these findings and show that under hypoxia, the expression of inhibitory synapse-associated genes like *Gephyrin* and *Collybistin* is down-regulated. Furthermore, a HIF-2α KO in astrocytes intensified the down-regulation in the neurons.

Map2k1, a member of the MAPK/ERK pathway, was shown to be less expressed in primary cilia of HIF-2α KO neurons (Leu *et al.*, 2023), which suggested that HIF-2 is an important regulator of the MAPK/ERK pathway at least in primary cilia of neurons. The study presented here did not report an overall effect of HIF-2α on this pathway in neurons by a neuronal HIF-2α KO, but *Map2k1* was expressed lower in neurons co-cultured with HIF-2α KO astrocytes. The MAPK/ERK signaling pathway plays a crucial role in controlling cell proliferation and survival (Guo *et al.*, 2020). This becomes especially significant during oxygen deficiency such as in stroke, where it acts to safeguard cells and tissues and facilitate the regeneration of damaged tissue. As discussed before, both EPO and VEGF can activate the MAPK/ERK

pathway by receptor binding, though this activation is not on a transcriptional level. How a HIF-2α KO in astrocytes then indirectly influences expression of Map2k1 needs to be further evaluated.

Strikingly, one further gene that was significantly less expressed in neurons co-cultured with HIF-2α KO astrocytes compared to a co-culture with WT astrocytes was *Hif-1α*. The main regulation of HIF-1α abundance and activity is post-transcriptionally through proteasomal degradation under normoxic conditions or stabilization under hypoxic conditions. The potential mechanism behind the reduced *Hif-1α* expression needs to be elucidated in future experiments. A potential consequence of the reduced expression might be that the respective neurons also show a dampened HIF-1α-dependent adaptation to the hypoxic incubation, together with an increased susceptibility to hypoxia-induced cell damage. This was for example shown for HIF-1α-deficient neurons in an in vitro study by Vangeison and colleagues (2008).

In summary, astrocytic HIF-2α appears to be important for the neuronal gene expression under hypoxic conditions. A loss of functional HIF-2α in astrocytes leads to higher neuronal expression of genes predominantly associated with excitatory synapses and the glutamatergic system with a further increase mostly in the expression under prolonged hypoxia. On the contrary, expression levels of genes associated with inhibitory, GABAergic synapses are reduced and expression further decreases under prolonged hypoxia. This indicates that during hypoxia, HIF-2α in astrocytes is important for fine-tuning the balance of excitatory and inhibitory neuronal circuits.

This study showed that the overall hypoxic response of neurons is diminished when HIF-2α is knocked out in astrocytes. Because of the lack of trophic support by the HIF-2α KO astrocytes, neurons seem to be unable to change their phenotype to a neuroprotective state and are incapable to reduce synaptic signaling in order to go into a survival mode. As excessive abundance or activation of glutamate receptors eventually causes excitotoxicity, HIF-2α of astrocytes seems to normally induce changes in neurons to reduce the potential effects of excessive receptor stimulation and activity under these energy-deprived conditions. Reduced neuronal *Vegf* and *Phd2* expression as negative feedback regulators additionally boosts the anti-neuroprotective mechanisms of a HIF-2α KO in astrocytes.

These findings continue the study of Leiton and colleagues (2018) who first reported on the particular functions of HIF-1 and HIF-2 in astrocytes regarding synaptic plasticity. They found that HIF-2α, not HIF-1α, in astrocytes is beneficial and supports synaptic plasticity and learning under mild hypoxia. When identifying important mechanisms responsible for the deficits in learning and LTP when HIF-2α is knocked out in astrocytes, they focused on analyses of the

glucose and lactate metabolism of astrocytes, where they found no HIF-2α-dependency in genes like Glut-1 and PDK-1.

The study presented here identified *Epo* and *Vegf* as significantly diminished factors in HIF-2α KO astrocytes that could potentially regulate processes of synaptic plasticity. Thus it seems contradictory that Leiton *et al.* found LTP impairment upon HIF-2α loss in astrocytes whereas the results presented in this study found enhanced expression levels of for example NDMA receptor subunits *Grin2a* and *Grin2b*, as NDMA receptors are also known to induce LTP and LTD events (Luscher and Malenka, 2012).

Conversely, the results presented here confirm and support other findings regarding the neurotrophic role of astrocytes, which is especially regulated by HIF-2. In addition, a closer look on the expression of synapse-associated genes showed that neurons failed to decrease the expression of genes important for reduction of synaptic signaling and transmission and the characteristic induction of hypoxia target genes was reduced when the HIF-2α-mediated support of astrocytes was missing.

4.4. Conclusion

In total, a HIF-2α KO in astrocytes resulted in more prominent effects on both cell types than a HIF-2α KO in neurons. By the use of a spatial separated co-culture system and the possibility to co-culture combinations of cell types with different genotypes (WT vs. HIF-2α KO), the discrimination of cell type-specific effects was possible. The in vitro co-culture studies demonstrated the broad effects of trophic factors secreted by astrocytes in regulating neuronal response and adaptation to hypoxia. Thereby, HIF-2α abundance in astrocytes plays a significant role and a loss of functional HIF-2α in astrocytes dampens the neuronal response to hypoxic stress, as astrocyte-derived neurotrophic factors like VEGF and EPO are less secreted into the synaptic cleft. Neurons respond to the lack of astrocytic HIF-2α with a diminished induction of hypoxia target genes like *Vegf* and *Phd2* and with higher expression of genes associated to the excitatory, glutamatergic system and lower expression of genes associated to the inhibitory, GABAergic system. HIF-2α in astrocytes seems to take part in regulating and fine-tuning the balance of excitatory and inhibitory synapses under hypoxic conditions whereas a HIF-2α KO seems to result in enhanced excitatory synaptic functions. Altogether, this potentially leads to a less neuroprotective phenotype in the neurons as synaptic transmission is not reduced and glutamate excitotoxicity is potentially enhanced.

This study further confirmed that EPO expression in astrocytes is dependent on HIF-2α and found that VEGF is a target gene of HIF-2α in astrocytes, too, although other studies reported different results.

PHDs, as HIF regulating enzymes, have been considered as potential therapeutic targets for different diseases, such as anemia in chronic kidney disease, as PHD inhibition leads to stabilization of HIFs. For neuroscience, this is especially interesting as several target genes of HIF show promoting effects in terms of post-stroke neuroprotection, neurogenesis and angiogenesis. Research on PHDs and their mechanisms of action, especially in terms of PHD1, PHD2 or PHD3-specific effects, as the PHD isoforms have certain preferences for hydroxylation of specific HIF isoforms, is currently ongoing. Here, it was shown that HIF-2α in astrocytes indirectly affects neuronal levels of *Phd2*, therefore, when functions and effects of PHD inhibitors are tested, direct and indirect effects in different cell types need to be considered.

The study furthermore illustrated the cell type-specific effects of HIF-2, as a neuronal loss of HIF-2α did not lead to changes in expression of synapse-associated genes. Neuronal HIF-2α seems to be of only limited importance at the synapse regarding the neuronal hypoxic response and regulation of important synaptic markers. None of the initially proposed potential target genes (1.3.2) could be verified as a HIF-2α-dependent synaptic gene in neurons. Of course, the genes tested in this study were exclusively chosen due to already known or potential connections with HIFs or hypoxia or because of their general function in synaptic formation and plasticity, based on for example the synaptic plasticity-related PCR profiler arrays. There might be changes in expression levels of other genes that have not been identified in this study. Transcriptomics technologies, for example RNA sequencing combined with gene function annotation is an option for further evaluation.

Although HIFs have been implicated in developmental processes even under normoxic conditions, this does not seem to be the case for HIF-2α regarding synapse-associated processes. Under normoxic conditions and during brain development, HIF-2α exhibited only restricted effects at the synapse. In the in vivo studies, a global HIF-2α KO did not lead to any outstanding differences in the expression of synapse-associated genes in cortex and hippocampus of adult animals even under environmentally enriched conditions. Plus, hippocampal tissue showed no gross morphological alterations between WT and HIF-2α KO animals. During development, young HIF-2α KO mice showed alterations in the expression of genes associated mainly with inhibitory synapse function, which were mostly up-regulated. However, these differences were no longer visible when mice were grown-up, indicating that these temporary effects are not fundamental for the animals.
It has to be taken into account that the brains of the HIF-2α KO animals used in the in vivo part have a global knockout in all NSCs-derived cell types. As the in vitro system clearly

demonstrated cell-type specific differences in the cellular response to a HIF-2α KO, further in vivo studies should consider this when developing future experiments.

4.5. Outlook

The experiments presented here mainly focused on descriptive analyses.
HIF-2α KO mice in vivo thereby showed differences in synaptic ultrastructure in the Stratum radiatum of the hippocampus as well as differences in gene expression levels of brain cell-specific markers or synapse-associated genes in neonatal HIF-2α KO mice compared to WT littermates, which diminished when mice got older.
Whether these effects have functional consequences in terms of synaptic transmission and plasticity need to be addressed in further experiments. One approach is the execution of electrophysiological measurements, for example by generating acute tissue slices of the hippocampus of HIF-2α KO and WT mice, where electrophysiological properties of individual neurons or circuits can be assessed. Especially the hippocampus is well suited for measurements of LTP and LTD. A major advantage of this technique is that the integrity of cellular architecture and synaptic circuits is preserved. To date, many protocols have been developed for an optimal preparation of the tissue (Lein *et al.*, 2011; Villers and Ris, 2013). Slices could furthermore be treated directly with different forms of hypoxia or HIF-stabilizing agents like dimethyloxaloylglycine (DMOG), a PHD inhibitor, and electric currents can be measured over a series of time. For longer-lasting experiments, organotypic slice cultures might be established from postnatal or adult brains as a three-dimensional ex vivo brain model. The slices can be cultured up to several weeks and used, amongst others, for further electrophysiological experiments like calcium imaging, genetic modifications or analysis by microscopy (Humpel, 2015).

Though a neuronal HIF-2α knockout did not show effects on gene expression levels in the neurons themselves, the influence of astrocytic HIF-2α on neuronal gene expression and hypoxic response in vitro is striking and requires further analysis. One further approach could be to study which exact paracrine factor of the astrocytes is responsible for the changed gene expression in neurons. This study reported a reduced gene expression of *Vegf* and *Epo* in the HIF-2α KO astrocytes, both of which are secreted factors that probably initiate changes in the neurons. To assess, which of both factors (or if at all) is responsible, siRNA experiments are an option to exclusively knock-down *Vegf* or *Epo* or both in WT astrocytes and compare the neuronal response to the experiments with the HIF-2α KO astrocytes.
Of further interest is which other parameters are changed in the neurons when co-cultured with HIF-2α KO astrocytes. Most studies so far investigated effects of astrocytes on neuronal

survival. As this study reported changed levels of genes associated to synaptic function, functional analyses of synaptic transmission and plasticity are of interest, especially as altered gene expression was associated with the glutamatergic system. Excessive glutamate levels or high stimulation of the respective receptors can lead to a Ca^{2+} overload and further excitotoxicity and neuronal death. Single-cell calcium imaging with use of chemical or genetically encoded calcium sensors or patch-clamp techniques are a method of choice to address functionality of neuronal circuits, as neuronal activity is accompanied with an influx of calcium ions. Of note, special experimental set-ups need to be developed, so that the cells can also be measured under hypoxic conditions. In connection with these experiments, it is interesting to analyze the relative occurrence of excitatory and inhibitory synapses and synaptic density changes, for example by immunocytological stainings and quantification for specific inhibitory or excitatory pre- and post-synaptic markers.

As neurons in co-culture with HIF-2α astrocytes express higher levels of excitatory-associated genes and lesser levels of inhibitory-associated genes, the question is whether the overall synaptic phenotype and balance between excitatory and inhibitory synapses has changed in these culture conditions.

Neurons are highly sensitive to glucose deprivation and changes in glucose and lactate metabolism occur during hypoxia. In general, adaptations in glucose metabolism in the brain are more attributed to HIF-1α. A recent study furthermore reported that in chronic hypoxia, glucose availability and hypoxic severity dictate the balance between HIF-1 and HIF-2 in astrocytes (Guo *et al.*, 2019). Agilent Technologies provides a tool to study how the neuronal metabolism and homeostasis changes under hypoxic conditions: the Seahorse XF Analyzer can measure two main metabolic pathways in real-time in living cells, namely mitochondrial respiration and glycolysis, by measuring the oxygen consumption rate and extracellular acidification rate. Analysis of these parameters in WT or HIF-2α KO neurons and astrocytes under both normoxic and hypoxic conditions will furthermore provide information on the functional metabolic outcome of a HIF-2α KO in these cells, especially as *Hif-1α* mRNA was significantly less abundant in neurons co-cultured with HIF-2α astrocytes.

Another aspect worth studying is synaptic maturation and aging. The in vitro experiments were so far only conducted in matured neurons with fully developed synapses, but the in vivo analyses of different age cohorts of WT and HIF-2α KO mice displayed potential effects of HIF-2α during early development of synapses. Thus, it is interesting to perform prospective experiments using the in vitro co-culture system of WT and HIF-2α KO neurons and astrocytes also with premature neurons still developing synaptic contacts.

5. REFERENCES

Adamcio, B., Sargin, D., Stradomska, A., Medrihan, L., Gertler, C., Theis, F., Zhang, M., Muller, M., Hassouna, I., Hannke, K., Sperling, S., Radyushkin, K., El-Kordi, A., Schulze, L., Ronnenberg, A., Wolf, F., Brose, N., Rhee, J. S., Zhang, W. and Ehrenreich, H. (2008). Erythropoietin enhances hippocampal long-term potentiation and memory. *BMC Biol, 6*, p. 37.

Adams, I. (1987). Plasticity of the synaptic contact zone following loss of synapses in the cerebral cortex of aging humans. *Brain Res, 424(2)*, p. 343-51.

Agnello, L., Lo Sasso, B., Vidali, M., Scazzone, C., Piccoli, T., Gambino, C. M., Bivona, G., Giglio, R. V., Ciaccio, A. M., La Bella, V. and Ciaccio, M. (2021). Neurogranin as a Reliable Biomarker for Synaptic Dysfunction in Alzheimer's Disease. *Diagnostics (Basel), 11(12)*.

Agostinho, P., Madeira, D., Dias, L., Simoes, A. P., Cunha, R. A. and Canas, P. M. (2020). Purinergic signaling orchestrating neuron-glia communication. *Pharmacol Res, 162*, p. 105253.

Ahmad-Annuar, A., Ciani, L., Simeonidis, I., Herreros, J., Fredj, N. B., Rosso, S. B., Hall, A., Brickley, S. and Salinas, P. C. (2006). Signaling across the synapse: a role for Wnt and Dishevelled in presynaptic assembly and neurotransmitter release. *J Cell Biol, 174(1)*, p. 127-39.

Ahmad, A., Ahmad, S., Glover, L., Miller, S. M., Shannon, J. M., Guo, X., Franklin, W. A., Bridges, J. P., Schaack, J. B., Colgan, S. P. and White, C. W. (2009). Adenosine A2A receptor is a unique angiogenic target of HIF-2alpha in pulmonary endothelial cells. *Proc Natl Acad Sci U S A, 106(26)*, p. 10684-9.

Al-Qahtani, J. M., Abdel-Wahab, B. A. and Abd El-Aziz, S. M. (2014). Long-term moderate dose exogenous erythropoietin treatment protects from intermittent hypoxia-induced spatial learning deficits and hippocampal oxidative stress in young rats. *Neurochem Res, 39(1)*, p. 161-71.

Almaguer-Melian, W., Merceron-Martinez, D. and Bergado-Rosado, J. (2023). A unique erythropoietin dosage induces the recovery of long-term synaptic potentiation in fimbria-fornix lesioned rats. *Brain Res, 1799*, p. 148178.

Almaguer-Melian, W., Merceron-Martinez, D., Delgado-Ocana, S., Alberti-Amador, E., Gonzalez-Gomez, R. and Bergado, J. A. (2018). Erythropoietin improves object placement recognition memory in a time dependent manner in both, uninjured animals and fimbria-fornix-lesioned male rats. *Horm Behav, 100*, p. 94-9.

Almaguer-Melian, W., Merceron-Martinez, D., Delgado-Ocana, S., Pavon-Fuentes, N., Ledon, N. and Bergado, J. A. (2016). EPO induces changes in synaptic transmission and plasticity in the dentate gyrus of rats. *Synapse, 70(6)*, p. 240-52.

Appelhoff, R. J., Tian, Y. M., Raval, R. R., Turley, H., Harris, A. L., Pugh, C. W., Ratcliffe, P. J. and Gleadle, J. M. (2004). Differential function of the prolyl hydroxylases PHD1, PHD2, and PHD3 in the regulation of hypoxia-inducible factor. *J Biol Chem, 279(37)*, p. 38458-65.

Apte, R. S., Chen, D. S. and Ferrara, N. (2019). VEGF in Signaling and Disease: Beyond Discovery and Development. *Cell, 176(6)*, p. 1248-64.

Arany, Z., Huang, L. E., Eckner, R., Bhattacharya, S., Jiang, C., Goldberg, M. A., Bunn, H. F. and Livingston, D. M. (1996). An essential role for p300/CBP in the cellular response to hypoxia. *Proc Natl Acad Sci U S A, 93(23)*, p. 12969-73.

Badawi, Y., Ramamoorthy, P. and Shi, H. (2012). Hypoxia-inducible factor 1 protects hypoxic astrocytes against glutamate toxicity. *ASN Neuro, 4(4)*, p. 231-41.

Barros, W., David, M., Souza, A., Silva, M. and Matos, R. (2019). Can the effects of environmental enrichment modulate BDNF expression in hippocampal plasticity? A systematic review of animal studies. *Synapse, 73(8)*, p. e22103.

Barrow, S. L., Constable, J. R., Clark, E., El-Sabeawy, F., Mcallister, A. K. and Washbourne, P. (2009). Neuroligin1: a cell adhesion molecule that recruits PSD-95 and NMDA receptors by distinct mechanisms during synaptogenesis. *Neural Dev, 4*, p. 17.

Barteczek, P., Li, L., Ernst, A. S., Bohler, L. I., Marti, H. H. and Kunze, R. (2017). Neuronal HIF-1alpha and HIF-2alpha deficiency improves neuronal survival and sensorimotor function in the early acute phase after ischemic stroke. *J Cereb Blood Flow Metab, 37(1)*, p. 291-306.

Basarsky, T. A., Parpura, V. and Haydon, P. G. (1994). Hippocampal synaptogenesis in cell culture: developmental time course of synapse formation, calcium influx, and synaptic protein distribution. *J Neurosci, 14(11 Pt 1)*, p. 6402-11.

Bayne, K. (2018). Environmental enrichment and mouse models: Current perspectives. *Animal Model Exp Med, 1(2)*, p. 82-90.

Bear, M. F., Connors, B. W. and Paradiso, M. A. (2018). Neurowissenschaften: Ein grundlegendes Lehrbuch für Biologie, Medizin und Psychologie.

Befani, C. and Liakos, P. (2018). The role of hypoxia-inducible factor-2 alpha in angiogenesis. *J Cell Physiol, 233(12)*, p. 9087-98.

Berra, E., Benizri, E., Ginouves, A., Volmat, V., Roux, D. and Pouyssegur, J. (2003). HIF prolyl-hydroxylase 2 is the key oxygen sensor setting low steady-state levels of HIF-1alpha in normoxia. *EMBO J, 22(16)*, p. 4082-90.

Bin Ibrahim, M. Z., Benoy, A. and Sajikumar, S. (2022). Long-term plasticity in the hippocampus: maintaining within and 'tagging' between synapses. *FEBS J, 289(8)*, p. 2176-201.

Bjorklund, O., Shang, M., Tonazzini, I., Dare, E. and Fredholm, B. B. (2008). Adenosine A1 and A3 receptors protect astrocytes from hypoxic damage. *Eur J Pharmacol, 596(1-3)*, p. 6-13.

Boison, D., Chen, J. F. and Fredholm, B. B. (2010). Adenosine signaling and function in glial cells. *Cell Death Differ, 17(7)*, p. 1071-82.

Budreck, E. C. and Scheiffele, P. (2007). Neuroligin-3 is a neuronal adhesion protein at GABAergic and glutamatergic synapses. *Eur J Neurosci, 26(7)*, p. 1738-48.

Burch, A., Tao-Cheng, J. H. and Dosemeci, A. (2017). A novel synaptic junction preparation for the identification and characterization of cleft proteins. *PLoS One, 12(3)*, p. e0174895.

Cao, W., Duan, J., Wang, X., Zhong, X., Hu, Z., Huang, F., Wang, H., Zhang, J., Li, F., Zhang, J., Luo, X. and Li, C. Q. (2014). Early enriched environment induces an increased conversion of proBDNF to BDNF in the adult rat's hippocampus. *Behav Brain Res, 265*, p. 76-83.

Carroll, V. A. and Ashcroft, M. (2006). Role of hypoxia-inducible factor (HIF)-1alpha versus HIF-2alpha in the regulation of HIF target genes in response to hypoxia, insulin-like growth factor-I, or loss of von Hippel-Lindau function: implications for targeting the HIF pathway. *Cancer Res, 66(12)*, p. 6264-70.

Chavez, J. C., Baranova, O., Lin, J. and Pichiule, P. (2006). The transcriptional activator hypoxia inducible factor 2 (HIF-2/EPAS-1) regulates the oxygen-dependent expression of erythropoietin in cortical astrocytes. *J Neurosci, 26(37)*, p. 9471-81.

Chen, A., Xiong, L. J., Tong, Y. and Mao, M. (2013). The neuroprotective roles of BDNF in hypoxic ischemic brain injury. *Biomed Rep, 1(2)*, p. 167-76.

Chen, J. F., Lee, C. F. and Chern, Y. (2014). Adenosine receptor neurobiology: overview. *Int Rev Neurobiol, 119*, p. 1-49.

Chen, V. S., Morrison, J. P., Southwell, M. F., Foley, J. F., Bolon, B. and Elmore, S. A. (2017). Histology Atlas of the Developing Prenatal and Postnatal Mouse Central Nervous System, with Emphasis on Prenatal Days E7.5 to E18.5. *Toxicol Pathol, 45(6)*, p. 705-44.

Chen, Z. Y., Warin, R. and Noguchi, C. T. (2006). Erythropoietin and normal brain development: receptor expression determines multi-tissue response. *Neurodegener Dis, 3(1-2)*, p. 68-75.

Choii, G. and Ko, J. (2015). Gephyrin: a central GABAergic synapse organizer. *Exp Mol Med, 47*, p. e158.

Christopherson, K. S., Ullian, E. M., Stokes, C. C., Mullowney, C. E., Hell, J. W., Agah, A., Lawler, J., Mosher, D. F., Bornstein, P. and Barres, B. A. (2005). Thrombospondins are astrocyte-secreted proteins that promote CNS synaptogenesis. *Cell, 120(3)*, p. 421-33.

Chung, W. S., Allen, N. J. and Eroglu, C. (2015). Astrocytes Control Synapse Formation, Function, and Elimination. *Cold Spring Harb Perspect Biol, 7(9)*, p. a020370.

Ciccarelli, R., D'alimonte, I., Ballerini, P., D'auro, M., Nargi, E., Buccella, S., Di Iorio, P., Bruno, V., Nicoletti, F. and Caciagli, F. (2007). Molecular signalling mediating the protective effect of A1 adenosine and mGlu3 metabotropic glutamate receptor activation against apoptosis by oxygen/glucose deprivation in cultured astrocytes. *Mol Pharmacol, 71(5)*, p. 1369-80.

Citri, A. and Malenka, R. C. (2008). Synaptic plasticity: multiple forms, functions, and mechanisms. *Neuropsychopharmacology, 33(1)*, p. 18-41.

Cockman, M. E., Masson, N., Mole, D. R., Jaakkola, P., Chang, G. W., Clifford, S. C., Maher, E. R., Pugh, C. W., Ratcliffe, P. J. and Maxwell, P. H. (2000). Hypoxia inducible factor-alpha binding and ubiquitylation by the von Hippel-Lindau tumor suppressor protein. *J Biol Chem, 275(33)*, p. 25733-41.

Coley, A. A. and Gao, W. J. (2018). PSD95: A synaptic protein implicated in schizophrenia or autism? *Prog Neuropsychopharmacol Biol Psychiatry, 82*, p. 187-94.

Colucci-D'amato, L., Speranza, L. and Volpicelli, F. (2020). Neurotrophic Factor BDNF, Physiological Functions and Therapeutic Potential in Depression, Neurodegeneration and Brain Cancer. *Int J Mol Sci, 21(20)*.

Corcoran, A., Kunze, R., Harney, S. C., Breier, G., Marti, H. H. and O'connor, J. J. (2013). A role for prolyl hydroxylase domain proteins in hippocampal synaptic plasticity. *Hippocampus, 23(10)*, p. 861-72.

Covello, K. L., Kehler, J., Yu, H., Gordan, J. D., Arsham, A. M., Hu, C. J., Labosky, P. A., Simon, M. C. and Keith, B. (2006). HIF-2alpha regulates Oct-4: effects of hypoxia on stem cell function, embryonic development, and tumor growth. *Genes Dev, 20(5)*, p. 557-70.

D'angelo, G., Duplan, E., Boyer, N., Vigne, P. and Frelin, C. (2003). Hypoxia up-regulates prolyl hydroxylase activity: a feedback mechanism that limits HIF-1 responses during reoxygenation. *J Biol Chem, 278(40)*, p. 38183-7.

Dandi, E., Kalamari, A., Touloumi, O., Lagoudaki, R., Nousiopoulou, E., Simeonidou, C., Spandou, E. and Tata, D. A. (2018). Beneficial effects of environmental enrichment on behavior, stress reactivity and synaptophysin/BDNF expression in hippocampus following early life stress. *Int J Dev Neurosci, 67*, p. 19-32.

Davis, C. K., Jain, S. A., Bae, O. N., Majid, A. and Rajanikant, G. K. (2018). Hypoxia Mimetic Agents for Ischemic Stroke. *Front Cell Dev Biol, 6*, p. 175.

Dienel, G. A. (2012). Brain lactate metabolism: the discoveries and the controversies. *J Cereb Blood Flow Metab, 32(7)*, p. 1107-38.

Dieterich, D. C. and Kreutz, M. R. (2016). Proteomics of the Synapse--A Quantitative Approach to Neuronal Plasticity. *Mol Cell Proteomics, 15(2)*, p. 368-81.

Dillman, A. A. and Cookson, M. R. (2014). Transcriptomic changes in brain development. *Int Rev Neurobiol, 116*, p. 233-50.

Duan, C. (2016). Hypoxia-inducible factor 3 biology: complexities and emerging themes. *Am J Physiol Cell Physiol, 310(4)*, p. C260-9.

Duan, L. J., Takeda, K. and Fong, G. H. (2014). Hypoxia inducible factor-2alpha regulates the development of retinal astrocytic network by maintaining adequate supply of astrocyte progenitors. *PLoS One, 9(1)*, p. e84736.

Dunwoodie, S. L. (2009). The role of hypoxia in development of the Mammalian embryo. *Dev Cell, 17(6)*, p. 755-73.

Epstein, A. C., Gleadle, J. M., Mcneill, L. A., Hewitson, K. S., O'rourke, J., Mole, D. R., Mukherji, M., Metzen, E., Wilson, M. I., Dhanda, A., Tian, Y. M., Masson, N., Hamilton, D. L., Jaakkola, P., Barstead, R., Hodgkin, J., Maxwell, P. H., Pugh, C. W., Schofield, C. J. and Ratcliffe, P. J. (2001). C. elegans EGL-9 and mammalian homologs define a family of dioxygenases that regulate HIF by prolyl hydroxylation. *Cell, 107(1)*, p. 43-54.

Faissner, A., Pyka, M., Geissler, M., Sobik, T., Frischknecht, R., Gundelfinger, E. D. and Seidenbecher, C. (2010). Contributions of astrocytes to synapse formation and maturation - Potential functions of the perisynaptic extracellular matrix. *Brain Res Rev, 63(1-2)*, p. 26-38.

Fandrey, J., Schodel, J., Eckardt, K. U., Katschinski, D. M. and Wenger, R. H. (2019). Now a Nobel gas: oxygen. *Pflugers Arch*.

Ghezzi, P. and Brines, M. (2004). Erythropoietin as an antiapoptotic, tissue-protective cytokine. *Cell Death Differ, 11 Suppl 1*, p. S37-44.

Giannone, G., Mondin, M., Grillo-Bosch, D., Tessier, B., Saint-Michel, E., Czondor, K., Sainlos, M., Choquet, D. and Thoumine, O. (2013). Neurexin-1beta binding to neuroligin-1 triggers the preferential recruitment of PSD-95 versus gephyrin through tyrosine phosphorylation of neuroligin-1. *Cell Rep, 3(6)*, p. 1996-2007.

Gordan, J. D., Bertout, J. A., Hu, C. J., Diehl, J. A. and Simon, M. C. (2007). HIF-2alpha promotes hypoxic cell proliferation by enhancing c-myc transcriptional activity. *Cancer Cell, 11(4)*, p. 335-47.

Grabrucker, A., Vaida, B., Bockmann, J. and Boeckers, T. M. (2009). Synaptogenesis of hippocampal neurons in primary cell culture. *Cell Tissue Res, 338(3)*, p. 333-41.

Gray, E. G. (1959). Electron microscopy of synaptic contacts on dendrite spines of the cerebral cortex. *Nature, 183(4675)*, p. 1592-3.

Gu, Y. Z., Moran, S. M., Hogenesch, J. B., Wartman, L. and Bradfield, C. A. (1998). Molecular characterization and chromosomal localization of a third alpha-class hypoxia inducible factor subunit, HIF3alpha. *Gene Expr, 7(3)*, p. 205-13.

Guo, M., Ma, X., Feng, Y., Han, S., Dong, Q., Cui, M. and Zhao, Y. (2019). In chronic hypoxia, glucose availability and hypoxic severity dictate the balance between HIF-1 and HIF-2 in astrocytes. *FASEB J, 33(10)*, p. 11123-36.

Guo, Y. J., Pan, W. W., Liu, S. B., Shen, Z. F., Xu, Y. and Hu, L. L. (2020). ERK/MAPK signalling pathway and tumorigenesis. *Exp Ther Med, 19(3)*, p. 1997-2007.

Gutierrez-Vera, B., Rivera-Olvera, A. and Escobar, M. L. (2022). Environmental enrichment attenuates conditioned taste aversion through the restoration of BDNF levels in the insular cortex. *Behav Brain Res, 430*, p. 113947.

Heinla, I., Leidmaa, E., Kongi, K., Pennert, A., Innos, J., Nurk, K., Tekko, T., Singh, K., Vanaveski, T., Reimets, R., Mandel, M., Lang, A., Lillevali, K., Kaasik, A., Vasar, E. and Philips, M. A. (2015). Gene expression patterns and environmental enrichment-induced effects in the hippocampi of mice suggest importance of Lsamp in plasticity. *Front Neurosci, 9*, p. 205.

Helan, M., Aravamudan, B., Hartman, W. R., Thompson, M. A., Johnson, B. D., Pabelick, C. M. and Prakash, Y. S. (2014). BDNF secretion by human pulmonary artery endothelial cells in response to hypoxia. *J Mol Cell Cardiol, 68*, p. 89-97.

Henneberger, C., Papouin, T., Oliet, S. H. and Rusakov, D. A. (2010). Long-term potentiation depends on release of D-serine from astrocytes. *Nature, 463(7278)*, p. 232-6.

Hewitson, K. S., Mcneill, L. A., Riordan, M. V., Tian, Y. M., Bullock, A. N., Welford, R. W., Elkins, J. M., Oldham, N. J., Bhattacharya, S., Gleadle, J. M., Ratcliffe, P. J., Pugh, C. W. and Schofield, C. J. (2002). Hypoxia-inducible factor (HIF) asparagine hydroxylase is identical to factor inhibiting HIF (FIH) and is related to the cupin structural family. *J Biol Chem, 277(29)*, p. 26351-5.

Hirabayashi, Y., Itoh, Y., Tabata, H., Nakajima, K., Akiyama, T., Masuyama, N. and Gotoh, Y. (2004). The Wnt/beta-catenin pathway directs neuronal differentiation of cortical neural precursor cells. *Development, 131(12)*, p. 2791-801.

Hodson, E. J., Nicholls, L. G., Turner, P. J., Llyr, R., Fielding, J. W., Douglas, G., Ratnayaka, I., Robbins, P. A., Pugh, C. W., Buckler, K. J., Ratcliffe, P. J. and Bishop, T. (2016). Regulation of ventilatory sensitivity and carotid body proliferation in hypoxia by the PHD2/HIF-2 pathway. *J Physiol, 594(5)*, p. 1179-95.

Hu, C. J., Sataur, A., Wang, L., Chen, H. and Simon, M. C. (2007). The N-terminal transactivation domain confers target gene specificity of hypoxia-inducible factors HIF-1alpha and HIF-2alpha. *Mol Biol Cell, 18(11)*, p. 4528-42.

Huang, E. J. and Reichardt, L. F. (2001). Neurotrophins: roles in neuronal development and function. *Annu Rev Neurosci, 24*, p. 677-736.

Huang, L. E., Gu, J., Schau, M. and Bunn, H. F. (1998). Regulation of hypoxia-inducible factor 1alpha is mediated by an O2-dependent degradation domain via the ubiquitin-proteasome pathway. *Proc Natl Acad Sci U S A, 95(14)*, p. 7987-92.

Humpel, C. (2015). Organotypic brain slice cultures: A review. *Neuroscience, 305*, p. 86-98.

Hwang, S., Ham, S., Lee, S. E., Lee, Y. and Lee, G. H. (2018). Hypoxia regulates the level of glutamic acid decarboxylase enzymes and interrupts inhibitory synapse stability in primary cultured neurons. *Neurotoxicology, 65*, p. 221-30.

Iommarini, L., Porcelli, A. M., Gasparre, G. and Kurelac, I. (2017). Non-Canonical Mechanisms Regulating Hypoxia-Inducible Factor 1 Alpha in Cancer. *Front Oncol, 7*, p. 286.

Irie, M., Hata, Y., Takeuchi, M., Ichtchenko, K., Toyoda, A., Hirao, K., Takai, Y., Rosahl, T. W. and Sudhof, T. C. (1997). Binding of neuroligins to PSD-95. *Science, 277(5331)*, p. 1511-5.

Ivan, M. and Kaelin, W. G., Jr. (2017). The EGLN-HIF O2-Sensing System: Multiple Inputs and Feedbacks. *Mol Cell, 66(6)*, p. 772-9.

Jaskiewicz, M., Moszynska, A., Kroliczewski, J., Cabaj, A., Bartoszewska, S., Charzynska, A., Gebert, M., Dabrowski, M., Collawn, J. F. and Bartoszewski, R. (2022). The transition from HIF-1 to HIF-2 during prolonged hypoxia results from reactivation of PHDs and HIF1A mRNA instability. *Cell Mol Biol Lett, 27(1)*, p. 109.

Jha, N. K., Jha, S. K., Sharma, R., Kumar, D., Ambasta, R. K. and Kumar, P. (2018). Hypoxia-Induced Signaling Activation in Neurodegenerative Diseases: Targets for New Therapeutic Strategies. *J Alzheimers Dis, 62(1)*, p. 15-38.

Jiang, B. H., Zheng, J. Z., Leung, S. W., Roe, R. and Semenza, G. L. (1997). Transactivation and inhibitory domains of hypoxia-inducible factor 1alpha. Modulation of transcriptional activity by oxygen tension. *J Biol Chem, 272(31)*, p. 19253-60.

Jones, E. G. (1994). Santiago Ramon y Cajal and the Croonian Lecture, March 1894. *Trends Neurosci, 17(5)*, p. 190-2.

Jones, E. V., Cook, D. and Murai, K. K. (2012). A neuron-astrocyte co-culture system to investigate astrocyte-secreted factors in mouse neuronal development. *Methods Mol Biol, 814*, p. 341-52.

Kaizuka, T. and Takumi, T. (2018). Postsynaptic density proteins and their involvement in neurodevelopmental disorders. *J Biochem, 163(6)*, p. 447-55.

Kallio, P. J., Okamoto, K., O'brien, S., Carrero, P., Makino, Y., Tanaka, H. and Poellinger, L. (1998). Signal transduction in hypoxic cells: inducible nuclear translocation and recruitment of the CBP/p300 coactivator by the hypoxia-inducible factor-1alpha. *EMBO J, 17(22)*, p. 6573-86.

Kins, S., Betz, H. and Kirsch, J. (2000). Collybistin, a newly identified brain-specific GEF, induces submembrane clustering of gephyrin. *Nat Neurosci, 3(1)*, p. 22-9.

Kleszka, K., Leu, T., Quinting, T., Jastrow, H., Pechlivanis, S., Fandrey, J. and Schreiber, T. (2020). Hypoxia-inducible factor-2alpha is crucial for proper brain development. *Sci Rep, 10(1)*, p. 19146.

Ko, C. Y., Tsai, M. Y., Tseng, W. F., Cheng, C. H., Huang, C. R., Wu, J. S., Chung, H. Y., Hsieh, C. S., Sun, C. K., Hwang, S. P., Yuh, C. H., Huang, C. J., Pai, T. W., Tzou, W. S. and Hu, C. H. (2011). Integration of CNS survival and differentiation by HIF2alpha. *Cell Death Differ, 18(11)*, p. 1757-70.

Koh, M. Y. and Powis, G. (2012). Passing the baton: the HIF switch. *Trends Biochem Sci, 37(9)*, p. 364-72.

Kong, T., Westerman, K. A., Faigle, M., Eltzschig, H. K. and Colgan, S. P. (2006). HIF-dependent induction of adenosine A2B receptor in hypoxia. *FASEB J, 20(13)*, p. 2242-50.

Kowianski, P., Lietzau, G., Czuba, E., Waskow, M., Steliga, A. and Morys, J. (2018). BDNF: A Key Factor with Multipotent Impact on Brain Signaling and Synaptic Plasticity. *Cell Mol Neurobiol, 38(3)*, p. 579-93.

Kunze, R., Zhou, W., Veltkamp, R., Wielockx, B., Breier, G. and Marti, H. H. (2012). Neuron-specific prolyl-4-hydroxylase domain 2 knockout reduces brain injury after transient cerebral ischemia. *Stroke, 43(10)*, p. 2748-56.

Lando, D., Peet, D. J., Gorman, J. J., Whelan, D. A., Whitelaw, M. L. and Bruick, R. K. (2002). FIH-1 is an asparaginyl hydroxylase enzyme that regulates the transcriptional activity of hypoxia-inducible factor. *Genes Dev, 16(12)*, p. 1466-71.

Lein, P. J., Barnhart, C. D. and Pessah, I. N. (2011). Acute hippocampal slice preparation and hippocampal slice cultures. *Methods Mol Biol, 758*, p. 115-34.

Leiton, C. V., Chen, E., Cutrone, A., Conn, K., Mellanson, K., Malik, D. M., Klingener, M., Lamm, R., Cutrone, M., Petrie, J. T., Sheikh, J., Dibua, A., Cohen, B. and Floyd, T. F. (2018). Astrocyte HIF-2alpha supports learning in a passive avoidance paradigm under hypoxic stress. *Hypoxia (Auckl), 6*, p. 35-56.

Leu, T., Denda, J., Wrobeln, A. and Fandrey, J. (2023). Hypoxia-Inducible Factor-2alpha Affects the MEK/ERK Signaling Pathway via Primary Cilia in Connection with the Intraflagellar Transport Protein 88 Homolog. *Mol Cell Biol, 43(4)*, p. 174-83.

Leu, T., Fandrey, J. and Schreiber, T. (2021). (H)IF applicable: promotion of neurogenesis by induced HIF-2 signalling after ischaemia. *Pflugers Arch, 473(8)*, p. 1287-99.

Li, C., Onouchi, T., Hirayama, M., Sakai, K., Matsuda, S., Yamada, N. O. and Senda, T. (2021). Morphological and functional abnormalities of hippocampus in APC(1638T/1638T) mice. *Med Mol Morphol, 54(1)*, p. 31-40.

Li, L., Saliba, P., Reischl, S., Marti, H. H. and Kunze, R. (2016). Neuronal deficiency of HIF prolyl 4-hydroxylase 2 in mice improves ischemic stroke recovery in an HIF dependent manner. *Neurobiol Dis, 91*, p. 221-35.

Lie, D. C., Colamarino, S. A., Song, H. J., Desire, L., Mira, H., Consiglio, A., Lein, E. S., Jessberger, S., Lansford, H., Dearie, A. R. and Gage, F. H. (2005). Wnt signalling regulates adult hippocampal neurogenesis. *Nature, 437(7063)*, p. 1370-5.

Liu, H. and Xia, Y. (2015). Beneficial and detrimental role of adenosine signaling in diseases and therapy. *J Appl Physiol (1985), 119(10)*, p. 1173-82.

Liu, Z., Yan, S., Wang, J., Xu, Y., Wang, Y., Zhang, S., Xu, X., Yang, Q., Zeng, X., Zhou, Y., Gu, X., Lu, S., Fu, Z., Fulton, D. J., Weintraub, N. L., Caldwell, R. B., Zhang, W., Wu, C., Liu, X. L., Chen, J. F., Ahmad, A., Kaddour-Djebbar, I., Al-Shabrawey, M., Li, Q., Jiang, X., Sun, Y., Sodhi, A., Smith, L., Hong, M. and Huo, Y. (2017). Endothelial adenosine A2a receptor-mediated glycolysis is essential for pathological retinal angiogenesis. *Nat Commun, 8(1)*, p. 584.

Lleo, A., Nunez-Llaves, R., Alcolea, D., Chiva, C., Balateu-Panos, D., Colom-Cadena, M., Gomez-Giro, G., Munoz, L., Querol-Vilaseca, M., Pegueroles, J., Rami, L., Llado, A., Molinuevo, J. L., Tainta, M., Clarimon, J., Spires-Jones, T., Blesa, R., Fortea, J., Martinez-Lage, P., Sanchez-Valle, R., Sabido, E., Bayes, A. and Belbin, O. (2019). Changes in Synaptic Proteins Precede Neurodegeneration Markers in Preclinical Alzheimer's Disease Cerebrospinal Fluid. *Mol Cell Proteomics, 18(3)*, p. 546-60.

Loboda, A., Jozkowicz, A. and Dulak, J. (2012). HIF-1 versus HIF-2--is one more important than the other? *Vascul Pharmacol, 56(5-6)*, p. 245-51.

Lohmann, C. and Kessels, H. W. (2014). The developmental stages of synaptic plasticity. *J Physiol, 592(1)*, p. 13-31.

Lopes, C. R., Cunha, R. A. and Agostinho, P. (2021). Astrocytes and Adenosine A(2A) Receptors: Active Players in Alzheimer's Disease. *Front Neurosci, 15*, p. 666710.

Lu, B., Pang, P. T. and Woo, N. H. (2005). The yin and yang of neurotrophin action. *Nat Rev Neurosci, 6(8)*, p. 603-14.

Lucas, F. R. and Salinas, P. C. (1997). WNT-7a induces axonal remodeling and increases synapsin I levels in cerebellar neurons. *Dev Biol, 192(1)*, p. 31-44.

Luscher, C. and Malenka, R. C. (2012). NMDA receptor-dependent long-term potentiation and long-term depression (LTP/LTD). *Cold Spring Harb Perspect Biol, 4(6)*.

Ma, L., Sebastian Garcia-Medina, J., Ortet, G., Lamanna, J. C. and Xu, K. (2021). Altered Behavioral Performance in the Neuron-Specific HIF-1- and HIF-2-Deficient Mice Following Chronic Hypoxic Exposure. *Adv Exp Med Biol, 1269*, p. 271-6.

Macias, D., Cowburn, A. S., Torres-Torrelo, H., Ortega-Saenz, P., Lopez-Barneo, J. and Johnson, R. S. (2018). HIF-2alpha is essential for carotid body development and function. *Elife, 7*.

Mahmoud, S., Gharagozloo, M., Simard, C. and Gris, D. (2019). Astrocytes Maintain Glutamate Homeostasis in the CNS by Controlling the Balance between Glutamate Uptake and Release. *Cells, 8(2)*.

Martens, L. K., Kirschner, K. M., Warnecke, C. and Scholz, H. (2007). Hypoxia-inducible factor-1 (HIF-1) is a transcriptional activator of the TrkB neurotrophin receptor gene. *J Biol Chem, 282(19)*, p. 14379-88.

Marti, H. H., Wenger, R. H., Rivas, L. A., Straumann, U., Digicaylioglu, M., Henn, V., Yonekawa, Y., Bauer, C. and Gassmann, M. (1996). Erythropoietin gene expression in human, monkey and murine brain. *Eur J Neurosci, 8(4)*, p. 666-76.

Martin, D., Xu, J., Porretta, C. and Nichols, C. D. (2017). Neurocytometry: Flow Cytometric Sorting of Specific Neuronal Populations from Human and Rodent Brain. *ACS Chem Neurosci, 8(2)*, p. 356-67.

Martinowich, K., Manji, H. and Lu, B. (2007). New insights into BDNF function in depression and anxiety. *Nat Neurosci, 10(9)*, p. 1089-93.

Maxwell, P. H., Wiesener, M. S., Chang, G. W., Clifford, S. C., Vaux, E. C., Cockman, M. E., Wykoff, C. C., Pugh, C. W., Maher, E. R. and Ratcliffe, P. J. (1999). The tumour suppressor protein VHL targets hypoxia-inducible factors for oxygen-dependent proteolysis. *Nature, 399(6733)*, p. 271-5.

Maynard, M. A., Evans, A. J., Hosomi, T., Hara, S., Jewett, M. A. and Ohh, M. (2005). Human HIF-3alpha4 is a dominant-negative regulator of HIF-1 and is down-regulated in renal cell carcinoma. *FASEB J, 19(11)*, p. 1396-406.

Mcgettrick, A. F. and O'neill, L. a. J. (2020). The Role of HIF in Immunity and Inflammation. *Cell Metab, 32(4)*, p. 524-36.

Megias, M., Emri, Z., Freund, T. F. and Gulyas, A. I. (2001). Total number and distribution of inhibitory and excitatory synapses on hippocampal CA1 pyramidal cells. *Neuroscience, 102(3)*, p. 527-40.

Metzen, E., Stiehl, D. P., Doege, K., Marxsen, J. H., Hellwig-Burgel, T. and Jelkmann, W. (2005). Regulation of the prolyl hydroxylase domain protein 2 (phd2/egln-1) gene: identification of a functional hypoxia-responsive element. *Biochem J, 387(Pt 3)*, p. 711-7.

Miranda, M., Morici, J. F., Zanoni, M. B. and Bekinschtein, P. (2019). Brain-Derived Neurotrophic Factor: A Key Molecule for Memory in the Healthy and the Pathological Brain. *Front Cell Neurosci, 13*, p. 363.

Missler, M., Sudhof, T. C. and Biederer, T. (2012). Synaptic cell adhesion. *Cold Spring Harb Perspect Biol, 4(4)*, p. a005694.

Mitroshina, E. V., Savyuk, M. O., Ponimaskin, E. and Vedunova, M. V. (2021). Hypoxia-Inducible Factor (HIF) in Ischemic Stroke and Neurodegenerative Disease. *Front Cell Dev Biol, 9*, p. 703084.

Mukandala, G., Tynan, R., Lanigan, S. and O'connor, J. J. (2016). The Effects of Hypoxia and Inflammation on Synaptic Signaling in the CNS. *Brain Sci, 6(1)*.

Nagai, A., Nakagawa, E., Choi, H. B., Hatori, K., Kobayashi, S. and Kim, S. U. (2001). Erythropoietin and erythropoietin receptors in human CNS neurons, astrocytes, microglia, and oligodendrocytes grown in culture. *J Neuropathol Exp Neurol, 60(4)*, p. 386-92.

Neves, G., Cooke, S. F. and Bliss, T. V. (2008). Synaptic plasticity, memory and the hippocampus: a neural network approach to causality. *Nat Rev Neurosci, 9(1)*, p. 65-75.

Nithianantharajah, J., Levis, H. and Murphy, M. (2004). Environmental enrichment results in cortical and subcortical changes in levels of synaptophysin and PSD-95 proteins. *Neurobiol Learn Mem, 81(3)*, p. 200-10.

Nobelprize.Org (2019). NobelPrize.org. Nobel Prize Outreach AB 2023. Fri. 9 Jun 2023. <https://www.nobelprize.org/prizes/medicine/2019/press-release/.

Noguchi, C. T., Asavaritikrai, P., Teng, R. and Jia, Y. (2007). Role of erythropoietin in the brain. *Crit Rev Oncol Hematol, 64(2)*, p. 159-71.

Novkovic, T., Mittmann, T. and Manahan-Vaughan, D. (2015). BDNF contributes to the facilitation of hippocampal synaptic plasticity and learning enabled by environmental enrichment. *Hippocampus, 25(1)*, p. 1-15.

Page, E. L., Robitaille, G. A., Pouyssegur, J. and Richard, D. E. (2002). Induction of hypoxia-inducible factor-1alpha by transcriptional and translational mechanisms. *J Biol Chem, 277(50)*, p. 48403-9.

Palay, S. L. (1956). Synapses in the central nervous system. *J Biophys Biochem Cytol, 2(4 Suppl)*, p. 193-202.

Paoletti, P., Bellone, C. and Zhou, Q. (2013). NMDA receptor subunit diversity: impact on receptor properties, synaptic plasticity and disease. *Nat Rev Neurosci, 14(6)*, p. 383-400.

Parpura, V. and Zorec, R. (2010). Gliotransmission: Exocytotic release from astrocytes. *Brain Res Rev, 63(1-2)*, p. 83-92.

Posfai, B., Cserep, C., Hegedus, P., Szabadits, E., Otte, D. M., Zimmer, A., Watanabe, M., Freund, T. F. and Nyiri, G. (2016). Synaptic and cellular changes induced by the schizophrenia susceptibility gene G72 are rescued by N-acetylcysteine treatment. *Transl Psychiatry, 6(5)*, p. e807.

Poth, J. M., Brodsky, K., Ehrentraut, H., Grenz, A. and Eltzschig, H. K. (2013). Transcriptional control of adenosine signaling by hypoxia-inducible transcription factors during ischemic or inflammatory disease. *J Mol Med, 91(2)*, p. 183-93.

Poulopoulos, A., Aramuni, G., Meyer, G., Soykan, T., Hoon, M., Papadopoulos, T., Zhang, M., Paarmann, I., Fuchs, C., Harvey, K., Jedlicka, P., Schwarzacher, S. W., Betz, H., Harvey, R. J., Brose, N., Zhang, W. and Varoqueaux, F. (2009). Neuroligin 2 drives postsynaptic assembly at perisomatic inhibitory synapses through gephyrin and collybistin. *Neuron, 63(5)*, p. 628-42.

Pugh, C. W. and Ratcliffe, P. J. (2017). New horizons in hypoxia signaling pathways. *Exp Cell Res, 356(2)*, p. 116-21.

Qu, Q., Sun, G., Murai, K., Ye, P., Li, W., Asuelime, G., Cheung, Y. T. and Shi, Y. (2013). Wnt7a regulates multiple steps of neurogenesis. *Mol Cell Biol, 33(13)*, p. 2551-9.

Rabie, T., Kunze, R. and Marti, H. H. (2011). Impaired hypoxic response in senescent mouse brain. *Int J Dev Neurosci, 29(6)*, p. 655-61.

Racca, C., Stephenson, F. A., Streit, P., Roberts, J. D. and Somogyi, P. (2000). NMDA receptor content of synapses in stratum radiatum of the hippocampal CA1 area. *J Neurosci, 20(7)*, p. 2512-22.

Rampon, C., Jiang, C. H., Dong, H., Tang, Y. P., Lockhart, D. J., Schultz, P. G., Tsien, J. Z. and Hu, Y. (2000). Effects of environmental enrichment on gene expression in the brain. *Proc Natl Acad Sci U S A, 97(23)*, p. 12880-4.

Rankin, E. B., Rha, J., Unger, T. L., Wu, C. H., Shutt, H. P., Johnson, R. S., Simon, M. C., Keith, B. and Haase, V. H. (2008). Hypoxia-inducible factor-2 regulates vascular tumorigenesis in mice. *Oncogene, 27(40)*, p. 5354-8.

Rey, F., Balsari, A., Giallongo, T., Ottolenghi, S., Di Giulio, A. M., Samaja, M. and Carelli, S. (2019). Erythropoietin as a Neuroprotective Molecule: An Overview of Its Therapeutic Potential in Neurodegenerative Diseases. *ASN Neuro, 11*, p. 1759091419871420.

Richter, S., Qin, N., Pacak, K. and Eisenhofer, G. (2013). Role of hypoxia and HIF2alpha in development of the sympathoadrenal cell lineage and chromaffin cell tumors with distinct catecholamine phenotypic features. *Adv Pharmacol, 68*, p. 285-317.

Rombo, D. M., Newton, K., Nissen, W., Badurek, S., Horn, J. M., Minichiello, L., Jefferys, J. G., Sebastiao, A. M. and Lamsa, K. P. (2015). Synaptic mechanisms of adenosine A2A receptor-mediated hyperexcitability in the hippocampus. *Hippocampus, 25(5)*, p. 566-80.

Rosenstein, J. M., Krum, J. M. and Ruhrberg, C. (2010). VEGF in the nervous system. *Organogenesis, 6(2)*, p. 107-14.

Rosiewicz, K. S., Muinjonov, B., Kunz, S., Radbruch, H., Chen, J., Juttner, R., Kerkering, J., Ucar, J., Crowley, T., Wielockx, B., Paul, F., Alisch, M. and Siffrin, V. (2023). HIF prolyl hydroxylase 2/3 deletion disrupts astrocytic integrity and exacerbates neuroinflammation. *Glia, 71(8)*, p. 2024-44.

Ruscher, K., Freyer, D., Karsch, M., Isaev, N., Megow, D., Sawitzki, B., Priller, J., Dirnagl, U. and Meisel, A. (2002). Erythropoietin is a paracrine mediator of ischemic tolerance in the brain: evidence from an in vitro model. *J Neurosci, 22(23)*, p. 10291-301.

Salceda, S. and Caro, J. (1997). Hypoxia-inducible factor 1alpha (HIF-1alpha) protein is rapidly degraded by the ubiquitin-proteasome system under normoxic conditions. Its stabilization by hypoxia depends on redox-induced changes. *J Biol Chem, 272(36)*, p. 22642-7.

Savtchenko, L. P., Antropov, S. N. and Korogod, S. M. (2000). Effect of voltage drop within the synaptic cleft on the current and voltage generated at a single synapse. *Biophys J, 78(3)*, p. 1119-25.

Savtchenko, L. P. and Rusakov, D. A. (2007). The optimal height of the synaptic cleft. *Proc Natl Acad Sci U S A, 104(6)*, p. 1823-8.

Schnell, P. O., Ignacak, M. L., Bauer, A. L., Striet, J. B., Paulding, W. R. and Czyzyk-Krzeska, M. F. (2003). Regulation of tyrosine hydroxylase promoter activity by the von Hippel-Lindau tumor suppressor protein and hypoxia-inducible transcription factors. *J Neurochem, 85(2)*, p. 483-91.

Schulz, K., Milke, L., Rubsamen, D., Menrad, H., Schmid, T. and Brune, B. (2012). HIF-1alpha protein is upregulated in HIF-2alpha depleted cells via enhanced translation. *FEBS Lett, 586(11)*, p. 1652-7.

Segura, I., Lange, C., Knevels, E., Moskalyuk, A., Pulizzi, R., Eelen, G., Chaze, T., Tudor, C., Boulegue, C., Holt, M., Daelemans, D., Matondo, M., Ghesquiere, B., Giugliano, M., Ruiz De Almodovar, C., Dewerchin, M. and Carmeliet, P. (2016). The Oxygen Sensor PHD2 Controls Dendritic Spines and Synapses via Modification of Filamin A. *Cell Rep, 14(11)*, p. 2653-67.

Semenza, G. L. (2012). Hypoxia-inducible factors: mediators of cancer progression and targets for cancer therapy. *Trends Pharmacol Sci, 33(4)*, p. 207-14.

Semenza, G. L., Agani, F., Booth, G., Forsythe, J., Iyer, N., Jiang, B. H., Leung, S., Roe, R., Wiener, C. and Yu, A. (1997). Structural and functional analysis of hypoxia-inducible factor 1. *Kidney Int, 51(2)*, p. 553-5.

Semple, B. D., Blomgren, K., Gimlin, K., Ferriero, D. M. and Noble-Haeusslein, L. J. (2013). Brain development in rodents and humans: Identifying benchmarks of maturation and vulnerability to injury across species. *Prog Neurobiol, 106-107*, p. 1-16.

Serocki, M., Bartoszewska, S., Janaszak-Jasiecka, A., Ochocka, R. J., Collawn, J. F. and Bartoszewski, R. (2018). miRNAs regulate the HIF switch during hypoxia: a novel therapeutic target. *Angiogenesis, 21(2)*, p. 183-202.

Serra, S., Vaisitti, T., Audrito, V., Bologna, C., Buonincontri, R., Chen, S. S., Arruga, F., Brusa, D., Coscia, M., Jaksic, O., Inghirami, G., Rossi, D., Furman, R. R., Robson, S. C., Gaidano, G., Chiorazzi, N. and Deaglio, S. (2016). Adenosine signaling mediates hypoxic responses in the chronic lymphocytic leukemia microenvironment. *Blood Adv, 1(1)*, p. 47-61.

Sharp, F. R. and Bernaudin, M. (2004). HIF1 and oxygen sensing in the brain. *Nat Rev Neurosci, 5(6)*, p. 437-48.

Sheng, M. and Kim, E. (2011). The postsynaptic organization of synapses. *Cold Spring Harb Perspect Biol, 3(12)*.

Simon, M. C. and Keith, B. (2008). The role of oxygen availability in embryonic development and stem cell function. *Nat Rev Mol Cell Biol, 9(4)*, p. 285-96.

Srinivas, V., Zhang, L. P., Zhu, X. H. and Caro, J. (1999). Characterization of an oxygen/redox-dependent degradation domain of hypoxia-inducible factor alpha (HIF-alpha) proteins. *Biochem Biophys Res Commun, 260(2)*, p. 557-61.

Sudhof, T. C. (2008). Neuroligins and neurexins link synaptic function to cognitive disease. *Nature, 455(7215)*, p. 903-11.

Sudhof, T. C. (2012). The presynaptic active zone. *Neuron, 75(1)*, p. 11-25.

Sudhof, T. C. (2013). Neurotransmitter release: the last millisecond in the life of a synaptic vesicle. *Neuron, 80(3)*, p. 675-90.

Sun, H., Zhang, J., Zhang, L., Liu, H., Zhu, H. and Yang, Y. (2010). Environmental enrichment influences BDNF and NR1 levels in the hippocampus and restores cognitive impairment in chronic cerebral hypoperfused rats. *Curr Neurovasc Res, 7(4)*, p. 268-80.

Thion, M. S. and Garel, S. (2017). On place and time: microglia in embryonic and perinatal brain development. *Curr Opin Neurobiol, 47*, p. 121-30.

Tian, H., Mcknight, S. L. and Russell, D. W. (1997). Endothelial PAS domain protein 1 (EPAS1), a transcription factor selectively expressed in endothelial cells. *Genes Dev, 11(1)*, p. 72-82.

Timmusk, T., Palm, K., Metsis, M., Reintam, T., Paalme, V., Saarma, M. and Persson, H. (1993). Multiple promoters direct tissue-specific expression of the rat BDNF gene. *Neuron, 10(3)*, p. 475-89.

Toriuchi, K., Kakita, H., Tamura, T., Takeshita, S., Yamada, Y. and Aoyama, M. (2020). Prolonged astrocyte-derived erythropoietin expression attenuates neuronal damage under hypothermic conditions. *J Neuroinflammation, 17(1)*, p. 141.

Trujillo, M., Mcelroy, T., Brown, T., Simmons, P., Ntagwabira, F. and Allen, A. R. (2021). Combined Mechanical and Enzymatic Dissociation of Mouse Brain Hippocampal Tissue. *J Vis Exp, (176)*.

Turovskaya, M. V., Gaidin, S. G., Vedunova, M. V., Babaev, A. A. and Turovsky, E. A. (2020). BDNF Overexpression Enhances the Preconditioning Effect of Brief Episodes of Hypoxia, Promoting Survival of GABAergic Neurons. *Neurosci Bull, 36(7)*, p. 733-60.

Vangeison, G., Carr, D., Federoff, H. J. and Rempe, D. A. (2008). The good, the bad, and the cell type-specific roles of hypoxia inducible factor-1 alpha in neurons and astrocytes. *J Neurosci, 28(8)*, p. 1988-93.

Vangeison, G. and Rempe, D. A. (2009). The Janus-faced effects of hypoxia on astrocyte function. *Neuroscientist, 15(6)*, p. 579-88.

Villers, A. and Ris, L. (2013). Improved preparation and preservation of hippocampal mouse slices for a very stable and reproducible recording of long-term potentiation. *J Vis Exp, (76)*.

Wahl, L. M., Pouzat, C. and Stratford, K. J. (1996). Monte Carlo simulation of fast excitatory synaptic transmission at a hippocampal synapse. *J Neurophysiol, 75(2)*, p. 597-608.

Wang, G. L., Jiang, B. H., Rue, E. A. and Semenza, G. L. (1995). Hypoxia-inducible factor 1 is a basic-helix-loop-helix-PAS heterodimer regulated by cellular O2 tension. *Proc Natl Acad Sci U S A, 92(12)*, p. 5510-4.

Wang, G. L. and Semenza, G. L. (1995). Purification and characterization of hypoxia-inducible factor 1. *J Biol Chem, 270(3)*, p. 1230-7.

Wang, H., Yuan, G., Prabhakar, N. R., Boswell, M. and Katz, D. M. (2006). Secretion of brain-derived neurotrophic factor from PC12 cells in response to oxidative stress requires autocrine dopamine signaling. *J Neurochem, 96(3)*, p. 694-705.

Wang, V., Davis, D. A., Haque, M., Huang, L. E. and Yarchoan, R. (2005). Differential gene up-regulation by hypoxia-inducible factor-1alpha and hypoxia-inducible factor-2alpha in HEK293T cells. *Cancer Res, 65(8)*, p. 3299-306.

Watts, M. E., Pocock, R. and Claudianos, C. (2018). Brain Energy and Oxygen Metabolism: Emerging Role in Normal Function and Disease. *Front Mol Neurosci, 11*, p. 216.

Weidemann, A., Kerdiles, Y. M., Knaup, K. X., Rafie, C. A., Boutin, A. T., Stockmann, C., Takeda, N., Scadeng, M., Shih, A. Y., Haase, V. H., Simon, M. C., Kleinfeld, D. and Johnson, R. S. (2009). The glial cell response is an essential component of hypoxia-induced erythropoiesis in mice. *J Clin Invest, 119(11)*, p. 3373-83.

Wenger, R. H. (2002). Cellular adaptation to hypoxia: O2-sensing protein hydroxylases, hypoxia-inducible transcription factors, and O2-regulated gene expression. *FASEB J, 16(10)*, p. 1151-62.

Wielockx, B., Grinenko, T., Mirtschink, P. and Chavakis, T. (2019). Hypoxia Pathway Proteins in Normal and Malignant Hematopoiesis. *Cells, 8(2)*.

Wiesener, M. S., Jurgensen, J. S., Rosenberger, C., Scholze, C. K., Horstrup, J. H., Warnecke, C., Mandriota, S., Bechmann, I., Frei, U. A., Pugh, C. W., Ratcliffe, P. J., Bachmann, S., Maxwell, P. H. and Eckardt, K. U. (2003). Widespread hypoxia-inducible expression of HIF-2alpha in distinct cell populations of different organs. *FASEB J, 17(2)*, p. 271-3.

Wong-Riley, M. T. and Besharse, J. C. (2012). The kinesin superfamily protein KIF17: one protein with many functions. *Biomol Concepts, 3(3)*, p. 267-82.

Xue, L. L., Du, R. L., Hu, Y., Xiong, L. L., Su, Z. Y., Ma, Z., Tan, Y. X., Liu, J., Hu, Q., Zhu, Z. Q., Liu, X. Z. and Wang, T. H. (2021). BDNF promotes neuronal survival after neonatal hypoxic-ischemic encephalopathy by up-regulating Stx1b and suppressing VDAC1. *Brain Res Bull, 174*, p. 131-40.

Zhang, R., Jiang, H., Liu, Y. and He, G. (2023). Structure, function, and pathology of Neurexin-3. *Genes & Diseases, 10(5)*, p. 1908-19.

Zhong, L., Kaleka, K. S. and Gerges, N. Z. (2011). Neurogranin phosphorylation fine-tunes long-term potentiation. *Eur J Neurosci, 33(2)*, p. 244-50.

Ziello, J. E., Jovin, I. S. and Huang, Y. (2007). Hypoxia-Inducible Factor (HIF)-1 regulatory pathway and its potential for therapeutic intervention in malignancy and ischemia. *Yale J Biol Med, 80(2)*, p. 51-60.

6. APPENDIX

6.1. Supplementary figures

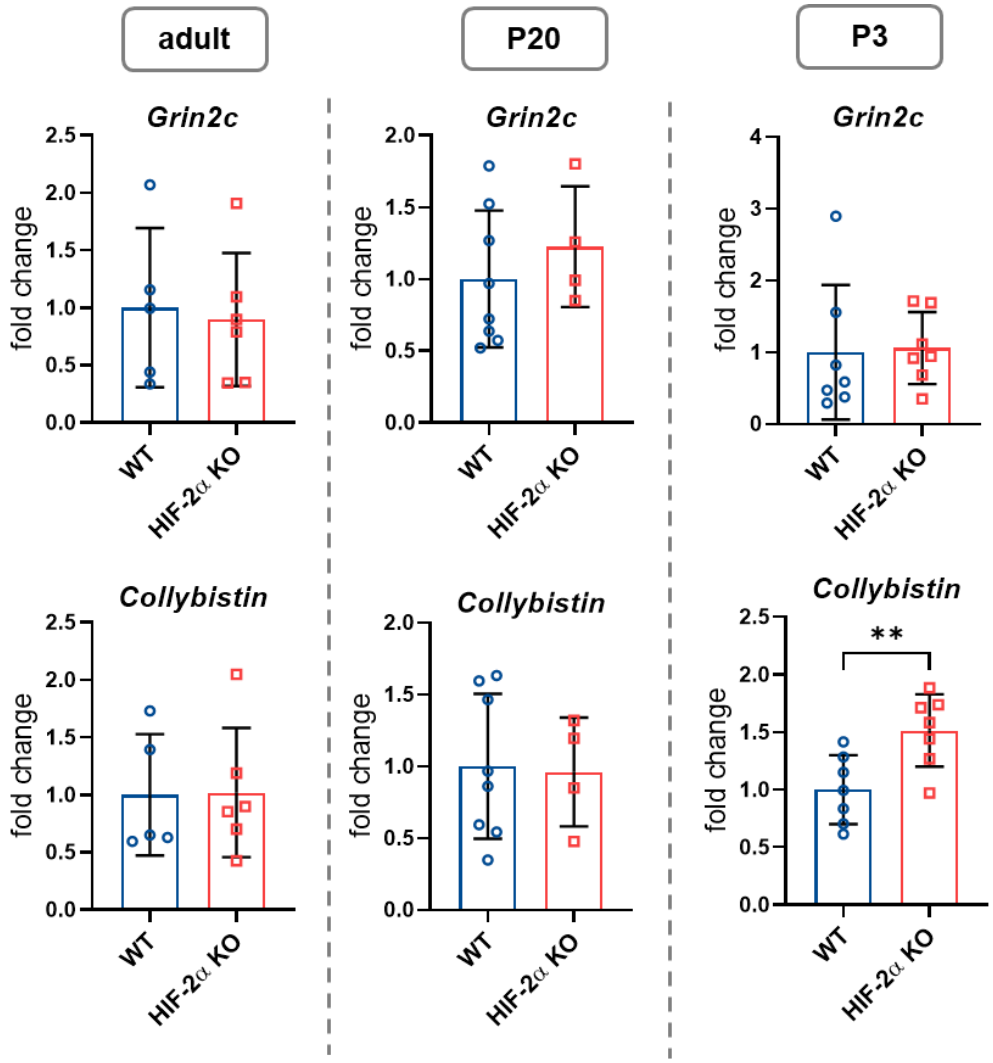

Figure 6.1: Expression analysis of additional genes in brain tissue of WT and HIF-2α KO mice - part 1.
Brain hemispheres of WT and HIF-2α KO mice of different ages (adult, P20 = 20 days postnatal, P3 = 3 days postnatal) were analyzed by qPCR for different brain- and synapse-associated genes. *Grin2c* = Glutamate [NMDA] receptor subunit epsilon-3, *Collybistin* = CDC42 guanine nucleotide exchange factor 9. Values were normalized to *Rpl13a* as HKG and changes in gene expression calculated as x-fold changes relative to the WT controls using the 2^-ΔCt method. Mean ± SD, unpaired t-test, $p < 0.05$ = *, n = 4-8 per genotype.

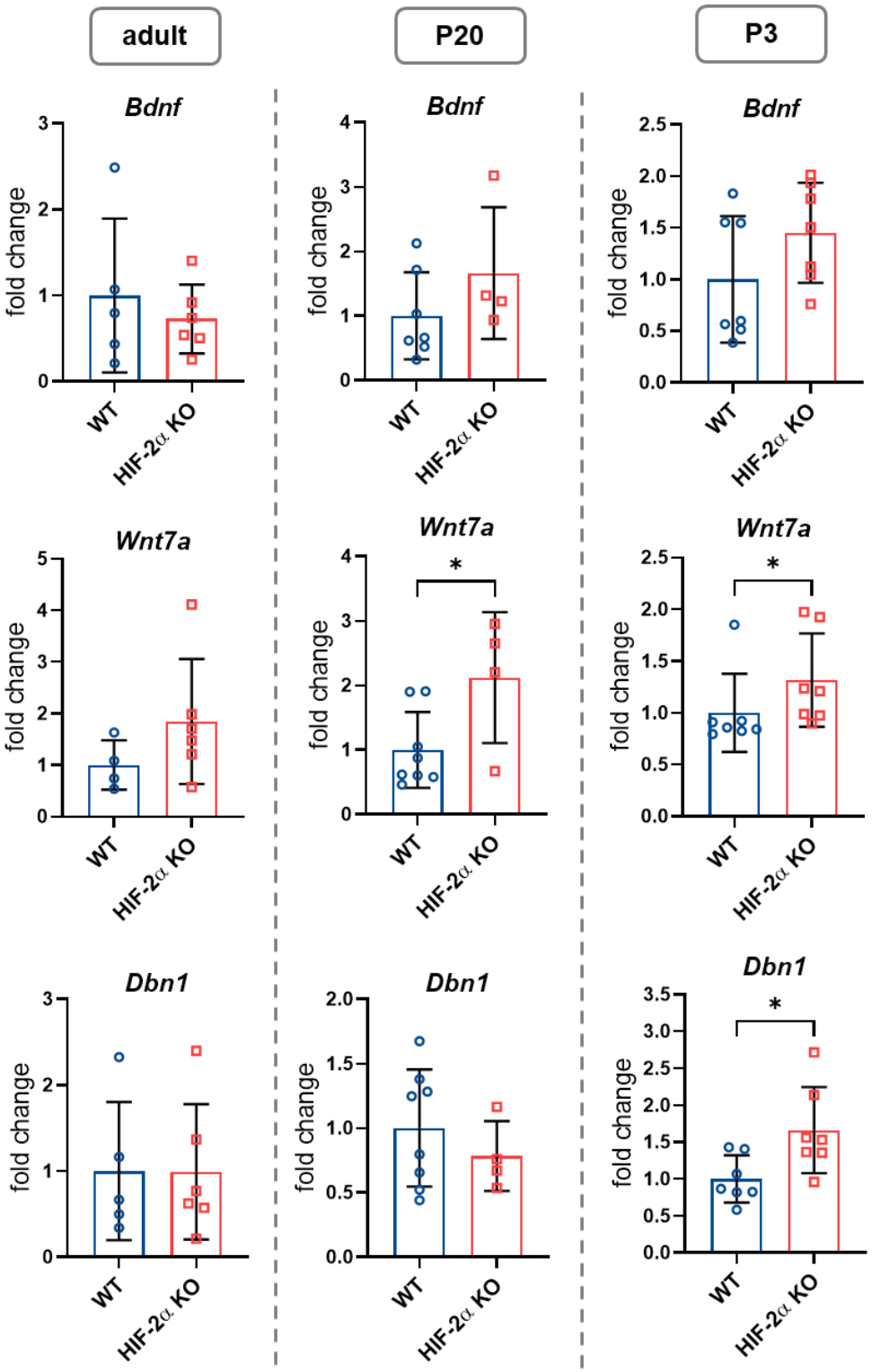

Figure 6.2: Expression analysis of additional genes in brain tissue of WT and HIF-2α KO mice - part 2.
Brain hemispheres of WT and HIF-2α KO mice of different ages (adult, P20 = 20 days postnatal, P3 = 3 days postnatal) were analyzed by qPCR for different brain- and synapse-associated genes. *Bdnf* = brain derived neutrophic factor, *Wnt7a* = Wnt family member 7A, *Dbn1* = Drebrin. Values were normalized to *Rpl13a* as HKG and changes in gene expression calculated as x-fold changes relative to the WT controls using the 2^-ΔCt method. Mean ± SD, unpaired t-test, $p < 0.05$ = *, n = 4-8 per genotype.

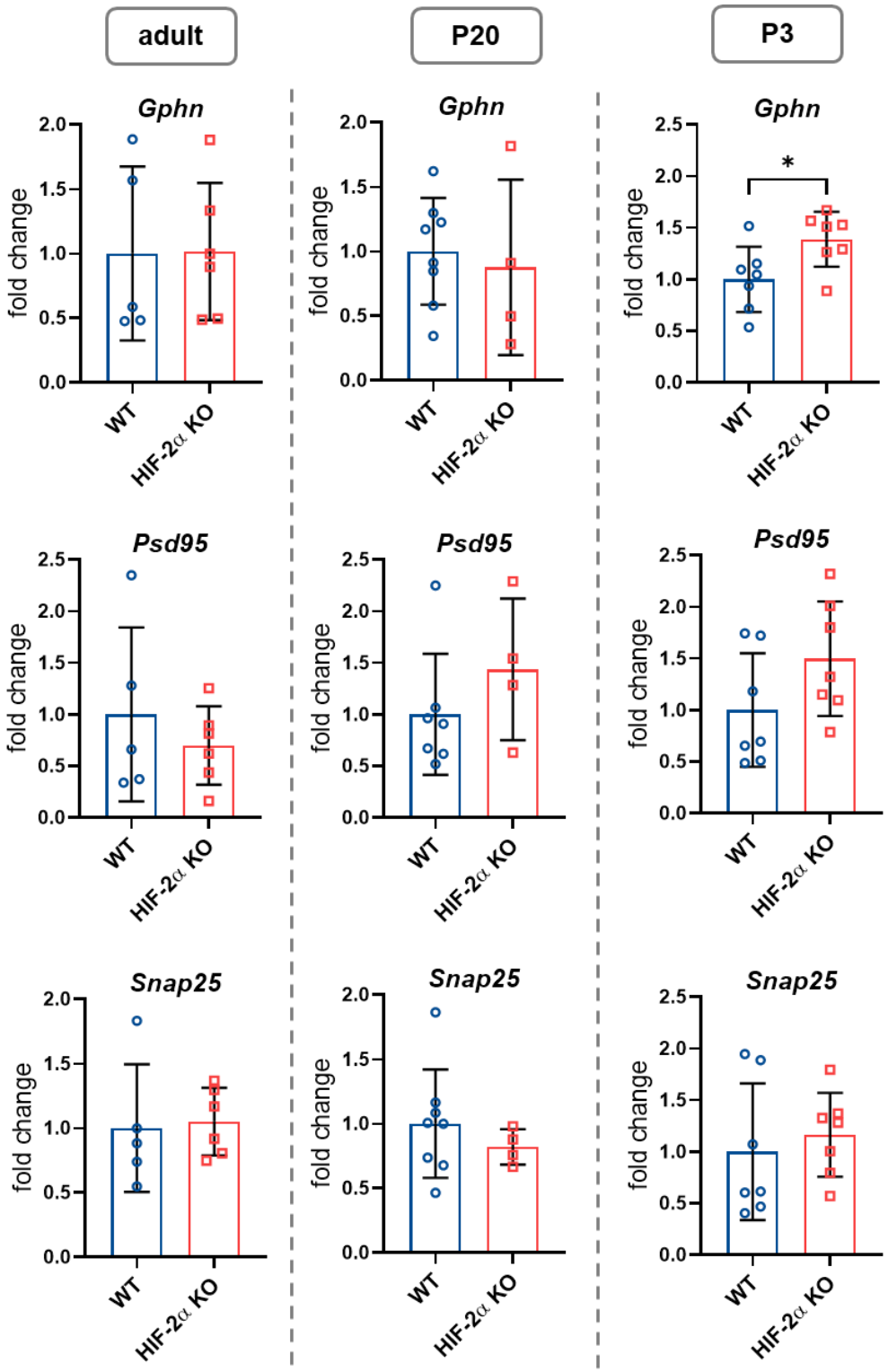

Figure 6.3: Expression analysis of additional genes in brain tissue of WT and HIF-2α KO mice - part 3.
Brain hemispheres of WT and HIF-2α KO mice of different ages (adult, P20 = 20 days postnatal, P3 = 3 days postnatal) were analyzed by qPCR for different brain- and synapse-associated genes. *Gphn* = Gephyrin - post-synaptic at inhibitory synapses, *Psd95* = post-synaptic density protein 95 - excitatory synapses, , *Snap25* = Synaptosomal-Associated Protein, 25kDa. Values were normalized to *Rpl13a* as HKG and changes in gene expression calculated as x-fold changes relative to the WT controls using the 2^-ΔCt method. Mean ± SD, unpaired t-test, $p < 0.05$ = *, n = 4-8 per genotype.

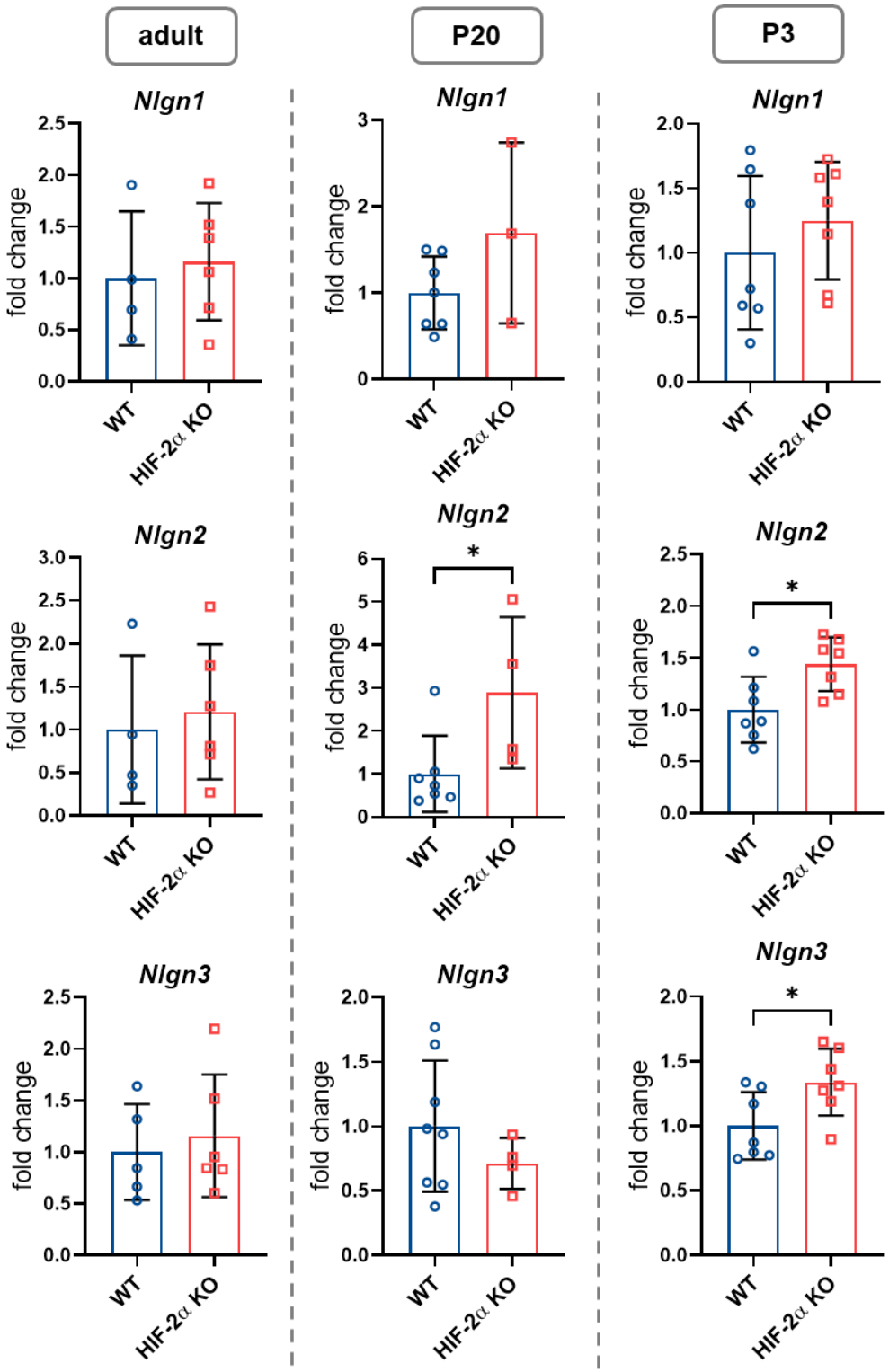

Figure 6.4: Expression analysis of *Neuroligin 1-3* in brain tissue of WT and HIF-2α KO mice.

Brain hemispheres of WT and HIF-2α KO mice of different ages (adult, P20 = 20 days postnatal, P3 = 3 days postnatal) were analyzed by qPCR for gene expression of cell adhesion molecules *Neuroligin 1-3* (*Nlgn 1-3*) of the post-synaptic membrane. Values were normalized to *Rpl13a* as HKG and changes in gene expression calculated as x-fold changes relative to the WT controls using the 2^-ΔCt method. Mean ± SD, unpaired t-test, $p < 0.05$ = *, n = 4-8 per genotype.

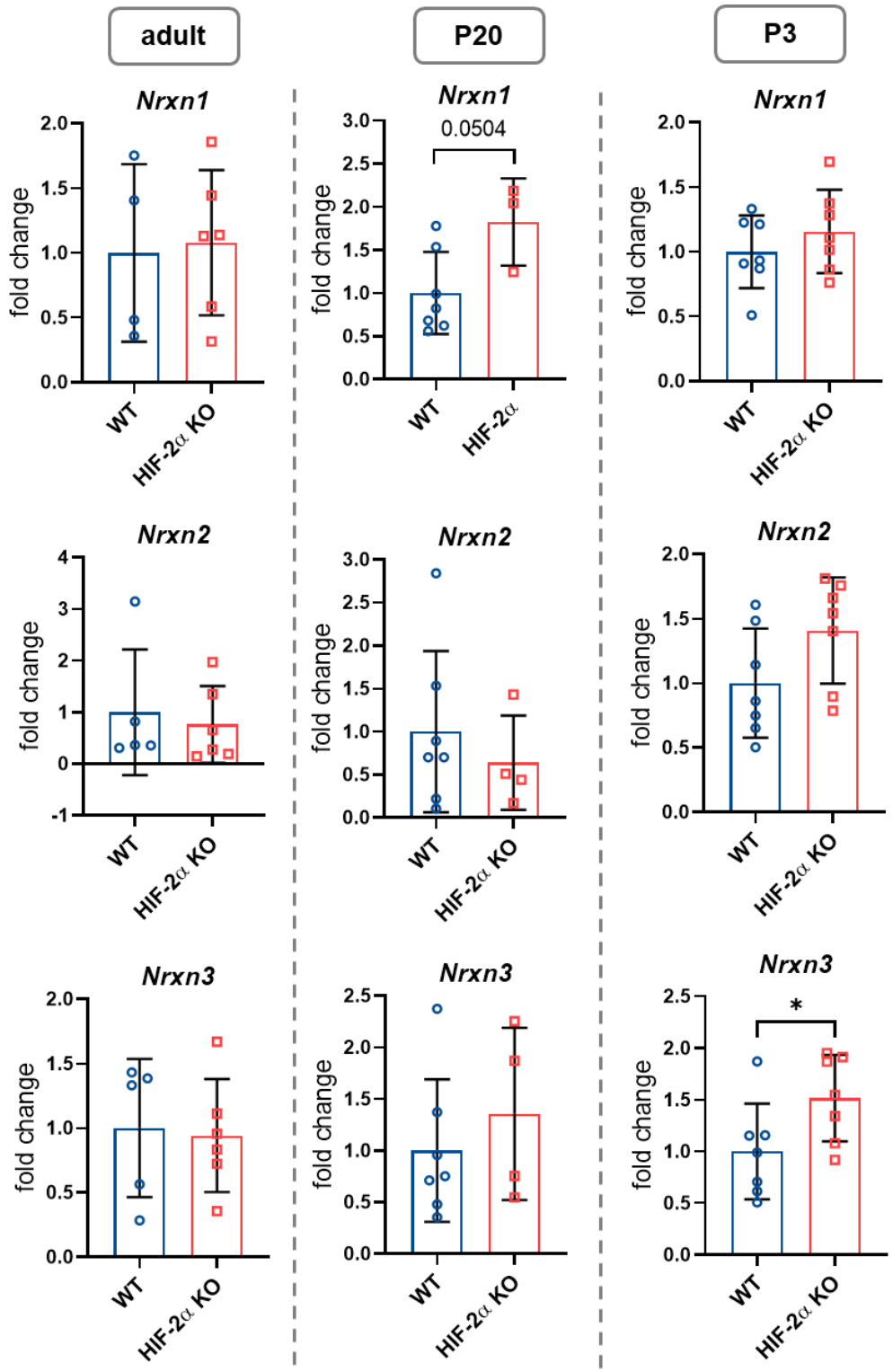

Figure 6.5: Expression analysis of *Neurexin 1-3* in brain tissue of WT and HIF-2α KO mice.

Brain hemispheres of WT and HIF-2α KO mice of different ages (adult, P20 = 20 days postnatal, P3 = 3 days postnatal) were analyzed by qPCR for gene expression of cell adhesion molecules *Neurexin 1-3* (*Nrxn 1-3*) of the pre-synaptic membrane. Values were normalized to *Rpl13a* as HKG and changes in gene expression calculated as x-fold changes relative to the WT controls using the 2^-ΔCt method. Mean ± SD, unpaired t-test, $p < 0.05$ = *, n = 4-8 per genotype.

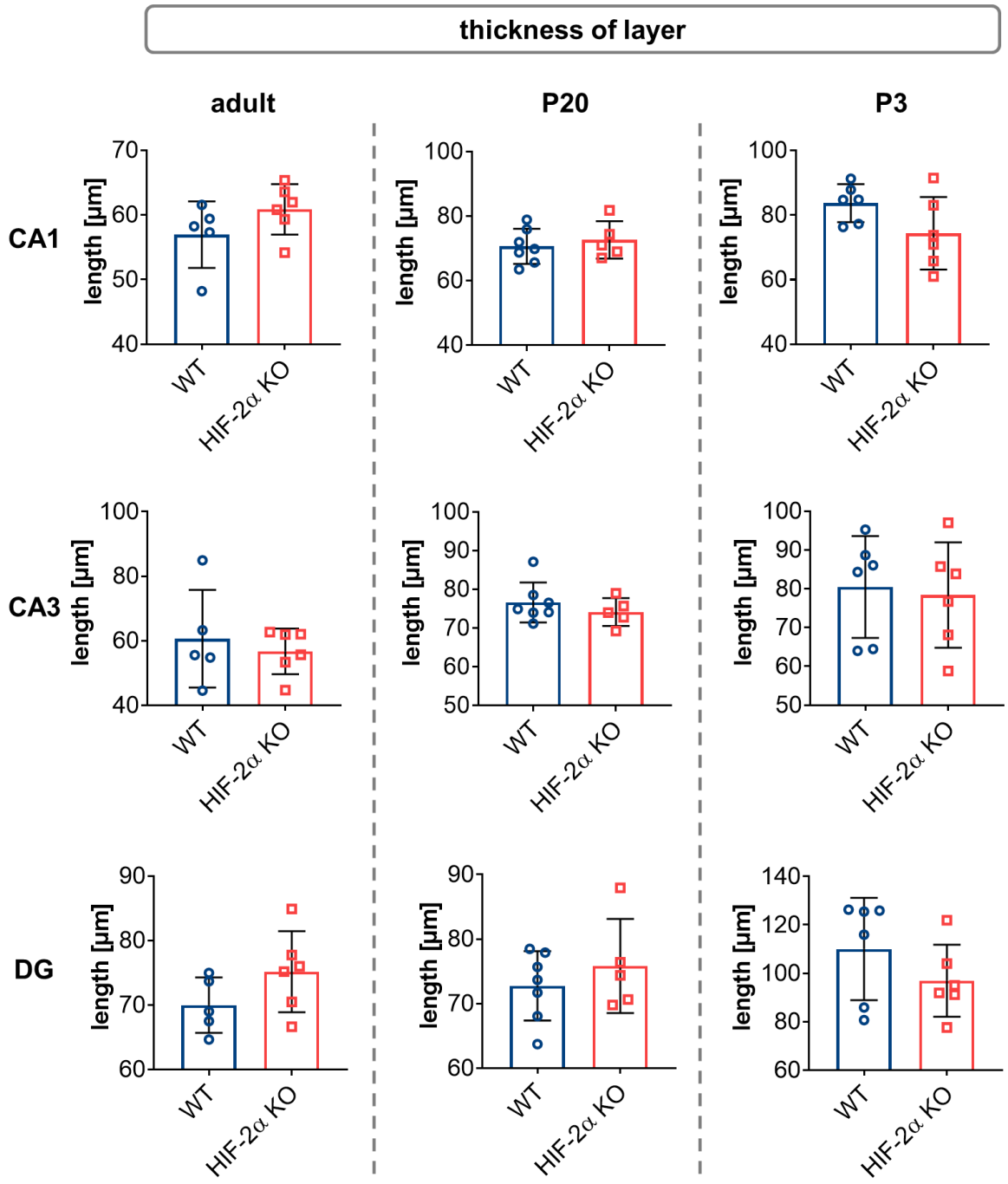

Figure 6.6: Additional analysis of the thickness of CA1, CA3 and DG hippocampal layers of WT and HIF-2α KO mice.

Brain hemispheres of WT and HIF-2α KO mice of different ages (adult, P20 = 20 days postnatal, P3 = 3 days postnatal) were serial-sectioned and Nissl-stained. The thickness of the nuclei layer of the CA1, CA3 and DG regions was measured as length in µm for both genotypes at all ages at an additional section. Mean ± SD, n = 5 - 7 per genotype and age.

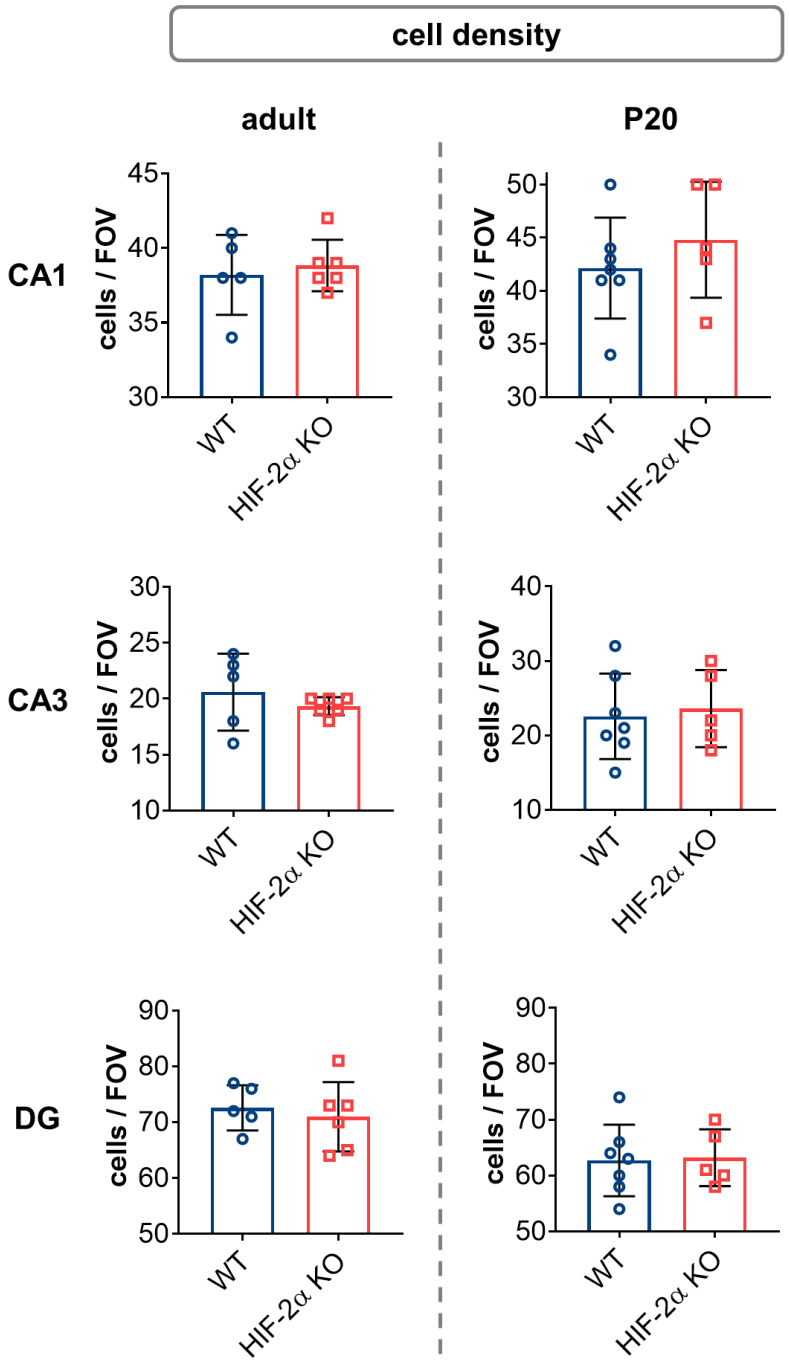

Figure 6.7: Additional analysis of the cell density of CA1, CA3 and DG hippocampal layers of WT and HIF-2α KO mice.

Brain hemispheres of WT and HIF-2α KO mice of different ages (adult, P20 = 20 days postnatal) were serial-sectioned and Nissl-stained. The density of the nuclei layer of the CA1, CA3 and DG regions was measured as cells/field of view (FOV) for both genotypes at an additional section. Mean ± SD, n = 5 - 7 per genotype and age.

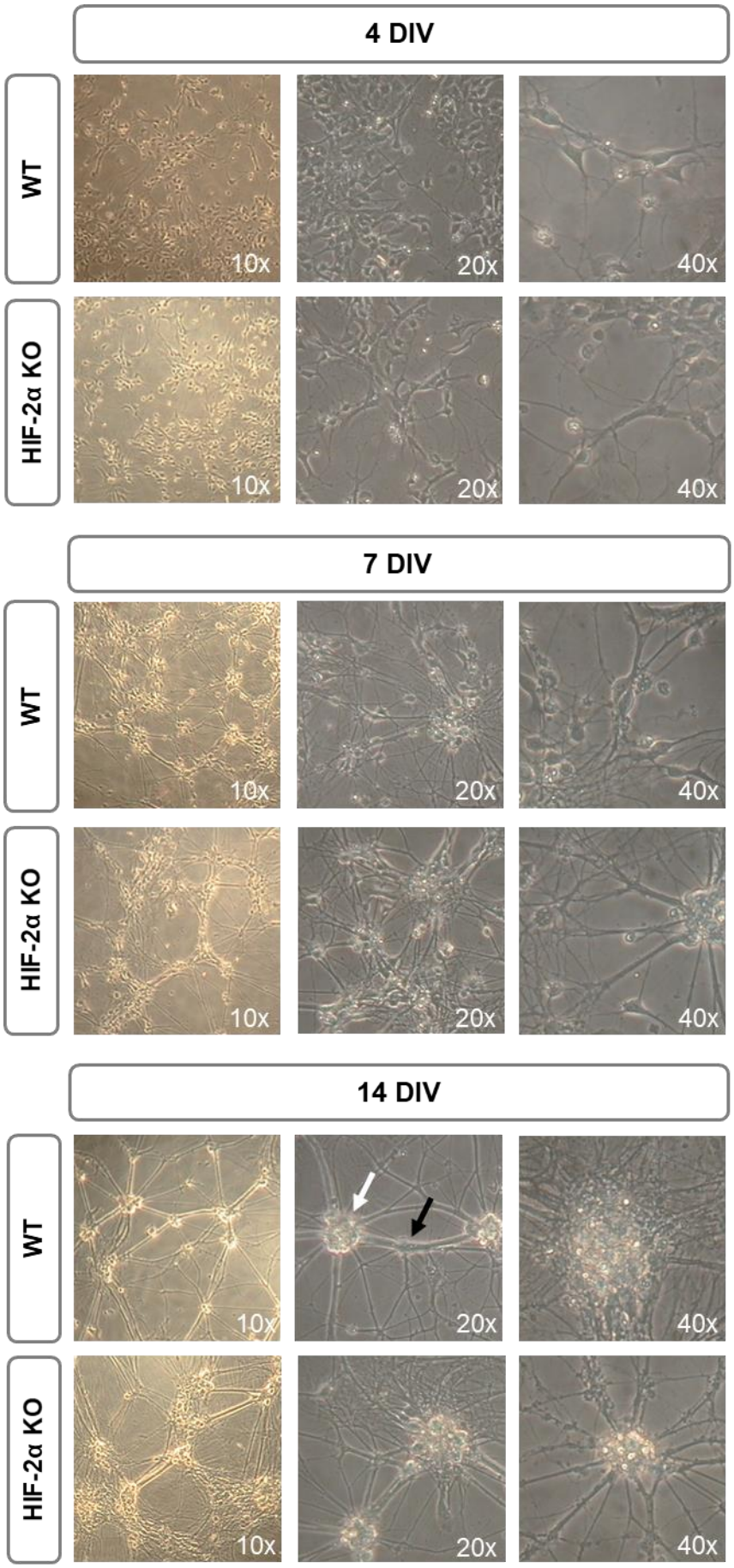

Figure 6.8: Example of neuronal clustering and aggregate formation.
Hippocampal WT or HIF-2α KO neurons were seeded in a neuron-astrocyte co-culture system and maintained for up to 14 DIV (days in vitro). Sometimes, neurons start to cluster and form aggregates (white arrow) with very thick dendritic branches ranging from one to another cluster (black arrow.

6.2. List of figures

Figure 1.1: Domain structure of human HIF subunits and isoforms (Davis *et al.*, 2018). 2
Figure 1.2: O_2-dependent regulation of hypoxia-inducible factors. 3
Figure 1.3: Different ways of HIFs for regulating processes that are directly or indirectly associated with maintaining oxygen balance. 4
Figure 1.4: Schematic overview of chemical synapses and synaptic transmission. 7
Figure 1.5: Pathological roles of hypoxia in neuronal dysfunction and neurodegeneration. ..10
Figure 1.6: HIF-1 and HIF-2 dependent mechanisms of cellular adaptation to brain hypoxia. 12
Figure 2.1: Schematic overview of the neuron-astrocyte co-culture system. 32
Figure 2.2: Region of interest for electron microscopy analysis. 46
Figure 2.3: Environmental enrichment study design. 48
Figure 2.4: Scheme of cage equipment for environmental enrichment. 49
Figure 3.1: Contour analysis of the hippocampi of WT and HIF-2α KO mice. 56
Figure 3.2: Analysis parameters and overview of Nissl-stained hippocampi of WT and HIF-2α KO mice. 57
Figure 3.3: Thickness of CA1, CA3 and DG hippocampal layers of WT and HIF-2α KO mice. 58
Figure 3.4: Cell density of CA1, CA3 and DG hippocampal layers of WT and HIF-2α KO mice. 59
Figure 3.5: RT^2 profiler PCR array for synaptic plasticity of brain hemispheres of adult WT and HIF-2α KO mice. 61
Figure 3.6: Detailed expression analysis of genes that showed changes in the RT^2 Profiler PCR array. 62
Figure 3.7: Expression analysis of (potentially) HIF-2α-associated genes in brain tissue of WT and HIF-2α KO mice. 63
Figure 3.8: Expression analysis of cell-type specific markers in brain tissue of WT and HIF-2α KO mice. 65
Figure 3.9: Expression analysis of potential targets of HIF-2α in brain tissue of WT and HIF-2α KO mice. 67
Figure 3.10: Overview of the TEM-analyzed synapses of WT and HIF-2α KO mice and the analysis parameters. 70
Figure 3.11: Analysis of hippocampal synapses of adult WT and HIF-2α KO mice. 71
Figure 3.12: RT^2 profiler PCR array for synaptic plasticity of the hippocampus of environmentally enriched WT and HIF-2α KO mice. 73

Figure 3.13: Detailed expression analysis of genes that were very highly up-regulated in the RT^2 Profiler PCR array. 75
Figure 3.14: Detailed expression analysis of genes that were highly up-regulated in the RT^2 Profiler PCR array. 76
Figure 3.15: Detailed expression analysis of genes that were moderately up-regulated in the RT^2 Profiler PCR array. 77
Figure 3.16: Detailed expression analysis of genes that were down-regulated in the RT^2 Profiler PCR array. 78
Figure 3.17: HIF-2α KO efficiency in hippocampal and cortical tissue of SC and EE housed mice. 78
Figure 3.18: Expression analysis of additional neuronal and synapse-associated genes in hippocampal and cortical tissue of SC and EE housed WT and HIF-2α KO mice. 79
Figure 3.19: Expression analysis of (potentially) HIF-2α-associated genes in hippocampal and cortical tissue of SC and EE housed WT and HIF-2α KO mice. 80
Figure 3.20: proBDNF and BDNF content in the hippocampus of SC and EE housed WT and HIF-2α KO mice. 82
Figure 3.21: proBDNF and BDNF content in the cortex of SC and EE housed WT and HIF-2α KO mice. 82
Figure 3.22: Tested parameters for optimization of a neuron-astrocyte co-culture system....84
Figure 3.23: Exemplary brightfield images for comparison of seeding density of hippocampal neurons and different coating reagents. 86
Figure 3.24: Immunofluorescence staining of neurons and astrocytes. 88
Figure 3.25: Exemplary brightfield images of maturing hippocampal HIF-2α KO neurons.....88
Figure 3.26: Exemplary brightfield images of WT neurons under normoxic or hypoxic incubation. 89
Figure 3.27: Neuron and astrocyte cDNA analysis of kit-extracted or phenol-chloroform-extracted RNA samples. 90
Figure 3.28: Pilot experiment for the expression of hypoxic target genes in astrocytes at different O_2 levels. 91
Figure 3.29: Timed expression of hypoxic target genes in astrocytes and neurons at 1% O_2. 93
Figure 3.30: HIF-2α KO efficiency in neurons and astrocytes under NOX and HOX conditions. 94
Figure 3.31: Stability of gene expression levels for astrocytic and neuronal markers under normoxic culture conditions. 96
Figure 3.32: Gene expression analysis in WT and HIF-2α KO astrocytes under HOX conditions. 98

Figure 3.33: Gene expression analysis of adenosine receptors in WT and HIF-2α KO astrocytes under HOX conditions. 99
Figure 3.34: Western Blot analysis for HIF-1α and HIF-2α in WT and HIF-2α KO astrocytes under HOX conditions. 101
Figure 3.35: Hif-1α expression in WT and HIF-2α KO astrocytes under HOX conditions. ...102
Figure 3.36: Gene expression analysis of hypoxia target genes in WT and HIF-2α KO neurons under HOX conditions. 103
Figure 3.37: Gene expression analysis of potential HIF-2α-dependent neuronal genes in WT and HIF-2α KO neurons under HOX conditions. 105
Figure 3.38: Gene expression analysis of *Bdnf* and *Wnt7a* in WT and HIF-2α KO neurons under HOX conditions. 106
Figure 3.39: Gene expression analysis of neuronal and synapse-associated genes in WT and HIF-2α KO neurons under HOX conditions. 108
Figure 3.40: Gene expression analysis of neuronal and synapse-associated genes in WT and HIF-2α KO neurons under HOX conditions. 110
Figure 3.41: Gene expression analysis of further genes of interest in WT and HIF-2α KO neurons under HOX conditions. 112
Figure 4.1: Altered gene expression in both WT and HIF-2α KO neurons + HIF-2α KO astrocytes. 132
Figure 6.1: Expression analysis of additional genes in brain tissue of WT and HIF-2α KO mice - part 1. 154
Figure 6.2: Expression analysis of additional genes in brain tissue of WT and HIF-2α KO mice - part 2. 155
Figure 6.3: Expression analysis of additional genes in brain tissue of WT and HIF-2α KO mice - part 3. 156
Figure 6.4: Expression analysis of *Neuroligin 1-3* in brain tissue of WT and HIF-2α KO mice. 157
Figure 6.5: Expression analysis of *Neurexin 1-3* in brain tissue of WT and HIF-2α KO mice. 158
Figure 6.6: Additional analysis of the thickness of CA1, CA3 and DG hippocampal layers of WT and HIF-2α KO mice. 159
Figure 6.7: Additional analysis of the cell density of CA1, CA3 and DG hippocampal layers of WT and HIF-2α KO mice. 160
Figure 6.8: Example of neuronal clustering and aggregate formation. 161

6.3. List of tables

Table 2.1: Used machines and devices and their manufacturer. 20
Table 2.2: Used consumables and plastic ware and their manufacturer. 21
Table 2.3: Used chemicals, reagents, supplements and enzymes and their manufacturer. 23
Table 2.4: Used buffers and media and their compositions. 25
Table 2.5: Antibodies used for Western Blot. 27
Table 2.6: Antibodies used for immunocytochemistry. 28
Table 2.7: Used oligonucleotides and primers. 28
Table 2.8: Used software and its purpose. 31
Table 2.9: RNA mix for cDNA synthesis. 38
Table 2.10: Reaction mix for cDNA synthesis. 39
Table 2.11: Protocol for cDNA synthesis. 39
Table 2.12: Reaction mix for PCR. 39
Table 2.13: Standard PCR program. 40
Table 2.14: Reaction mix for qPCR. 41
Table 2.15: qPCR program. 41
Table 2.16: Composition of stacking and separation gel of a SDS-PAGE. 44
Table 2.17: Protocol for tissue sample dehydration. 51

6.4. List of abbreviations

°C	degree Celsius
AMPA	α-amino-3-hydroxy-5-methyl-4-isoxazolepropionic acid
ANOVA	analysis of variance
APS	ammonium persulfate
AraC	cytosine ß-D-arabinofuranoside
ARNT	aryl hydrocarbon receptor nuclear translocator
ATP	adenosine triphosphate
bp	base pairs
BSA	bovine serum albumin
CaMKII	calcium/calmodulin-dependent protein kinase II
cAMP	cyclic adenosine monophosphate
cDNA	complementary DNA
Ct	cycle of threshold
d	day(s)
DAPI	4′,6-diamidino-2-phenylindole
DEPC	diethyl pyrocarbonate

dH_2O	distilled water
DMSO	dimethyl sulfoxide
DNA	deoxyribonucleic acid
DNAse I	deoxyribonuclease I
EE	environmental enrichment / environmentally enriched
EM	electron microscopy
EPAS1	endothelial PAS domain protein 1
EPSP	excitatory post-synaptic potential
EtOH	ethanol
FCS	fetal calf serum
FIH	factor-inhibiting HIF
FOV	field of view
gDNA	genomic DNA
GLUT1 / GLUT3	glucose transporter 1 / 3
GTC	guanidinium thiocyanate
h	hour(s)
H_2O	water
HBSS	Hanks' balanced salt solution
HCl	hydrochloric acid
HIF	hypoxia-inducible factor
HKG	housekeeping gene
HOX	hypoxia
HRE	hypoxia-responsive element
IP3	inositol triphosphate
IPSP	inhibitory post-synaptic potential
kDa	kilo Dalton
KO	knockout
kV	kilo Volt
LTD	long-term depression
LTP	long-term potentiation
M	molar
MCAO	middle cerebral artery occlusion
min	minute(s)
mRNA	messenger RNA
NaCl	sodium chloride
NaOAc	sodium acetate
NaOH	sodium hydroxide

NGS	normal goat serum
NMDA	N-methyl-D-aspartate
Nonidet® P40	NP40
NOX	normoxia
NP40	Nonidet® P40
NSC	neural stem cells
NTP	nucleotide triphosphate
ODD	oxygen-dependent degradation domain
OGD	oxygen-glucose deprivation
ON	overnight
P/S	penicillin/streptavidin
PBS	phosphate-buffered saline
PCR	polymerase chain reaction
PFA	paraformaldehyde
PHD	prolyl hydroxylase
PI	proteinase inhibitor
PKA	protein kinase A
PSD	post-synaptic density
PVDF	polyvinylidene fluoride
qPCR	quantitative PCR
REML	restricted maximum likelihood
ribProt	ribosomal protein
RNA	ribonucleic acid
ROS	reactive oxygen species
rpm	rounds per minutes
RT	room temperature
RT-PCR	reverse transcriptase PCR
SC	standard housing / standard housed
SD	standard deviation
SDS	sodium dodecyl sulfate
sec	second(s)
TAE	Tris-acetate-EDTA
TEM	transmission electron microscopy
TEMED	N,N,N′,N′-Tetramethylethylenediamine
Tris	tris(hydroxymethyl)-aminomethane
U	units
UV	ultraviolet

V	Volt
VHL	von Hippel-Lindau protein
WT	wild-type / wildtypic

6.5. List of publications and congress contributions

Scientific papers

Quinting, T., Heymann, A. K., Bicker, A., Nauth, T., Bernardini, A., Hankeln, T., Fandrey, J. and Schreiber, T. (2021). Myoglobin Protects Breast Cancer Cells Due to Its ROS and NO Scavenging Properties. *Front Endocrinol (Lausanne)*, 12, p. 732190.

Wrobeln, A., Jagers, J., **Quinting, T.**, Schreiber, T., Kirsch, M., Fandrey, J. and Ferenz, K. B. (2020). Albumin-derived perfluorocarbon-based artificial oxygen carriers can avoid hypoxic tissue damage in massive hemodilution. *Sci Rep, 10(1)*, p. 11950.

Kleszka, K., Leu, T., **Quinting, T.**, Jastrow, H., Pechlivanis, S., Fandrey, J. and Schreiber, T. (2020). Hypoxia-inducible factor-2alpha is crucial for proper brain development. *Sci Rep, 10(1)*, p. 19146.

Schreiber, T., Salhofer, L., **Quinting, T.** and Fandrey, J. (2019). Things get broken: the hypoxia-inducible factor prolyl hydroxylases in ischemic heart disease. *Basic Res Cardiol, 114(3)*, p. 16.

Schreiber, T., **Quinting, T.**, Dittmer, U., Fandrey, J. and Sutter, K. (2017). Hypoxia-inducible factor 1alpha is Essential for Macrophage-mediated Erythroblast Proliferation in Acute Friend Retrovirus Infection. *Sci Rep, 7(1)*, p. 17236.

Posters

Quinting, T., Jastrow, H., Fandrey, J. and Schreiber, T. (2023). The influence of hypoxia-inducible factor-2α on synaptic architecture and function under normoxia and hypoxia. 12th Young Physiologist Symposium, Kiel, Germany.

Quinting, T., Jastrow, H., Fandrey, J. and Schreiber, T. (2022). The influence of hypoxia-inducible factor-2α on synaptic architecture and function under normoxia and hypoxia. 21st Day of Science at the Medical Faculty, University of Duisburg-Essen, Essen, Germany.

Quinting, T., Jastrow, H., Fandrey, J. and Schreiber, T. (2022). The influence of hypoxia-inducible factor-2α on synaptic architecture and function under normoxia and hypoxia. Europhysiology, Copenhagen, Denmark.

Quinting, T., Jastrow, H., Fandrey, J. and Schreiber, T. (2022). The influence of hypoxia-inducible factor-2α on synaptic architecture and function. 11th Young Physiologist Symposium, Essen, Germany.

Quinting, T., Fandrey, J. and Schreiber, T. (2019). Regulation of Synaptic Plasticity by Hypoxia-inducible Factor-2α. 98th Annual Meeting of the German Physiological Society (DPG), Ulm, Germany.

Quinting, T., Fandrey, J. and Schreiber, T. (2019). Regulation of Synaptic Plasticity by the Hypoxia-inducible Factor-2 alpha in Hypoxia. Festival of Neuroscience of the British Neuroscience Association (BNA), Dublin, Ireland.

Online Presentations

Quinting, T., Fandrey, J. and Schreiber, T. Regulation of synaptic plasticity by the hypoxia-inducible factor-2α (2021). 20st Day of Science at the Medical Faculty, University of Duisburg-Essen, Essen, Germany.

Quinting, T. HIF-2α - the “super athlete gene” (2021) Science Slam at the Annual Retreat of the Graduate School of Biomedical Science (BIOME), Core “Ischemia, Reperfusion and Angiogenesis”, Essen, Germany.

Quinting, T., Fandrey, J. and Schreiber, T. Regulation of synaptic plasticity by the hypoxia-inducible factor-2α (2020). 19th Day of Science at the Medical Faculty, University of Duisburg-Essen, Essen, Germany.

ACKNOWLEDGEMENTS

CURRICULUM VITAE

DECLARATIONS